Hinc patriam sustinet
Instituto Superior de Agronomia
Universidade de Lisboa

Avaliação da composição e estrutura ripária Mediterrânica baseada em SIG e Detecção Remota

TESE APRESENTADA PARA OBTENÇÃO DO GRAU DE DOUTOR EM ENGENHARIA FLORESTAL E DOS RECURSOS NATURAIS

MARIA DO ROSÁRIO PEREIRA FERNANDES

ORIENTADORA: Doutora Maria Teresa Ferreira da Cunha Cardoso
CO-ORIENTADOR: Doutor José Miguel Oliveira Cardoso Pereira
CO-ORIENTADORA: Doutora Francisca Constança Frutuoso de Aguiar

JÚRI:
Presidente: Reitor da Universidade de Lisboa

Vogais:
Doutora Marta González del Tánago
Professora Titular
Universidade Politécnica de Madrid, Espanha

Doutor Rui Manuel Victor Cortes
Professor Catedrático
Escola de Ciências Agrárias e Veterinárias da Universidade de Trás-os-Montes e Alto Douro

Doutor José Miguel Oliveira Cardoso Pereira
Professor Catedrático
Instituto Superior de Agronomia da Universidade de Lisboa

Doutora Maria Teresa Marques Ferreira da Cunha Cardoso
Professora Associada com Agregação
Instituto Superior de Agronomia da Universidade de Lisboa

Doutora Maria Manuela Queiroz Martins Mantero Morais
Professora Auxiliar
Escola de Ciências e Tecnologia da Universidade de Évora

Doutora Maria Graça Corte-Real Mira da Silva Abrantes
Professora Auxiliar
Instituto Superior de Agronomia da Universidade de Lisboa

Lisboa

U LISBOA | UNIVERSIDADE DE LISBOA

2013

Resumo

As florestas ripárias são responsáveis por numerosas funções consideradas fundamentais para a preservação da qualidade ecológica dos corredores fluviais. O objectivo desta tese é a caracterização dos padrões estruturais e composicionais da vegetação ripária e relacioná-los com a qualidade ecológica dos ecossistemas fluviais através de deteção remota e de sistemas de informação geográfica.

As análises de separabilidade permitiram caracterizar e distinguir vários padrões espectrais e comportamentos óticos divergentes entre os principais tipos de florestas ripárias em Portugal. As análises de espectroradiometria possibilitaram a identificação das bandas ótimas para distinção remota da espécie exótica invasora, cana (*Arundo donax*), face à vegetação envolvente, tendo em conta a variabilidade espectral sazonal da vegetação.

As técnicas de geoestatística combinadas com a aplicação de métricas de paisagem, em imagens de elevada resolução espacial, permitiram o reconhecimento remoto dos padrões estruturais de florestas ribeirinhas e de zonas ripárias invadidas por cana. Foi obtida uma relação entre os padrões de degradação observados e um gradiente de pressão humana exercido nas zonas envolventes aos corredores fluviais. A combinação de atributos espectrais e geométricos permitiu aumentar o grau de precisão da cartografia semi-automática de cana em habitats ripários.

Palavras-chave: vegetação ripária, deteção remota, qualidade ecológica, traços óticos, atributos espectrais e geométricos

Abstract

Riparian forests are responsible for many functions considered essential to the preservation of the ecological condition of fluvial corridors. The aim of this thesis is to characterize the structural and compositional patterns of the riparian vegetation in relation to its ecological quality using remote detection and geographic information systems.

Separability analyses allowed to characterize and distinguish the spectral patterns and divergent optical behavior between the main riparian forests of Portugal. Spectroradiometry analyses enable the identification of the optimal bands for the remote detection of the alien invasive species *Arundo donax*, giant reed, from the surrounding vegetation, taking into account its seasonal spectral variability.

The Geostatistical techniques combined with the application of landscape metrics, in high spatial resolution images, allowed the remote identification of the structural patterns for riparian forests and for the riparian areas invaded by the giant reed. It was obtained a relation between the observed degradation patterns and a gradient of human disturbance in the surrounding areas of fluvial corridors. The combination of the spectral and geometric attributes allowed to increasing giant reed mapping accuracy in riparian habitats, using a semi-automatic technique.

Keywords: Riparian vegetation, remote detection, ecological condition, optical traits, spectral and geometric attributes

Agradecimentos

A todas as pessoas que contribuíram para o desenvolvimento e conclusão desta tese gostaria de exprimir o meu agradecimento, entre elas:

À Professora Teresa Ferreira, pela orientação científica, condições e oportunidades concedidas, amizade e confiança depositada.

À Doutora Francisca Aguiar, pelos valiosos ensinamentos, revisão detalhada de todos os manuscritos, constante disponibilidade e amizade incondicional.

Ao Professor José Miguel Pereira, pelas valiosas sugestões sobretudo metodológicas, incentivo e espírito crítico.

Aos colegas do "Waterlobby", nomeadamente à Ana Mendes, André Fabião, João Oliveira, José Maria Santos, Patrícia Rodriguez-González, Rui Rivaes e Susana Amaral, pelo companheirismo e amizade. Ao Paulo Branco, pelas críticas construtivas e discussões científicas empolgantes, ao Pedro Segurado pelas sugestões estatísticas e ao António Albuquerque pelo apoio nas saídas de campo. Ao colega do grupo de deteção remota do ISA, João Silva, pela partilha de ideias e apoio na elaboração e correção dos últimos dois artigos.

Ao Instituto Geográfico Português pela cedência das imagens aéreas multiespectrais ao abrigo do programa FIGIEE.

À Fundação para a Ciência e a Tecnologia pelo suporte financeiro atribuído pela Bolsa de Doutoramento (SFRH/BD/44707/2008).

Aos projectos "Ripidurable"-Interreg IIIC-SUD e "Ricover"-Interreg IV-B SUDOE que proporcionaram os meios financeiros para a concretização de parte do plano de trabalhos.

A todos os familiares e amigos, uma palavra de gratidão pelo incentivo e amizade. Um especial agradecimento à Mafalda Silva pela revisão dos textos em português.

Aos meus pais pelo apoio e carinho permanente.

À Matilde e ao Miguel por temperarem os meus dias com sorrisos e traquinices.

Ao Filipe, simplesmente por existires…

Indice

PARTE I

Introdução

Capítulo 1

Introdução

1.1 Objetivos e estrutura da tese

Esta dissertação tem como objetivo geral estudar os padrões estruturais e composicionais da vegetação ripária Mediterrânica, utilizando metodologias e técnicas de deteção remota e sistemas de informação geográfica e relacioná-los com a integridade ecológica dos corredores fluviais. Os objectivos particulares englobam: 1) avaliar a capacidade de distinção espectral de florestas ripárias e a existência de diferentes comportamentos óticos; 2) explorar a capacidade de descrição da estrutura da vegetação ripária com base em métricas de paisagem e aferir a influência dos usos do solo ao longo de um gradiente de pressão antropogénico; 3) aferir a detetabilidade remota das zonas ripárias invadidas por cana e identificar os atributos ótimos para cartografia da invasora.

A dissertação encontra-se estruturada em quatro partes. A primeira parte, a Introdução, descreve os objetivos e o enquadramento geral da tese bem como a estrutura seguida no decurso da dissertação. No capítulo 1 é apresentado o estado de arte no que se refere ao estudo da vegetação ripária nos sistemas mediterrânicos, bem como a evolução da deteção remota no estudo das galerias ribeirinhas, enquadrando a presente dissertação no atual contexto das duas áreas.

A segunda e a terceira partes representam o núcleo desta dissertação. Cada parte é constituída por dois capítulos, apresentados sob a forma de artigo científico, redigidos em Inglês, que pretendem de forma interdependente responder a questões científicas e/ou metodológicas. Dos quatro artigos que compõem as Partes II e III, três encontram-se publicados em revistas científicas e o quarto encontra-se em revisão. A apresentação dos artigos foi mantida igual à que se encontra publicada havendo diferenças nas formatações inerentes às especificidades de cada revista.

A presente dissertação engloba um conjunto de trabalhos que, tendo como elemento comum a caracterização da vegetação ripária com metodologias remotas, pretendem aferir através de atributos estruturais (fragmentação, continuidade longitudinal, largura ripária) e composicionais (composição florística, percentagem de cobertura, dominância, variabilidade) a qualidade ecológica das galerias ripárias. Ao longo da tese é utilizada uma abordagem de crescente especificidade, quer ao nível da escala, quer ao nível dos atributos estudados. No capítulo 2 é realizada uma abordagem à escala regional, sendo avaliados padrões de estrutura e composição florística de diferentes tipologias ripárias em função de um gradiente latitudinal bioclimático, tendo em conta unicamente locais de referência, i.e., locais minimamente

alterados pela ação humana. Seguidamente, o capítulo 3 detalha a caracterização da componente estrutural da vegetação ripária, neste caso ao nível da bacia hidrográfica, em função de diferentes usos do solo, incluindo locais de reduzida perturbação, mas também locais de elevada pressão antropogénica. No capítulo 4 é estudada a condição ecológica ripária através da avaliação remota da substituição dos padrões florísticos naturais pela espécie exótica invasora, *Arundo donax* L., sendo selecionado um troço de rio muito perturbado. Nos capítulos 4 e 5 é ainda abordada a dimensão temporal do sistema fluvial, ao avaliar a variabilidade sazonal da assinatura espectral da cana (capítulo 4) e a maior ou menor detetabilidade inter-anual desta, em função da variabilidade da matriz espectral envolvente e das diferentes características das imagens resultantes de períodos de aquisição distintos.

Esta tese pretende realizar uma ligação entre duas áreas difíceis de conciliar. Por um lado a ecologia fluvial, que estudando a interação entre organismos e comunidades aquáticas e a sua relação com o meio ambiente encara com alguma relutância a adoção de novas abordagens, envolvendo observações estruturais consideradas redutoras quando comparadas com o detalhe e a visão holística das diversas dimensões do sistema fluvial, obtida pelo contato direto com o campo. Por outro lado, os especialistas na área da deteção remota encontram-se muitas vezes focados nas questões tecnológicas e no desafio constante de desenvolver novas metodologias com análises estatísticas complexas, mas, por vezes, de difícil adequabilidade de escala à elevada complexidade dos ecossistemas ripários. Esta tese espera ser um exemplo de sinergia produtiva entre as duas áreas. Finalmente, salientar que foi preocupação constante ao longo desta dissertação traduzir os ensinamentos teórico-científicos resultantes de cada capítulo em implicações claras para a intervenção na gestão e monitorização das galerias ribeirinhas.

1.2 A vegetação ripária nos sistemas fluviais mediterrânicos

As galerias ribeirinhas são ecótonos de elevada dinâmica entre os ecossistemas aquáticos e terrestres, apresentando um conjunto de funções ecológicas inerentes à sua complexidade estrutural e biológica consideradas fundamentais para a manutenção das condições ecológicas gerais dos sistemas fluviais (Malanson 1993; Naiman e Décamps 1997). As zonas ripícolas em regiões semiáridas, como é o caso de grande parte do território da bacia mediterrânica, são consideradas “oásis lineares” devido à importância acrescida das funções relacionadas com a regulação biofísica do meio, do suporte ecológico de comunidades e do funcionamento como corredores de migração para a fauna, na mitigação dos efeitos resultantes dos

constrangimentos geomorfológicos e climáticos destas regiões (Naiman et al., 1993). A manutenção desta diversidade funcional em ecossistemas ribeirinhos está intimamente associada ao conceito de integridade ecológica, como sendo a capacidade do sistema ripário preservar a comunidade biológica correspondente ao seu estado natural, tendo em conta o tipo de habitat tipológico específico, de acordo com os princípios de resiliência e resistência, for forma a preservar os processos funcionais endógenos e exógenos (Angermeier e Karr, 1994).

Os últimos trinta anos de estudos sobre vegetação ripária em sistemas fluviais portugueses permitiram reconhecer a especificidade e elevada complexidade destas comunidades traduzida numa elevada heterogeneidade estrutural e composicional (Aguiar e Ferreira, 2005). Embora os estudos realizados tivessem salientado a dificuldade do reconhecimento de tipologias naturais de vegetação, devido à influência milenar da perturbação humana, foi possível encontrar padrões florísticos e composicionais gerais, modelados primariamente por um gradiente climático e hidrogeológico latitudinal (Aguiar et al., 2000; Ferreira e Aguiar, 2006; Aguiar et al., 2012). Estas tipologias composicionais (composição florística, percentagem de cobertura, riqueza e frequência de ocorrência) e estruturais (fragmentação, continuidade longitudinal, largura ripária) correspondem aos atributos biológicos representativos de condições pouco perturbadas encontradas para cada região, isto é, locais classificados como de referência. Assim, nas regiões localizadas no extremo norte do gradiente latitudinal, de clima temperado húmido, com linhas de água de caráter permanente, predominam as florestas ripárias caducifólias de salgueirais, amiais e freixiais, de elevada complexidade vertical com sobreposição dos estratos arbóreo, arbustivo e herbáceo. As galerias ripárias destas zonas apresentam padrões de média conectividade longitudinal e lateral e larguras ripárias que podem atingir os 10m. Por oposição, no extremo sul do gradiente, as comunidades ripárias típicas de cursos de água com regimes temporários e sujeitos a acentuada secura estival são substituídas por espécies perenifólias como o loendro (*Nerium oleander* L., ou esclerófitas como o tamujo (*Flueggea tinctoria* (L.) G.L.Webster) e a tamargueira (*Tamarix africana* Poiret) (Aguiar et al., 1999). Estas galerias são naturalmente estreitas e esparsas sendo, muito vezes, representadas só pelo estrato arbustivo e herbáceo e pela presença de espécies resilientes adaptadas às condições de aridez.

Nos sistemas fluviais mediterrâneos a distribuição das espécies ripárias é ainda função de um gradiente longitudinal associado a fatores geomorfológicos locais (origem do substrato, largura do canal, declive) responsável pela heterogeneidade florística e estrutural encontrada entre a cabeceira e a foz. De um modo geral, os trabalhos de Aguiar e Ferreira, 2005; Aguiar et al.,

2009; 2012 revelam um aumento da complexidade em termos estruturais, mas também de riqueza e composição florística, de montante para jusante, devido ao aumento da disponibilidade de nutrientes e à existência de solos profundos que permitem a colonização e o estabelecimento de comunidades mais complexas. No entanto, estas tipologias de afiliação geográfica e os padrões espaciais de composição florística, são fortemente condicionados por variáveis locais, associadas à perturbação humana, como a regularização dos cursos de água e a ocupação agrícola e urbana do uso do solo (Décamps et al., 1988; Corbacho et al., 2003; Ferreira et al., 2005; Hooke, 2006). Com exceção das grandes assimetrias geográficas e climáticas, que claramente distinguem galerias ribeirinhas com diferentes padrões de riqueza e integridade estrutural, a combinação e sobreposição das variáveis locais geológicas, hidromorfológicas e antropogénicas ditam a panóplia de padrões ripários espaciais encontrados para o restante território, como é o caso da presença de comunidades monoespecíficas de amiais ribeirinhos encontrada em solos aluviais de forte utilização agrícola ou os salgueirais arbustivos típicos de cursos de água com regimes torrenciais em rios regularizados. Estes trabalhos apontam para o aumento da fragmentação e para a diminuição da riqueza e cobertura de espécies ripárias nativas em sistemas fluviais fortemente humanizados, bem como a existência de padrões de substituição de comunidades nativas por espécies exóticas, associados a processos de intensificação dos usos agrícolas do solo e canalização de rios para retificação do perfil longitudinal e transversal.

A preservação e recuperação da diversidade funcional dos ecossistemas ripários, atendendo ao princípio da integridade ecológica, é objetivo comum de instrumentos legais nacionais e internacionais, como a Directiva Comunitaria 2000/60/EC, transposta para Portugal pela Lei nº 58/2005 de 29 de Dezembro e complementada pelo Dec. Lei nº 77/2006 de 30 de Março, conhecida como Directiva-Quadro da Água da União Europeia (DQA), mas também de inúmeros projetos nacionais e de cooperação internacional associados à temática do restauro fluvial. As espécies e as comunidades, os padrões de cobertura e de fragmentação encontrados nas zonas ripárias podem ser utilizados para avaliação da integridade ecológica global do sistema fluvial, na monitorização do estado de conservação e, consequentemente, na identificação de áreas para restauro através da estimativa do desvio em relação às situações de referência.

Nas últimas décadas diversos trabalhos têm sido dedicados ao desenvolvimento de metodologias para avaliação da qualidade ecológica das galerias ribeirinhas, onde se salientam o Índice Multimétrico Ibérico (IMPI) (Ferreira et al., 2005), o Índice de Qualidade Ribeirinho

(González-del-Tánago et al., 2006), o Índice de Qualidade de Bosques Ribeirinhos (Munné et al., 2003) e o Índice de Vegetação Ripária (RVI) (Aguiar et al., 2009). Enquanto alguns autores dão particular relevância à determinação da qualidade ecológica através da vertente composicional (Looy et al., 2008), para outros, ela é sobretudo estabelecida através de atributos estruturais e funcionais como a continuidade longitudinal e lateral e a percentagem de cobertura (González-del-Tánago, 2006; Aguiar et al., 2009). No caso de avaliações expeditas baseadas em apreciações visuais de parâmetros ripários são usados maioritariamente critérios qualitativos (Ward et al., 2003; Dixon et al., 2006) de elevada subjetividade e difícil comparação. No entanto, todas apresentam como ponto fraco o facto de recorrem a um exaustivo e dispendioso trabalho de campo com limitações na aplicabilidade da metodologia em zonas de difícil acesso e em áreas extensas.

Dentro deste contexto, a deteção remota entendida como a possibilidade de adquirir informação sobre um objeto sem entrar em contato com o mesmo (Lillesand e Kiefer, 1994), representa um potencial contributo para avaliação da qualidade ecológica da vegetação ripária. A aplicação destes métodos permite ultrapassar parte das limitações dos métodos tradicionais de inventariação no campo (Muller, 1997; Goetz, 2006) e a possibilidade de monitorização de áreas sujeitas a restauro devido à automatização de diversos processos. A utilidade da deteção remota nos estudos ripários está intrinsecamente relacionada com a componente espacial e com a necessidade fundamental de conhecer a localização e a distribuição da vegetação (Turner et al., 2003). Os padrões espaciais traduzem processos ecológicos (Turner, 1989; Goetz, 2006). Dito de outra maneira, os parâmetros ripários obtidos através da análise de imagens, como os padrões de descontinuidade longitudinal e transversal, a largura ripária, o maior ou menor contraste espectral das manchas de vegetação ripária com a matriz envolvente, traduzem a natureza e a magnitude dos processos e das funções ecológicas podendo ser usados na avaliação da integridade ripária, quer a nível local quer a nível regional.

1.3 A deteção remota das galerias ribeirinhas

As duas últimas décadas têm mostrado um progresso significativo no desenvolvimento dos Sistemas de Informação Geográfica (SIG), na crescente disponibilização de imagens de satélite com maior resolução e nas novas técnicas de extração de informação a partir de imagens. Os estudos realizados em galerias ribeirinhas, com recurso a técnicas de deteção remota, refletem essa evolução e têm vindo a contribuir para a otimização da gestão e monitorização destas

zonas devido à possibilidade de caraterizar com detalhe, de forma objectiva e regular os ecossistemas ripários. Os diversos trabalhos realizados neste âmbito podem ser sistematizados em três grandes categorias, de acordo com os objetivos a que se propõem: 1) classificação e produção de cartografia temática; 2) determinação de parâmetros relacionados com a integridade do ecossistema ripário e 3) deteção de alterações. O Quadro 1 apresenta uma síntese destes trabalhos enumerando os atributos avaliados segundo estas categorias e a respetiva área de estudo. O Quadro 2 sumaria as características básicas dos sensores utilizados nos referidos trabalhos, relativamente ao tipo de plataforma, resolução espacial e espectral das imagens.

O primeiro grande grupo de trabalhos refere-se à classificação de imagens e a consequente produção de cartografia temática é a aplicação de carácter mais elementar da utilização da deteção remota no estudo das zonas ripárias. Os mapas produzidos podem apresentar a distribuição geográfica de métricas ripárias estruturais, como a largura total do "buffer ripário" (Goetz et al., 2003; Bentrup e Kellerman 2004; Baker et al., 2007; Booth et al., 2007; Makkeasorn et al., 2009) ou fornecerem informação quanto à localização e distribuição de espécies e comunidades ripárias nativas e/ou exóticas (Dowling e Accad, 2003; Nagler et al., 2005; Johansen e Phinn, 2006).

Na cartografia de representação de atributos estruturais, as aplicações mais simples utilizam um sistema de classificação só com uma classe, sendo o objetivo a distinção da zona ripária dentro de uma matriz geográfica (Schuft et al., 1999; Reed e Carpenter,2002; Goetz et al., 2003). Há autores que utilizam um sistema de "buffer ripário" constante e incremental (faixas ripárias contíguas) (Schuft et al., 1999; Congalton et al., 2002; Yang, 2007), com ganhos em termos de processamento de informação, mas redução da precisão quanto à localização e à descrição da forma da galeria ribeirinha. Nas aplicações mais complexas, é utilizado um sistema de classificação com diversas classes de vegetação ripária, sendo este construído com base em critérios muito diversos. Reed e Carpenter (2002) e Fernandes et al. (2011) utilizam um sistema de classificação baseado nos diferentes estratos de vegetação (arbóreo, arbustivo e herbáceo), enquanto outros trabalhos baseiam-se em atributos fisionómicos e de persistência foliar para construção das classes (Weber e Dunno, 2001). Existem ainda critérios relacionados com a similaridade dos valores e benefícios ecológicos produzidos por cada classe para o sistema ripário (Congalton et al., 2002; Gergel et al., 2007; Tormos et al., 2010), e sistemas construídos com base nos diferentes estágios de sucessão da vegetação (Johansen et al., 2007a.

Quadro 1 – Estudos de deteção remota aplicados a zonas ripárias de acordo com as principais aplicações e atributos estudados.

Aplicação	Atributo	Designação	Localização	Referência
Cartografia	Estrutural	Cartografia do buffer ripário	Iowa, US	Narumalani et al., 1997
			Oregon, US	Schuft et al., 1999
			Califórnia, US	Butt et al., 2001
			Queensland, Austrália	Apan et al., 2002
			Arizona, US	Davis et al., 2002
			Wisconsin, US	Reed e Carpenter, 2002
			Paraná, Brasil	Antunes et al., 2003
			Maryland,US	Goetz et al., 2003
			Kansas, US	Bentrup e Kellerman., 2004
			Virginia, US	Baker et al., 2007
			Nevada, US	Booth et al., 2007
			Hunter, Australia	Yang, 2007
			Espanha	Ivits et al., 2009
			Texas, US	Makkeasorn et al., 2009
		Cartografia de classes de vegetação ripária	Arizona, US	Weber e Dunno, 2001
			Oregon, US	Congalton et al., 2002
			California, US	DiPietro et al., 2002
			Wisconsin, US	Reed e Carpenter, 2002
			British Columbia, Canadá	Gergel et al., 2007
			Vancouver, Canada	Johansen et al., 2007a
			Queensland, Austrália	Johansen et al., 2010
			França	Tormos et al., 2010
			Portugal	Fernandes et al., 2011
	Composicional	Cartografia de espécies nativas	Texas, US	Lonard et al., 2000
			Texas, US	Nagler et al., 2005
			Queensland, Austrália	Johansen e Phinn, 2006
			Nevada, US	Booth et al., 2007
			New Mexico, US	Akasheh, et al., 2008
			Texas e Mississippi, US	Zomer et al., 2009
		Cartografia de comunidades ripárias nativas	Texas, US	Lonard et al., 2000
			Queensland, Australia	Dowling e Accad, 2003
			Texas, US	Nagler et al., 2005
			Queensland, Australia	Johansen e Phinn, 2006
			New Mexico, US	Akasheh, et al., 2008
			Texas e Mississippi, US	Zomer et al., 2009
		Cartografia de exóticas	California, US	DiPietro et al., 2002
			Texas, US	Everitt et al., 2004
			Idaho, US	Gleenn et al., 2005
			California, US	Hamada et al., 2007
			Wisconsin, US	Pengra et al., 2007
			California, US	Andrew e Ustin, 2008
			New Mexico, US	Akasheh, et al., 2008
			Texas, US	Everitt et al., 2008
			Mexico/US	Yang et al., 2012
			Portugal	Fernandes et al., (submited)

Quadro 1 (cont)

Aplicação	Atributo	Designação	Localização	Referência
Determinação de parâmetros	Estrutural	Cobertura da vegetação ripária	California, US Oregon, US Queensland, Austrália Queensland, Austrália Darwin, Australia Queensland, Austrália Hunter, Austrália Espanha	Nagler et al., 2001 Congalton et al., 2002 Dowling e Accad, 2003 Johansen e Phinn, 2006 Johansen et al., 2007a Johansen et al., 2010 Yang, 2007 Ivits et al., 2009
		Largura	Oregon, US Queensland, Austrália Oregon, US Wisconsin, US Queensland, Austrália Virginia, US Nevada, US França	Schuft et al., 1999 Apan et al., 2002 Congalton et al., 2002 Reed e Carpenter, 2002 Johansen e Phinn, 2006 Baker et al., 2007 Booth et al., 2007 Tormos et al., 2010
		Extensão longitudinal	Oregon, US Arizona, US Wisconsin, US France	Schuft et al., 1999 Weber e Dunno, 2001 Reed e Carpenter, 2002 Tormos et al., 2010
		Fragmentação (inclui a quantificação das zona sem vegetação)	Oregon, US Queensland, Austrália França Kansas, US Darwin, Austrália Virginia, US Portugal	Schuft et al., 1999 Apan et al., 2002 Tormos et al., 2010 Bentrup e Kellerman Johansen et al., 2007 Baker et al., 2007 Fernandes et al., 2011
		Conetividade	Oregon, US Wisconsin, US Darwin, Australia Queensland, Austrália	Schuft et al., 1999 Reed e Carpenter, 2002 Johansen et al., 2007a Johansen et al., 2010
		Configuração	Queensland, Austrália Portugal	Apan et al., 2002 Fernandes et al., 2011
		Estrutura vertical	Queensland, Austrália Califórnia, USA Queensland, Austrália	Dowling e Accad, 2003 Nagler et al., 2005 Johansen et al., 2010
	Morfológico	Vigor vegetativo	Texas, Arizona, USA British Columbia, Canadá	Lonard et al., 2000 Weber e Dunno, 2001 Gergel et al., 2007
		Indice de área foliar	California, USA Queensland, Austrália	Nagler et al., 2001 Johansen e Phinn, 2006 Zomer et al., 2009
		Biomassa		

Composicional	Assinaturas espectrais de espécies nativas	Califórnia, US New Mexico, US South Africa Texas e Mississippi, US Califórnia, US Portugal	Nagler et al., 2001 Akasheh et al., 2008 Adam e Mutanga, 2009 Zomer et al., 2009 Ustin e Santos, 2010 Fernandes et al., 2013a
	Assinaturas espectrais de comunidades nativas	Califórnia, US Queensland, Australia Texas e Mississippi, US Portugal	DiPietro et al., 2002 Johansen e Phinn, 2006 Zomer et al., 2009 Fernandes et al., 2013a
	Assinaturas espectrais de espécies exóticas	Califórnia, US California, US New Mexico, US Uganda Califórnia, US Mexico/US Portugal	DiPietro et al., 2002 Andrew e Ustin, 2008 Akasheh et al., 2008 Cavalli et al., 2009 Ustin e Santos, 2010 Yang et al., 2012 Fernandes et al., 2013b

Deteção de alterações

Estrutural	Buffer ripário	Espanha Texas, US	Ivits et al., 2009 Makkeasorn et al., 2009
	Cobertura da vegetação ripária	Texas, USA Darwin, Austrália	Lonard et al., 2000 Johansen et al., 2007b
	Conetividade, Largura, Dimensão e forma das manchas ripárias	Queensland, Austrália	Apan et al., 2002
Composicional	Espécies e comunidades ripárias nativas	Califórnia, US	Nagler et al., 2005
	Espécies e comunidades ripárias nativas e exóticas	New Mexico, US	Akasheh et al., 2008
	Espécies invasoras	Idaho, US	Glenn et al., 2005

O segundo grande grupo de trabalhos tem como objetivo comum a determinação remota de parâmetros estruturais e composicionais que representam, quer direta quer indiretamente, medidas de funcionalidade e de integridade dos ecossistemas ripários. Na maior parte dos casos são estabelecidas relações empíricas entre as variáveis extraídas nas imagens e os atributos intrínsecos da vegetação, provenientes de informação recolhida em campo. Como exemplo destas relações pode indicar-se a estimativa dos valores de biomassa e produtividade primária com base no ajuste dos melhores modelos de regressão entre medições de campo e valores de reflectância das imagens (Nagler et al., 2001; Johansen e Phinn, 2006; Cavalli et al., 2009). Outros atributos morfológicos representativos de medidas de qualidade ecológica do sistema, como, por exemplo, o vigor vegetativo e o índice de massa foliar, podem também ser avaliados de forma indireta através do cálculo de índices espectrais como é o caso do Índice da Vegetação por Diferença Normalizada (NDVI) (Lonard et al., 2000; Nagler et al., 2001; Weber e Dunno, 2001; Gergel et al., 2007; Zomer et al., 2009) ou outros índices desenvolvidos no sentido de mitigar os problemas relacionados com o efeito do solo nas medições espectrais. (Johansen e Phinn, 2006). A avaliação do vigor vegetativo pode também ser realizada de forma indireta através da presença de assinaturas espectrais atípicas que permitem detetar a presença de árvores mortas (Lonard et al., 2000). Dentro dos atributos estruturais frequentemente avaliados remotamente, e que representam medidas diretas da integridade funcional do ecossistema ripário, encontram-se a percentagem de cobertura ripária, a conectividade longitudinal e lateral e a fragmentação. Recentemente, devido à utilização de imagens óticas de maior resolução espacial, como é o caso das Ikonos, QuickBird, OrbView-3, Spot HRG e WorldView-2, tem sido avaliada a configuração das manchas de vegetação, através da utilização de descritores numéricos geométricos, e caracterizada a sua relação com a naturalidade do sistema ripário (Apan et al., 2002; Fernandes et al., 2011). Manchas de vegetação lenhosa de grandes dimensões com configurações complexas e meandrizadas representam galerias ripárias em bom estado de conservação por oposição a manchas de configurações simples e lineares. São ainda conhecidos trabalhos que avaliam a estrutura vertical da vegetação ripária, recorrendo a leituras em sistemas de Light Detection and Ranging (LiDAR) (Dowling e Accad, 2003) ou ainda em imagens óticas, usando o tamanho da sombra para inferir quanto à altura da vegetação (Nagler et al., 2001; Nagler et al., 2005; Fernandes et al., 2011) caraterizando a componente tridimensional do sistema ripário.

No entanto, a aferição da qualidade ecológica das zonas ripárias deve representar uma visão holística e integradora das diversas componentes descritoras do ecossistema. Desta forma, a avaliação remota da componente composicional é, a par da avaliação da componente estrutural, uma necessidade em todo este processo. Zonas ripárias caracterizadas pela

presença de grandes manchas de vegetação, com elevada conectividade podem, no entanto, estar associadas a zonas de reduzida integridade com baixa funcionalidade ecológica para todo o sistema fluvial. Neste caso a degradação está associada a processos de substituição da vegetação nativa por espécies exóticas. Neste campo, a recente disponibilização de instrumentos e sensores hiperespectrais, com centenas de bandas contíguas ao longo do espectro eletromagnético, têm permitido a caracterização da vertente composicional através da identificação de assinaturas espectrais, não só de espécies (Akasheh et al., 2008; Adam e Mutanga, 2009; Zomer et al., 2009; Ustin e Santos, 2010; Fernandes et al., 2013a e comunidades nativas (DiPietro et al., 2002; Zomer et al., 2009; Fernandes et al., 2013a), mas também das espécies exóticas mais comuns nos sistemas ripários (DiPietro et al., 2002; Andrew e Ustin, 2008; Akasheh et al., 2008; Cavalli et al., 2009; Ustin e Santos, 2010; Yang et al., 2012). Estes trabalhos base, permitiram averiguar a separabilidade espectral destas espécies face à vegetação envolvente, determinar as bandas do espectro eletromagnético onde essa distinção é maximizada e desta forma fornecer orientações na produção de cartografia temática (Nagler et al., 2001; Fernandes et al., 2013). São, no entanto, ainda reduzidos os trabalhos que integram simultaneamente a avaliação remota das duas componentes nos estudos sobre zonas ripárias.

O terceiro grupo de trabalhos tem como objetivo a deteção de alterações num dado período temporal, quer ao nível da percentagem de cobertura e composição florística (Glenn et al., 2005; Nagler et al., 2005; Akasheh et al., 2008), quer em termos de variação da fragmentação, de conetividade longitudinal, tranversal e largura total (Ivits et al., 2009; Johansen et al., 2007; Lonard et al., 2000; Makkeasorn et al., 2009). Noutras áreas da ecologia, a aplicação da deteção remota a estudos temporais é largamente utilizada para previsão de cenários futuros, através da estimativa da influência dos fatores externos, quer ambientais quer fatores de pressão humana. No entanto, nos estudos de deteção remota aplicada a vegetação ripária, esta vertente ainda não se encontra desenvolvida.

Quadro 2- Principais características dos sensores utilizados nos trabalhos de deteção remota aplicada a estudos ripários, relativamente ao tipo de plataforma, sensor utilizado, resolução espacial e espectral.

Plataforma	Sensor	Resolução espectral					Resolução espacial					**Referência**
		Pancromático	Multiespectral (visível e/ou infravermelho)	Multiespectral < 20 bandas	Multiespectral >20 bandas	Hiperespectral	< 1m	1-5m	5-20m	> 20m	> 500m	
Aérea	Sensores digitais	X					X					Booth et al., 2007
		X						X				Schuft et al., 1999 Congalton et al., 2002
		X							X			Reed e Carpenter, 2002 Baker et al., 2007
		X								X		Bentrup e Kellerman, 2004
			X				X					Butt et al., 2001 Nagler et al., 2001 Davis et al., 2002 Everitt et al., 2004 Nagler et al., 2005 Akasheh et al., 2008 Tormos et al., 2010 Fernandes et al., 2011 Fernandes et al.,2013 (a)
			X					X				Yang, 2007
	ATLAS (airborne terrestrial application sensor)			X				X				Weber e Dunno, 2001
	AVIRIS (airborne visible infrared spectrometer					X			X			DiPietro et al., 2002 Ustin e Santos, 2010
	CCD (hyperspectral digital camera)					X			X			Yang et al., 2012
	HyMap					X		X				Glenn et al., 2005 Andrew e Ustin, 2008

												Ustin e Santos, 2010
	PROBE-1					X		X				Zomer et al., 2009
	SOC-700					X	X					Hamada et al., 2007
	Câmara de video		X				X					Lonard et al., 2000 Davis et al., 2002 Everitt et al., 2004
	LIDAR (light detection and ranging	X						X				Dowling e Accad, 2003
Orbital	AVHRR (Advanced Very High Resolution Radiometer)			X						X	X	Ivits et al., 2009 Johansen et al
	SPOT-4 SPOT-5 SPOT-5 XS		X						X			Yang, 2007 Everitt et al., 2008 Tormos et al., 2010
	Landsat- TM ou ETM+ (Thematic Mapper ou Enhanced Thematic Mapper Plus			X						X		Apan et al., 2002 Congalton et al., 2002 Johansen e Phinn, 2006 Yang, 2007 Cavalli et al., 2009 Makkeasorn et al., 2009
	Hyperion					X				X		Pengra et al., 2007
	Ikonos		X					X				Antunes et al., 2003 Goetz et al., 2003 Johansen e Phinn, 2006
	QuickBird		X					X				Gergel et al., 2007 Johansen et al., 2007(b) Everitt et al., 2008
	WorldView-2			X				X				Fernandes et al., submitted
Terrestre	Espectroradiometro					X	X					Adam e Mutanga, 2009 Zomer et al., 2009 Ustin e Santos, 2010 Fernandes et al., 2013 (b)

Na deteção remota de ecossistemas ripários, sobretudo em zonas mediterrâneas, o maior constrangimento prende-se com a necessidade de utilização de imagens de elevada resolução espacial, e metodologias de extração de informação ajustadas à natureza linear, e à largura residual destas zonas face à utilização secular das margens dos rios para uso agrícola, combinada com a intrínseca heterogeneidade espacial destas comunidades (Congalton et al., 2002; Davis et al., 2002; Muller, 1997). Os erros de classificação mais comuns prendem-se com a dificuldade de isolar assinaturas espectrais que representam diversidade florística, existência de diferentes estratos e densidades, e mistura de reflectâncias combinadas de vegetação, solo nu e molhado (Weber e Dunno, 2001). Os trabalhos cujos objetivos passavam pela cartografia de detalhe e distinção entre espécies, com base na informação numérica extraída em imagens multiespectrais de média resolução espacial, como é o caso das Landsat e das SPOT, apresentavam níveis de precisão bastante reduzidos, entre 25 a 50% (Johansen and Phinn, 2006 Lonard et al., 2000, Nagler., 2005) quando comparados com imagens de elevada resolução espacial. Para se obter precisões cartográficas elevadas, era necessário o uso de fotografias aéreas de elevada resolução espacial, sendo, no entanto, usadas técnicas de fotointerpretação, ou seja, de extração de informação através da análise visual das imagens e não da sua componente numérica (Schuft et al., 1999; Weber e Dunno, 2001; Congalton et al., 2001; Reed e Carpenter, 2002; Dowling e Accad, 2003). Além disso, a utilização de imagens com resoluções espaciais mais grosseiras poder conduzir a uma sobreavaliação da largura e do nível de conetividade entre as manchas de vegetação. Só o detalhe das resoluções finas permite reconhecer as relações de influência entre os fatores externos, quer ambientais quer de uso do solo, ao detectar e cartografar com precisão padrões de fragmentação e configurações geométricas características de processos de degradação ripária (Baker et al., 2007; Fernandes et al., 2011).

O aparecimento de imagens de elevada resolução espacial, em plataformas orbitais e de sensores hiperespectrais, tem permitido melhorar as classificações obtidas na caracterização remota das zonas ripárias. Em particular, as imagens hiperespectrais permitem a caracterização dos perfis espectrais da vegetação no contínuo, mas todas elas têm obrigado a um ajustamento dos métodos de processamento e análise de imagens, de extração de informação, redução de redundância e de ruído, devido ao incremento de variabilidade capturada por estes sensores. Os estudos tradicionais são sobretudo focados nas características espectrais da vegetação, através da utilização simples ou combinada de máscaras espaciais e algoritmos supervisionados e não supervisionados (Congalton et al.,

2001; Apan et al., 2002; Goetz et al., 2003). Estes trabalhos utilizam métodos estatísticos paramétricos, como técnicas de ordenação, para determinação das bandas ótimas ou combinações lineares de bandas para potenciar a separabilidade entre classes. Nos trabalhos mais recentes, há uma tendência para combinar informação remota proveniente de diferentes categorias, como é o caso da componente geométrica ou da textura, para aumentar o grau de precisão final. A classificação orientado por objeto (Antunes et al., 2003; Gergel et al., 2007; Johansen et al., 2007a,b; Fernandes et al., submetido) combinada com o uso de técnicas estatísticas não paramétricas, como as árvores de classificação e regressão (Goetz et al., 2003; Andrew e Ustin, 2008), as redes neuronais e os algoritmos "fuzzy", têm permitido obter informação cada vez mais detalhada das zonas ripárias, quer na sua componente biofísica, quer estrutural, quer composicional.

No decorrer desta dissertação houve ainda necessidade de recolher informação específica sobre as particularidades da deteção remota, quando aplicada à vegetação de zonas áridas e semi-áridas, como é o caso das galerias ripárias localizados no sul de Portugal continental. Estas apresentam adaptações quer ao nível da comunidade (galerias naturalmente esparsas com reduzida cobertura), quer ao nível da planta (folha coriáceas, cobertura da epiderme com ceras, reduzida evapotranspiração) que resultam dos condicionalismos ambientais traduzindo-se em traços funcionais (Aguiar et al., 2012) e em comportamentos óticos particulares, como é o caso do menor contraste espectral e dos reduzidos valores de reflectância na zona do infravermelho próximo, que necessitam de técnicas e abordagens metodológicas adaptadas, no sentido de compreender o funcionamento destes sistemas numa perspectiva remota (Okin et al., 2001).

1.4 Referências bibliográficas

Adam E., Mutanga O., 2009. Spectral discrimination of papyrus vegetation (*Cyperus papyrus* L.) in swamp wetlands using field spectrometry. ISPRS Journal of Photogrammetry and Remote Sensing 64 (6), 612-620.

Aguiar F.C., Cerdeira J.O., Martins M.J., Ferreira M.T., 2012 (on-line). Riparian forests of Southwestern Europe: are functional trait and species composition assemblages constrained by environment? Journal of Vegetation Science. http://onlinelibrary.wiley.com/doi/10.1111/jvs.12009/abstract

Aguiar F.C., Ferreira M.T., 2005. Human-disturbed landscapes: effects on composition and

integrity of riparian woody vegetation in the Tagus River basin, Portugal. Environmental Conservation 32 (1), 30-41.

Aguiar F.C., Ferreira M.T., Albuquerque A., Rodriguez-Gonzalez P., Segurado P., 2009. Structural and functional responses of riparian vegetation to human disturbance: performance and scale-dependence. Fundamental and Applied Limnology 175 (3), 249-267.

Aguiar F.C., Ferreira M.T., Moreira I., Albuquerque A., 2000. Riparian types in Mediterranean basin. Aspects of Applied Biology 58, 221-232.

Andrew M.E., Ustin S.L., 2008. The role of environmental context in mapping plants with hyperspectral image data. Remote Sensing of Environment 112 (12), 4301-4317.

Angermeier P.L., Karr J.K., 1994. Biological integrity versus biological diversity as policy directives. BioScience 44 (10), 690-697.

Antunes A.F., Lingnau C., Silva J.C., 2003 Object oriented analysis and semantic network for high resolution image classification. Anais XI SBSR, Instituto Nacional Pesquisas Espaciais, Belo Horizonte, 273-279.

Akasheh O.Z., Neale C.M.U., Jayanthi H., 2008. Detailed mapping of riparian vegetation in the middle Rio Grande River using high resolution multi-spectral airborne remote sensing. Journal of Arid Environments 72,1734-1744.

Apan A.A., Raine S.R., Paterson M.S., 2002. Mapping an analysis of changes in the riparian landscape structure of Lockyer Valley catchment Queensland, Australia. Landscape and Urban Planning 59, 43-57.

Baker M.E., Weller D.E., Jordan T.E., 2007. Effects of stream map resolution on measures of riparian buffer distribution and nutrient potential. Landscape Ecology 27 (7), 973-992.

Bentrup G., Kellerman. 2004. Where should buffers go? Modelling riparian habitat connectivity in northeast Kansas. Journal of Soil and Water Conservation, 59 (5), 209-215.

Booth D.T., Cox S.E., Simonds G., 2007. Riparian monitoring using 2-cm GSD aerial photography. Ecological Indicators 7, 636-648.

Butt A.Z., Ayers M., Swanson S., Tueller P., 2001. Riparian corridor assessment: combining vegetation and stream morphology classifications into a GIS database. In American Water Resources Association. Technical Publication Series TP S-98-1.

Cavalli R.M., Laneve G., Fusilli L., Pignatti S., Santini F., 2009. Remote sensing water Observation for supporting Lake Victoria weed management. Journal of Environmental Management 90, 2199-2211.

Congalton R.G., Birch K., Jones R., Schriever J., 2002. Evaluating remotely sensed techniques for mapping riparian vegetation. Computers and Electronics in Agriculture 37, 113-126.

Corbacho C., Sánchez J.M., Costillo E., 2003. Patterns of structural complexity and human disturbance of riparian vegetation in agricultural landscapes of Mediterranean area. Agriculture Ecosystems and Environment 95 (2-3), 495–507.

Davis P.A., Staid M.I., Plescia J.B., Johnson J.R., 2002. Evaluation of airborne image data for mapping riparian vegetation within the Grand Canyon. Report of U.S. Geological Survey. Arizona

Décamps H., Fortune M., Gazelle F., Patou G., 1988. Historical influence of man on the riparian dynamics of fluvial landscape. Landscape Ecology 1 (3), 163-173.

DiPietro D., Ustin S.L., Underwood E., 2002. Mapping the invasive plant *Arundo donax* and associated riparian vegetation using AVIRIS. AVIRIS Airborne Geoscience Workshop Proceedings, Pasadena, CA.

Dixon I., Douglas M., Dowe J., Burrows D., 2006. Tropical rapid appraisal of riparian condition version 1. River management technical guidelines. No7 Land and Water Australia, Canberra, Australia.

Dowling R., Accad A., 2003. Vegetation classification of the riparian zone along the Brisbane River, Queensland, Australia, using light detection and ranging (lidar) data and forward looking digital video. Canadian Journal of Remote Sensing 29 (5), 556-563.

Everitt J.H., Yang C., Alaniz M.A., Davis M.R., Nibling F.L., Deloach C.J., 2004. Canopy spectra of giant reed and associated vegetation. Journal of Range Management 57 (5), 561-569.

Everitt J.H., Yang C., Fletcher R., Deloach C.J., 2008. Comparison of QuickBird and SPOT 5 satellite imagery for mapping giant reed. Journal of Aquatic Plant Management 46, 77-82.

Ferreira M.T., Aguiar F.C., 2006. Riparian and aquatic vegetation in Mediterranean-type streams (western Iberia). Limnetica 25 (1-2), 411-424.

Ferreira M.T., Aguiar F.C., Nogueira C., 2005. Changes in riparian woods over space and time:

influence of environment and land use. Forest Ecology and Management 212 (1–3), 145-159.

Ferreira M., Rodríguez-González P., Aguiar F., Albuquerque A., 2005. Assessing biotic integrity in Iberian rivers: Development of a multimetric plant index. Ecological Indicators 5 (2), 137-149.

Gergel S.E., Stange Y., Coops N.C., Johansen K., Kirby KR., 2007. What is the value of a good map? An example using high spatial resolution imagery to aid riparian restoration. Ecosystems 10 (5), 688-702.

Glenn NF., Weber K.T., Prather T.S., Lass L.W., Pettingill J., 2005. Hyperspectral data processing for repeat detection of small infestations of leafy spurge. Remote Sensing of Environment 95 (3), 399-412.

Goetz S., 2006. Remote Sensing of Riparian Buffers: Past Progress and Future Prospects. Journal of the American Water Resources Association 42 (1), 133-143.

Goetz S.J., Wright R.K., Smith A.J., Zinecker E., Schaub E., 2003. IKONOS imagery for resource management: Tree cover, impervious surfaces, and riparian buffer analyses in the mid-Atlantic region. Remote Sensing of Environment 88 (1), 195-208.

González del Tánago M., García de Jalón D., Lara F., Garilleti R., 2006. Índice RQI para la valoración de las riberas fluviales en el contexto de la directiva marco del agua. Ingeniería Civil 143, 97-108.

Hamada Y., Stow D.A., Coulter L.L., Jafolla J.C., Hendricks L.W., 2007. Detecting Tamarisk species (*Tamarix* spp.) in riparian habitats of Southern California using high spatial resolution hyperspectral imagery. Remote Sensing of Environment 109 (2), 237-248.

Hooke, J.M., 2006. Human impacts on fluvial systems in the Mediterranean region. Geomorphology 79 (3-4), 311-335.

Ivits E., Cherlet M., Mehl W., Sommer S., 2009. Estimating the ecological status and change of riparian zones in Andalusia assessed by multitemporal AVHHR datasets. Ecological Indicators 9 (3), 422-431.

Johansen K., Coops N.C., Gergel S.E., Stange Y., 2007a. Application of high spatial resolution satellite imagery for riparian and forest ecosystem classification. Remote Sensing of Environment 110 (1), 29-44.

Johansen K., Phinn S., 2006. Mapping structural parameters and species composition of

riparian vegetation using IKONOS and Landsat ETM+ Data in Australian Tropical Savannahs. Photogrammetric Engineering and Remote Sensing *72*(1), 71-80.

Johansen K., Phinn S., Dixon I., Douglas M., Lowry J., 2007b. Comparison of image and rapid field assessments of riparian zone condition in Australian tropical savannas. Forest Ecology and Management 240 (1-3), 42-60.

Johansen K., Phinn S., Witte C., 2010. Mapping of riparian zone attributes using discrete return LiDAR, QuickBird and SPOT-5 imagery: Assessing accuracy and costs. Remote Sensing of Environment 114 (11), 2679-2691.

Lillesand T.M., Kiefer R.W., 1994. Remote Sensing and Image Interpretation. John Wiley and Sons, New York.

Lonard R.I., Judd F.W., Everitt J.H., Escobar D.E., Davis M.R., Crawford M.M., Desai M.D., 2000. Evaluation of color-infrared photography for distinguishing annual changes in riparian forest vegetation of the lower Rio Grande in Texas. Forest Ecology and Management 128 (1-2), 75-81.

Looy K.V., Meire P., Wasson J.G., 2008. Including riparian vegetation in the definition of morphologic reference conditions for large rivers: a case study for Europe's western plains. Environmental Management 41 (5), 625-639.

Makkeasorn A., Chang N., Li J. 2009. Seasonal change detection of riparian zone with remote sensing images and genetic programming in a semi-arid watershed. Journal of Environmental Management 90 (2), 1069-1080.

Malanson G.P., 1993. Riparian landscapes. Cambridge University Press, Cambridge.

Muller E., 1997. Mapping riparian vegetation along rivers: old concepts and new methods. Aquatic Botany 58 (3-4), 411-437.

Munné A., Prat N., Solà C., Bonada N., Rieradevall M., 2003. A simple field method for assessing the ecological quality of riparian habitat in rivers and streams, QBR index. Aquatic Conservation: Marine and Freshwater Ecosystems 13, 147-164.

Nagler P.L., Glenn E.P., Huete A.R., 2001. Assessment of spectral vegetation indices for riparian vegetation in the Colorado River delta, Mexico. Journal of Arid Environments 49 (1), 91-110.

Nagler P.L., Glenn E.P., Hursh K., Curtis C., Huete, A.R. 2005. Vegetation mapping for

change detection on an arid-zone river. Environmental Monitoring and Assessment 109 (1-3), 255-274.

Naiman R.J., Décamps H., 1997. The ecology of interfaces: riparian zones. Annual Review of Ecology, Evolution and Systematics 28, 621-658.

Naiman R.J., Décamps H., Pollock M., 1993. The role of riparian corridors in maintaining regional biodiversity. Ecological Applications 3 (2), 209-212.

Okin G.S., Roberts D.A., Murray B., Okin W.J., 2001. Practical limits on hyperspectral vegetation discrimination in arid and semiarid environments. Remote Sensing of Environment 77 (2), 212-225.

Pengra B.W., Johnston C.A., Loveland T.R., 2007. Mapping an invasive plant, *Phragmites australis*, in coastal wetlands using the EO-1 Hyperion hyperspectral sensor. Remote Sensing of Environment 108 (1), 74-81.

Reed T., Carpenter S.R., 2002. Comparisons of P-Yield, Riparian Buffer Strips, and land Cover in Six Agricultural Watersheds. Ecosystems 5 (6), 568-577.

Schuft M.J., Moser T.J., Wigington P.J., Stevens D.L., McAllister L.S., Chapman S., Ernst T.L., 1999. Development of landscape metrics for characterizing riparian-stream networks. Photogrammetric Engineering and Remote Sensing 65 (10), 1157-1167.

Turner M.G., 1989. Landscape ecology: the effect of pattern on process. Annual Review of Ecology, Evolution and Systematics 20, 171-197.

Turner W., Spector S., Gardiner N., Fladeland M., Sterling E., Steininger M., 2003. Remote sensing for biodiversity science and conservation. Trends in Ecology and Evolution 18 (6), 306-314.

Ustin S.L., Santos M.J., 2010. Spectral identification of native and non-native plant species. In: Proceedings of ASD and IEEE GRS; Art, Science and Applications of Reflectance Spectroscopy Symposium, Vol. II, Boulder, Colorado, February 23-25, pp17.

Ward T.A., Tate K.W., Atwill E.R., 2003. Visual assessment of riparian health. Rangeland Monitoring Series, Publication 8089. University of California.

Weber R.M., Dunno G.A., 2001. Riparian vegetation mapping and image processing techniques, Hopi Indian Reservation, Arizona. Photogrammetric Engineering and Remote Sensing 67 (2), 179-186.

Yang X., 2007. Integrated of remote sensing and geographic information systems in riparian

vegetation delineation and mapping. International Journal od Remote Sensing, 28(2), 353-370.

Yang C., Goolsby J.A., Everitt J.H., Du Q., 2012. Applying six classifiers to airborne hyperspectral imagery for detecting giant reed. Geocarto International 27(5), 413-424.

Zomer R.J., Trabucco, A., Ustin S.L., 2009. Building spectral libraries for wetlands land cover classification and hyperspectral remote sensing. Journal of Environmental Management 90 (7), 2170-2177.

PARTE II

Caracterização dos padrões estruturais e composicionais da vegetação ripária

Capítulo 2

Spectral separability of riparian forests from small and medium-sized rivers across a latitudinal gradient using multispectral imagery

2.1 Síntese

O capítulo 2, da segunda parte, testa a distinção espectral de florestas ripárias em função de critérios florísticos composicionais, utilizando imagens aéreas multiespectrais de elevada resolução espacial (RGB-NIR, 50 cm pixel). Compara-se a separabilidade espectral de formações ripárias lenhosas em rios de pequena e de média dimensão no sentido de investigar a possibilidade de detetar remotamente as diferenças resultantes da influência de um gradiente climático e de dimensão da bacia hidrográfica nos padrões florísticos composicionais das galerias ribeirinhas. Partindo de vinte seis locais de referência, i.e, corredores fluviais minimamente perturbados, de três zonas bioclimáticas (temperada, mediterrânea e de transição) são extraídas amostras espectrais representativas da variabilidade florística encontrada em cada local e com base em metodologias de análise e manipulação de imagem (normalização, criação de regiões de interesse, aplicação de índices de separabilidade e análise multivariada) são identificados diferentes níveis de distinção espectral entre as florestas ripárias. Relaciona-se a variabilidade estrutural e florística de cada floresta com o maior ou menor nível de separabilidade espectral e explora-se a convegência no comportamento ótico, modelado em função do gradiente climático, que justifica os diferentes graus de distinção espectral entre as florestas ripárias da zona temperada, da zona mediterrânea e da zona de transição. Neste trabalho é também apresentado pela primeira vez a nosso conhecimento, um quadro de síntese que relaciona os traços morfológicos, fenológicos e ecológicos, quer ao nível da folha quer ao nível da copa, das diferentes florestas ripárias com as implicações no comportamento espectral das diferentes tipologias ripárias. São ainda identificadas as assinaturas espectrais das espécies dominantes em cada uma das regiões bioclimáticas e discutida a sua relevância na identificação remota de áreas prioritárias para restauro, devido à possibilidade de determinação dos desvios florísticos em relação aos padrões espectrais de referência.

2.2 Artigo

Spectral separability of riparian forests from small and medium-sized rivers across a latitudinal gradient using multispectral imagery

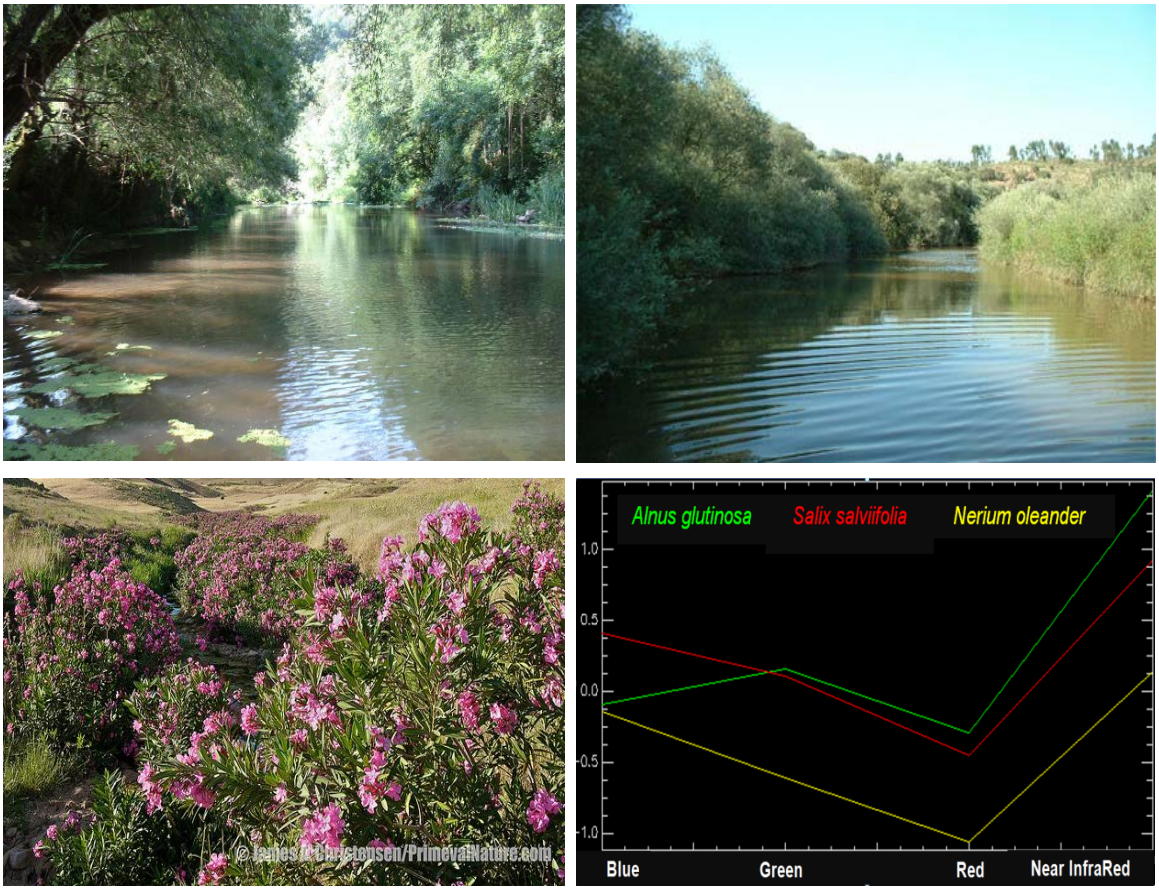

Publicado como: Fernandes MR, Aguiar FC, Ferreira MT, Pereira JMC. 2013. Spectral separability of riparian forests from small and medium-sized rivers across a latitudinal gradient using multispectral imagery. *International Journal of Remote Sensing*, 33 (7) 2375-2401.

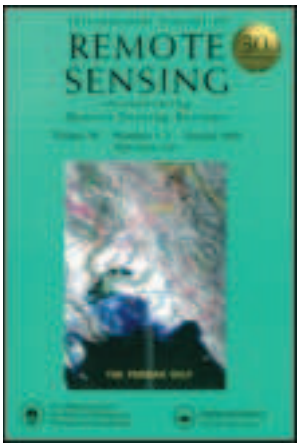

International Journal of Remote Sensing
Publication details, including instructions for authors and subscription information:
http://www.tandfonline.com/loi/tres20

Spectral separability of riparian forests from small and medium-sized rivers across a latitudinal gradient using multispectral imagery

Maria Rosário Fernandes [a] , Francisca Constança Aguiar [a] , Maria Teresa Ferreira [a] & Jose Miguel Cardoso Pereira [a]
[a] Forest Research Centre, Technical University of Lisbon, School of Agriculture, Tapada da Ajuda, 1349-017, Lisbon, Portugal
Version of record first published: 11 Dec 2012.

To cite this article: Maria Rosário Fernandes , Francisca Constança Aguiar , Maria Teresa Ferreira & Jose Miguel Cardoso Pereira (2013): Spectral separability of riparian forests from small and medium-sized rivers across a latitudinal gradient using multispectral imagery, International Journal of Remote Sensing, 33:7, 2375-2401

To link to this article: http://dx.doi.org/10.1080/01431161.2012.744491

International Journal of Remote Sensing
Vol. 33, No. 7, 10 April 2013, 2375–2401

Taylor & Francis
Taylor & Francis Group

Spectral separability of riparian forests from small and medium-sized rivers across a latitudinal gradient using multispectral imagery

Maria Rosário Fernandes*, Francisca Constança Aguiar, Maria Teresa Ferreira, and Jose Miguel Cardoso Pereira

Forest Research Centre, Technical University of Lisbon, School of Agriculture, Tapada da Ajuda, 1349-017 Lisbon, Portugal

(*Received 18 October 2011; accepted 4 August 2012*)

Spectral discrimination between riparian forests is a challenging issue due to the inherent complexity of species composition and the high spatial structural variability of these vegetation types. This study aimed to evaluate spectral separability among riparian forests, in small and medium-sized river catchment areas, in three bioclimatic zones of Portugal (temperate, transitional, and Mediterranean). We also assess the spectral differences using only the dominant riparian woody species in each riparian forest class, namely *Alnus glutinosa*, *Salix salviifolia*, and *Nerium oleander*.

Pixel values were extracted from high-resolution airborne multispectral imagery (red, green, blue, and near-infrared, 50 cm pixels) of 26 riparian forests located in the three bioclimatic zones. Spectral separability was calculated using the transformed divergence (TD) distance. Discriminant analysis (DA) was used to select the bands that contribute most to the spectral separability and for the classification accuracy assessment of the riparian forests. Species composition and percentage of canopy closure were collected for all the riparian forests in a field campaign and subjected to hierarchical clustering in order to validate the spectral separability analyses. Optical traits derived from field data were used to interpret the spectral differences between riparian forest classes.

The greatest spectral separability was observed between the temperate and the Mediterranean riparian forest classes. Global classification accuracy for the DA was 86.3% for riparian forest classes along medium-sized rivers and 70.1% in small-sized ones. The high floristic and spatial structure variability was responsible for the misclassification errors that occurred between the transitional and the other riparian forest classes. The spectral separability using only the dominant species was greater than that obtained using the overall species assemblages of the riparian forests. *Alnus glutinosa* had the highest level of classification accuracy, and this may be related to its peculiar yellowish-green tone. DA also revealed that all spectral bands were needed in order to distinguish the riparian forest classes.

This study provided evidence that the spectral discrimination of riparian forests can be explained on the basis of differences in species composition and cover, and by a convergence of optical traits, at both leaf and canopy levels. Spectral signatures of these riparian forests and related spectral signatures of key species are useful tools for evaluating the floristic deviations of actual riparian forests from their near-natural benchmarks.

*Corresponding author. Email: mrfernandes@isa.utl.pt

ISSN 0143-1161 print/ISSN 1366-5901 online

http://dx.doi.org/10.1080/01431161.2012.744491
http://www.tandfonline.com

1. Introduction

Riparian forests are complex ecosystems located in dynamic transitional zones between aquatic and terrestrial ecosystems, and function as energy and ecological corridors, supporting, receiving, and transporting biota (Malanson 1993). They are primarily shaped by climate and hydrogeomorphology (Hynes 1970) and present an upstream–downstream gradient expressed in varying species composition, diversity, and spatial structure. Site-specific attributes, such as slope, substrate features, size of catchment area, and flow regime, also contribute to differences in species composition and spatial structure (lateral and longitudinal continuity, strata complexity, and riparian width) between riparian forests.

Riparian forests in Western Iberia are green corridors along rivers, clearly distinct from the surrounding ecosystems and usually seen as linear oases embedded in a complex landscape matrix. Previous studies in this region have found that the clear latitudinal climatic and orographic gradient between northern and southern regions correspond to different types of riparian forests (Aguiar et al. 2000). In addition, clear differences in the spatial structure of riparian forests have been detected along the longitudinal river gradient and according to the land use in the river surroundings (Aguiar and Ferreira 2005).

Riparian forest types have been classified via species composition, the abundance of dominant or characteristic species (e.g. Aguiar, Moreira, and Ferreira 2001; Renofalt, Nilsson, and Jansson 2005), or the functional attributes of vegetation (e.g. Heráult and Honnay 2007). However, there is a need to fully understand the biogeographical variation in riparian forests for management and restoration purposes. Field surveys are the usual data source, but they are spatially limited, non-exhaustive, and resource consuming.

Several studies have been focused on the spectral discrimination and supervised or unsupervised image classification of different forest types, such as evergreen needleleaf forest *versus* deciduous broadleaf forest (Shao et al. 1996; Xiao et al. 2002), rain forest types (Thessler et al. 2008), and tropical forest types (Tottrup 2004). However, as far as we know, no analogous studies have been conducted for riparian forests.

Most research using remote sensing concerns the spatial structure of riparian vegetation – for example, assessing corridor width, fragmentation (Congalton et al. 2002), and tree clearing (Schuft et al. 1999; Johansen and Phin 2006), rather than their spectral characteristics. In particular, Hall, Huemmrich, and Goward (1990), Lonard et al. (2000), Nagler, Glenn, and Huete (2001), and Johansen and Phinn (2006) have explored the possibility of remotely mapping intrinsic features of riparian vegetation, such as percentage of foliage cover, leaf area index (LAI), and tree height, in order to help river conservation and management and assess degradation patterns (Fernandes, Aguiar, and Ferreira 2011), whereas Weber and Dunno (2001) studied the distinction between the riparian buffer and the adjacent land use. Nevertheless, when spectral information is explored for riparian vegetation studies, the focus has usually been on target native species (Hamada et al. 2007; Pengra, Johnston, and Loveland 2007; Adam and Onisimo 2009) or alien invasive species (Dipietro et al. 2002; Underwood, Ustin, and DiPietro 2003), which frequently form homogeneous stands. These monotypic stands provide pure spectral signatures (Zomer, Trabucco, and Ustin 2009), which often result in an accurate classification of vegetation types. However, riparian forests are usually composed of a mixture of species and strata, creating a spectrally complex behaviour. Spectral discrimination of vegetation types still remains a thorny issue (Goetz et al. 2003) due to the influence of extraneous factors, such as illumination and observation geometry, atmospheric effects, and variable moisture content (Cochrane 2000). Where biological constraints are concerned, several species may have similar biochemical composition, causing spectral overlapping (Schmidt and Skidmore 2003), and variations in the spectral signature may occur within species (Price 1994).

Recently, Ustin, and Gamon (2010) proposed an ecological remote-sensing approach that incorporates the concept of optical types and basic ecological principles. Optical types are defined as distinguishable types of vegetation detectable by their optical properties from remote measurements – i.e. measurements of the absorption and scattering properties of plant canopies across the electromagnetic spectrum. These types incorporate the structural, physiological, and phenological properties of the vegetation (Gamon 2008), which can be applied to assess the spectral separability of heterogeneous vegetation types, such as riparian forests.

High spatial resolution imagery (<5 m) is essential to the spectral analysis of riparian vegetation, due to the limited width of the riparian zone and the complexity of its spatial structure (Muller 1997; Congalton et al. 2002; Davis et al. 2002; Goetz 2006).

Airborne multispectral images (four bands: blue, green, red, near-infrared (NIR)) can yield higher spatial resolutions (<1 m) and be cost competitive compared to high-resolution satellite images. Furthermore, some studies have demonstrated that broad bands located in the visible and NIR regions are suited for the remote assessment of riparian cover, especially in semi-arid regions (Neale 1997; Belluco et al. 2006). Similar classification performances for vegetation have been obtained with multispectral and hyperspectral data (Belluco et al. 2006), showing that spatial resolution is, in some cases, the greatest constraint on obtaining high classification accuracy. Traditionally, airborne images in the form of aerial photographs were used to visually estimate some spatial structural attributes of riparian vegetation. More recently, the numerical data present in each band have been used as a discriminatory variable in the classification of riparian areas (Marcus et al. 2002; Akasheh, Neale, and Jayanthi, 2008), for vegetation mapping in wetlands (Belluco et al. 2006), and for forest inventory (Foody et al. 2005; Tuominen and Pekkarien 2005).

In this study, we explored the spectral separability of riparian forests in two types of catchment areas (small and medium-sized rivers) in three bioclimatic zones (riparian forest classes). This work is designed to provide supporting information for management and restoration purposes, in order to help identify the conservation status of riparian forests, based on species composition, rather than just the use of spatial structure. This is essential because the studied region is frequently invaded by exotic plant species that alter the functioning and the ecosystem services of riparian forests. In addition, the identification of key species in riparian forests is needed in order to characterize and evaluate the condition of riparian zones.

We consider that riparian vegetation is characterized by fito-associations and consequently by the spatial structure and distribution of diverse ecological plant assemblages (riparian synecological units). Spectral signatures of riparian units are thus a combination of leaf characteristics, canopy structure, and soil background (Schmidt and Skidmore 2003). We therefore hypothesize that despite the inherent spectral complexity of riparian forests and of the riparian habitat, it is possible to find a supra-level of physiological and phenological homogeneity that is capable of allowing for the spectral separability of riparian forest classes. In other words, we assume that reflectance variance is significantly larger among riparian forest classes than within riparian forest classes in both small and medium-sized river areas. We also expect riparian forests along small-sized rivers to be more homogeneous than riparian forests in medium-sized river areas in each bioclimatic zone, thus allowing a better separation of the riparian forests in the smaller catchments. In order to validate the spectral separability, we assessed the level of dissimilarity between each riparian forest class based on its species composition.

Additionally, we identified the most frequent and abundant species in each riparian forest class (hereafter, dominant species) and tested their spectral separability. This approach

allowed us to recognize the spectral signature of key species in each riparian forest type for the purpose of evaluating the conservation status of riparian forests.

Finally, we identified the most important bands that allow riparian forest classes to be spectrally separated and interpreted the differences in the reflectance values using the respective optical traits.

2. Methods

Figure 1 presents a workflow for the methodological procedures, which are detailed in the following subsections.

2.1. Study area and sampling design

This study was conducted along small and medium-sized rivers throughout mainland Portugal in southern Europe. The country presents a large latitudinal variability in geomorphology, climate, land use, and vegetation. The southern regions (south of the River Tagus) are characterized by extensive agricultural land, scattered human settlements, typical Mediterranean shrublands, and cork–oak woodlands. The summers are hot and dry, and the yearly rainfall is usually below 600 mm. The northern regions present a diverse landscape, with small landownership parcels and multiple land uses, mild summers (up to 18°C), and rainier winters (up to 3500 mm of annual precipitation).

In our research, we defined bioclimatic zones using the ombrothermic criterion of Rivas-Martinez (Rivas-Martínez, Sanchez-Mata, and Costa 1999, 2004) and a threshold level of 1200 mm for the mean annual precipitation (P). The Rivas-Martinez classification is based on the four-monthly summer ombrothermic index (Ios4) (Equation (1)), which is obtained through the ratio between the sum of the monthly total precipitation and the sum of the monthly temperature of the four driest months (May–August):

$$\text{Ios4} = (P_{\text{pMay}} + P_{\text{pJune}} + P_{\text{pJuly}} + P_{\text{pAugust}})/(T_{\text{pMay}} + T_{\text{pJune}} + T_{\text{pJuly}} + T_{\text{pAugust}}) \times 10, \quad (1)$$

where P_{p} is the total monthly precipitation (in mm) and T_{p} is the mean monthly temperature (in tenths of degrees Celsius, °C). If the temperature is lower than 0°C, the values are not included in the calculations.

Three bioclimatic zones (Figure 2) were defined according to the following criteria: temperate – $P > 1200$ mm and Ios4 > 2; transitional – $P < 1200$ mm and Ios4 [1, 2]; and Mediterranean – $P < 1200$ mm and Ios4 < 1.

Climatic variables (800 m resolution) were extracted from the WORLDCLIM database (http://www.worldclim.org/). ArcGIS (version 9.1, ESRI, Redlands, CA, USA) was used to store the data and perform the bioclimatic classification.

Thirteen sites along small-sized rivers (catchment from 80 to 300 km^2) and 13 sites along medium-sized rivers (catchment from 300 to 2000 km^2) were positioned in the bioclimatic zones (Figure 2). The sites are 100 m-long river stretches and include the overall riparian forests. They were selected from the Water Institute (www.inag.pt) reference database of sites, because they had no or minimal anthropogenic stress regarding physicochemical conditions, hydromorphological conditions, and riparian integrity.

2.2. Image acquisition and normalization

High-resolution airborne multispectral images (0.5 m spatial resolution) were obtained for each site. The 26 images were acquired during the spring and early summer of 2007 with

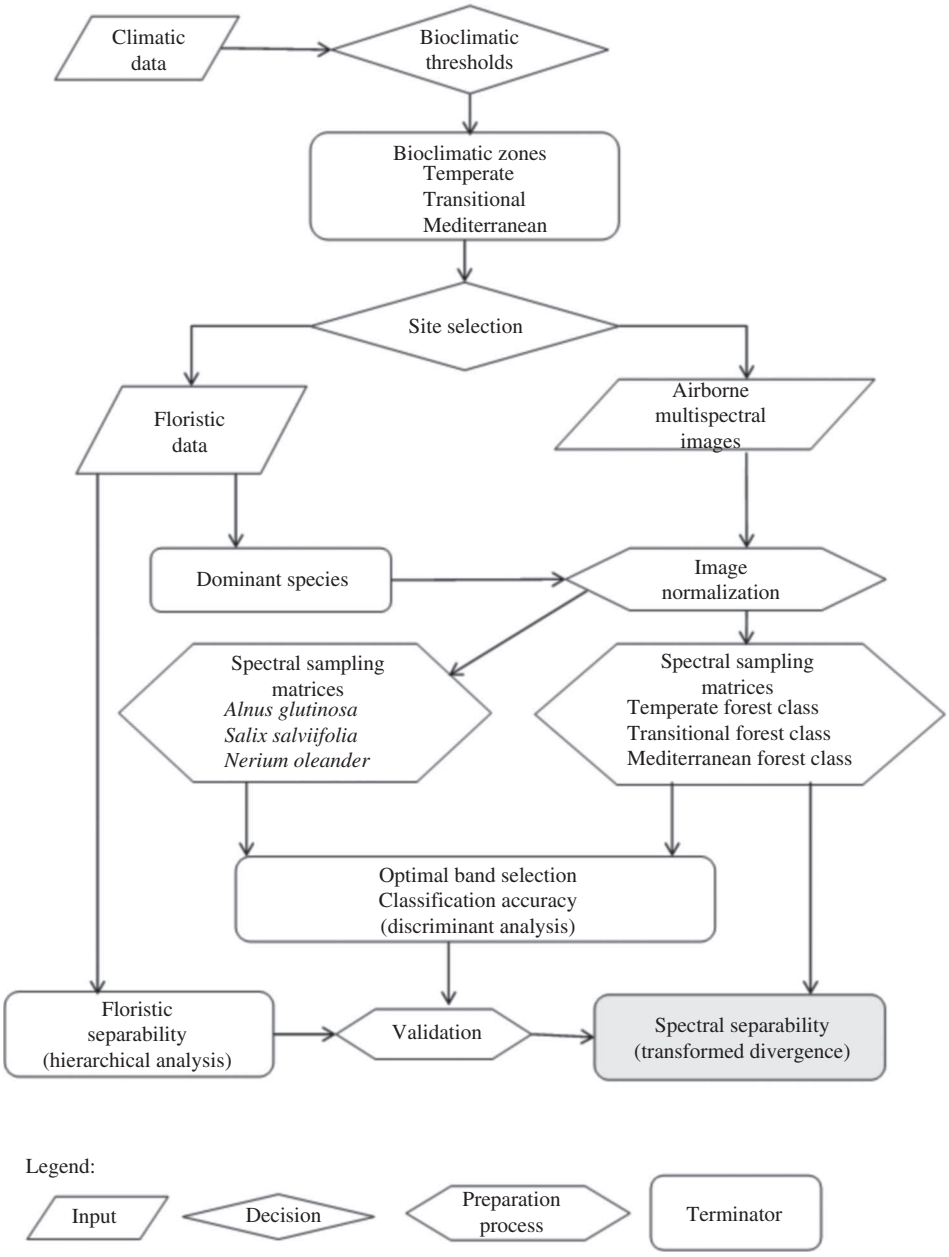

Figure 1. Workflow for the methodological procedures.

an Ultracam D and a DMC-Intergraph camera with interference filters forming spectral bands in the blue (0.390–0.580 mm), green (0.420–650 mm), red (0.590–0.690 mm), and NIR (0.675–0.900 mm) wavelengths of the electromagnetic spectrum. The images had a nominal overlap of 60% along flight lines with an imaging altitude of 5800 m and were subjected to orthorectification using a 5 m resolution raster digital elevation model (DEM). To reduce the effects of bidirectional reflectance and exposure fall off, only the innermost

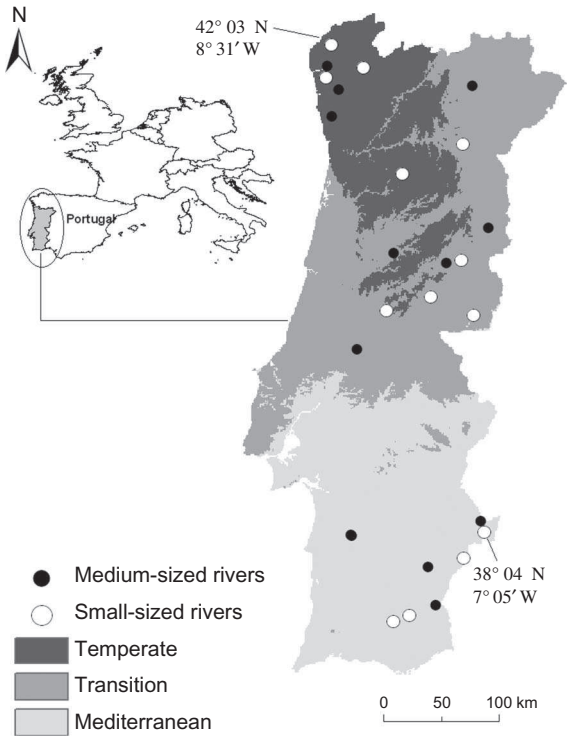

Figure 2. Map of Portugal with the bioclimatic zones and the location of the studied sites in the small- and medium-sized rivers. Top-left map shows the location of Portugal in Europe.

part of the images was retained for the final mosaic. Antivignetting filters were used to reduce the radiometric distortions commonly present in airborne digital images (Neale and Crowther 1994). All the geometric and radiometric calibrations were conducted by Instituto Geográfico Português (http://www.igeo.pt/). Each band was saved as a TIFF file with pixel values varying between 0 and 255 digital numbers (DNs).

Normalization (N) was performed to allow scene-to-scene comparison, smoothing the differences in brightness due to changes in the solar zenith angle. The band intensity data were relative grey levels – i.e. radiometric signals, as used by Quackenbush, Hopkins, and Kinn (2000), and not reflectance values. Without normalization, the variables with large variability would have higher weights in the covariance-weighted distance matrix used to compute class separation (Lillesand and Kiefer 2000; Tuominen and Pekkarinen 2005). The histogram of each image was centred at 0 and the standard deviation at 1, by replacing each original pixel value with the following equation:

$$N_{\lambda ij} = (\mathrm{DN}_{\lambda ij} - \mu_\lambda)/\sigma_\lambda, \tag{2}$$

where $N_{\lambda ij}$ is the normalized value for pixel ij in band λ, $\mathrm{DN}_{\lambda ij}$ is the original DN (0–255) for pixel ij in band λ, μ_λ is the mean value of the image in band λ, and σ_λ is the standard deviation of the image in band λ. Finally, a multiband mosaic of 13 images for each river type was performed in ENVI (version 4.5, ITT Visual Information Solutions, Boulder, CO, USA).

2.3. Spectral sampling

We geographically identified the 26 sites in the airborne multispectral images, and in each site manually digitalized nearly 90 polygons composed of 5–8 pixels, in order to capture the overall spectral variability of the riparian forests (Lillesand and Kiefer 2000). These digitalized polygons represent the spectral samples or training samples of each riparian forest class. We thereby obtained the spectral matrix for each riparian forest class, which is composed of the pixel values for the four bands. The number of training samples followed the criteria established by Schowengerdt (1983) and Jensen (1996), where the minimum number of collected pixels by class (in our case, three riparian forest classes) is the number of bands multiplied by 100 in order to improve the estimation of the mean vector and the covariance matrices. The mean vector describes the average or expected position of the pixels of training samples in the multispectral vector space (in our case, $n = 4$ dimensions, four bands) for each riparian forest class (Richards and Jia 2006). We also prefer to use a large number of small-sized training samples instead of few large polygons in order to reduce spatial autocorrelation in the data (Congalton 1988). The spectral matrix samplings were used to obtain the spectral signatures of the vegetation of the riparian forests. The spectral signature of vegetation is characterized by a transition of low reflectance values in the visible region (400–700 nm) to high reflectance values in the NIR region (700–1300 nm) – the so-called red edge.

Although in our studied sites the riparian forests were visually clearly distinct from the adjoining vegetation, the training samples were collected inside the riparian canopies, avoiding boundaries with other cover types (Chuvieco 1996) and selecting only bright green pixels, avoiding shadowing pixels and reducing soil background effects.

To test whether the most frequent and abundant species in each riparian forest class (hereafter, dominant species) make a strong contribution to the spectral separability of riparian forests, training samples of dominant species were collected. These species were identified in the images using field data and knowledge of typical morphological and phenological features.

2.4. Spectral separability analysis and band selection

The spectral separability between each pair of riparian forest classes (temperate vs Mediterranean, temperate vs transition, and Mediterranean vs transition) was calculated using the transformed divergence (TD) distance to the spectral samplings collected from the airborne multispectral images (extracted pixel values for the blue, green, red, and NIR bands) for both medium-sized and small-sized rivers. The TD distance represents a measure of the average distance between two class density functions (Swain and Davis 1978). Compared to other separability indices, such as the Jeffries-Matusita, the TD distance is computationally more efficient (Richards and Jia 2006).

Spectral separability was calculated as follows (Richards and Jia 2006):

$$d_{ij} = {}^1\!/_2 \mathrm{tr}\left\{(\mathbf{C}_i - \mathbf{C}_j)\left(\mathbf{C}_j^{-1} - \mathbf{C}_i^{-1}\right)\right\} + {}^1\!/_2 \mathrm{tr}\left\{\left(\mathbf{C}_i^{-1} + \mathbf{C}_j^{-1}\right)(\mu_i - \mu_j)(\mu_i - \mu_j)^t\right\} \quad (3)$$

$$\mathrm{TD}_{ij} = 2000\,(1 - \exp(-dij/8))\,,$$

where i and j are the two classes under comparison, $\mathbf{C}_i$ is the covariance matrix of signature i, $\mu_\mathbf{i}$ is the mean vector of signature i, and tr is the trace of the subject matrix.

The TD varies between 0 and 2. A TD value of 2.0 indicates perfect separability, whereas a value of 0 indicates complete overlap between the class signatures. Values greater than 1.7 are considered to represent good separability.

We also calculated the TD distance of all pair combinations of sites belonging to each riparian forest class and separately for the small and medium-sized rivers – i.e. we calculated the intraspectral separability of the riparian forest classes.

Other techniques, such as Classification and Regression Trees or Random Forests, could be used to identify the optimal band or combination of bands for the spectral separability of the riparian forests. However, discriminant analysis (DA) has been used for similar purposes in recent studies (Thenkabail et al. 2004; Thessler et al. 2008; Pu and Liu 2011) and is suited for measuring the likelihood of success of classifications when groups are known *a priori*. In this study, we used a stepwise forward DA (F to enter = 0.15, F to remove = 0.10, tolerance = 0.001), which begins with no variables in the model. At each step, one enters the variable that contributes most to the discriminatory power of the model as measured by Wilks' Lambda – the likelihood ratio criterion. When none of the unselected variables meets the entry criterion, the forward selection process stops. Partial Wilks' Lambda and 1-Tolerance were also calculated. Wilks' Lambda is used to test the null hypothesis that the groups have identical means. The smaller the values, the greater the doubt that is cast upon that null hypothesis. The 1-Tolerance computes the respective variable redundancy.

We then performed the DA using only the dominant riparian species of each riparian forest class. Independent images were reserved for validation of the DA corresponding to about 25% of the overall spectral samples. All analyses were performed with STATISTICA version 6.0 (StatSoft, Inc., Tulsa, OK, USA) and Matlab 6.5 (MathWorks, Natick, MA, USA).

2.5. Field data and validation

A field campaign was performed in the spring and early summer of 2004–2005 in order to collect floristic data (species composition and species cover). Sampling sites were 100 m-long river stretches and included both river margins. Woody species were surveyed and identified at species taxonomic level for each sampling site (species composition). Additionally, the riparian woody species abundance in the sampled area was visually estimated by the percentage of canopy closure (species cover). The GPS location of each site was recorded to ensure that field data were coincident with the spectral sampling.

Hierarchical clustering of field data (matrix of sites vs riparian woody species percentage of canopy closure) was performed separately for the riparian forests along the small and medium-sized rivers. The classification makes it possible to aggregate similar sites based on the species composition. Unlike the DA, the number of groups is not established *a priori* and must be determined from the data. The algorithm used in hierarchical clustering analysis starts with a matrix of pairwise dissimilarities (distance). Using a recursive process, it aggregates the sites until they are all clustered. We used 1-Pearson's R distance and a single linkage rule (Podani 1994) to determine how the dissimilarities between clusters were recalculated (Quinn and Keough 2002). Occasional species (cover $<0.5\%$) were discarded from the analysis. We applied an arcsine square-root transformation of the data in order to follow the normal distribution (Quinn and Keough 2002).

3. Results

3.1. Spectral separability of the riparian forests

The spectral sampling was performed for the riparian forest classes designated as Mediterranean, transitional, and temperate riparian forest classes. Table 1 summarizes the global spectral separability among these classes. All spectral differences between riparian forest classes were higher for the medium-sized rivers in comparison with the small-sized rivers. The highest spectral separability was observed between the temperate and the Mediterranean riparian forest classes for medium-sized rivers (TD = 1.9), followed by the small-sized rivers (TD = 1.6). The transitional riparian forest class did not present a consistent spectral separation from the other riparian forest classes except for the Mediterranean riparian forest class in the case of the medium-sized rivers.

The DA confusion matrix (Table 2) for the spectral sampling showed an overall classification accuracy of 86.3% for the riparian forest classes from medium-sized rivers and 70.1% from the small-sized ones. Misclassification occurred mainly between the transitional and the other two riparian forest classes. Transitional pixels were mostly misclassified as temperate, especially in the case of small-sized rivers. The validation procedure performed with a set of independent pixels resulted in a decrease of around 10% in the overall accuracy for both small and medium-sized rivers. All bands were selected by the stepwise discriminant models as predictor variables (Table 3), although the red band was primarily selected for both small and medium-sized rivers. The NIR band showed a small discriminatory ability, particularly for the small-sized rivers, albeit presenting a low level of redundancy, as revealed by the 1-Tolerance, when compared with visible bands (blue, green, and red) of the electromagnetic spectrum. The lowest values of reflectance were found in the Mediterranean vegetation of the medium-sized rivers (Figure 3).

The highest spectral variability (Figure 4) was found in the transitional riparian forest class for both small and medium-sized rivers, and in the temperate riparian forest class for small-sized rivers, in contrast to the temperate and Mediterranean riparian forest classes for the medium-sized rivers.

Table 1. Values of the TD distance for the riparian forest classes in the small and medium-sized rivers for the temperate (Temp), transitional (Trans), and Mediterranean (Med) regions.

	Temp *versus* Med	Temp *versus* Trans	Med *versus* Trans
Small-sized rivers	1.6	1.0	0.6
Medium-sized rivers	1.9	1.2	1.5

Table 2. Classification matrix (rows = number of observed pixels; columns = number of predicted pixels) of the DA for the riparian forest classes in the small and medium-sized rivers for the temperate (Temp), transitional (Trans), and Mediterranean (Med) regions.

	Small-sized rivers				Medium-sized rivers			
	Temp	Trans	Med	Total	Temp	Trans	Med	Total
Temp	1569	162	14	1745	1281	80	8	1369
Trans	663	1585	386	2634	437	1638	60	2135
Med	159	575	1431	2165	12	127	1645	1784
Predicted classifications								
(percentage of correct cases)	89.9	66.1	60.2	70.1	93.6	92.2	76.7	86.3
(percentage after validation)	68.0	52.2	58.2	60.5	71.9	74.9	85.3	77.5

Table 3. Selected bands (by decreasing order of selection), Partial Wilk's Lambda, F to remove, and 1-Tolerance of the discriminant model in the small and medium-sized rivers ($p < 0.001$).

Variables in the model	Partial Wilk's Lambda	F to remove	1-Tolerance
Small-sized rivers			
Red	0.6	1391.1	0.8
Blue	0.9	475.7	0.8
Green	0.9	447.5	0.9
NIR	0.9	387.5	0.4
Medium-sized rivers			
Red	0.4	5254.7	0.8
Green	0.8	711.8	0.9
NIR	0.8	830.8	0.4
Blue	0.9	229.3	0.8

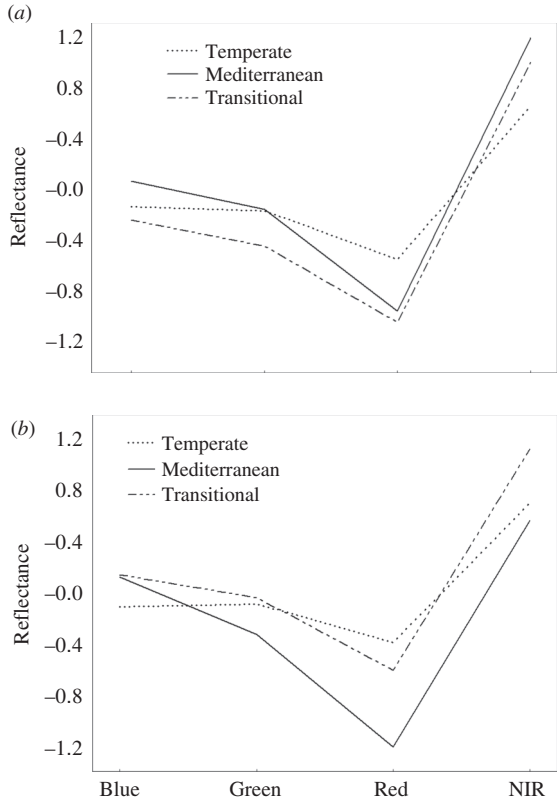

Figure 3. Spectral signatures (average values) of the temperate, transitional, and Mediterranean riparian forest classes in the (*a*) small-sized rivers and (*b*) medium-sized rivers.

3.2. Spectral separability of the dominant riparian species

Figure 5 illustrates the results of the spectral separability (discriminant scores) of the dominant species of each riparian forest class, namely *Alnus glutinosa* (for the temperate class), *Salix salviifolia* (for the transitional class), and *Nerium oleander* (for the Mediterranean

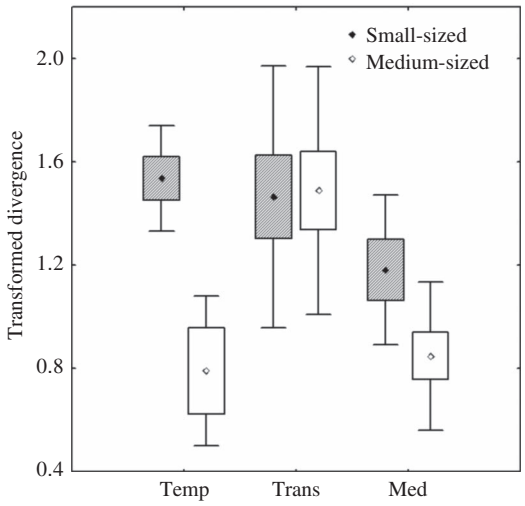

Figure 4. Intraspectral separability of riparian forest classes in the small- and medium-sized rivers (average ± standard deviation) for the temperate (Temp), transitional (Trans), and Mediterranean (Med) regions.

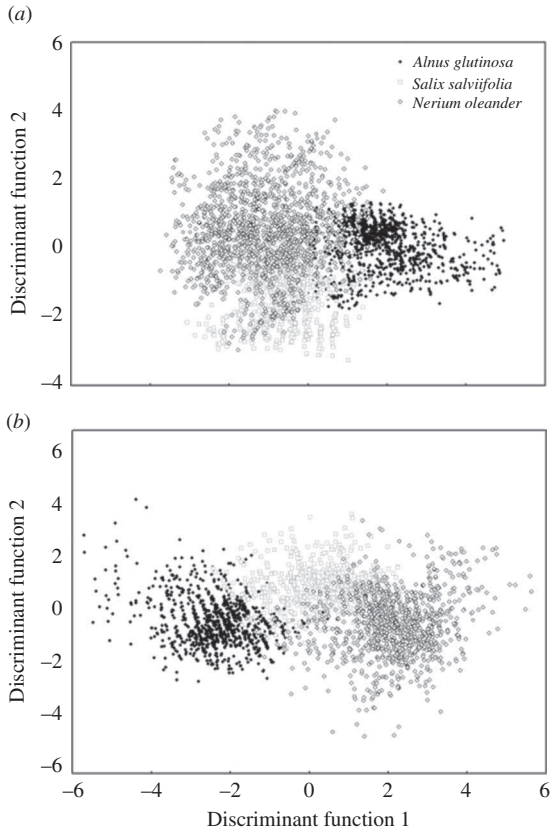

Figure 5. Scatter plot of the discriminant function canonical scores for *Alnus glutinosa*, *Salix salviifolia*, and *Nerium oleander* for the (*a*) small-sized rivers and (*b*) medium-sized rivers.

class). DA results (Table A1) showed that spectral signatures of the dominant riparian species are separable for both river types and that those of medium-sized rivers were more accurately classified than those of small-sized rivers. The global level of classification accuracy was 81.9% for the small-sized rivers and 92.2% for medium-sized rivers, and 71.2% and 75.4%, respectively, after validation. Misclassifications mainly occurred between the *S. salviifolia* and *N. oleander* pixels, mainly in the case of the small-sized rivers. All bands were selected for the discriminant models, but the NIR band was primarily selected over the visible bands for both small and medium-sized rivers, contrary to the results found for the spectral separability using all the species assemblages of the riparian forest classes.

Figure 6 shows a true-colour composition image (blue, green, and red bands) in which the tone differences make it possible to visually distinguish two dominant species. The true-colour composition images show that *S. salviifolia* has a more greyish tone than *A. glutinosa*, whereas *N. oleander* presented a dark green canopy, and in some images, pink pixels, due to the colour of the flowers. *Alnus glutinosa* could easily be distinguished from the surrounding species in the riparian zone, both in field observations and in true-colour composition images, due to the yellowish-green tone exhibited by the canopy at the outset of the flowering period.

3.3. Floristic analysis and validation

Eighteen trees, shrubs, and woody climbers from 13 families and 15 genera were found at the field sites.

Figure 7 shows the percentage of canopy closure of the five most abundant species in the study area in each bioclimatic zone, and Table A2 shows the species list, along with the relative frequency of species occurrence (number of sites where a species occurs out of the total number of sites). Clear differences in the species composition and spatial structure of the surveyed sites were observed between the three riparian forest classes. Temperate riparian forests were mainly composed of deciduous species such as alder (*A. glutinosa* (L.) Gaertner), ash (*Fraxinus angustifolia* Vahl.), and willow (*Salix* L. spp.) in contrast to the evergreen shrub vegetation found in the Mediterranean riparian forests. However, alder dominated several temperate riparian forest sites along medium-sized rivers. Mediterranean riparian forests were mainly composed of oleander (*N. oleander* L.), Ibero-African spurge

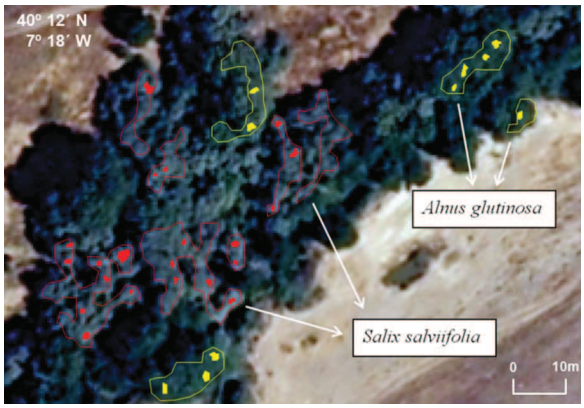

Figure 6. Delimitation of canopies and training samples of *Salix salviifolia* (red patches) and *Alnus glutinosa* (yellow patches) in the transitional region (small-sized river from the Tagus Basin).

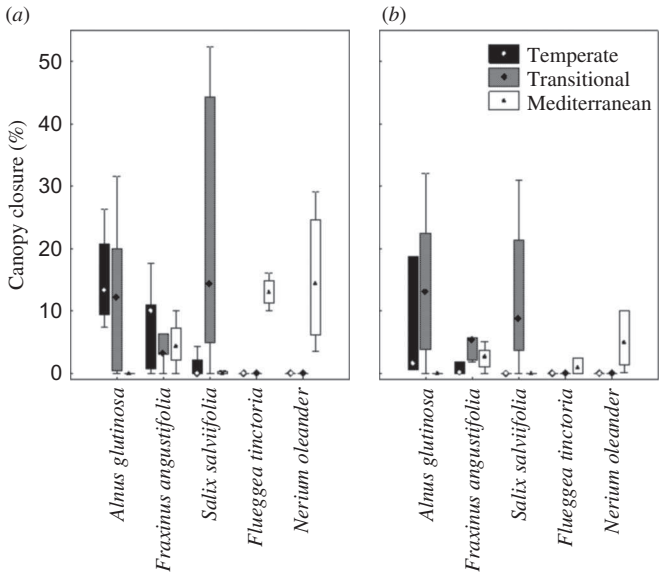

Figure 7. Percentage of canopy closure (box: median; percentile 25; whisker: minimum, maximum) of the dominant species for the riparian forest classes in the (*a*) small-sized rivers and (*b*) medium-sized rivers.

(*Flueggea tinctoria* (L.) G.L. Webster), and African tamarisk (*Tamarix africana* Poiret), which were recorded at 92%, 69%, and 38% of the sites, respectively (Table A2). The transitional riparian forest class had a high cover of *S. salviifolia* (Figure 7) and displayed the highest floristic diversity of all the riparian forest classes (Table A2). Where the spatial structure was concerned, in the temperate riparian forest class, most of the sampling sites usually had continuous stands and presented various vegetation strata, whereas transitional riparian forests were also continuous but with a single stratum. The Mediterranean riparian forests were mainly composed of sparsely distributed shrubby species.

Figure 8 shows dendrograms of the hierarchical clustering of the floristic data for the riparian forest along the small and medium-sized rivers. Two clusters were obtained for both river types at the 0.7 cutting level of 1-Pearson's *R* distance. For small-sized rivers, one group included all Mediterranean riparian forests and one transitional riparian forest, and the other group was composed of the remaining transitional and temperate riparian forests. In the case of the medium-sized rivers, the classification also separates the Mediterranean riparian forests from the transitional and temperate riparian forests.

4. Discussion

4.1. Spectral traits of the riparian forests

Spectral vegetation patterns result from the combination of leaf-level and canopy-level spectra. The main source of spectral variability at the leaf level is not only the proportion of photosynthetic pigments, but also water, leaf, N, and non-pigment biochemical constituents (e.g. proteins, lignin, and cellulose) combined with the leaf morphological features, such as cell wall thickness, air spaces, and cuticular wax (Cochrane 2000; Schmidt and Skidmore 2003). The spectral signature of vegetation is characterized by a transition from low reflectance values in the visible region (400–700 nm) to high reflectance values

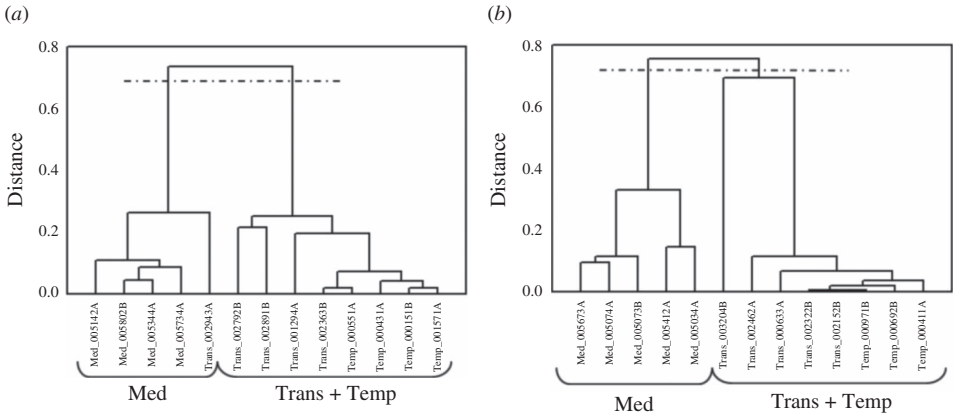

Figure 8. Groups obtained from floristic data for the (*a*) small-sized and (*b*) medium-sized rivers using arcsine square-root transformed cover, 1-Pearson's *R* distance, and single linkage rule. Codes of the georeferenced sampling sites are given in the *x*-axis.

in the NIR region (700–1300 nm) – the so-called red edge. The intense chlorophyll absorption, which is mainly explained by the concentration of chlorophyll-*a,* chlorophyll-*b*, and carotenoids, rules the spectral behaviour in the visible region, while the scattering of the radiation, which is largely related to the ratio of mesophyll cell surface to intercellular air spaces, drives the spectral patterns in the NIR region. The canopy-level spectra result from multiple relationships among vegetation traits, which influence the reflectance values, such as the strata complexity, crown volume, number of gaps, and foliage density.

In this study, we hypothesized that diverse riparian forest classes distributed along a climatic gradient present phenological, physiological, and ecological traits that are remotely detachable and characteristic of each riparian forest class. While this was clearly observed for the temperate and the Mediterranean riparian forest classes, either in their spectral or in their floristic patterns, the transitional riparian forest class could not be discriminated from others. The differences in species composition, diversity, and cover between and within riparian forest classes help explain these results. Table 4 combines information from field observations and bibliography relative to leaf and canopy traits of the riparian forest classes and their implications for spectral behaviour of the vegetation. The general leaf-level and canopy-level traits determine the spectral patterns of the vegetation and consequently the level of distinctiveness between riparian forest classes. Temperate and Mediterranean riparian forest classes have distinct traits that optimize the achievement and efficient use of water, light, and nutrients. This is the case of the leaf persistence (deciduous vs evergreen), the foliage density, and morphological leaf traits. On the other hand, diverse strategies within a riparian forest class converge towards a similar spectral behaviour. For example, the diverse strategies for adapting to water stress adopted by the species of the Mediterranean riparian forest class, such as the small leaf angles, low foliage cover, and minor photosynthetic activity (Valiente-Banuet et al. 2010), have a convergent effect on how these plants absorb, scatter, and reflect light and lead to smaller reflectance values when compared with other riparian forest classes (Table 4). Plants that are adapted to thorny environments tend to have limited rates of stem elongation, small crown diameters, and lateral branching and are more densely clumped along the stem (Rautiainen et al. 2008; Olinger 2011). These traits were observed in the Mediterranean shrubs of the study area and were especially evident in the *F. tinctoria*.

Table 4. Leaf and canopy traits of the riparian forest classes and implications for spectral behaviour of the vegetation based on field observations and bibliographic references.

	Riparian forest traits			Spectral traits	
Traits	Temperate	Transitional	Mediterranean	Implications for spectral behaviour	References
Leaf					
Anatomy	Mesomorphic, medium thickened	Mainly mesomorphic	Scleromorphic, firm, and stiff leaves with thickened epidermis and cuticular wax coatings	Increasing reflectance values in the NIR region with thicker cuticules	Slaton, Hunt, and Smith (2001), Kühn, Durka, and Klotz (2004), and Valladares and Sánchez-Gómez (2006)
Water content	High	Intermediate	Low	Increasing reflectance in the visible and in NIR regions towards low water contents	Ollinger (2011)
Physiognomy	Mixture of bifacial and unifacial	Mixture of bifacial and unifacial	Unifacial	Higher NIR reflectance in the adaxial leaf surface compared with the abaxial leaf	Ollinger (2011)
Orientation	Mainly flat	Mainly flat	More inclined	Higher overall reflectance, but especially in NIR region with the flattening of the leaves	Johnson et al. (2005), Valiente-Banuet et al. (2010), and Ollinger (2011)
Colour	Green	Greyish-Green	Dark green	Darkening effect in the visible and NIR regions of the Mediterranean vegetation Brightness values lower for Mediterranean than for temperate vegetation	Matheson and Ringrose (1994)

(*Continued*)

Table 4. (*Continued*).

	Riparian forest traits			Spectral traits	
Traits	Temperate	Transitional	Mediterranean	Implications for spectral behaviour	References
Photochemical pigments	High chlorophyll content	High chlorophyll content	Low chlorophyll content	Positive correlation between the red edge and the chlorophyll contents; red shift for high chlorophyll content and blue shift for low contents	Chen and Chen (2008)
Leaf persistence	Deciduous	Mainly deciduous	Evergreen	Seasonal variability of reflectance properties mainly in deciduous vegetation	
Ecological					
Tolerance to water stress	Low	Low	High	Blue shift of the red edge	Anderson and Perry (1996), Kenro, Yoshiko, and Nobuhito (2000), Okin et al. (2001), and Calvão and Palmeirim (2004)
				Low reflectance values in the green and NIR regions for Mediterranean vegetation	
				Low remote detectability for drought-tolerant species with adjacent land uses	

Canopy					
Clumping level	Low clumped canopies	Variable	High clumped canopies	Differences in light scattering, deeper light penetration, and reduction in light interception with increasing clumping level Reduced NIR reflectance in high clumped canopies	Walcroft et al. (2005)
Crown diameter	High	Variable	Low	Decreasing reflectance across the infrared region towards low crown diameters	Rautiainen et al. (2008)
Foliage density	High LAI	High LAI	Low LAI	Increasing reflectance for increasing LAI at NIR region	Nagler et al. (2001), Osborne and Woodward (2001), Valladares and Sánchez-Gómez (2006), and Ollinger (2011)
				LAI and normalized difference vegetation index (NDVI) are usually positively related, but to a lesser extent for Mediterranean vegetation	

(*Continued*)

Table 4. (*Continued*).

	Riparian forest traits			Spectral traits	
Traits	Temperate	Transitional	Mediterranean	Implications for spectral behaviour	References
Crown gaps	Low	Medium	High	Multiple scattering with increasing number of gaps, high photoabsorption probability, and lower reflectance (recollision theory)	Smolander and Stenberg (2005)
Strata complexity	Complex; trees and shrubs	Simple; mainly trees	Simple; mainly shrubs	Reflectance decreases with increasing canopy complexity due to shadowing traps	Alvarez-Añorve et al. (2008)

The leaf traits of this species are associated with low reflectance values, especially in the NIR region. One of the strategies Mediterranean plants adopt in order to handle water scarcity and high radiation is a reduction in transpiration rates (Valiente-Banuet et al. 2010), which are associated with a low reflectance that can be attained by means of small leaf insertion angles. The leaf angle plays an important role in resource optimization due to its effects on light interception, leaf temperature, nutrient efficiency, and also transpiration rates. Leaf angle is broadly included in canopy radiative transfer models and presents lower reflectance, as leaf orientation shifts from horizontal (high angles of leaf insertion) to vertical (small angles of leaf insertion). This reflectance pattern (small reflectance values) was observed in the spectral signature of the Mediterranean riparian forest class and reflects an adaptation to drought environments. In addition, at the canopy level, some traits such as strata complexity can have an effect that is the opposite to the overall spectral behaviour. This is the case of the temperate riparian forest class (where we observed a larger number of strata compared to the transitional class), which thus had lower than expected reflectance values.

Taking the dominant species of each riparian forest class instead of the overall floristic variability into account led to an increase in the accuracy of the DA classification (Table A1). In particular, the high level of classification accuracy for *A. glutinosa* may be related to the higher spectral reflectance observed in the spectral signature of this species (not shown), in the case of both small and medium-sized rivers, when compared with the other two dominant riparian species. This characteristic can be connected with some phenological aspects, such as the peculiar yellowish-green tone of this species, which clearly differs from the surrounding riparian species in the early growing period, both in field and in true-colour composite images. This can be a powerful result for the discrimination and mapping of more monotypic forests composed of this species.

4.2. Spectral separability of riparian forest along small-sized versus medium-sized rivers

The spectral separability found in the riparian forests along medium-sized rivers was higher than that in the riparian forests along small-sized rivers. In the case of the medium-sized rivers, the temperate riparian forest class was dominated by alder, whereas along the small-sized rivers plant communities were a mixture that included alder, willow, and ash. Since the images were captured in the early vegetative period, alders presented a brilliant yellowish-green colour, whereas along the small-sized rivers this pattern was masked by coexistence with other riparian species. A similar pattern was observed for the medium-sized rivers of the Mediterranean riparian forest class, where riparian forests showed a greater dominance by oleanders than in the case of the small-sized rivers.

Mediterranean and transitional riparian forest classes could not be consistently discriminated for the small-sized rivers (TD = 0.5). The low spectral separability could be related to the presence of *F. angustifolia* in both riparian forest classes and to the high cover of *S. salviifolia* in the transitional class. The *S. salviifolia* displayed a grey colour which when combined with species with a dark tone, such as *Salix atrocinerea* (see Table A2), results in low reflectance, similar to the spectral results of the Mediterranean riparian forest class. The spectral separability for these classes is greater in medium-sized rivers. Although the species composition is similar to that of small-sized rivers, the species cover clearly differs. The Mediterranean riparian forest class of the medium-sized river areas has a lower species cover than the transitional riparian forest class. In addition, we observed a high cover of

understory hygrophilous vegetation, which displays a spectral behaviour similar to shadowing because it reduces the reflectance values of the overall spectral sampling (Karnieli et al. 1996; Otterman 1996).

4.3. Spectral separability in the visible versus the NIR regions

Whereas the spectral variability in the visible region is largely dependent on the leaf level, due to the two dominant light-harvesting components (pigments and water), the spectral variability in the NIR region is also dependent on the canopy-level spectra (Ollinger 2011).

In this study, only the combination of all bands provided a good separability among the riparian vegetation classes in agreement with Schmidt and Skidmore (2003) in a coastal wetland, although the bands in the visible region (especially the red band) had a higher discriminant ability compared with the NIR. The Mediterranean vegetation did not display a clear red edge (see Table 4) characteristic for most vegetation types. The visible region is also sensitive to changes in leaf-level traits that occur in short periods of time (Ollinger 2011), such as the yellowish-green tone of alders during the few weeks of the early growing period. In contrast, the NIR region is also dependent on changes in canopy architecture. However, when the spectral performance of the dominant riparian species was explored, the NIR region was primarily selected in the discriminant model. This agrees with Hurcom, Harrison, and Taberner (1996), who recorded differences in the spectral performance of species typical of semi-arid regions in the NIR region. In Hurcom's study, the spectral responses were very predictable in the visible region, but the reflectance varied considerably in the NIR region, which was attributed to specific species traits. In this study, the atypical behaviour of the NIR reflectance in the Mediterranean region (small reflectance in the NIR region) was not so marked when we used the *N. oleander* instead of the overall Mediterranean riparian forest class. When the *N. oleander* species is compared, for instance with *F. tinctoria*, it has rather different traits – the species has large lanceolate leaves and fruits and low clumped canopies. These findings enhance the potential development of semi-automatic geographical information system (GIS)/remote-sensing tools for riparian management.

5. Conclusions and implications for riparian forest management

Our study provides evidence that riparian forests subjected to distinct environmental constraints are spectrally separable. This occurs when morphological, phenological, and spatial structural traits of the component species converge to create a high level of intraclass spectral evenness. In particular, we observed marked spectral patterns, along with a species composition that is characteristic of Mediterranean riparian vegetation. The riparian forest class in the middle of the climatic gradient presents a high floristic variability, which translates into a very heterogeneous spectral behaviour, creating misclassification with the other riparian forest classes. Spectral vegetation patterns are the result of complex interrelations among multiple traits, with effects right across all wavelengths, but particularly variable in the NIR region.

The linkage between species composition from field observations and the spectral information from airborne imaging can provide a low-cost basis on which to differentiate and map riparian forests in order to prioritize areas for restoration. Remote identification of degraded riparian areas is usually performed by detecting fragmentation patterns (i.e. canopy gaps) and/or narrow riparian forests. However, degraded riparian zones are often composed of large and continuous exotic stands – the giant reed (*Arundo donax*), for instance. This study made it possible to identify spectral signatures of three types of

near-natural riparian forests that can be used as preliminary tests for riparian degradation patterns related to species composition when applied to other spectral samplings. For instance, detection of high spectral reflectance patterns in Mediterranean zone riparian vegetation could be an indication of invasions by exotic species, since the spectral signature showed lower values of reflectance in the absence of invaders in our study.

We concluded that riparian forest classes along medium-sized rivers were more spectrally separable compared with those of small-sized river areas, due to differences in species diversity, and to cover that creates more homogeneous stands. Spectral vegetation patterns are a consequence of complex interrelations among multiple traits, with effects that run right across all wavelengths, but are highly variable in the NIR region. As a consequence, all the bands of the images are needed in order to distinguish the various riparian forest classes. For similar studies in other regions, the catchment area should be taken into consideration, given this study's dissimilar results for the different river types. The small-sized rivers displayed a large variability in our study area, either in species composition or in spatial structure, and this reduces the ability to spectrally discriminate riparian forests.

Detecting key species in riparian habitats can provide an indication as to the riparian stage of succession and the conditions under which plant communities succeed one another. The spectral signatures of species identified in this study can be used in the creation of spectral libraries, and their absence in the case of the respective riparian forest type reflects a poor ecological condition. Moreover, the high spectral separability of *A. glutinosa*, when compared with the other two key species (*N. oleander* and *S. salviifolia*), is a very good result for the remote discrimination approach.

Our study also showed that the optimal season for spectral vegetation discrimination depends on the key species or forest type. The peculiar and very distinct yellowish-green tone of *A. glutinosa* at the beginning of the vegetative period is coincident with the optimal season for using remote-sensing techniques to spectrally separate wetland vegetation types (Anderson and Perry 1996). However, other species present useful optical characteristics in other seasons. One example is the pink colour of *N. oleander* flowers in the peak of summer, as we have observed in this study.

Further research on the discrimination of riparian forests can be done by adding spatial, textural, or contextual information to the spectral information, thereby improving mapping accuracy for riparian forests.

Acknowledgements

This study received backing from EU funds (ERDF) from the project RICOVER River Recovery in SW Europe (Interreg IVB-SOE1/P2/P248) and from the Forest Research Centre (CEF) through FEDER/POCI 2010. Maria R. Fernandes and Francisca C. Aguiar were supported by doctoral and postdoctoral scholarships from the Foundation for Science and Technology, Portugal, SFRH/BD/44707/2008 and SFRH/BPD/29333/2006, respectively. We acknowledge the assistance of Instituto Geográfico Português (IGP), which provided the airborne multispectral images through the FIGEE programme, and of the National Water Institute (INAG IP), which made the floristic data available to us.

References

Adam, E., and M. Onisimo. 2009. "Spectral Discrimination of Papyrus Vegetation (*Cyperus Papyrus* L.) in Swamp Wetlands Using Field Spectrometry." *ISPRS Journal of Photogrammetry and Remote Sensing* 64: 612–20.

Aguiar, F. C., and M. T. Ferreira. 2005. "Human-Disturbed Landscapes: Effects on Composition and Integrity of Riparian Woody Vegetation in Tagus River Basin, Portugal." *Environmental Conservation* 32: 30–41.

Aguiar, F. C., M. T. Ferreira, I. Moreira, and A. Albuquerque. 2000. "Riparian Types in a Mediterranean Basin." *Aspects of Applied Biology* 58: 221–32.

Aguiar, F. C., I. Moreira, and M. T. Ferreira. 2001. "Exotic and Native Vegetation Establishment Following Channelization of a Western Iberian River." *Regulated Rivers: Research and Management* 17: 509–26.

Akasheh, O. Z., C. M. U. Neale, and H. Jayanthi. 2008. "Detailed Mapping of Riparian Vegetation in the Middle Rio Grande River Using High Resolution Multi-Spectral Airborne Remote Sensing." *Journal of Arid Environments* 72: 1734–44.

Alvarez-Añorve, M., M. Quesada, and E. de la Barrer. 2008. "Remote Sensing and Plant Functional Groups. Physiology, Ecology, and Spectroscopy in Tropical Systems." In *Hyperspectral Remote Sensing of Tropical and Sub-Tropical Forests*, edited by M. Kalacska and Sánchez Azofeifa, 27–45. Montreal: CRC Press.

Anderson, J. E., and J. E. Perry. 1996. "Characterization of Wetland Plant Stress Using Leaf Spectral Reflectance: Implications for Wetland Remote Sensing." *Wetlands* 16: 477–87.

Belluco, E., M. Camuffo, S. Ferrari, L. Modenese, S. Silvestri, A. Marani, and M. Marani. 2006. "Mapping Salt-Marsh Vegetation by Multispectral and Hyperspectral Remote Sensing." *Remote Sensing of Environment* 105: 54–67.

Calvão, T., and J. M. Palmeirim. 2004. "Mapping Mediterranean Scrub with Satellite Imagery: Biomass Estimation and Spectral Behavior." *International Journal of Remote Sensing* 25: 1–14.

Chen, J., and C. Chen. 2008. "Correlation Analysis Between Indices of Tree Leaf Spectral Reflectance and Chlorophyll Content." In *Proceedings of Commission VII. ISPRS Congress Beijing*, edited by C. Jun, J. Jie, and J. van Genderen, Beijing, China, July 3–11, 2008, 231 pp.

Chuvieco, E. 1996. *Fundamentos De Teledetección Espacial*. 3ª Edición revisada, 469–84. Madrid: Rialp.

Cochrane, M. A. 2000. "Using Vegetation Reflectance Variability for Species Level Classification of Hyperspectral Data." *International Journal Remote Sensing* 21: 2075–87.

Congalton, R. G. 1988. "Using Spatial Autocorrelation Analysis to Explore the Error in Maps Generated From Remotely Sensed Data." *Photogrammetric Engineering and Remote Sensing* 54: 587–92.

Congalton, R. G., K. Birch, R. Jones, and J. Schriever. 2002. "Evaluating Remotely Sensed Techniques for Mapping Riparian Vegetation." *Computers and Electronics in Agriculture* 37: 113–26.

Davis, P. A., M. I. Staid, J. B. Plescia, and J. R. Johnson. 2002. *Evaluation of Airborne Image Data for Mapping Riparian Vegetation within the Grand Canyon*. Arizona: USGS. Report of US Geological Survey.

Dipietro, D., S. L. Ustin, and E. Underwood. 2002. "Mapping the Invasive Plant *A*rundo *d*onax and Associated Riparian Vegetation Using AVIRIS." In *AVIRIS Airborne Geoscience Workshop Proceedings*, Pasadena, CA.

Fernandes, M. R., F. C. Aguiar, and M. T. Ferreira. 2011. "Assessing Riparian Vegetation Structure and the Influence of Land Use Using Landscape Metrics and Geostatistical Tools." *Landscape and Urban Planning* 99: 166–77.

Foody, G. M., P. M. Atkinson, P. W. Gething, N. A. Ravenhill, and C. K. Kelly. 2005. "Identification of Specific Tree Species in Ancient Semi-Natural Woodland from Digital Aerial Sensor Imagery." *Ecological Applications* 15: 1233–44.

Gamon, J. A. 2008. "Tropical Remote Sensing – Opportunities and Challenges." In *Hyperspectral Remote Sensing of Tropical and Subtropical Forests*, edited by M. Kalacska and G. A. Sanchez-Azofeifa, 297–304. Montreal: CRC Press.

Goetz, S. J. 2006. "Remote Sensing of Riparian Buffers: Past Progress and Future Prospects." *Journal of the American Water Resources Association* 42: 133–43.

Goetz, S. J., R. K. Wright, A. J. Smith, E. Zinecker, and E. Schaub. 2003. "IKONOS Imagery for Resource Management: Tree Cover, Impervious Surfaces, and Riparian Buffer Analyses in the Mid-Atlantic Region." *Remote Sensing of Environment* 88: 195–208.

Hall, F. G., K. F. Huemmrich, and S. N. Goward. 1990. "Use of Narrow Band Spectra to Estimate Fraction of Absorbed Photosynthetically Active Radiation 3." *Remote Sensing of Environment* 32: 47–54.

Hamada, Y., D. A. Stow, L. L. Coulter, J. C. Jafolla, and L. W. Hendricks. 2007. "Detecting Tamarisk Species (Tamarix Spp.) in Riparian Habitats of Southern California Using High Spatial Resolution Hyperspectral Imagery." *Remote Sensing of Environment* 109: 237–48.

Hérault, B., and O. Honnay. 2007. "Using Life-History Traits to Achieve a Functional Classification of Habitats." *Applied Vegetation Science* 10: 73–80.

Hurcom, S. J., A. R. Harrison, and M. Taberner. 1996. "Assessment of Biophysical Vegetation Properties Through Spectral Decomposition Techniques." *Remote Sensing of Environment* 56: 203–14.

Hynes, H. B. N. 1970. *The Ecology of Running Waters*, 555 pp. Toronto: University of Toronto Press.

Jensen, J. R. 1996. *Introductory Digital Image Processing. a Remote Sensing Perspective*. 2nd ed. Upper Saddle River, NJ: Prentice Hall.

Johansen, K., and S. Phinn. 2006. "Mapping Structural Parameters and Species Composition of Riparian Vegetation Using IKONOS and Landsat ETM+ Data in Australian Tropical Savannahs." *Photogrammetric Engineering and Remote Sensing* 72: 71–80.

Johnson, D. M., W. K. Smith, T. C. Vogelmann, and C. R. Brodersen. 2005. "Leaf Architecture and Direction of Incident Light Influence Mesophyll Fluorescence Profiles." *American Journal of Botany* 92: 1425–31.

Karnieli, A., M. Shachak, H. Tsoar, E. Zaady, Y. Kaufman, A. Danin, and W. Porter. 1996. "The Effect of Microphytes on the Spectral Reflectance of Vegetation in Semiarid Regions." *Remote Sensing of Environment* 57: 88–96.

Kenro, N., K. Yoshiko, and O. Nobuhito. 2000. "Spectral Reflectance, Photosynthesis, and Water Deficit Stress of Tree Leaves." *Journal of Remote Sensing Society of Japan* 20: 230–40.

Kuhn, I., W. Durka, and S. Klotz. 2004. "BiolFlor: A New Plant-Trait Database as a Tool for Plant Invasion Ecology." *Diversity and Distributions* 10: 363–5.

Lillesand, T. M., and R. W. Kiefer. 2000. *Remote Sensing and Image Interpretation*. 4th ed. New York: Wiley.

Lonard, R. I., F. W. Judd, J. H. Everitt, D. E. Escobar, M. R. Davis, M. M. Crawford, and M. D. Desai. 2000. "Evaluation of Color-Infrared Photography for Distinguishing Annual Changes in Riparian Forest Vegetation of the Lower Rio Grande in Texas." *Forest Ecology and Management* 128: 75–81.

Malanson, G. P. 1993. *Riparian Landscapes*. Cambridge: Cambridge University Press.

Marcus, W. A., R. A. Marston, C. R. Colvard Jr., and R. D. Gray. 2002. "Mapping the Spatial and Temporal Distributions of Woody Debris in Streams of the Greater Yellowstone Ecosystem, USA." *Geomorphology* 44: 323–35.

Matheson, W., and S. Ringrose. 1994. "The Development of Image Processing Techniques to Assess Changes in Green Vegetation Cover Along a Climatic Gradient Through Northern Territory, Australia." *International Journal of Remote Sensing* 15: 17–47.

Muller, E. 1997. "Mapping Riparian Vegetation Along Rivers: Old Concepts and New Methods." *Aquatic Botany* 58: 411–37.

Nagler, P. L., E. P. Glenn, and A. R. Huete. 2001. "Assessment of Spectral Vegetation Indices for Riparian Vegetation in the Colorado River Delta, Mexico." *Journal of Arid Environments* 49: 91–110.

Neale, C. M. 1997. "Classification and Mapping of Riparian Systems Using Airborne Multispectral Videography." *Restoration Ecology* 5: 103–12.

Neale, C. M., and B. G. Crowther. 1994. "An Airborne Multi-Spectral Video/Radiometer Remote Sensing System: Development and Calibration." *Remote Sensing of Environment* 49: 187–94.

Okin, G. S., D. A. Roberts, B. Murray, and W. J. Okin. 2001. "Practical Limits on Hyperspectral Vegetation Discrimination in Arid and Semiarid Environments." *Remote Sensing of Environment* 77: 212–25.

Ollinger, S. V. 2011. "Sources of Variability in Canopy Reflectance and the Convergent Properties of Plants." *New Phytologist* 189: 375–94.

Osborne, C. P., and F. I. Woodward. 2001. "Biological Mechanisms Underlying Recent Increases in the NDVI of Mediteterranean Shrublands." *International Journal of Remote Sensing* 22: 1895–907.

Otterman, J. 1996. "Desert-Scrub as the Cause of Reduced Reflectances in Protected Versus Impacted Sandy Arid Areas." *International Journal of Remote Sensing* 17: 615–19.

Pengra, B. W., C. A. Johnston, and T. R. Loveland. 2007. "Mapping an Invasive Plant, *Phragmites Australis*, in Coastal Wetlands Using the EO-1 Hyperion Hyperspectral Sensor." *Remote Sensing of Environment* 108: 74–81.

Podani, J. 1994. *Multivariate Data Analysis in Ecology and Systematics. A Methodological Guide*, 176 pp. The Hague: SPB Academic Publishing.

Price, J. C. 1994. "How Unique Are Spectral Signatures? " *Remote Sensing of Environment* 49: 181–6.
Pu, R., and D. Liu. 2011. "Segmented Canonical Discriminant Analysis of *in situ* Hyperspectral Data for Identifying 13 Urban Tree Species." *International Journal of Remote Sensing* 32, 8: 2207–26.
Quackenbush, L. J., P. F. Hopkins, and G. J. Kinn. 2000. "Developing Forestry Products from High Resolution Digital Aerial Imagery." *Photogrammetric Engineering and Remote Sensing* 66: 1337–46.
Quinn, G. P., and M. J. Keough. 2002. *Experimental Design and Data Analysis for Biologists*. Cambridge: Cambridge University Press.
Rautiainen, M., M. Mõtus, P. Stenberg, and S. Ervasti. 2008. "Crown Envelope Shape Measurements and Models." *Silva Fennica* 42: 19–33.
Renofalt, B. M., C. Nilsson, and R. Jansson. 2005. "Spatial and Temporal Patterns of Species Richness in a Riparian Landscape." *Journal of Biogeography* 32: 2025–37.
Richards, J. A., and X. Jia. 2006. *Remote Sensing Digital Image Analysis*. 4th ed. New York: Springer.
Rivas-Martínez, S. 2004. Global Bioclimatics (Clasificación Bioclimática de la Tierra). Accessed May 18, 2012. http://www.ucm.es/info/cif/book/bioc/bioc2.pdf.
Rivas-Martínez, S., D. Sanchez-Mata, and M. Costa. 1999. "North American Boreal and Western Temperate Forest Vegetation." *Itinera Geobotanica* 12: 5–16.
Schmidt, K. S., and A. K. Skidmore. 2003. "Spectral Discrimination of Vegetation Types in a Costal Wetland." *Remote Sensing of Environment* 85: 92–108.
Schowengerdt, R. A. 1983. *Techniques for Image Processing and Classification in Remote Sensing*. New York: Academic Press.
Schuft, M. J., T. J. Moser, P. J. Wigington, D. L. Stevens, L. S. McAllister, S. S. Chapman, and T. L. Ernst. 1999. "Development of Landscape Metrics for Characterizing Riparian-Stream Networks." *Photogrammetric Engineering and Remote Sensing* 65: 1157–67.
Shao, G., G. Zhao, S. Zhao, H. H. Shugart, S. Wang, and J. Schaller. 1996. "Forest Cover Types Derived From Landsat Thematic Mapper Imagery for Changbai Mountain Area of China." *Canadian Journal of Forest Research* 26: 206–16.
Slaton, M. R., E. R. Hunt, and W. K. Smith. 2001. "Estimating Near-Infrared Leaf Reflectance from Leaf Structural Characteristics." *American Journal of Botany* 88: 278–84.
Smolander, S., and P. Stenberg. 2005. "Simple Parameterizations of the Radiation Budget of Uniform Broadleaved and Coniferous Canopies." *Remote Sensing of Environment* 94: 355–63.
Swain, P. H., and S. M. Davis. 1978. *Remote Sensing: The Quantitative Approach*. New York: McGraw-Hill.
Thenkabail, P. S., E. A. Enclona, M. S. Ashton, and B. van Der Meer. 2004. "Accuracy Assessments of Hyperspectral Waveband Performance for Vegetation Analysis Applications." *Remote Sensing of Environment* 91: 354–76.
Thessler, S., S. Sesnie, Z. Bendaña, K. Ruokolainen, E. Tomppo, and B. Finegan. 2008. "Using *k*-n and Discriminant Analyses to Classify Rain Forest Types in a Landsat TM Image Over Northern Costa Rica." *Remote Sensing of Environment* 112, 5: 2485–94.
Tottrup, C. 2004. "Improving Tropical Forest Mapping Using Multi-Date Landsat TM Data and Pre-Classification Image Smoothing." *International Journal of Remote Sensing* 25: 717–30.
Tuominen, S., and A. Pekkarinen. 2005. "Performance of Different Spectral and Textural Aerial Photograph Features in Multi-Source Forest Inventory." *Remote Sensing of Environment* 94: 256–68.
Underwood, E. C., S. L. Ustin, and D. DiPietro. 2003. "Mapping Nonnative Plants Using Hyperspectral Imagery." *Remote Sensing of Environment* 86: 150–61.
Ustin, S. L., and J. A. Gamon. 2010. "Remote Sensing of Plant Functional Types." *New Phytologist* 186: 795–816.
Valiente-Banuet, A., M. Verdú, F. Valladares, and P. Garcia-Fayos. 2010. "Functional and Evolutionary Correlations of Steep Leaf Angles in the Mexical Shrubland." *Oecologia* 163: 25–33.
Valladares, F., and D. Sánchez-Gómez. 2006. "Ecophysiological Traits Associated with Drought in Mediterranean Tree Seedlings: Individual Responses Versus Interspecific Trends in Eleven Species." *Plant Biology* 8: 688–97.
Walcroft, A. S., K. J. Brown, W. S. F. Schuster, D. T. Tissue, M. H. Turnbull, K. L. Griffin, and D. Whitehead. 2005. "Radiative Transfer and Carbon Assimiliation in Relation to Canopy Architecture, Foliage Area Distribution and Clumping in a Mature Temperate Rainforest Canopy in New Zealand." *Agricultural and Forest Meteorology* 135: 326–39.

Weber, R. M., and G. A. Dunno. 2001. "Riparian Vegetation Mapping and Image Processing Techniques, Hopi Indian Reservation, Arizona." *Photogrammetric Engineering and Remote Sensing* 67: 179–86.

Xiao, X., S. Boles, J. Liu, D. Zhuang, and M. Liu. 2002. "Characterization of Forest Types in Northeastern China, Using Multi-Temporal SPOT-4 VEGETATION Sensor Data." *Remote Sensing of Environment* 82: 335–48.

Zomer, R. J., A. Trabucco, and S. L. Ustin. 2009. "Building Spectral Libraries for Wetlands Land Cover Classification and Hyperspectral Remote Sensing." *Journal of Environmental Management* 90: 2170–7.

Appendix

Table A1. Classification matrix (rows = number of observed pixels; columns = number of predicted pixels) of the DA for the dominant riparian species for the temperate (*Alnus glutinosa*), transitional (*Salix salviifolia*), and Mediterranean (*Nerium oleander)* regions in small and medium-sized river catchment areas.

	Small-sized rivers				Medium-sized rivers			
	Alnus glutinosa	*Salix salviifolia*	*Nerium oleander*	Total	*Alnus glutinosa*	*Salix salviifolia*	*Nerium oleander*	Total
Alnus glutinosa	745	6	0	751	648	0	0	648
Salix salviifolia	14	317	62	393	0	406	40	446
Nerium oleander	102	229	802	1133	5	89	522	616
Predicted classifications								
(percentage of correct cases)	99.2	80.7	70.8	81.9	100.0	91.0	84.7	92.2
(percentage after cross-validation)	83.6	83.8	53.1	71.2	88.8	56.4	71.5	75.4

Table A2. Species composition of each bioclimatic zone and relative frequency of species occurrence expressed in percentage.

Species	Bioclimatic zone		
	Mediterranean	Transitional	Temperate
Trees			
Alnus glutinosa (L.) Gaertner		87	42
Celtis australis L.		12	
Frangula alnus Miller		37	33
Fraxinus angustifolia Vahl *angustifolia*	61	87	42
Populus nigra L.	15	31	
Salix alba L.		25	
Salix atrocinerea Brot.	15	65	42
Salix neotricha Goerz		12	
Salix salvifolia Brot.	7	75	8
Shrubs			
Crataegus monogyna Jacq.		68	25
Erica arborea L.	7		8
Flueggea tinctoria (L.) G.L. Webster	69	6	
Laurus nobilis L.			16
Nerium oleander L.	92		
Sambucus nigra L.		6	8
Tamarix africana Poiret	38	6	
Woody climbers			
Hedera hibernica (G. Kirchn.) Bean		37	42
Rubus ulmifolius Schott	62	75	25

Capítulo 3

Assessing riparian vegetation structure and the influence of land use using landscape metrics and geostatistical tools

3.1 Síntese

O capítulo 3, da segunda parte, explora a capacidade de prever a estrutura da vegetação ripária (continuidade longitudinal, largura ripária) em função da pressão antropogénica, num total de 80 km de troços de rio localizados na bacia hidrográfica do Tejo. A influência dos diferentes usos do solo nos padrões espaciais da vegetação ripária arbórea, herbácea e arbustiva é avaliada recorrendo a descritores numéricos, geográficos e topológicos, recolhidos sobre ortofotomapas de elevada resolução espacial (50 cm pixel) e a métodos de análise multivariada e geoestatística. A estrutura ripária é caracterizada e traduzida quantitativamente, utilizando métricas de paisagem (número de manchas, dimensão média da mancha, índice fractal, índice de conectividade, índice de difusão e justaposição) traduzindo-se o resultado num gradiente de qualidade fluvial que posteriormente é relacionado com o uso do solo em faixas de 30 m (uso proximal) e de 200 m (uso distal). Descrevem-se pela primeira vez, as principais implicações ecológicas e significado das diferentes métricas de paisagem em ecossistemas ripários e o seu potencial na avaliação remota do estado de integridade ripária, em função de padrões estruturais espaciais. Aborda-se a possibilidade de combinação de métricas de diferentes categorias na prioritização para restauro de habitats ribeirinhos. As principais conclusões deste trabalho são discutidas em função da sua aplicabilidade na gestão e conservação de galerias ribeirinhas referindo-se a necessidade de ajustar os referenciais relativos à estrutura da vegetação ripária para outras regiões. Destacam-se sobretudo as galerias ripárias que se encontram em locais de reduzida perturbação humana, como as cabeceiras de rios, e que naturalmente apresentam padrões espaciais de elevada fragmentação longitudinal e lateral em função dos constrangimentos geológicos e ambientais. Finalmente, reconhece-se a possibilidade de utilização das métricas de paisagem numa pré-classificação de degradação ripária associada à composição florística, devido à possibilidade de indentificação de padrões espaciais e de configuração geométrica característicos da substituição das margens dos rios por espécies exóticas invasoras, nomeadamente, pela cana (*Arundo don*ax L.).

3.2 Artigo

Assessing riparian vegetation structure and the influence of land use using landscape metrics and geostatistic tools

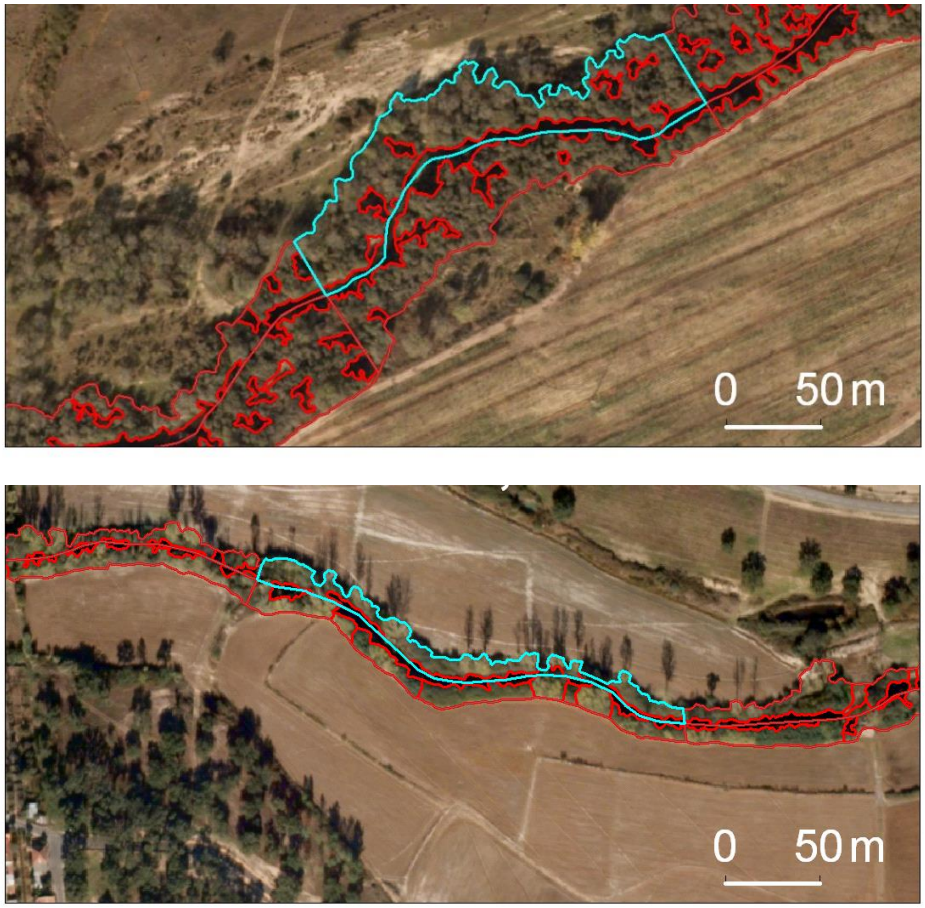

Publicado como: Fernandes MR, Aguiar FC, Ferreira MT. 2011. Assessing riparian vegetation structure and the influence of land use using landscape metrics and geostatistical tools. *Landscape and Urban Planning* 99(2): 166-177.

Landscape and Urban Planning 99 (2011) 166–177

Contents lists available at ScienceDirect

Landscape and Urban Planning

journal homepage: www.elsevier.com/locate/landurbplan

Assessing riparian vegetation structure and the influence of land use using landscape metrics and geostatistical tools

Maria R. Fernandes*, Francisca C. Aguiar, Maria T. Ferreira

Forest Research Centre, Instituto Superior de Agronomia, Tapada da Ajuda, 1349-017 Lisbon, Portugal

ARTICLE INFO

Article history:
Received 22 February 2010
Received in revised form 12 August 2010
Accepted 1 November 2010
Available online 26 November 2010

Keywords:
Riparian landscapes
Land cover
Human influence
Spatial patterns
Buffer
Autocorrelation

ABSTRACT

Riparian areas are among the most threatened habitats in the world, due to human activities and land use in adjacent areas. In this study we sought to identify landscape metrics for describing the spatial patterns of riparian vegetation affected by land use. We also hypothesize that land use in the immediate vicinity of the riparian area (considered as a 30-m buffer) can have a greater effect on the structure of riparian vegetation than that in an enlarged buffer (i.e. 200 m). The study was conducted in the highly humanized River Tagus watershed (Central Portugal; Western Iberia), along over 80 km of river stretches. Riparian vegetation and land use data were obtained from high-resolution digital images (RGB-NIR 0.5 m × 0.5 m, spring 2005). Patch analyst was used to calculate landscape metrics related to the spatial configuration, isolation, inter-connectivity, and distribution of patches of three riparian cover classes (tree, shrub, and herbaceous). We quantified and accounted for the global and local spatial autocorrelation of data. Data treatment included redundancy analysis and geostatistic methods. Results showed that only a combined interpretation of various landscape metrics can consistently describe the spatial patterns of riparian vegetation. Riparian vegetation near agricultural areas (irrigation crops, rice fields, orchards, and vineyards), presented a low number of much smaller riparian tree patches with less complex shapes, and a low interspersion of the patch distribution. We found that proximal land use affects the structure of riparian vegetation more than distal land use – an important consideration for the establishment of streamside protection buffers.

1. Introduction

Riparian zones are responsible for many ecological functions considered crucial to the preservation of river ecological conditions (Forman, 1995; Naiman and Décamps, 1997); they are, however, severely altered due to adjacent human activity and land use, especially in Mediterranean areas (Corbacho et al., 2003; Décamps et al., 1988; Gallego-Fernández et al., 1999; Hooke, 2006; von Schiller et al., 2008). Numerous studies have observed that the composition and spatial patterns of riparian vegetation can be significantly influenced by land use (Aguiar and Ferreira, 2005; Allan, 2004; Ferreira et al., 2005; Inoue and Nakagoshi, 2001), but few studies relate the influence of land use at increasing distances from the fluvial systems in rivers and riparian ecosystems (but see Bott et al., 2006; Bunn and Davies, 2000; McIntyre and Hobbs, 1999).

Stream management and restoration programs have broadly recognized the urgent need to develop methodologies for evaluating ecological river quality from multiple perspectives. Some studies have focused on floristic composition (Looy et al., 2008), structural and functional attributes, such as the longitudinal and lateral continuity of riparian vegetation (González-del-Tánago and Garcia-Jalón, 2006), percentage of canopy cover, canopy continuity, and tree clearing (Aguiar et al., 2009; Johansen and Phinn, 2006), but all of them require intensive field surveys. Other methods are fast and visually based, but do not involve quantification (Dixon et al., 2006; Ward et al., 2003). In other cases, the riparian zone is mapped in a fixed buffer using remotely sensed image data (Congalton et al., 2002; Schuft et al., 1999; Yang, 2007), but the mismatch between the established riparian buffer and the existent riparian zone usually cause errors in the estimation of vegetation cover. Efficient and quantitative remote measurements of the structure of riparian vegetation are thus needed in watershed studies in order to provide on-the-ground management guidelines for these ecosystems. Image-based methods, satellite images or airborne digital images, become increasingly more cost-effective than field assessments when a higher level of detail is necessary (Johansen and Phinn, 2006). Moreover, high spatial resolution imagery (<5 m × 5 m pixels) is essential for mapping riparian vegetation, due to the limited width of riparian zones and the high spatial variability (Congalton et al., 2002; Davis et al., 2002; Muller, 1997).

* Corresponding author. Tel.: +351 213653380; fax: +351 213653338.
E-mail addresses: mrfernandes@isa.utl.pt, rosario.pereira.fernandes@gmail.com (M.R. Fernandes).

0169-2046/$ – see front matter © 2010 Elsevier B.V. All rights reserved.
doi:10.1016/j.landurbplan.2010.11.001

Table 1
Structural categories, summary description, acronyms, units and range of landscape metrics; formulae and detailed calculation from McGarigal and Marks (1994). Main ecological implications based mainly on Forman and Godron (1981) and Forman (1995), and applications of landscape metrics to the riparian vegetation.

Structural category	Landscape metrics	Acronym	Units and range	Description	Main ecological implications	Applications for riparian woods
Area/density	Number of Patches	NP	None [1,∞]	Basic statistics of the spatial configuration	Productivity, biogeochemical cycling and species dynamics	Simple indicators of riparian fragmentation
	Mean Patch Size	MPS	Square meters [0,∞]			
	Patch Size Coefficient of Variation	PSCV	Percentage [0,∞]	Variability in the size of patches	Biological diversity	Heterogeneity in the structure of riparian vegetation
Shape	Mean Shape Index	MSI	None [1,∞]	Complexity of shapes. Approaches 1 for shapes with simple perimeters.	Interactions with the adjacent matrix–edge effects	Spatial configuration of riparian vegetation, in terms of complexity of riparian patches
Area/edge	Mean Fractal Dimension Index	MPFD	None [1,2]	Fractal dimension: ratio of perimeter per unit area. Increases as patches become more irregular	Lateral connectivity	
Isolation/proximity	Mean Nearest-Neighbor Distance	MNN	Meters [0,∞]	Minimum distance between patches of the same class, based on the shortest distance between their edges	Flows of energy and biomass and biological diversity–connectivity effects	Isolation of riparian patches, inter-connectivity
	Mean Proximity Index	MPI	None [0,∞]	Increases as the patches of the corresponding patch type become less isolated and less fragmented.	Ecological neighborhood	Degree of isolation and fragmentation of riparian patches
					Habitat and refugia discontinuity	
Contagion/interspersion	Interspersion and Juxtaposition Index	IJI	Percentage [0,100]	Proximity of patches in each class. High values correspond to proportionate distribution of patch type adjacencies	Equitability between patches–community dynamics	Distribution of riparian patches
					Persistence and resilience of communities	

The spatial patterns of riparian vegetation can influence ecological processes, such as flows of biomass, energy and nutrients, biological diversity and species dynamics (Rex and Malanson, 1990, Turner, 1989). Patches – homogenous areas differing from their surroundings in origin and dynamics – are the fundamental units of landscapes (Forman and Godron, 1981; Wiens, 1976). Helpful tools, such as landscape metrics using Geographical Information System (GIS) techniques, can characterize the structure of riparian vegetation (Apan et al., 2002). Landscape metrics are numeric descriptors that quantify patch configuration and the spatial relationships among patches, such as distribution, isolation and interspersion, and can consequently be used as expressions of ecological processes (Table 1). For instance, the Mean Shape Index – a configuration landscape metric which relates the patch area and its perimeter – can be used to evaluate the edge effect. Convoluted shapes indicate large boundaries, expressing high interactions with the adjacent matrix (Forman, 1995). Reduced connectivity and fragmental patterns indicated by Mean Proximity Index and Mean Nearest-Neighbor Distance, particularly in woody vegetation, represent poorer stream ecological conditions (Schuft et al., 1999). Also, the structure of riparian vegetation, the longitudinal continuity of vegetation patches, their aggregation, configuration, expansion limits, and distribution in the riparian zone, can reveal the level of human disturbance and can be used as an indicator of the status of the riparian zone (Johansen et al., 2007).

The traditional statistical approaches to exploring the spatial distribution of vegetation across a landscape generally ignore the spatial dependence of the data and assume the independence of the samples (Miller et al., 2007). However, one of the basic principles of both geographic and ecological theory is the direct relationship between proximity and similarity (Tobler, 1979). The elements that are closer to one another in an ecosystem tend to be influenced by the same processes and tend to present a greater degree of likeness (Legendre and Fortin, 1989) – a phenomenon called spatial autocorrelation. Spatial autocorrelation measures the correlation of a variable with itself through space, that means the lack of independence between pairs of observation at given distances in space (Legendre, 1993). Disregarding the spatial component in an ecological analysis can lead to erroneous results, since it is a source of bias in most ecological studies. The present study quantifies and accounts for the global and local spatial autocorrelation of the data. We mapped riparian patches and land use using airborne digital images (RGB-NIR spatial resolution 0.5 m × 0.5 m) of impaired landscapes in order to address the following questions:

- Can landscape metrics be used to characterize the structure of riparian vegetation?
- What landscape metrics are most suitable for detecting alterations in spatial patterns of riparian vegetation due to land use pressure?
- Does the land use in the immediate vicinity of the riparian zone have more influence on the spatial structure of riparian vegetation than the distal land use?

Fig. 1. Iberian Peninsula, showing the River Tagus watershed (Portuguese part), and the location of the four studied watersheds.

2. Methods

2.1. Site description

The study was conducted on four tributaries along the left margin of the River Tagus (Chouto, Margem, Muge and Sôr) (Fig. 1), all with similar climate and geomorphology. The studied stretches are mostly spread over calcareous Mesozoic formations and have a Mediterranean climate, with a high seasonal variability of rainfall patterns. According to the *Atlas do Ambiente* (http://www.iambiente.pt/atlas/), the annual runoff ranges from 200 to 300 mm, with an annual average rainfall of 600–800 mm and an annual average temperature of 15–17.5 °C. The land use in the study area is very heterogeneous, including small-scale agriculture, including orchards, vineyards, maize, pine and eucalyptus forests, Mediterranean shrublands, cork oaklands, and scattered human settlements.

2.2. Field sampling and hydrogeomorphology

Floristic surveys were carried out during the summer of 2004. Sampling sites ($n = 15$) were 200 m long sections of the riverbank at approximately 3 km intervals along the studied fluvial stretches. We recorded riparian woody species, tree and shrubs, and estimated percentage canopy cover using five classes: (1)<10%, (2)≥10–25%, (3)≥ 25–50%, (4) ≥50–75% and (5) ≥75%. We also recorded the total number of herbaceous species, and identified the most abundant ones (more than 5% cover).

The hydrogeomorphological characteristics of the streams – namely valley morphology, channel width, dominant substrates of riverbanks, and land use in the floodplain – were obtained from both field observations and GIS layers.

2.3. Structure of the riparian vegetation and land use assessment

A GIS was used to store and organize the data obtained from the on-screen photo interpretation of 1:5000 airborne digital images (RGB-NIR spatial resolution 0.5 m × 0.5 m; ortho-rectified and mosaicked, flyover date spring 2005). We studied 21 km of the River Sôr, 33 km of the River Muge, 16 km of the River Margem, and 13 km of the River Chouto.

The riparian zone is defined as the area from the edge of the stream bank to the external visible line of the canopy where an abrupt change in vegetation height, type and amount occurs (Johansen and Phinn, 2006).

We first divided the river reaches under study into 250 m long sections (sampling units). The lateral limits of the riparian zone were then manually digitalized for both riverbanks (Fig. 2a). Polygons of homogeneous strata of riparian vegetation – riparian patches – were delineated and classified into riparian vegetation

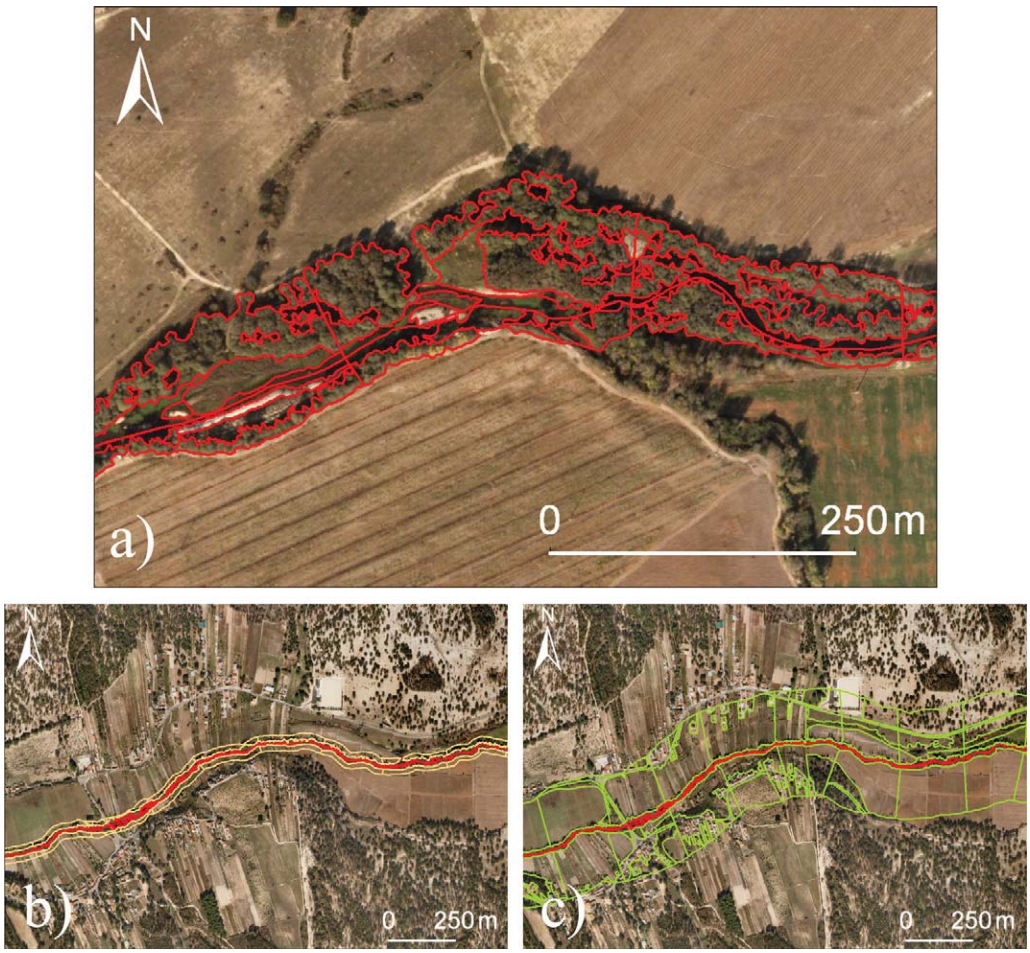

Fig. 2. Illustration of: (a) sampling units and riparian patches, perpendicular lines divide contiguous sampling units, River Sôr; (b) 30 m land use buffer, River Muge; and (c) 200 m land use buffer, River Muge.
IGP.

cover classes, within each sampling unit: (i) trees; (ii) shrubs; and (iii) herbaceous. This was done using visual screening of image features, namely the spatial variation in pixel intensity pattern and the local contrast (gray level differences). Tree cover class had a higher variability in these textural features than the other classes, with the herbaceous class being the most homogenous of all. Areas with shadow were removed from the inner part of riparian patches to capture the overall complexity of their shapes.

Landscape metrics related with the spatial configuration, isolation, inter-connectivity, and distribution of riparian vegetation were calculated within each sampling unit for each riparian cover class using the patch analyst – vector format (ArcGis9) extension. Spearman Rank correlations (R) were initially used to evaluate the relationships between the landscape metrics available in the software. The correlated metrics ($|R| > 0.8$; $p < 0.01$) were eliminated to avoid redundancy in the data. Table 1 describes the selected landscape metrics, namely the Number of Patches, Mean Patch Size, Patch Size Coefficient of Variation, Mean Shape Index, Mean Fractal Dimension Index, Mean Nearest-Neighbor Distance, Mean Proximity Index, Interspersion and Juxtaposition Index, as well as their main ecological implications and contribution to the characterization of the structure of the riparian vegetation.

A connectivity distance of 5 m was applied to the Mean Proximity Index calculation, as used by Schuft et al. (1999) in the characterization of riparian-stream networks.

Two buffers (30 m and 200 m) were used to evaluate the influence on the riparian vegetation structure of proximal and distal land use (Fig. 2). Fifty sampling units scattered across the study area were used to identify the existing land uses; for this we used on-screen photo interpretation, along with information from 1:25,000 scale military maps from the Portuguese Army Geographic Institute (www.igeoe.pt). Four land use classes ordered by increasing physical and ecological impact in the riparian areas were considered: (1) agroforestry, including oak and cork-oak woodlands, natural pastures, scrublands, fallow ground, extensive crops, and mixed woodland; (2) forestry, including plantations of pine and eucalyptus; (3) agriculture, including irrigation crops, rice fields, orchards, and vineyards; and (4) urban, including settlements and industrial areas. The agroforestry class is dominated by the "*montados*", a traditional agrosilvopastoral system characterized by long agricultural rotations and closed nutrient cycles without fertilizers and pesticides (Plieninger and Wilbrand, 2004). The main ecological consequences of this land use type include the removal of bank vegetation and a decreasing rate of natural regeneration; the other land uses in the study area present manifold and more severe physical and ecological consequences for riparian areas and inhabitant communities than the agroforestry class (Table 2).

Patches of land use were delimited for each buffer within each sampling unit. Land use classes were evaluated in terms of percentage of area occupied, after grouping the patches of the same class. Roads were also taken into account and quantified in length (km) for each sampling unit and land use buffer.

During the summer of 2007, field observations were made in about 25% of the total study area in order to validate the photo

Table 2
Main direct physical effects and potential ecological consequences of the land uses for the riparian areas in the study area.

Land use class	Main direct physical effects on the riparian area	Potential ecological consequences for the riparian vegetation
Agroforestry	Bank vegetation removal by grazing	Removal of riparian vegetation removed and hampering of natural regeneration
Forestry	Replacement of the riparian woods by forest plantations	Reduction of the structural and biological diversity of the riparian woods
	Increase in runoff, sediment load and bank erosion by timber extraction	Fragmentation of riparian woods
		Loss of habitat complexity
Agriculture	Superficial water extraction and groundwater pumping	Water stress, increased mortality, decreased growth rate and crown volumes of riparian vegetation
	Replacement of the riparian woods by agricultural land and irrigation channels	Fragmentation of riparian woods
	Inputs of nutrients and pesticides	Alteration of the nutrient cycling and imbalance of the inhabitant biological communities
		Introduction and excessive growth of exotic species
Urban (including roads)	Increase in runoff and sediments by the impervious surfaces	Riparian vegetation stress
	Riparian habitat reallocation by linearization and channelization for flood control	Fragmentation of riparian woods
	Replacement of the riparian habitat by access roads and urban infrastructures	Pollution and unsuitable conditions for the establishment of riparian vegetation
		Alteration of the nutrient cycling and contamination of riparian habitat by pollutants
		Introduction of exotic species

interpretation, to confirm the correct allocation of riparian and land use cover classes.

2.4. Spatial autocorrelation assessment

Moran's *I* statistics (Moran, 1950) were used to estimate general patterns of spatial dependency. Moran's *I* is frequently used in geostatistical and ecological studies (Fortin et al., 2002; Segurado et al., 2006), and is obtained by dividing the spatial covariation by the total variation of a given attribute. Global Moran's *I* evaluates whether the pattern expressed is clustered, dispersed, or random. When the *z* score indicates statistical significance, a Moran's *I* value near +1.0 indicates clustering, while a value near −1.0 indicates dispersion, and 0 or near to 0 represents no spatial autocorrelation, that means a random pattern.

We calculated Global Moran's *I* using three different configurations of distance matrices: (i) the "inverse distance criterion", which includes all the sampling units and gives a lower weight with increasing distances from a given sampling unit; (ii) the "threshold distance", which only includes the sampling units within a distance of 1000 m; and (iii) the "first continuity order", which only includes the sampling units that share boundaries, the left and right contiguous sampling units.

A semivariogram function (Cressie, 1991; Wackernagel, 2003; Webster and Oliver, 2007) was applied to the riparian vegetation data, for the four streams, in order to calculate the spatial independence distance between sampling units. A variogram function is a mathematical description that relates the variance (or dissimilarity) of samples from a given attribute with the distance that separates them (Isaacs and Srivastava, 1989). Because nearby samples tend to have similar attribute values, low variance among samples is expected in the semivariogram. The variance increases asymptotically to the limit value, as the distances between samples increase. Samples that are separated by distances below this limit are spatially autocorrelated, whereas samples that are farther apart are independent, because the expected variance is not significantly different from the asymptotic value. The distance value between samples at which spatial autocorrelation is considered insignificant is named "range" (Oline and Grant, 2002).

We also calculated the Local Moran's *I* (Anselin, 1995) – a measure of contagion that includes the effect of the spatial neighborhood (Keitt et al., 2002; Segurado and Araújo, 2004). The Local Moran's *I* have a spatial autocorrelation value for each sampling unit, rather than the single value of the Global Moran's *I*.

The spatial dependence of the land use variables was not evaluated, because ensuring the spatial independence of the biological variable means that unbiased correlations between dependent and independent variables are guaranteed (Lennon, 2000).

2.5. Influence of land use on the structure of riparian vegetation

Constrained ordination procedures were performed in CANOCO version 4.5 (ter Braak and Smilauer, 2002) to determine the influence of land use on the structure of the riparian vegetation ($n = 330$ sampling units). The gradient lengths of the landscape metrics datasets were evaluated with Detrended Correspondence Analysis. As the gradient lengths were lower than 4 standard deviation units (Leps and Smilauer, 2003) thus indicating a linear response, Redundancy Analysis (RDA) was used.

The effect of the spatial component in our data was analysed using two approaches: (1) by incorporating the spatial component into the landscape metrics dataset; and (2) by removing the spatial autocorrelation. For the first approach, RDA runs were performed: (i) using just land use variables; (ii) using land use variables and the Local Moran's *I* matrix as co-variable (i.e. spatial variables); and (iii) using the spatial and the land use variables together.

For the second approach, we performed RDA using spatially independent sampling units. The distance between sampling units was defined by the "range" values obtained by the application of a semivariogram function to the landscape metrics (see Section 2.4). The subsampling method was defined to maximize the sample size, and avoided the duplication of any sampling unit. More precisely, the independent subsamples were obtained by systematically using an sampling unit that was separated from the following one by the "range" value: for instance, the first subsample begins with the inclusion of sampling $unit_1$, the second subsample begins in sampling $unit_2$, and so forth.

In both approaches the landscape metric datasets for the three riparian cover classes were centred and standardized and the correlation matrix was used to make them comparable. RDA runs were performed with forward selection of land use variables, and unrestricted Monte Carlo permutation tests for each one. A cut-off point of 0.10 was adopted. Variance inflation factors were examined to detect co-linearity between the land use variables. The total vari-

Table 3
Minimum and maximum values of landscape metrics; average (± SD) for each riparian cover class ($n = 330$ sampling units). Acronyms for landscape metrics are given in Table 1. Dominant riparian taxa, observed percentage cover class in parentheses, average species richness ± SD for the tree, shrub and herbaceous cover classes ($n = 15$ field surveys).

	Riparian cover classes		
	Tree	Shrub	Herbaceous
Landscape metrics			
NP	1.00–14.00 (3.43 ± 2.29)	1.00–11.00 (2.23 ± 1.62)	1.00–8.00 (1.92 ± 1.12)
MPS	21.67–11268.02 (1000.57 ± 1387.17)	5.41–4770.42 (413.94 ± 626.97)	6.73–2183.67 (420.70 ± 501.30)
PSCV	6.60–211.81 (84.29 ± 41.10)	2.67–151.54 (63.20 ± 34.03)	9.01–128.58 (57.57 ± 30.49)
MSI	1.03–5.47 (2.00 ± 0.76)	1.08–4.15 (1.79 ± 0.57)	1.16–5.70 (2.12 ± 0.93)
MPFD	1.47–2.13 (1.69 ± 0.11)	1.46–2.67 (1.73 ± 0.17)	1.45–2.69 (1.78 ± 0.17)
MNN	0.37–171.70 (15.10 ± 23.94)	0.80–210.70 (34.49 ± 45.13)	1.80–134.50 (28.35 ± 29.29)
MPI	2.43–4584.94 (379.34 ± 651.59)	1.12–539.37 (81.96 ± 126.11)	2.26–114.37 (25.35 ± 28.15)
IJI	0–22.66 (10.00 ± 5.37)	1.27–24.99 (11.63 ± 4.89)	0–19.97(8.91 ± 5.71)
Floristic composition			
Dominant taxa (cover class)	*Salix salviifolia* (3) *Salix atrocinerea* (3) *Fraxinus angustifolia* (3) *Populus nigra* (2) *Alnus glutinosa* (2) *Salix alba* (1)	*Sambucus nigra* (2) *Rubus ulmifolius* (1) *Crataegus monogyna* (1) *Tamarix africana* (1) *Frangula alnus* (1)	*Juncus* sp. *Scirpus holoschoenus* *Cyperus longus* *Agrostis stolonifera* *Mentha suaveolens* *Holcus lanatus*
Average species richness (± SD)	4 ± 1.3	1.2 ± 1	25 ± 6.5

ance – also called 'total inertia' – explained by each combination was obtained by the sum of all canonical unconstrained eigenvalues (ter Braak and Smilauer, 2002).

Multiple linear regressions were performed to evaluate the relationship between the various types of land use and the landscape metrics. To identify the land use classes that contributed most to explaining the structure of the riparian vegetation, we used forward selection procedures and counted the number of significant regressions ($p < 0.05$) per land use class and land use buffer, for each landscape metric. STATISTICA software version 6.0 (StatSoft Inc., 2001) was used for the regression analyses.

In addition, we compared the expected and the observed responses of the landscape metrics to land use. Bibliographic sources, such as Aguiar et al. (2000), Aguiar and Ferreira (2005), Guirado et al. (2007), Schuft et al. (1999), Shandas and Alberti (2009), Timm et al. (2004), Wu et al. (2000), and expert judgment were used to suggest the behaviour, positive or negative relationships, of the landscape metrics influenced by land use.

3. Results

3.1. Riparian composition and hydrogeomorphology

Stretches of the Margem and the Chouto and the upstream section of the Sôr are of medium valley width. The riparian formations are dominated by willows, namely *Salix salviifolia* and *Salix atrocinerea*. The deep soils of the downstream section of the Margem support riparian woods dominated by ashes (*Fraxinus angustifolia*) and alders (*Alnus glutinosa*). The shrub strata is dominated by hawthorns (*Crataegus monogyna*), black elders (*Sambucus nigra*), and alder buckthorns (*Frangula alnus*). *Tamarix africana* was found in the most near-natural upstream section of the River Sôr. A patch mosaic of small-scale agriculture including orchards, vineyards and maize, and scattered human settlements dominated the landscape of these valleys.

The Rivers Muge and Sôr presented a relatively larger valley and channel width than the previous rivers, and their downstream sections often presented sand bars. Riparian woods were mainly composed of willows, and occasionally ashes and hawthorn. Isolated groups of black poplar (*Populus nigra*) were also found in the middle section of the Sôr. The most degraded areas were frequently composed of a sole shrub strata of *Salix* sp., surrounded by sedges of bramble ticket (*Rubus ulmifolius*) Eroded embankments with fine substrates were frequently invaded by the giant reed (*Arundo donax*). Large regular patches of rice, maize and other irrigation crops dominated the landscape near the riparian zone.

The natural regeneration of ashes and willows was frequently observed in the inner banks.

Forests of Mediterranean shrublands, cork oaklands, and pine and eucalyptus forests were widespread on the floodplain.

3.2. Structure of riparian vegetation

The study area encompassed 330 sampling units, which resulted in the delimitation of 3900 patches of riparian vegetation.

Table 3 summarizes the overall characteristics of the structure of the riparian vegetation using landscape metrics and the dominant taxa found for each cover class. The tree cover class was mostly composed of willows, ashes and alders. This class was the most abundant, and presented the largest riparian patches (Mean Patch Size values) when compared to the other riparian cover classes, although a higher variability of the patch size (Patch Size Coefficient of Variation values) was also found. The highest number of tree cover patches (Number of Patches values) was found in the upstream sampling units of the River Sôr, whereas lower values occurred close to urban areas and small farms, or associated with areas with large widths of riparian vegetation, at least more than 30 m. Landscape metrics associated with the connectivity – namely the Mean Nearest-Neighbor Distance and the Mean Proximity Index – provide evidence of a higher connectivity of tree cover class in comparison to the other riparian cover classes. The high Mean Fractal Dimension Index values found for this riparian cover class corresponded to complex shapes with meandering forms, associated with large riparian widths. We even found a small number of riparian tree patches with Mean Fractal Dimension Index values that exceeded the maximum value usually referred to in the literature (see Table 1).

Riparian shrub strata frequently included black elder, hawthorn and dyer's buckthorn. Patches of shrubs were smaller than the tree patches, but presented less fragmentation.

Under the canopies, the vegetation was dominated by a community of grasses, reeds, rushes and other vascular species associated with wet environments.

Where the herbaceous cover class was concerned, higher Mean Patch Size (MPS) values occurred near irrigation crops or associated with temporary sand deposits; also, higher Mean Shape Index (MSI) values were associated with elongated shapes, which were a frequent characteristic of this riparian cover class.

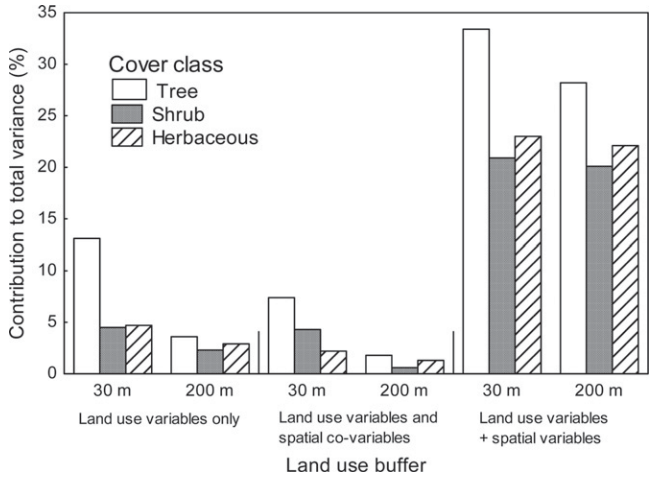

Fig. 3. RDA results expressed by the contribution of land use variables to explaining the total variance of riparian cover classes, using three approaches: (1) solely land use variables, (2) land use variables and spatial co-variables, and (3) land use and spatial variables, with the 30 m and 200 m land use buffers (330 sampling units).

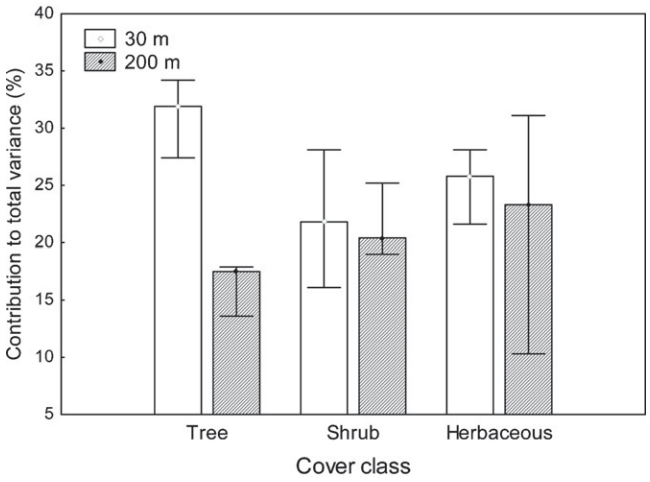

Fig. 4. Average, minimum and maximum RDA results expressed by the contribution of land use variables to explaining the total variance of riparian cover classes, using spatial independent sampling units (28 sampling units per subsample) for the 30 m and 200 m land use buffers.

All riparian cover classes presented low Interspersion and Juxtaposition Index values, meaning that the riparian patches were not proportionately distributed in the study area.

The classification by on-screen photo interpretation agreed with the field observations. The few differences that were found were related to recent local disturbances, such as vegetation removal due to sand extraction.

3.3. Spatial autocorrelation assessment

The results of the Global Moran's *I* and its statistical significance for the three configurations of the distance matrix indicated the presence of spatial autocorrelation in most of the landscape metrics across the studied area (Appendix 1). The Mean Proximity Index had a spatial random pattern, except for the shrub cover class; nor did the Mean Nearest-Neighbor Distance reveal a significant clustered pattern for any of the riparian cover classes. No clear dispersed patterns were found. We observed clear differences in the spatial patterns for the riparian cover classes using the various configurations of the distance matrix, which indicates the existence of local spatial autocorrelation patterns. In addition, when the restriction of the sampling unit neighborhood was applied to the tree cover class, with a threshold distance and first continuity order approaches, we observed a higher spatial autocorrelation value than using the inverse distance criteria, which included all the sampling units. This means that the tree cover class had a higher spatial dependence at a local level than at the global level.

The application of a semivariogram function to the landscape metrics for the four streams resulted in an estimation of the "range" value that varied between 2395 m and 2963 m. In order to ensure that sampling units were spatially independent, we therefore used the value of 3000 m between sampling units. The subsampling resulted in 9 combinations ($n = 28$) of different sampling units (see Section 2.5 for detailed subsampling method).

3.4. Influence of land use on the structure of riparian vegetation

Fig. 3 shows the results of the contribution of the land use variables to the total variance of the structure of the riparian vegetation obtained from the RDA runs for the three approaches.

On the whole, the explained variance using the proximal land use (30 m land use buffer) presented consistently higher values than that using the distal land use (200 m land use buffer). This pattern was also observed for stream sections with slightly different valley morphologies, namely the Margem/Chouto and Muge/Sôr.

Another consistent pattern that emerges in the overall RDA analyses was the decrease in the explained variance upon removal of the spatial component (Local Moran's *I* as co-variable). The explained variance that results from using the spatial and the land use variables together, ranged from 20.1% to 33.4%. These results indicate that the structure of the riparian vegetation is more dependent on its spatial component than on the land use variables from either buffer. This means that part of the variance of the riparian vegetation is explained by neighboring values. We also observed higher total variance for the tree cover class than for the other riparian cover classes.

Fig. 4 illustrates the contribution of land use variables, proximal and distal land use buffers, to an explanation of the total variance of the riparian cover classes, using combinations of spatially independent sampling units (9 subsamples; 28 sampling units per subsample). We observed a high increase of the total variance when compared with the previous approach, where we used non-independent sampling units (Fig. 3). Likewise, the proximal land use buffer had a greater influence on the overall riparian cover classes than the distal land use buffer. This trend was especially evident for the tree cover class. For the herbaceous cover class, a high variability was detected in relation to the results of the 9 RDAs we performed.

3.5. Influence of land use classes on the tree cover class

We used the tree cover class to evaluate the influence of the different land use classes, since it was best represented in the study area and displayed the highest percentage of variance explained by land use variables, compared to the other cover classes (Figs. 3 and 4).

Using both early findings from the literature and expert judgement, we suggested a negative relationship between most of the landscape metric values and the tree cover class when influenced by human land use, except in the case of the Mean Nearest-Neighbor Distance, and Number of Patches (Table 4). We therefore expected that increasing land use pressure would result in a high number of patches (expressed by Number of Patches), and smaller patches (expressed by Mean Patch size) with less complex shapes (expressed by low Mean Fractal Dimension Index values, and low

Table 4
Expected and observed responses of landscape metrics to the increasing areas occupied by each land use (↑-positive relation; ↓-negative relation) for the tree cover class. Number of significant multiple regression analyses ($p < 0.05$) of landscape metrics and land use variables (30 m and 200 m land use buffers) using spatial independent sampling units (9 subsamples; 28 sampling units per subsample). Acronyms for landscape metrics are given in Table 1.

Landscape metrics	Expected response	Observed response									
		Agroforestry		Forestry		Agriculture		Urban		Roads	
		30 m	200 m	30 m	200 m	30 m	200 m	30 m	200 m	30 m	200 m
NP	↑	↑ 1				↓ 5	↓ 1			↓ 1	
MPS	↓	↓ 3				↓ 7					
PSCV	↓	↓ 1		↓1	↓ 1	↓ 4	↓ 1				↑ 1
MSI	↓	↓ 2				↓ 6	↓ 1				
MPFD	↓	↓ 1	↓ 1		↓ 1	↓ 3	↓ 1	↓ 1			
MNN	↑	↑ 2	↓ 1	↑1			↑ 1			↑ 1	↑ 1
MPI	↓	↑ 1	↓ 1			↓ 2	↓ 1		↓ 1		↑ 1
IJI	↓	↓ 2		↑1		↓ 7	↓ 1	↓ 1	↓ 2	↑ 1	

Mean Shape Index values), but more isolated patches (high Mean Nearest-Neighbor Distance values and low Mean Proximity Index values). We also expected more homogeneous riparian patches, (expressed by lower Patch Size Coefficient of Variation values), and low interspersion of the patch distribution (expressed by low Interspersion and Juxtaposition Index values) along a gradient of land use pressure.

In general, the observed responses of the landscape metrics were concordant with the expected ones (Table 4). Agriculture presented the highest number of significant regressions (p-value < 0.05) with virtually all the landscape metrics, the exception being the fragmentation metrics Mean Nearest-Neighbor Distance and Mean Proximity Index. We observed a low number of much smaller riparian tree patches, with less jagged shapes, and a low interspersion of the patch distribution with increasing agricultural areas in the land use buffer – mainly in the 30 m buffer. For the other land uses the general patterns of degradation were similar to those found for agriculture, though supported by a low number of significant responses. We also observed an increase in the degradation pattern across the land use pressure gradient, from agroforestry to urban land use (Fig. 5).

We selected two landscape metrics with a high number of significant regressions with the agriculture in the 30 m land use buffer, to illustrate the response of the landscape metrics to the increase of the agricultural area (Fig. 6). The Mean Patch Size presented lower values and low variability with the increasing agricultural area. The same pattern was observed for the Mean Shape Index, albeit with higher variability with increasing agricultural areas.

4. Discussion

4.1. Structure of the riparian vegetation

Numerous studies on the ecology and management of riparian zones seek to relate human disturbances in the surrounding landscapes with degradation of riparian vegetation (Baker et al., 2007; Malanson and Cramer, 1999). The use of field-based methods over large riparian areas is very time-consuming and often results in the

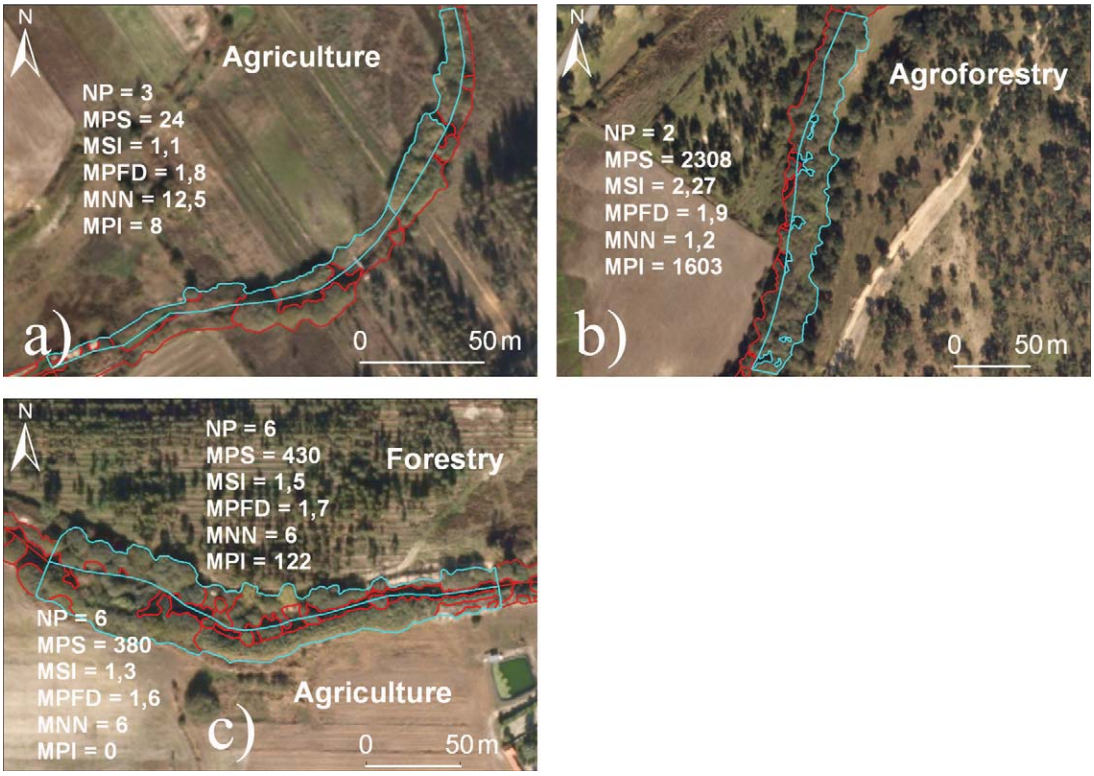

Fig. 5. Values of the landscape metrics for the tree cover class with adjacent land use of: (a) agriculture, River Chouto; (b) agroforestry, River Chouto; and (c) forestry and agriculture, River Muge.

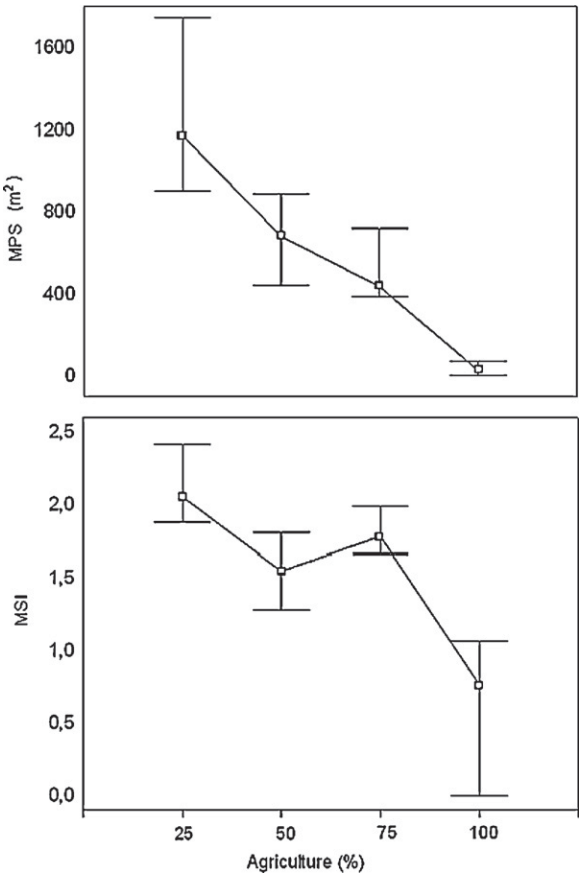

Fig. 6. Median, 25, and 75 quartiles for the Mean Patch Size (MPS) and Mean Shape Index (MSI) for the tree cover class with the increase of the agricultural areas in the 30 m buffer (9 subsamples; 28 sampling units per subsample).

loss of the overall perception of the landscape, making it difficult to propose management guidelines, like forestation of degraded areas, stock management, establishment of riparian buffers, control of invasive plants, or to help managers prioritize the places to restore, improve, or protect. Landscape metrics, such as Mean Patch Size, Mean Nearest-Neighbor Distance, or Mean Proximity Index, can be used as proxies of riparian width, longitudinal continuity and fragmentation (Johansen and Phinn, 2006), and therefore indicate the status of the riparian vegetation. The present study uses a set of landscape metrics and proposes a combined approach in order to characterize the structure of the riparian vegetation. It is widely recognized that combining landscape metrics from the same category, such as the Number of Patches and Mean Patch Size (Apan et al., 2002), is necessary for there to be a reliable evaluation of the structure of riparian vegetation.

In addition to confirming this, the present study points to the advantage of a complementary approach using landscape metrics from diverse categories. For instance, the joint use of area/density and shape metrics, such as the Number of Patches and Mean Shape Index, and metrics of connectivity (e.g. Mean Nearest-Neighbor Distance, Mean Proximity Index), helps characterize the structure of riparian vegetation. This was the case with wide well-preserved riparian vegetation stretches, which consistently displayed large connected tree patches with complex shapes, whereas herbaceous vegetation was characterized by elongated and connected patches with simple shapes. These findings can also help to identify highly degraded riparian zones, such as those in Portugal's coastal watersheds, which are invaded by the alien species *Arundo donax* L. (giant reed). The giant reed forms dense, monotypic stands, and thus high connected patches, but with simple stretched shapes, which can be identified using a combination of landscape metrics like the Mean Nearest-Neighbor Distance, Mean Proximity Index, Mean Shape Index and Number of Patches. However, knowledge of the hydrogeomorphological background of watercourses is still indispensable, since the narrow riparian zones that are naturally found in first-order streams mimic the degraded riparian vegetation, with small linear patches and low inter-connectivity.

The shrub and herbaceous cover classes were naturally underestimated, due to the superimposition of canopies. However, distinguishing between the tree and shrub cover classes is feasible using the type of high-resolution images to which we had access. Most studies using remote sensing have only considered the riparian woody vegetation, shrubs and trees (Apan et al., 2002; Schuft et al., 1999). Whereas for more detailed assessments, it is necessary to characterize the canopy and subcanopy surface topography, and other remote sensing techniques, such as the LIDAR sensors, broad beam, full return with high sampling rates (Goetz, 2006), are recommended.

4.2. Spatial autocorrelation assessment

This work also points to the importance of quantifying and taking into account the spatial component of the data, which is particularly relevant in riparian vegetation studies, due to its linear nature. In the present study most of the landscape metrics revealed a high global spatial autocorrelation, and also local patterns of spatial dependence. By mapping the Local Moran's *I* it is possible to identify the sampling units with highest spatial dependence (Fig. 7a) and spatial independence (Fig. 7b), per landscape metric, which can provide site-specific information for management of degraded areas. Exceptionally, the connectivity metric Mean Proximity Index showed a spatially random pattern for the tree cover class; however, this could be explained by the selection of the connectivity threshold (5 m), rather than by spatial independence of data distribution. The spatial autocorrelation patterns we observed can be explained by historical factors (Dormann, 2007; Segurado et al., 2006), or biotic factors (Legendre, 1993), or environmental variables (Legendre and Fortin, 1989). This study also suggests a spatial autocorrelation evaluation procedure for the influence of the surrounding land use in the riparian structure, using two approaches: incorporation of the spatial component; and the use of spatially independent Sampling Units. The former procedure revealed a high dependency of the data on the spatial component, and a decrease in the extent to which land use variables helped explain the total variance of the structure of riparian vegetation. The second approach, by removing the spatial autocorrelation, led to a significant increase in the variance explained by land use, although we inevitably lost biological information due to subsampling.

4.3. Influence of land use in the structure of the riparian vegetation

In general, there was an agreement between the expected and the observed responses of the landscape metrics due to the influence of land use. The present study clearly showed that riparian tree patches affected by nearby agricultural areas are characterized by a low number of small patches, whereas in the riparian areas of Cedar River, USA, Timm et al. (2004) observed degraded riparian areas with numerous small patches. For management purposes, a clear referential of well-preserved riparian vegetation in the region is therefore needed in order to define the near-natural spatial patterns and to further identify possible changes due to land use. This result can be also due to different magnitudes of land use pressure; thus low numbers of small patches in our area can be indicative of a highly degraded landscape. In contrast to our results, Apan et al. (2002) did not observe differences in patch configurations

Fig. 7. Morans' *I* and *z*-score for the Mean Patch Size (MPS) for the tree cover class. Illustration of: (a) high spatial dependence (River Sôr); and (b) spatial independence (River Muge).

(namely Mean Shape Index and Mean Fractal Dimension Index values), possibly due to the coarse resolution of the mapping resources (Baker et al., 2007). The low representation of the remaining land use classes in the study area did not make it possible to achieve a consistent pattern in the relationships between the land uses and the structure of riparian vegetation. Nevertheless, the values of the landscape metrics point towards the degradation of the riparian vegetation along the land use pressure gradient, from agroforestry to urban land uses.

This study found that the proximal land use has a greater effect on the structure of the riparian vegetation than distal land use, as has been suggested by studies in other geographic areas (Bott et al., 2006; Bunn and Davies, 2000; von Schiller et al., 2008) and by a precursor study in the River Tagus watershed by Ferreira et al. (2005). The latter stated that the "proximity and extension of land use patches interplay to influence the degree of changes in the riparian areas". In fact, an increment of around 14% of explained variance was achieved at the 30 m land use buffer, compared to the distal land use buffer. Even so, a large part of the variability in the structure of the riparian vegetation remained unexplained. Natural disturbances, such as fire, and the flash-flow hydrological regime typical of Mediterranean rivers, as well as site-specific human disturbances, such as tree clearing, sand extraction, and channel re-profiling, can help to explain part of the structure of riparian vegetation (McIntyre and Hobbs, 1999). The composition of riparian vegetation, especially the tree and shrub cover classes, could also partially explain the variability of the spatial patterns of riparian vegetation, and it is essential to detect non-native vegetation patches. We therefore advocate a comprehensive approach to the evaluation of the conservation status of riparian vegetation, which should be based on the interpretation of a set of landscape metrics and supported by *a posteriori* on-ground vegetation survey methods.

5. Conclusions and implications for riparian management

The structure of riparian vegetation can give essential clues for riparian management, and its assessment through landscape metrics can help prioritize where to restore, enhance, or protect riparian zones. Below we present the main findings of the present study and their implications for riparian management:

5.1. Spatial patterns of riparian vegetation can be consistently described with a combination of landscape metrics from various categories

Although it is important to use various configuration, isolation, fragmentation and distribution-based landscape metrics to assess degradation in detail, the ultimate selection of landscape metrics rely on the management or conservation goals in question. In certain situations, only one or two metrics are necessary. For instance, the Mean Proximity Index can be used to restore the longitudinal connectivity of riparian corridors for the movement or dispersal of a given target-species. A threshold distance for the species is defined *a priori* as the minimum distance between patches required for the use of the riparian area as an ecological corridor. The stretches that need to be restored are identified when the metric value is zero. For a quick identification of fragmented areas, the Mean Nearest-Neighbor Distance combined with the Mean Patch Size can give an idea of the overall degradation. On the other hand, when seeking to identify which riparian areas to protect, we suggest the use of spatial configuration metrics associated with ecological fluxes and species dynamics, such as the Mean Shape Index, Mean Patch Size and Mean Fractal Dimension Index, combined with metrics that evaluate fragmentation. The results of landscape metrics can be easily mapped on a GIS platform, thereby allowing the visualization of critical areas, and can also be used to monitor the success of the restoration or conservation actions.

High spatial resolution imagery – pixel size less than five metres – is required in order to assess the structure of riparian vegetation, and principally for the spatial configuration metrics Mean Shape Index and Mean Fractal Dimension Index. This resolution is needed to capture the complexity of the shape of riparian patches. Besides spatial resolution, other characteristics of the images must be considered. The radiometric resolution, which is the number of digital levels used to express the data collected by the sensor, should possess a minimum of eight bits (0–255 digital numbers). Otherwise the discrimination of the riparian cover classes by the perception of the grey level scale will be impaired. Where spectral resolution – the width and the number of the spectral bands of the sensor – is concerned, a "true color image" given by the combination of the blue, green and red bands in the visible region is appropriate to the application of this approach, since it does not make use of the numerical information in the bands.

5.2. Proximal land use has a greater effect on the structure of riparian vegetation than distal land use, especially in areas occupied by agriculture

Understanding the importance of the land uses and related human activities in river surroundings can undoubtedly help take practical managerial decisions. In Portugal there are no legislative tools that are specifically designed to limit the human pressures near riparian zones. The width of streamside public areas depends solely on the size of catchment areas. Protection buffers ought to take account of the impact of the different land uses on the river sur-

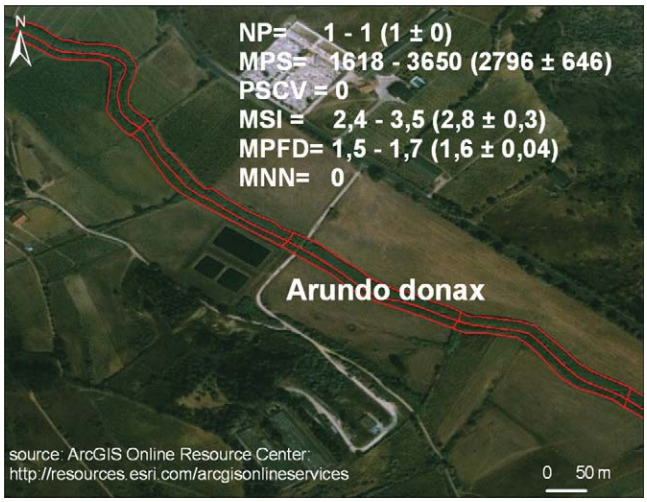

Fig. 8. Invasion of riverbanks by the giant reed; minimum and maximum values of landscape metrics; average ± SD in parentheses for giant reed patches (16 sampling units at River Aveiras, 4 km).
"World User Imagery" from the ArcGIS Resourcer Center (http://www.resources.esri.com/arcgisonlineservices), spatial resolution 1–2 m.

roundings and include measures that restrict access to the riparian area, sand extraction from riverbanks, and clear-cuts of riparian vegetation. Where possible, ecologically sustainable land uses in the proximity of the riparian area, such as the traditional agro-forestry systems, must be encouraged.

5.3. The pattern of degradation of riparian vegetation is characterized by a reduction in the number, size and complexity of riparian tree patches, along with a disproportionate patch distribution within the riparian landscape

One of the main contributions made by the present study was the characterization of the spatial patterns of the structure of riparian vegetation when impacted by land use. However, caution must be observed: (i) when transposing the present results to other regions; it is crucial to define a structural benchmark by assessing the patterns of near-natural riparian vegetation which is as unimpaired by human land use and other pressures as possible; (ii) with riparian areas invaded by alien, or composed of forestry species; in general, it is to be expected that connected and large riparian patches will correspond to well-preserved riparian areas, but they can be the result of monospecific stands of non-riparian or non-native species; (iii) with the spatial component of data; spatial autocorrelation can influence the results obtained when assessing effects of land use.

5.4. Additional outcomes of the present study for riparian management

Landscape metrics can be used to identify areas invaded by alien plants, such as those caused by the giant reed. The present approach is being improved for detecting and mapping invaded areas by the use of the spectral reflectance signature of this species. The giant reed form usually simple, large and elongated patches, that extend in continuous and almost monospecific stands along riverbanks (Fig. 8).

The present study also provided evidence that using just the tree cover class to characterize the structural features of woody riparian vegetation does not lead to a substantial loss of information. This has the advantage of being less time-consuming, especially in digitalizing the riparian patches, and also overcomes the problem of underestimated shrubby canopies.

Mapping the spatial autocorrelation of the riparian vegetation can provide additional management information. Riparian stretches that present autocorrelation can be object of the same management actions. It is to be expected that the vegetation structure along stretches that present spatial dependence will present similar responses to managerial activities, such as the restoration of longitudinal connectivity. The detection of local autocorrelation patterns can help locate site-specific riparian areas with similar patterns in the contiguous adjacencies within the riparian area, and also areas of transition with regard to changes in structural features, such as the fragmentation or diverse distribution of riparian patches.

Acknowledgements

This study received backing from the project RIPIDURABLE "Gestion Durable de Ripisylves" (INTERREG III-C Sul - 3S0125I), and from the Forest Research Centre, CEF through FEDER/POCI 2010. Maria R. Fernandes and Francisca C. Aguiar were supported by doctoral and post-doctoral scholarships from the Foundation for Science and Technology, Portugal, SFRH/BPD/29333/2006 and SFRH/BD/44707/2008, respectively. We acknowledge the Instituto Geográfico Português (IGP), which provided the airborne digital images through the FIGEE program. Thanks are also due to Pedro Segurado for suggestions concerning methods for estimating the spatial autocorrelation.

Appendix A. Supplementary data

Supplementary data associated with this article can be found, in the online version, at doi:10.1016/j.landurbplan.2010.11.001.

References

Aguiar, F.C., Ferreira, M.T., 2005. Human-disturbed landscapes: effects on composition and integrity of riparian woody vegetation in the Tagus River basin, Portugal. Environ. Conserv. 32 (1), 30–41.
Aguiar, F.C., Ferreira, M.T., Moreira, I., Albuquerque, A., 2000. Riparian types in Mediterranean basin. Aspects Appl. Biol. 58, 221–232.
Aguiar, F.C., Ferreira, M.T., Albuquerque, A., Rodriguez-Gonzalez, P., Segurado, P., 2009. Structural and functional responses of riparian vegetation to human disturbance: performance and scale-dependence. Fundam. Appl. Limnol. 175, 249–267.
Allan, J.D., 2004. Landscapes and riverscapes: the influence of land use on stream ecosystems. Ann. Rev. Ecol. Syst. 35, 257–284.
Anselin, L., 1995. Local indicators of spatial association-LISA. Geogr. Anal. 27, 93–115.
Apan, A.A., Raine, S.R., Paterson, M.S., 2002. Mapping an analysis of changes in the riparian landscape structure of Lockyer Valley catchment Queensland, Australia. Landscape Urban Plan. 59, 43–57.
Baker, M.E., Weller, D.E., Jordan, T.E., 2007. Effects of stream map resolution on measures of riparian buffer distribution and nutrient potential. Landscape Ecol. 27 (7), 973–992.
Bott, T.L., Montgomery, D.S., Newbold, J.D., Arscott, D.B., Dow, C.L., Aufdenkampe, A.K., Jackson, J.K., Kaplan, L.A., 2006. Ecosystem metabolism in streams of the Catskill Mountains (Delaware and Hudson River watersheds) and Lower Hudson Valley. J. N. Am. Benthol. Soc. 25, 1018–1044.
Bunn, S.E., Davies, P.M., 2000. Biological processes in running waters and their implications for the assessment of ecological integrity. Hydrobiologia 442/443, 61–70.
Congalton, R.G., Birch, K., Jones, R., Schriever, J., 2002. Evaluating remotely sensed techniques for mapping riparian vegetation. Comput. Electron. Agric. 37, 113–126.
Corbacho, C., Sánchez, J.M., Costillo, E., 2003. Patterns of structural complexity and human disturbance of riparian vegetation in agricultural landscapes of Mediterranean area. Agric. Ecosyst. Environ. 95, 495–507.
Cressie, N., 1991. Statistics for Spatial Data. John Wiley and Sons, New York.
Davis, P.A., Staid, M.I., Plescia, J.B., Johnson, J.R., 2002. Evaluation of Airborne Image Data for Mapping Riparian Vegetation within the Grand Canyon. Report of U.S Geological Survey, Arizona.
Décamps, H., Fortune, M., Gazelle, F., Patou, G., 1988. Historical influence of man on the riparian dynamics of fluvial landscape. Landscape Ecol. 1, 163–173.
Dixon, I., Douglas, M., Dowe, J., Burrows, D., 2006. Tropical Rapid Appraisal of Riparian Condition Version 1. River Management Technical Guidelines. No.7 Land and Water Australia, Canberra, Australia.
Dormann, C.F., 2007. Effects of incorporating spatial autocorrelation into the analysis of species distribution data. Global Ecol. Biogeogr. 16, 129–138.

Ferreira, M.T., Aguiar, F.C., Nogueira, C., 2005. Changes in riparian woods over space and time: influence of environment and land use. Forest Ecol. Manage. 212 (1–3), 145–159.
Forman, R.T.T., 1995. Land Mosaics: The Ecology of Landscapes and Regions. Cambridge University Press, Cambridge.
Forman, R.T.T., Godron, M., 1981. Patches and structural components for a landscape ecology. Bioscience 31, 733–740.
Fortin, M.-J., Dale, M.R.T., Hoef, J., 2002. Spatial analysis in ecology. Encyclopedia of Environmetrics, 4. John Wiley Sons, Ltd., Chichester, pp. 2051–2058.
Gallego-Fernández, J.B., García-Mora, M.R., García-Novo, F., 1999. Small wetlands lost: a biological conservation hazard in Mediterranean landscapes. Environ. Conserv. 26 (3), 190–199.
Goetz, S.J., 2006. Remote sensing of riparian buffers: past progress and future prospects. J. Am. Water Resour. Assoc. 2, 133–143.
González-del-Tánago, M., Garcia-Jalón, D., 2006. Attributes for assessing the environmental quality of riparian zones. Limnetica 25 (1–2), 389–402.
Guirado, M., Pino, J., Roda, F., 2007. Comparing the role of site disturbance and landscape properties on understory species richness in fragmented periurban Mediterranean forests. Landscape Ecol. 22, 117–129.
Hooke, J.M., 2006. Human impacts on fluvial systems in the Mediterranean region. Geomorphology 79, 311–335.
Inoue, M., Nakagoshi, M., 2001. The effects of human impact on spatial structure of the riparian vegetation along the Ashida river, Japan. Landscape Urban Plan. 53, 111–121.
Isaacs, E.H., Srivastava, M., 1989. An Introduction to Applied Geostatistics. Oxford University Press, New York, p. 146.
Johansen, K., Phinn, S., 2006. Mapping structural parameters and species composition of riparian vegetation using IKONOS and Landsat ETM+ Data in Australian Tropical Savannahs. Photogramm. Eng. Remote Sens. 72 (1), 71–80.
Johansen, K., Coops, N.C., Gergel, S.E., Stange, Y., 2007. Application of high spatial resolution satellite imagery for riparian and forest ecosystem classification. Remote Sens. Environ. 110 (1), 29–44.
Keitt, T.H., Bjornstad, O.N., Dixon, P.M., Citron-Pousty, S., 2002. Accounting for spatial pattern when modelling organism–environment interactions. Ecography 25, 616–625.
Legendre, P., 1993. Spatial autocorrelation: trouble or new paradigm? Ecology 74, 1659–1673.
Legendre, P., Fortin, M., 1989. Spatial pattern and ecological analysis. Vegetation 80, 107–138.
Lennon, J.J., 2000. Red-shifts and red herrings in geographical ecology. Ecography 23, 101–113.
Leps, J., Smilauer, P., 2003. Multivariate Analysis of Ecological Data using CANOCO. Cambridge University Press, Cambridge, UK.
Looy, K.V., Meire, P., Wasson, J.G., 2008. Including riparian vegetation in the definition of morphologic reference conditions for large rivers: a case study for Europe's western plains. Environ. Manage. 41, 625–639.
Malanson, G.P., Cramer, B.E., 1999. Landscape heterogeneity, connectivity and critical landscapes for conservation. Divers. Distrib. 5, 27–39.
McGarigal, K., Marks, B.J., 1994. FRAGSTATS Spatial Pattern Analysis Program for Quantifying Landscape Structure. Forest Science Department, Oregon State University, Corvallis.
McIntyre, S., Hobbs, R.A., 1999. A framework for conceptualizing human effects on landscapes and its relevance to management and research models. Conserv. Biol. 13 (6), 1282–1292.
Miller, J., Franklin, J., Aspinall, R., 2007. Incorporating spatial dependence in predictive vegetation models. Ecol. Model. 202, 225–242.
Moran, P.A.P., 1950. Notes on continuous stochastic phenomena. Biometrika 37, 17–23.
Muller, E., 1997. Mapping riparian vegetation along rivers: old concepts and new methods. Aquat. Bot. 58, 411–437.
Naiman, R.J., Décamps, H., 1997. The ecology of interfaces: riparian zones. Ann. Rev Ecol. Syst. 28, 621–658.
Oline, D.K., Grant, M.C., 2002. Scaling patterns of biomass and soil properties: an empirical analysis. Landscape Ecol. 17 (1), 13–26.
Plieninger, T., Wilbrand, C., 2004. Land use, biodiversity conservation, and rural development in the dehesas of Cuatro Lugares, Spain. Agrofor. Syst. 51, 23–34.
Rex, K.D., Malanson, G.P., 1990. The fractal shape of riparian patches. Landscape Ecol. 4, 249–258.
Schuft, M.J., Moser, T.J., Wigington, P.J., Stevens, D.L., McAllister, L.S., Chapman, S.S., Ernst, T.L., 1999. Development of landscape metrics for characterizing riparian-stream networks. Photogramm. Eng. Remote Sens. 65 (10), 1157–1167.
Segurado, P., Araújo, M.B., 2004. An evaluation of methods for modelling species distributions. J. Biogeogr. 31, 1555–1568.
Segurado, P., Araújo, M.B., Kunin, E., 2006. Consequences of spatial autocorrelation for niche-based models. J. Appl. Ecol. 43, 433–444.
Shandas, V., Alberti, M., 2009. Exploring the role of vegetation fragmentation on aquatic conditions: linking upland with riparian areas in Puget Sound lowland streams. Landscape Urban Plan. 90, 66–75.
StatSoftm, Inc., 2001. STATISTICA (Data Analysis Software System) ver 6. StatSoft, Inc., www.statsoft.com.
ter Braak, C.J.F., Smilauer, P., 2002. CANOCO Reference Manual and CanoDraw for Windows User's Guide: Software for Canonical Community Ordination (version 4.5) Ithaca. Microcomputer Power, NY.
Timm, R.K., Small, J.W., Leschine, T.M., Lucchetti, G., 2004. A screening procedure for prioritizing riparian management. Environ. Manage. 33 (1), 151–161.
Tobler, W., 1979. Cellular geography. In Miller, J. Franklin J., Aspinall, R., 2007 Incorporating spatial dependence in predictive vegetation models. Ecol. Model. 202, 225–242.
Turner, M.G., 1989. Landscape ecology: the effect of pattern on process. Annu. Rev Ecol. Syst. 20, 171–197.
von Schiller, D., Martí, E., Riera, J.L., Ribot, M., Marks, J.C., Sabater, F., 2008. Influence of land use on stream ecosystem function in a Mediterranean catchment. Freshwater Biol. 53, 2600–2612.
Wackernagel, H., 2003. Multivariate Geostatistics: An Introduction with Applications, 3rd ed. Springer, Berlin.
Ward, T.A., Tate, K.W., Atwill, E.R., 2003. Visual Assessment of Riparian Health. Rangeland Monitoring Series, Publication 8089, University of California.
Webster, R., Oliver, M.A., 2007. Geostatistics for Environmental Scientists, 2nd ed. John Wiley and Sons.
Wiens, J.A., 1976. Population responses to patchy environments. Annu. Rev. Ecol. Syst. 7, 81–120.
Wu, X.B., Thurow, T.L., Whisenant, S.G., 2000. Fragmentation and changes in hydrologic function of tiger bush landscapes, south-west Niger. J. Ecol., 790–800.
Yang, X., 2007. Integrated of remote sensing and geographic information systems in riparian vegetation delineation and mapping. Int. J. Remote Sens. 28 (2), 353–370.

PARTE III

Cartografia de Arundo donax L. e sua relação com o estado de integridade ripária

Capítulo 4

Spectral discrimination of giant reed (*Arundo donax* L.): a seasonal study in riparian areas

4.1 Síntese

Tendo como fundamento os resultados obtidos na segunda parte, a terceira parte desta dissertação visa aprofundar a detetabilidade remota das zonas ripárias invadidas por cana (*Arundo donax* L.), explorando a sua relação com o estado de integridade das galerias ribeirinhas. Após prévia prospeção de campo, são selecionados quatro troços de rio localizados na bacia hidrográfica do Tejo e das ribeiras do Oeste representativos do elevado grau de invasibilidade em zonas ripárias pela cana. No capítulo 4 é usada espectroradiometria de campo (FieldSpec3 – com amplitude espectral que varia desde os 350 aos 2500 mm, e 2151 bandas) e índices de separabilidade espectral (distâncias de Jeffries-Matusita e de Bhattacharya) para avaliar a distinção da cana face à vegetação envolvente (herbácea e lenhosa) bem como em relação ao caniço (*Phragmites australis* (Cav.) Trin. ex Steud.), espécie nativa e com características morfológicas semelhantes à da cana. São ainda recolhidas amostras espectrais em formações de cana sujeitas a medidas de controlo mecânico para avaliar a influência das ações humanas na identificação remota da espécie. As amostras de reflectância são recolhidas durante o período vegetativo e de senescência por forma a incluir a variação espectral sazonal de cada classe de vegetação, sendo os resultados discutidos em função dos atributos fenológicos, morfológicos e estruturais das formações de cana e das restantes classes de vegetação com os respetivos traços óticos. As bandas ótimas para a discriminação espectral da cana face à vegetação envolvente, são identificadas recorrendo a um procedimento estatístico hierárquico não paramétrico, com testes de Kruskal-Wallis seguidos da árvores de classificação e regressão (CART). O resultado é testado em três imagens de satélite simuladas, largamente usadas para cartografia ambiental: Landsat, IKONOS e SPOT. No final do trabalho são apresentados os pontos fortes e fracos da detetabilidade remota da cana em habitats ripários, bem como as implicações dos resultados obtidos na selecção da tipologia de imagens para cartografia de cana em áreas ripárias.

4.2 Artigo

Spectral discrimination of giant reed (*Arundo donax* L.): a seasonal study in riparian areas

Publicado como: Fernandes MR, Aguiar FC, Silva JMN, Ferreira MT, Pereira JMC. 2013. Spectral discrimination of giant reed (Arundo donax L.): a seasonal study in riparian areas. *Journal of Photogrammetry and Remote Sensing* 80, 80-90.

ISPRS Journal of Photogrammetry and Remote Sensing 80 (2013) 80–90

Contents lists available at SciVerse ScienceDirect

ISPRS Journal of Photogrammetry and Remote Sensing

journal homepage: www.elsevier.com/locate/isprsjprs

Spectral discrimination of giant reed (*Arundo donax* L.): A seasonal study in riparian areas

Maria Rosário Fernandes *, Francisca C. Aguiar, João M.N. Silva, Maria Teresa Ferreira, José M.C. Pereira

Universidade Técnica de Lisboa, Instituto Superior de Agronomia, Centro de Estudos Florestais, Tapada da Ajuda, 1349-017 Lisboa, Portugal

ARTICLE INFO

Article history:
Received 15 May 2012
Received in revised form 6 November 2012
Accepted 21 March 2013

Keywords:
Giant reed
Common reed
Phenological period
Riparian vegetation
Invasive plant species
Field spectroradiometry

ABSTRACT

The giant reed (*Arundo donax* L.) is amongst the one hundred worst invasive alien species of the world, and it is responsible for biodiversity loss and failure of ecosystem functions in riparian habitats. In this work, field spectroradiometry was used to assess the spectral separability of the giant reed from the adjacent vegetation and from the common reed, a native similar species.

The study was conducted at different phenological periods and also for the giant reed stands regenerated after mechanical cutting (giant reed_RAC). A hierarchical procedure using Kruskal–Wallis test followed by Classification and Regression Trees (CART) was used to select the minimum number of optimal bands that discriminate the giant reed from the adjacent vegetation. A new approach was used to identify sets of wavelengths – wavezones – that maximize the spectral separability beyond the minimum number of optimal bands. Jeffries Matusita and Bhattacharya distance were used to evaluate the spectral separability using the minimum optimal bands and in three simulated satellite images, namely Landsat, IKONOS and SPOT.

Giant reed was spectrally separable from the adjacent vegetation, both at the vegetative and the senescent period, exception made to the common reed at the vegetative period. The red edge region was repeatedly selected, although the visible region was also important to separate the giant reed from the herbaceous vegetation and the mid infrared region to the discrimination from the woody vegetation. The highest separability was obtained for the giant reed_RAC stands, due to its highly homogeneous, dense and dark-green stands. Results are discussed by relating the phenological, morphological and structural features of the giant reed stands and the adjacent vegetation with their optical traits. Weaknesses and strengths of the giant reed spectral discrimination are highlighted and implications of imagery selection for mapping purposes are argued based on present results.

1. Introduction

The giant reed or cane (*Arundo donax* L.), is an alien invasive riparian species that significantly threatens global biodiversity and riparian ecosystem functions in many regions of the world (Cushman and Gaffney, 2010; Everitt et al., 2008; Ge et al., 2008; Herrera and Dudley, 2003) causing numerous management, ecological and economic problems in the southwestern US, especially in California, and in many sub-tropical and warm-temperate regions of the world (Everitt et al., 2004; Ge et al., 2008). The giant reed is a tall-growing perennial grass, belonging to the *Poaceae* family. Flowering occurs in later summer and dries completely if the roots are not connected with groundwater. Giant reed invasions form large, monotypic and impenetrable stands that contribute to the degradation of the riparian habitat for native fauna, deplete water resources and trap sediments (Everitt et al., 2004; Quinn and Holt, 2008). Moreover, heavy infestations of giant reed frequently obstruct river flow and damage adjoining lands (Dudley, 2000).

In Portugal, the giant reed is largely widespread in western and southern coastal rivers where it was introduced for erosion control, as windbreaks, to confine properties and as a tutor for creeper-cultivated plants (Aguiar et al., 2007). There are some doubts on its geographic origin, and some authors consider this species as naturalized in Iberia, however it is included in the Annex I of Executive Law of 565/99 (Ministério do Ambiente, 1999), which legislate the introduction, use and commercialization of alien species.

There is a lack of knowledge about its spatial distribution and abundance and about the effectiveness of control measures, usually mechanical or combined with herbicides. Many water resource managers point giant reed as one of the major invasive plants in

* Corresponding author. Tel.: +351 213653380; fax: +351 213653338.
E-mail addresses: mrfernandes@isa.utl.pt (M.R. Fernandes), fraguiar@isa.utl.pt (F.C. Aguiar), joaosilva@isa.utl.pt (J.M.N. Silva), terferreira@isa.utl.pt (M.T. Ferreira), jmcpereira@isa.utl.pt (J.M.C. Pereira).

0924-2716/$ - see front matter © 2013 International Society for Photogrammetry and Remote Sensing, Inc. (ISPRS) All rights reserved.
http://dx.doi.org/10.1016/j.isprsjprs.2013.03.007

rivers and drainage ditches, with consequent financial losses (Aguiar et al., 1996). However, there are no studies at national level of the environmental damages and economic costs of *Arundo donax* invasions. Usually, giant reed invasions have been identified through field campaigns or by visual interpretation of aerial photographs. However, these hand-mapping tools are very time consuming and require intensive validation procedures to ensure that analyst interpretation is reliable (Goetz et al., 2003; Underwood et al., 2003). Other alternatives, such as random sampling methods, although more cost-time efficient, may generate a biased estimated distribution of invasion (Barnett et al., 2007). Systematic and comprehensive monitoring programs to detect invasions, perform time-series evaluations, and assessing the success of previous management activities should not be accomplished with subjectivity (Goetz, 2006). Thus, remote sensing techniques that use spectral information gather information and integrate it in geographical information systems to perform accurate automated mapping, are less costly and time consuming, with the advantage of covering large areas.

Spectral discrimination of vegetation species still remains a challenge due to the overlap of spectral signatures among species. Also, within species, spectral signatures can vary as a function of physiological and phenological changes throughout the year (Cochrane, 2000; Goetz et al., 2003; Hestir et al., 2008). Moreover, these variations may also occur due to foliage age (Roberts et al., 1998) and position in the canopy, among other factors. Few studies have shown how spectral signatures vary seasonally, investigated differences in growth forms, or even assessed the feasibility of distinguishing similar morphological co-occurring species.

Environmental spectroscopy using field spectrometers and airborne imaging spectrometers, has made substantial progress in recent years. The newest hyperspectral instruments, have more than 100 spectral channels of relative narrow bandwidths (5–10 nm) and have been successfully used to identify invasive species (Adam and Mutanga, 2009; Andrew and Ustin, 2008; DiPietro et al., 2002; Hamada et al., 2007; Noujdina and Ustin, 2008; Taylor et al., 2012; Underwood et al., 2003, 2007; Vaiphasa et al., 2007; Yang et al., 2012). Although hyperspectral data improves species discrimination by capitalizing on the biochemical and structural vegetation properties, it has to deal with a high dimensional complexity (Cochrane, 2000; Marcus et al., 2003; Underwood et al., 2003). Several methods can be used to reduce dimensionality, and amongst those Classification and Regression Trees (CART) have been successfully used for the specific purpose of mapping invasions in riparian areas (Andrew and Ustin, 2008; Hestir et al., 2008.) CART is a nonparametric statistic model, which presents a very intuitive interpretation, little data preparation requirements and the capability to easily process large amount of data (Breiman et al., 1984). It has been stated to be suitable to deal with the continuum of the waveband data and their inherent vegetation spectral variability (Hansen and DeFries, 2004; Ustin and Santos, 2010).

Previous studies focused on identifying the minimum number of optimal bands for vegetation discrimination (Adam and Mutanga, 2009; Schmidt and Skidmore, 2003; Thenkabail et al., 2004; Vaiphasa et al., 2005) However, this minimum subset of bands can diverge, depending on the feature reduction technique used and it is likely that more than one subset can discriminate vegetation similarly (Adam and Mutanga, 2009). Although the identification of several wavebands in the same region seems to be initially redundant, these adjacent wavebands contain valuable spectral information (Hamada et al., 2007) with the same level of discriminatory power, compared with the minimum number of optimal wavebands (Steinberg and Golovnya, 2007).

The main goal of this study is to evaluate the spectral separability of the giant reed from surrounding vegetation, in different phenological periods, using field spectrometry. Secondary objectives are:

- to test the spectral separability of giant reed from the native morphospecies *Phragmites australis* (Cav.) Trin. ex Steud, the common reed;
- to explore the differences in the spectral separability of giant reed some weeks after mechanical harvesting from the surrounding vegetation;
- to calculate an optimal subset of wavezones, that is a group of neighboring wavelengths where spectral separability is optimal – in addition to the minimum number of optimal wavebands needed for the discrimination of the various vegetation types;
- to compute the spectral separability of the various vegetation types (giant reed, common reed, and surrounding vegetation) using simulated imagery of three satellites largely used in the assessment of riparian quality, namely the Landsat, Ikonos and Spot.

2. Methods

2.1. Study area

The study was conducted in the riparian areas of River Aveiras and River Alcabrichel, between 39°10′N, 9°19′W and 39°06′N, 8°49′W, Western Portugal. The climate is typically Mediterranean with mild winters and hot dry summers. Annual rainfall ranges between 500 mm and 800 mm. The studied rivers have frequent winter flood peaks, followed by a gradual flow decline and subsequent drying during late spring and summer. The studied area has a calcareous geological background, and riverbeds are composed predominantly by sand and gravel, with riverbanks of sandy soils. The study area is densely populated and characterized by small agricultural patches (orchards, rice, maize and grazing lands) and industrial areas. Most rivers in the region are regulated and impacted due to water abstraction, sand extraction, effluent discharges, riparian vegetation cutting and channelization. Numerous rivers stretches are devoid of the riparian shrubby and woody strata, which have been replaced by monotypic stands of giant reed.

2.2. Spectral sampling

The sampling locations were selected following a prospective field survey performed in early Spring, 2010. We looked for representative invaded riparian areas, that is, monotypic and continuous (more than 300 m long) stands of giant reed. Dense canopies and stands ranging from six to seven meters width were considered requirements for minimizing effects of soil and water background on the in situ spectral sampling.

Spectral sampling was conducted in May 2010, which was considered the best season for the giant reed vegetative period (Ferreira et al., 2002), and in February 2011 for the senescent period. We collected the giant reed spectra some weeks after mechanical harvesting, hereafter designated by giant reed_RAC (RAC-regeneration after cutting), also in May 2010, although this phenological period can occur throughout the year. A field spectroradiometer (FieldSpec3, Analytical Spectral Devices (ASD) (2010)) was used to perform the spectral measurements on giant-reed, coexisting plant populations, namely riparian woody vegetation, herbaceous vegetation and of the morphospecies *P. australis*, the common reed.

A bucket truck with 4.5 m boom length was used in order to collect the spectral samples above the vegetation canopies. Spectral samples were taken every 10 m, for 500 m, in each sampling location, to avoid autocorrelation, at about 1.5 m above vegetation canopy, and with a 25° field of view.

The FieldSpec3 has a fiber optic bundle for light collection and covers the range 350–2500 nm. The visible and near infrared region (350–1050 nm) is measured with a spectral resolution of

3 nm at a sampling interval of 1.4 nm. The mid infrared region (1000–2500 nm) is measured with a spectral resolution of 10 nm at a sampling interval of 2.0 nm. All spectral samples were collected under sunny, cloudless and windless conditions and between 10:00 am–03:00 pm, during the vegetative period, and 11:00 am–02:00 pm, during the senescent period. A white reference calibration – Spectralon panel – was used to normalize for variations in atmospheric conditions and to convert the measurements into relative reflectance, allowing the comparison of spectral samples acquired at different periods (Milton et al., 2009).

Table 1 summarizes the number of spectral samples collected for giant reed and for the surrounding vegetation, in each phenological stage. Woody vegetation was measured only during the vegetative period, since the riparian woody vegetation was composed of deciduous species, mainly alders, willows and ashes.

2.3. Data analysis

2.3.1. Data dimensionality reduction and classification accuracy

A hierarchical analysis was performed to reduce data dimensionality ($n = 2151$ bands) to the most sensitive wavelengths able to discriminate the giant reed from the surrounding vegetation, in each phenological period, using the approach of Adam and Mutanga (2009). First, a Kruskal–Wallis test was performed to identify the wavelengths where significant spectral reflectance differences occur among all vegetation types. Kruskal–Wallis is a rank-based non-parametric test used to compare multiple independent samples. Compared with the equivalent one-way ANOVA, it has the advantage of calculating a unique initial table with the p-value of the test for all the wavelengths and all vegetation types, simultaneously. If the p-value is small, one can reject H_0 and conclude that the vegetation types have different spectral reflectance distributions (Hollander and Wolfe, 1999; Quinn and Keough, 2002). We select a 95% confidence level to ensure that no crucial wavelengths for the discrimination of vegetation types were left out. Then, a post hoc Dunn test was performed at each significant wavelength, for all pairs (giant reed vs. herbaceous vegetation; giant reed vs. woody vegetation; giant reed vs. common reed) for the vegetative, the senescent periods and for giant reed_RAC.

We used Classification and Regression Trees (CART) to further reduce the number of wavelengths previously selected by the post hoc Dunn's test. CART was also used to assess the classification accuracy for the giant reed and for the adjacent vegetation. CART is a nonparametric and nonlinear method that classifies the data using a top-down sequential binary splitting mechanism based on a set of rules. In this study, we developed a classification tree, since the independent variable (spectral reflectance) is continuous and the dependent variable is categorical (vegetation type). With this technique, data are consequently split into two subsets showing the least impurity, i.e. by reducing the deviance from the mean of the dependent variable or in other words, maximizing the homogeneity inside each child node relative to the dependent variable. A cost complexity pruning method was used to obtain a final tree that represents a compromise between minimizing the error and the tree complexity. In the end of the algorithm only the spectral bands that produce small misclassification rates, and simultaneously avoid the "overfitting" of the model, were selected. We additionally used another approach for the final selection of the optimal bands, so-called wavezones. To identify the wavezones, besides using the CART primary splitters, we used all surrogate wavelengths that had simultaneously an association level of 1 with each primary splitter and a level of improvement for the CART model equal to each primary splitter. This method was originally proposed by Breiman et al. (1984) to assign values to missing data, by measuring the degree of suitability of a variable to substitute another variable. However, in this study we used this method to identify all spectral bands in the vicinity of each primary splitter, with the same optimal ability to separate the vegetation types. For more information about CART see Breiman et al. (1984) and Tso and Mather (2009).

Finally, we explored future application of this work with satellite or airborne images. The spectral data were divided into broad spectral regions: blue (350–449 nm), green (450–549 nm), red (550–649 nm), red-edge (650–749 nm), near infrared (750–1299 nm) and mid infrared (1300–2500 nm).

The atmospheric water absorption bands were placed between 1360–1420 nm, 1810–1960 nm and 2450–2500 nm during the vegetative period, and between 1360–1400 nm, 1820–1920 nm and 2450–2500 nm during the senescent period. These bands were excluded from the CART analysis.

Additionally, the red edge position was determined, i.e. the wavelength of maximum positive slope, for each vegetation class, by calculating the highest peak in the first derivative of the spectrum. The red edge position is a spectral feature that is frequently used to characterize vegetation types, since it is a stable estimation of foliar chlorophyll and nitrogen contents. It is less sensitive to the effect of leaf and canopy biophysical parameters and environmental conditions (Cochrane, 2000; Filella and Peñuelas, 1994).

2.3.2. Spectral separability

The spectral separability between giant reed and the other vegetation types was measured by computing the Jeffries–Matusita (JM) and the Bhattacharya (BT) distances using the optimal primary splitter bands selected by the CART analysis. Both JM and BT represent a measure of the average distance between two class density functions (Swain and Davis, 1978; Richards and Jia, 2006). The JM distance has an asymptotic behavior with lower and upper values that vary, respectively, between 0 and 1.414. A JM value of 1.414 indicates a perfect separability, whereas a value of 0 corresponds to a complete overlap between the spectral signatures. The BT distance does not have an upper limit, thus allowing for the identification of the highest spectral separability between giant reed and the adjacent vegetation.

A separability analysis between the giant reed and the other vegetation types, for all phenological periods and for giant reed_RAC and the other vegetation types, was computed by simulating data of three satellites: Ikonos, Landsat and SPOT. Ikonos is a high multispectral resolution satellite (3.2 m of spatial resolution) with four wavelength bands, namely: blue (450–520 nm), green (520–600 nm), red (630–690 nm) and near infrared (760–900 nm). The Enhanced Thematic Mapper Plus (ETM+) carried on Landsat satellite is a medium spatial resolution satellite (30 m) with seven wavelength bands: blue (450–515 nm), green (525–605 nm), red (630–690 nm), near infrared (775–900 nm), mid infrared (1550–1750 nm and 2090–2350 nm), and one band positioned in the thermal region (10.40–12.50 μm), not used in this study. The

Table 1
Number of spectral samples collected for giant reed, common reed, giant reed_RAC, and adjacent vegetation classes, during the vegetative and senescent period; RAC – regeneration after cutting.

Vegetation	Phenological period	# Spectral samples
Giant reed	Vegetative	105
	Senescent	75
	Giant reed_RAC	25
Herbaceous vegetation	Vegetative	45
	Senescent	25
Woody vegetation	Vegetative	55
Common reed	Vegetative	30
	Senescent	45

imaging device HRVIR supported by SPOT satellite is a medium spatial resolution satellite (20 m) and has four bands: green (500–590 nm), red (610–680 nm), near infrared (780–890 nm) and mid infrared (1580–1750 nm) (Richards and Jia, 2006). Satellite data were reproduced by averaging reflectance values collected with the Fielspec3 in the spectral ranges of each sensor.

A classification error (ε) was calculated for all separability results using the relationship established by Lee and Choi (2000) for the estimate error of the Gaussian maximum likelihood classifier from the Bhattacharya distance. According to the referred study, Bhattacharya distance values higher than 4 correspond to a classification error smaller than 0.2%.

All analyses were performed with IBM SPSS Statistics version 19 and Matlab 6.5.

3. Results

Significant differences were observed in the spectral reflectance amongst all the vegetation types, throughout the spectral range under analysis (n = 2049 wavelengths in the vegetative period, n = 2086 wavelengths in the senescent period and n = 2059 wavelengths in the RAC stage) using the Kruskal–Wallis tests, at 95% confidence level. The post hoc Dunn tests allowed a slight reduction in the number of significant wavelengths for the discrimination between the giant reed and the adjacent vegetation. The only exception occurred between the giant reed and the common reed, where only few wavelengths separated the two species in the vegetative period (Fig. 1).

The remaining significant wavelengths were further reduced using CART to obtain the optimal minimum number of wavelengths (primary splitters). The smallest number (three) of primary splitters was obtained for the giant reed vs. common reed in the vegetative period, while 28 bands significantly discriminate the giant reed from the herbaceous vegetation and from the woody vegetation, both in the vegetative period.

Table 2 shows the optimal wavelengths that discriminate giant reed from the adjacent vegetation, in each phenological period. These wavelengths were spread all over the spectral range of analysis, but were frequently located in the red edge region.

The spectral signatures of the vegetation types in each phenological stage are shown in Fig. 2. They all exhibit the typical spectral signature of vegetation, characterized by a transition from low reflectance in the visible region to high reflectance in the near infrared region, followed by two regions of decreasing reflectance due to the water absorption bands. The only exception was the low reflectance observed in the near infrared for common reed in the senescent period. The optimal wavezones (all variables, CART surrogate method) for the discrimination of giant reed from the adjacent vegetation are highlighted by grey shaded areas in Fig. 2. These wavezones are composed, in all cases, by a set of wavelengths contiguous to each initial discrete primary splitter, although the number of wavelengths that compose each wavezone is highly variable.

The spectral separability of giant reed from adjacent vegetation was maximal (JM = 1.414) when the optimal minimum subset of bands selected by CART (Table 3) was used. This result was consistent for all phenological periods, with the exception of the separability between the giant reed and the common reed in the vegetative period. In fact, the spectral discrimination of giant reed from the common reed morphospecies, was only observed for the senescent period and when wavelengths mainly located in the visible region were used.

Spectral separability between giant reed and herbaceous vegetation was higher in the vegetative period than in the senescent period. Slightly smaller values were observed for the separability from woody vegetation (Table 3).

The lowest classification accuracy was obtained for herbaceous vegetation (70.6%) in the senescent period and the high CART depth (4.3) for the herbaceous vegetation in the vegetative period (Appendix A). The number of bands able to discriminate herbaceous vegetation from giant reed was also highly variable between phenological periods, but the highest number of optimal bands for discrimination between the two groups was found in the vegetative period (Table 2, Fig. 2).

The spectral separability of giant reed from woody vegetation was obtained with the largest subset of wavezones (Fig. 1). These wavezones were located in the visible and near infrared regions, but there were also a large number of bands located in the mid infrared region (Fig. 2).

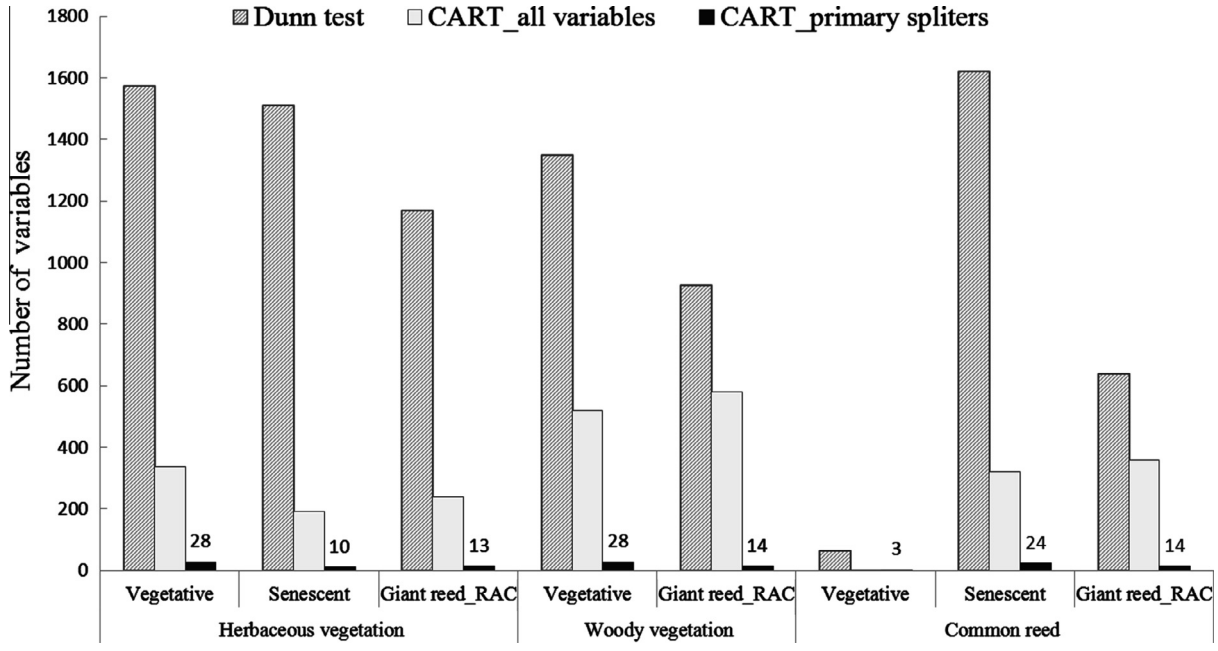

Fig. 1. Number of significant variables selected by post hoc Dunn tests and CART with all variables (surrogate method) and primary splitters (number of variables is shown), for the spectral discrimination of giant reed and giant reed_RAC from the adjacent vegetation classes during the vegetative and senescent periods; RAC – regeneration after cutting.

Table 2
Wavelengths (nm) selected by CART (primary spliters), in the spectral discrimination of giant reed and giant reed_RAC from the adjacent vegetation classes, during the vegetative and senescent periods, in each spectral region; RAC – regeneration after cutting.

		Giant reed vs. adjacent vegetation		
		Herbaceous vegetation (nm)	Woody vegetation (nm)	Common reed (nm)
Vegetative	Blue (350–449)	350	352, 355, 356, 372, 426, 445	–
	Green (450–549)	450, 522, 524, 528	450, 519	–
	Red (550–649)	609, 611, 612, 613, 621, 637, 649	620, 622, 632, 647, 649	–
	Red edge (650–749)	650, 681, 709, 737, 740, 747	650, 680, 694, 743, 746	–
	Near infrared (750–1299)	750, 1219	757, 758, 1155	–
	Mid infrared (1300–2061)	1441, 1444, 1508, 1598, 2094, 2340, 2408, 2432	1300, 1352, 1356, 1570, 2006, 2014, 2020	1974, 1976, 1981
Senescent	Blue (350–449)	–		352, 355, 357, 366, 386, 431
	Green (450–549)	520		462, 464, 474, 539, 543, 547
	Red (550–649)	550		550, 592, 597, 599
	Red edge (650–749)	693, 726, 738		702, 748, 749
	Near infrared (750–1299)	750, 1157, 1159		763
	Mid infrared (1300–2061)	1929, 2275		1300, 1354, 1940, 1966
Giant reed_RAC	Blue (350–449)	350	414	446, 448
	Green (450–549)	450	450, 526	450, 487
	Red (550–649)	550, 552	550, 649	550, 571
	Red edge (650–749)	700, 743	650, 713	732, 746, 747
	Near infrared (750–1299)	750, 754, 759, 829, 833, 852	762, 1245	752, 764
	Mid infrared (1300–2061)	1428	1300, 1354, 1358, 1360, 1490, 1786	1473, 1474, 1801

However, the highest values of spectral separability were found for the giant reed_RAC assemblages relatively to adjacent vegetation (Table 3). Bhattacharya values ranged from 34.46 to 77.50, respectively, for giant reed_RAC vs. common reed, and giant reed_RAC vs. herbaceous vegetation. Spectral reflectance of giant reed_RAC had the highest value in the red edge region, compared to the reflectance values of the other vegetation types in all phenological periods (near 50%), explained by the peak of greenness derived from the lush growth of these stands. Likewise, the CART classification accuracy for the giant reed_RAC with the adjacent vegetation was highest compared with giant reed, both in the vegetative and senescent periods (Appendix A).

The classification trees of giant reed in the vegetative period obtained with CART were more complex compared with the senescent period and the giant reed_RAC, i.e. they were deeper, and had more terminal nodes (Appendix A).

Wavelength surrogates of primary splitters were much more abundant in the visible compared with the mid-infrared, pointing out the uniqueness of the information provided in the bands located between 1300 nm and 2500 nm. Furthermore, the number of wavelengths identified by the CART surrogate method in the red edge region was very high when compared with the other spectral regions.

The red edge position of the common reed, herbaceous vegetation and woody vegetation was located at shorter wavelengths when compared with that of the giant reed (Table 4) in the vegetative period. On the contrary, the giant reed_RAC had the red edge position at the longest wavelengths of all vegetation types. Also, the herbaceous vegetation in the senescent period had a double peak and the common reed had its first derivative maximum outside the red edge region.

Using the simulated satellite bands all spectral separability values between giant reed and adjacent vegetation types were lower compared with the optimal bands selected by our methodology (Table 5). The simulated Landsat data obtained the highest spectral separability and the simulated SPOT data the lowest spectral discrimination of the three simulated satellite sensors.

4. Discussion and conclusion

4.1. Spectral discrimination of giant reed and spectral variability

Field spectrometry is able to capture a wide range of spectral variability in individuals of the same species or population. Some spectral characteristics of the vegetation can only be detected using field devices positioned very close to the canopies (Ustin and Santos, 2010). Consequently, discrimination between species using field spectrometry is very challenging, but results are consistent due to the incorporation of the existing spectral variability. Even more demanding is the selection of the finest subset of bands that can maximize the spectral separability between different types of vegetation.

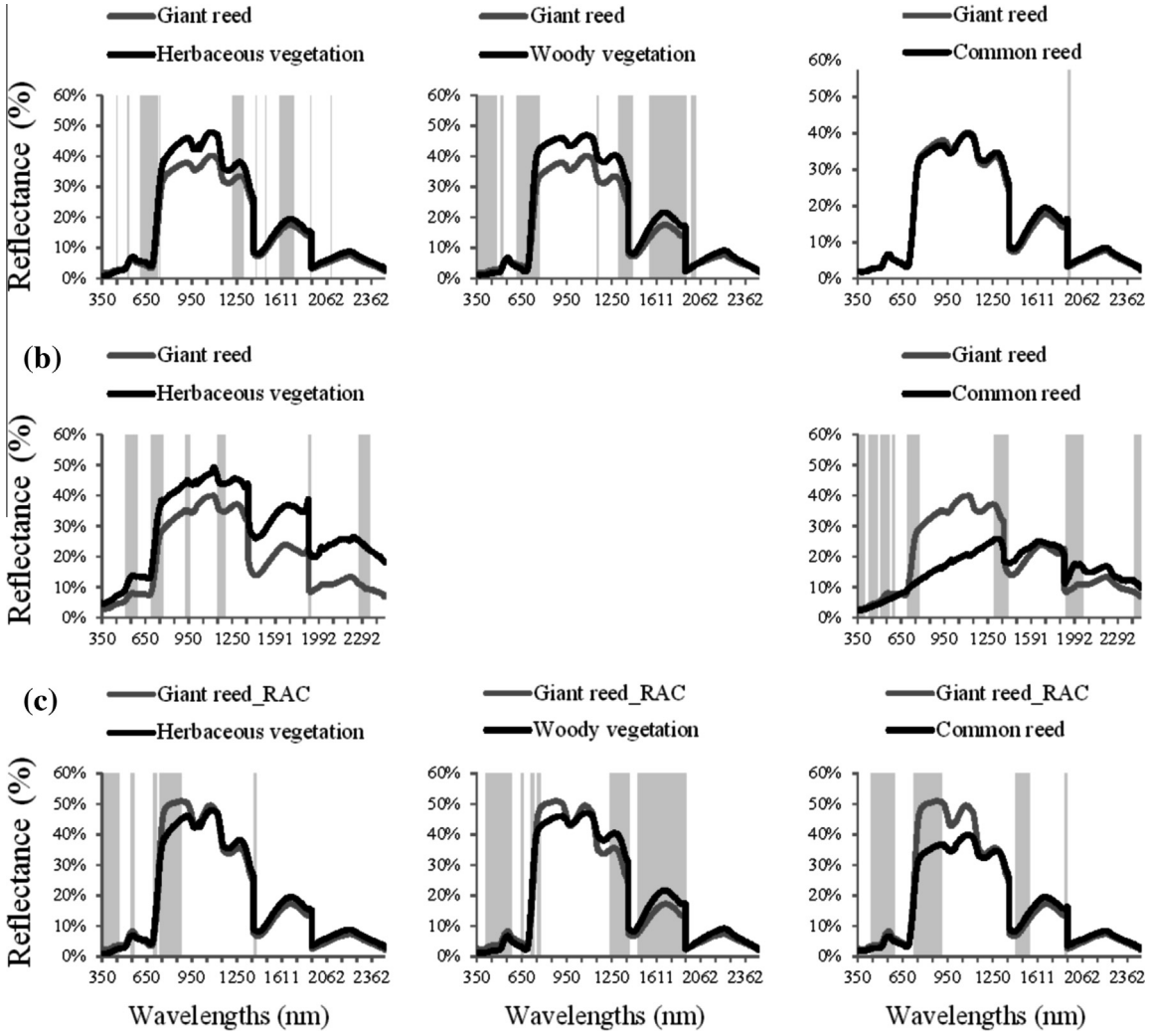

Fig. 2. Spectral signatures of each class pair in the (a) vegetative period, (b) senescent period and (c) giant reed_RAC. The grey areas show the wavebands where there are significant differences between each class pair selected by the CART, all variables, surrogate method.

Table 3
Spectral discrimination of giant reed and giant reed_RAC from the adjacent vegetation classes, during the vegetative and senescent periods. JM – Jeffries Matusita distance; BT – Bhattacharya distance; RAC – regeneration after cutting.

Phenological period		Giant reed vs. adjacent vegetation		
		Herbaceous vegetation	Woody vegetation	Common reed
Vegetative	JM	1.414	1.414	0.740
	BT	29.04	23.94	0.32
	(ε)	*	*	(23.33%)
Senescent	JM	1.414	–	1.414
	BT	15.97	–	20.48
	(ε)	*		*
Giant reed_RAC	JM	1.414	1.414	1.414
	BT	77.50	49.53	34.46
	(ε)	*	*	*

* Classification error smaller than 0.2%.

In this study, we found that giant reed was spectrally separable from the surrounding vegetation in both phenological periods, exception made for the giant reed and the common reed in the vegetative period, which are spectrally indistinguishable. The Kruskall–Wallis and the post hoc Dunn tests, although useful for an initial dimensionality reduction approach, were not able to identify the most sensitive bands for the giant reed discrimination. The hierarchical procedure, using CART, allowed for an adequate data dimensionality reduction and the identification of the most sensitive subset of bands, with the highest spectral separability (JM = 1.414), within each spectral region. The bands selected by CART with the surrogate method have the advantage of amplifying the areas of maximum separability between the giant reed and the other vegetation types. For instance, it is more obvious with this

Table 4
Red edge position for the giant reed, giant reed_RAC and the adjacent vegetation classes during the vegetative and senescent periods; RAC – regeneration after cutting.

Vegetation	Phenological period	Red edge position
Giant reed	Vegetative	724
	Senescent	722
	Giant reed_RAC	730
Herbaceous vegetation	Vegetative	718
	Senescent	717, 760
Woody vegetation	Vegetative	719
Common reed	Vegetative	719
	Senescent	763

method (Fig. 2) that the near infrared region and the green region are important for the discrimination of giant reed and common reed than by only using the primary splitters (Table 2). Likewise, the importance of the mid infrared region in the discrimination of giant reed from woody vegetation is emphasized by identifying the optimal wavezones compared with the primary splitters. This procedure can be used to select the most suitable satellite imagery, since the most sensitive zones of separability do correspond to a large number of surrogates.

4.2. Spectral discrimination of giant reed and relative spectral traits

Spectral discrimination of different types of vegetation is ruled by a combination of leaf and canopy spectral characteristics. In this study, wavelengths located in the near infrared region, and especially in the red edge, were recurrently selected in the discrimination of giant reed from adjacent vegetation. These results were also found in similar studies (e.g. Cochrane, 2000; Everitt et al., 2004; Hamada et al., 2007; Schmidt and Skidmore, 2003) that also revealed a high species-specific variability reflectance in this region. The giant reed has a high chlorophyll content combined with very high biomass production and photosynthetic rates (Papazoglou et al., 2005; Rossa et al., 1998). High concentration of chlorophyll and high values of leaf area index cause a displacement in the red edge position towards longer wavelengths (Chen and Chen, 2008; Ollinger, 2011), the so-called "red-shift" of the red edge, as noted in this study (Table 4). Moreover, other non-pigment biochemical constituents are also responsible for leaf-level spectral variability. Giant reed stems and leaves contain a wide array of noxious chemicals, including numerous alkaloids (Bell, 1997) that can also contribute to spectral distinction from adjacent vegetation. At the canopy-level, differences in foliage density, strata-complexity, crown gaps and "clumping level" can explain the spectra variability between giant reed and adjacent vegetation (Nagler et al., 2001; Ollinger, 2011). For instance, giant reed is characterized by forming very dense populations in connected monotypic stands, with a small number of canopy gaps when compared with the riparian woody vegetation (Fernandes et al., 2011). These canopy characteristics of the giant reed may provide particular spectral traits responsible for the decrease in reflectance in the near infrared region (Fig. 2) due to photon trapping (Alvarez-Añorve et al., 2008).

However, our study also identified the optimal bands for the discrimination of the giant reed in the visible and in the mid infrared region. While the spectral variability in the mid infrared region is mainly associated with differences in vegetation water content, in the visible, spectral differences between giant reed and the other vegetation types are mainly associated with variations in foliage cover and in plant pigments. Similar results were observed by Everitt et al. (2004) who considered the visible wavelengths, especially the green region, as crucial for giant reed discrimination. The giant reed stands observed displayed a mixture of branches of several orders, with the youngest leaves having a dark-green color, whereas the older leaves were often damaged and with a yellowish tone. In the senescent period, most of the leaves had a yellowish-brown color, but even at the peak of senescent, there still were some greenish leaves, apparently due to the water availability in the river channel (Fig. 3).

The herbaceous vegetation was mainly composed of a mixture of annual grasses, displaying various shades of green in both phenological periods. This floristic diversity can be responsible for a more complex CART classification of herbaceous vegetation in the vegetative period (CART depth = 4.3). However, in the senescent period the spectral variability was also associated with a patchy spatial pattern of bare soil, green plants and dried plants (Fig. 3b) which can explain the relatively poor classification accuracy (70.6%) (Appendix A) and the double peak of the red edge position (Table 4). The woody vegetation varies mainly between the light-green of alder, the grey-green of black willow, and the dark-green of ash. The complex three-dimensional structure of the woody vegetation is also responsible for the scattering patterns, which helps to explain why the near infrared and mid infrared regions are so important to distinguish this vegetation type.

4.3. Drawbacks and strengths of giant reed discrimination

As expected, the giant reed and common reed were not spectrally distinguishable in the vegetative period, as observed by Everitt et al. (2004) in invaded riparian areas of Texas, US.

These two species can be considered as morphospecies, since they have similar characteristics: Both are tall-growing, perennial

Table 5
Simulation of the spectral discrimination of giant reed and giant reed_RAC from the adjacent vegetation classes during the vegetative and senescent periods using three satellite sensors; JM – Jeffries Matusita distance; BT – Bhattacharya distance; RAC – regeneration after cutting.

Phenological period		Giant reed vs. adjacent vegetation								
		Herbaceous vegetation			Woody vegetation			Common reed		
		Ikonos	Landsat	SPOT	Ikonos	Landsat	SPOT	Ikonos	Landsat	SPOT
Vegetative	JM	1.314	1.340	1.170	1.403	1.411	1.296	0.830	1.250	1.203
	BT	1.99	2.28	1.15	4.15	5.40	1.833	0.42	1.52	1.28
	(ε)	(2.47%)	(1.68%)	(7.34%)	*	*	(3.08%)	(19.85%)	(4.69%)	(6.28%)
Senescent	JM	1.383	1.412	1.302	–	–	–	1.405	1.408	1.405
	BT	3.13	5.86	1.88	–	–	–	4.39	4.84	4.37
	(ε)	(0.50%)	*	(2.89%)				*	*	*
Giant reed_RAC	JM	1.411	1.413	1.383	1.413	1.414	1.388	1.404	1.414	1.413
	BT	5.45	7.67	3.15	7.71	12.91	3.30	4.25	10.47	7.16
	(ε)	*	*	(0.50%)	*	*	(0.51%)	*	*	*

* Classification error smaller than 0.2%.

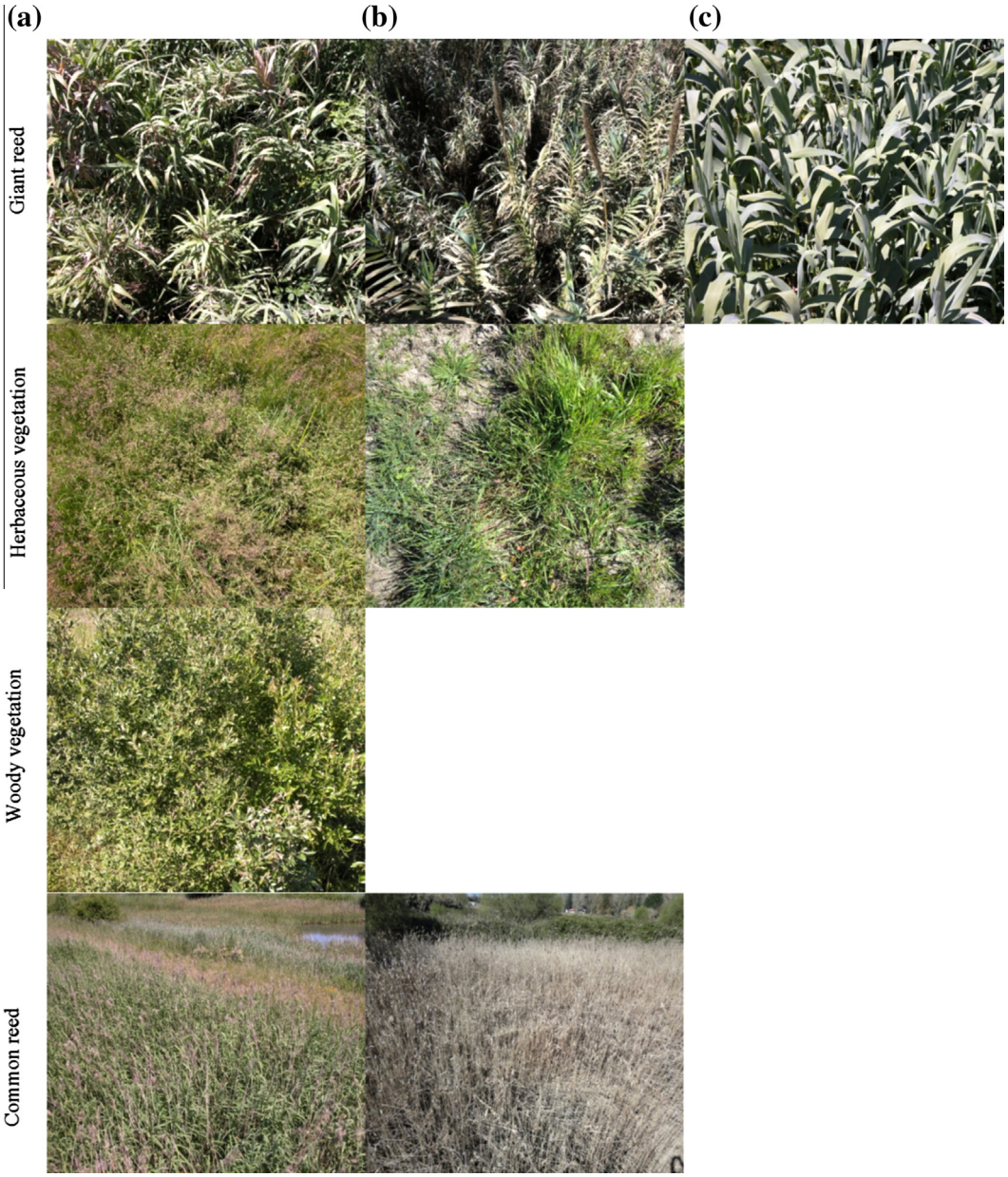

Fig. 3. Canopy and leaf characteristics of the giant reed and the adjacent vegetation classes during the (a) vegetative period, (b) senescent period, and for (c) giant reed_RAC; RAC – regeneration after cutting.

grass species, with green flowers arranged in a dense white plume (Pengra et al., 2007). The spectral distinction between the two species is only possible during the senescent period, when all common reed stands have a yellowish-brown color, with spectral signature atypical for vegetation (Fig. 2b), whereas the giant reed displays a mixture of green and yellowish-brown biomass (Fig. 3).

An interesting result was that the highest values of spectral separability were found between giant reed_RAC and adjacent vegetation, when compared with the giant reed without control measures. Regeneration of giant reed stands can occur in any season, only dependent on water supply. Giant reed_RAC represents the first year canes which are un-branched. These primary leaves are longer and wider than the second single year or older branched leaves and thus form highly homogeneous, dense dark-green stands (Decruyenaere and Holt, 2005) (Fig. 3c). The red edge was positioned at the longest wavelengths compared with the other vegetation types analysed (Table 4), which seems related to the high primary productivity and intensive vegetative growth. The high discriminant ability founded for regenerated stands can be very useful for mapping potential post-control invasions.

4.4. Selection of imagery and its implications for giant reed mapping

This study is a preliminary approach for giant reed effective mapping, using airborne or satellite imagery. The optimal wavelengths for the spectral discrimination of giant reed are only available in hyperspectral imagery. However, most of the current hyperspectral sensors are airborne, and image acquisitions is costly and coverage is limited. On the other hand, hyperspectral sensors available in satellite platforms, like the Hyperion imagery, still have low spatial resolution (30 m). Spatial resolution and especially high-scale resolution is crucial when assessing riparian ecological condition (Schuft et al., 1999). This is particularly true in Mediterranean areas, due to the limited width of riparian zones and high spatial variability (Congalton et al., 2002; Davis et al., 2002).

In our study, only the spectral potential of three sensors was assessed to detect giant reed invasions. In our simulated data, Landsat images were the most suitable, since it has a higher number of available bands (six) when compared with the simulated Ikonos or SPOT images (four), but also because two of the bands are positioned in the mid infrared region, which was found to be important to distinguish giant reed from woody vegetation (Fig. 2). Landsat imagery is still considered a highly cost-effective way to map invasions extensively. However, due to its coarse spatial resolution, high accuracy mapping only is feasible after giant reed become dense and largely widespread (Congalton et al., 2002; He et al., 2011; Underwood et al., 2003). Thus, selection of a very high spatial resolution multispectral imagery, such as Ikonos or QuickBird can, in some cases, produce better results, when compared with hyperspectral imagery with moderate spatial resolution, due to the drawback of the sub pixel spectral mixing (Carter et al., 2009). Additionally, high spatial resolution imagery allows for more accurate interpretation of the shape and texture of ground features (Goetz et al., 2003). Giant reed stands have a peculiar spatial structure characterized by elongated, with low edge complexity and highly-connected patches that can be remotely assessed and quantified using landscape metrics (Fernandes et al., 2011).

However, final selection of the imagery relies on a combination of the mapping goals and dominant surrounding land use. Based on our results, hyperspectral imagery with high spatial resolution is still needed to accurately distinguish giant reed from heterogeneous adjacent herbaceous vegetation, since high separability regions are concentrated in narrow wavezones, found throughout the spectral range under analysis (Fig. 2). Contrarily, to identify the regeneration of stands after cutting, high spatial resolution image, with coarse spectral resolution can be used, since the separability regions are located in broad wavezones in visible and in near infrared region. Similarly, imagery with broad spectral bands, mainly located in the visible region, is sufficient for the goal of distinguishing the giant reed from the common reed in the senescent period. For spectral discrimination of giant reed and the woody vegetation, additional information in the mid infrared region is necessary.

Further research on mapping giant reed invasions can be done by adding texture and context information (e.g. common reed is preferentially located in the river channel, whereas the giant reed occupies mainly riverbanks) to the discrimination classification process.

Acknowledgements

This study received backing from the EU funds (ERDF) from the project RICOVER "River Ricovery in the SW Europe" (Interreg IVB – SOE1/P2/P248) and from the Centro de Estudos Florestais, CEF through FEDER/POCI 2010. Maria R. Fernandes and Francisca C. Aguiar were supported by doctoral and post-doctoral scholarships from the Foundation for Science and Technology, Portugal, SFRH/BD/44707/2008 and SFRH/BPD/29333/2006, respectively. We are also grateful to the Engineer António Albuquerque for the precious help in the field prospection and field campaigns.

Appendix A.

		Giant reed vs. Herbaceous vegetation					
		Number nodes	Number terminal nodes	Tree depth	Giant reed	Herbaceous	Overall classification
Vegetative	Blue	3	2	1	99.0	97.1	98.6
	Green	11	6	5	95.2	88.6	93.6
	Red	15	8	7	100.0	62.9	90.7
	Red edge	15	8	4	99.0	100.0	99.3
	Near infrared	5	3	2	99.0	71.4	92.1
	Mid infrared	17	9	7	98.1	97.1	97.9
	Average	11	6	4.3	98.3	86.1	95.3
Senescent	Green	3	2	1	96.0	60.0	90.0
	Red	3	2	1	96.0	60.0	90.0
	Red edge	7	4	3	100.0	80.0	96.7
	Near infrared	7	4	3	100.0	53.3	92.2
	Mid infrared	5	3	2	98.7	100.0	98.9
	Average	5	3	2	98.1	70.6	93.5
Giant reed_RAC	Blue	3	2	1	100.0	100.0	100.0
	Green	7	4	3	100.0	100.0	100.0
	Red	5	3	2	80.0	85.7	84.0
	Red edge	5	3	2	100.0	100.0	100.0
	Near infrared	13	7	4	100.0	100.0	100.0
	Mid infrared	3	2	1	73.3	97.1	90.0
	Average	6	3.5	2.1	92.2	97.1	95.6

		Giant reed vs. Woody vegetation					
		Number nodes	Number terminal nodes	Tree depth	Giant reed	Woody	Overall classification
Vegetative	Blue	13	7	4	97.1	91.1	95.3
	Green	11	6	3	98.1	91.1	96.0
	Red	15	8	5	99.0	62.2	88.0
	Red edge	11	6	4	99.0	100.0	99.3
	Near infrared	7	4	3	97.1	77.8	91.3
	Mid infrared	15	8	4	100.0	93.3	98.0

Appendix A (*continued*)

	Average	12	6.5	3.8	98.3	85.9	94.6
Giant reed_RAC	Blue	3	2	1	100.0	97.8	98.3
	Green	5	3	2	100.0	100.0	100.0
	Red	9	5	4	100.0	97.8	98.3
	Red edge	5	3	2	100.0	100.0	100.0
	Near infrared	5	3	2	93.3	100.0	98.3
	Mid infrared	13	7	4	100.0	100.0	100.0
	Average	6.6	3.8	25	98.8	99.2	99.1

		Giant reed vs. Common reed					
		Number nodes	Number terminal nodes	Tree depth	Giant reed	Common reed	Overall classification
Vegetative	Mid infrared	13	7	4	97.1	75.0	93.6
	Average	13	7	4	97.1	75.0	93.6
Senescent	Blue	15	8	6	97.3	75.6	89.2
	Green	13	7	5	100.0	91.1	96.7
	Red	13	7	5	98.7	91.1	95.8
	Red edge	7	4	3	98.7	100.0	99.2
	Near infrared	3	2	1	96.0	100.0	97.5
	Mid infrared	9	5	3	100.0	97.8	99.2
	Average	10	5.5	3.8	98.4	92.6	96.2
Giant reed_RAC	Blue	11	6	5	100.0	100.0	100.0
	Green	7	4	3	100.0	100.0	100.0
	Red	13	7	6	100.0	90.0	94.3
	Red edge	7	4	3	100.0	100.0	100.0
	Near infrared	3	2	1	100.0	95.0	97.1
	Mid infrared	9	5	3	93.3	90.0	91.4
	Average	8.3	4.6	3.5	98.8	95.8	97.1

References

Adam, E., Mutanga, O., 2009. Spectral discrimination of papyrus vegetation (*Cyperus papyrus* L.) in swamp wetlands using field spectrometry. ISPRS Journal of Photogrammetry and Remote Sensing 64 (6), 612–620.

Aguiar, F.C., Ferreira, M.T., Albuquerque, A., Moreira, I., 2007. Alien and endemic flora on reference and non-reference sites from Mediterranean type-streams of Portugal. Aquatic Conservation: Marine and Freshwater Ecosystems 17 (4), 335–347.

Aguiar, F.C., Moreira, I., Ferreira, M.T., 1996. Perception of aquatic weed problems by water resources managers: a Percepção da Vegetação Aquática Infestante pelas Entidades Gestoras dos Recursos Hídricos. Revista de Ciências Agrárias 19 (4), 35–56.

Alvarez-Añorve, M., Quesada, M., de la Barrer, E., 2008. Remote sensing and plant functional groups. Physiology, ecology, and spectroscopy in tropical systems. In: Kalacska, M., Sánchez-Azofeifa, A. (Eds.), Hyperspectral Remote Sensing of Tropical and Sub-Tropical Forests, pp. 27–45.

Andrew, M.E., Ustin, S.L., 2008. The role of environmental context in mapping plants with hyperspectral image data. Remote Sensing of Environment 112 (12), 4301–4317.

Barnett, D.T., Stohlgren, T.J., Jarnevich, C.S., Chong, G.W., Ericson, J.A., Davern, T.R., Simonson, S.E., 2007. The art and science of weed mapping. Environmental Monitoring and Assessment 132 (1–3), 235–252.

Bell, G.P., 1997. Ecology and management of *Arundo donax*, and approaches to riparian habitat restoration in Southern California. In: Brock, J.H., Wade, M., Pysek, P., Green, D. (Eds.), Plant Invasions: Studies from North America and Europe. Backhuys Publishers, Leiden, The Netherlands, pp. 103–113.

Breiman, L.J.H., Friedman, R.A., Olshen, R., Stone, C.J., 1984. Classification and Regression Trees. Chapman & Hall/CRC, New York.

Carter, G.A., Lucas, K.L., Blossom, G.A., Lassitter, C.L., Holiday, D.M., Mooneyhan, D.S., Fastring, D.R., Holcombe, T.R., Griffith, J.A., 2009. Remote sensing and mapping of Tamarisk along the Colorado River, USA: a comparative use of summer-acquired Hyperion, Thematic Mapper and Quickbird data. Remote Sensing 1 (3), 318–329.

Chen, J., Chen, C., 2008. Correlation analysis between indices of tree leaf spectral reflectance and chlorophyll content. In: Proceedings of Commission VII. ISPRS Congress Beijing, 3–11 July, Beijing, China, pp. 231.

Cochrane, M.A., 2000. Using vegetation reflectance variability for species level classification of hyperspectral data. International Journal of Remote Sensing 21 (10), 2075–2087.

Congalton, R.G., Birch, K., Jones, R., Schriever, J., 2002. Evaluating remotely sensed techniques for mapping riparian vegetation. Computers and Electronics in Agriculture 37 (1), 113–126.

Cushman, J.H., Gaffney, K.A., 2010. Community-level consequences of invasion: impacts of exotic clonal plants on riparian vegetation. Biological Invasions 12 (8), 2765–2776.

Davis, P.A., Staid, M.I., Plescia, J.B., Johnson, J.R., 2002. Evaluation of Airborne Image Data for Mapping Riparian Vegetation within the Grand Canyon. Open-File Report of U.S. Geological Survey, Arizona. <http://geopubs.wr.usgs.gov/open-file/of02-470/> (accessed 02.11.12).

Decruyenaere, J.G., Holt, J.S., 2005. Ramet demography of a clonal invader, *Arundo donax* (Poaceae), Southern California. Plant and Soil 277 (1–2), 41–52.

DiPietro, D., Ustin, S.L., Underwood, E., 2002. Mapping the Invasive Plant Arundo Donax and Associated Riparian Vegetation Using AVIRIS. AVIRIS Airborne Geoscience Workshop Proceedings, Pasadena, CA.

Dudley, T.L., 2000. Arundo donax. In: Bossard, C.C., Randal, J.M., Hoshovsky, M.C. (Eds.), Invasive Plants of California's Wildlands, first ed. Univ. of California Press, Berkeley, California, pp. 53–58.

Everitt, J.H., Yang, C., Alaniz, M.A., Davis, M.R., Nibling, F.L., Deloach, C.J., 2004. Canopy spectra of giant reed and associated vegetation. Journal of Range Management 57 (5), 561–569.

Everitt, J.H., Yang, C., Fletcher, R., Deloach, C.J., 2008. Comparison of QuickBird and SPOT 5 satellite imagery for mapping giant reed. Journal of Aquatic Plant Management 46, 77–82.

Ferreira, M.T., Albuquerque, A., Aguiar, F.C., Catarino, L.F., 2002. Seasonal and yearly variations of macrophytes in a Southern Iberian River. International Association of Theoretical and Applied Limnology 27 (7), 3833–3837.

Fernandes, M.R., Aguiar, F.C., Ferreira, M.T., 2011. Assessing riparian vegetation structure and the influence of land use using landscape metrics and geostatistical tools. Landscape and Urban Planning 99 (2), 166–177.

FieldSpec® 3 User Manual, ASD Document 600540 Rev. J, 2010. Analytical Spectral Devices, Inc., Boulder, CO, USA. <http://support.asdi.com/Products/Products.aspx> (accessed 06.11.12).

Filella, I., Peñuelas, J., 1994. The red edge position and shape as indicators of plant chlorophyll content, biomass and hydric status. International Journal of Remote Sensing 15 (7), 1459–1470.

Ge, S., Carruthers, R.I., Spencer, D.F., Yu, Qian., 2008. Canopy assessment of biochemical features by ground-based hyperspectral data for an invasive species, giant reed (*Arundo donax*). Environmental Monitoring and Assessment 147 (1–3), 271–278.

Goetz, S.J., Wright, R.K., Smith, A.J., Zinecker, E., Schaub, E., 2003. IKONOS imagery for resource management: Tree cover, impervious surfaces, and riparian buffer analyses in the mid-Atlantic region. Remote Sensing of Environment 88 (1–2), 195–206.

Goetz, S.J., 2006. Remote sensing of riparian buffers: past progress and future prospects. Journal of the American Water Resources 42 (1), 133–143.

Hamada, Y., Stow, D.A., Coulter, L.L., Jafolla, J.C., Hendricks, L.W., 2007. Detecting Tamarisk species (*Tamarix* spp.) in riparian habitats of Southern California using high spatial resolution hyperspectral imagery. Remote Sensing of Environment 109 (2), 237–248.

Hansen, M.C., DeFries, R.S., 2004. Detecting long-term global forest change using continuous fields of tree-cover maps from 8-km Advanced Very High Resolution Radiometer (AVHRR) data from the years 1982–99. Ecosystems 7 (7), 695–716.

He, K.S., Rocchini, D., Neteler, M., Nagendra, H., 2011. Benefits of hyperspectral remote sensing for tracking plant invasions. Diversity and Distributions 17 (3), 381–392.

Herrera, A.M., Dudley, T.L., 2003. Reduction of riparian arthropod abundance and diversity as a consequence of giant reed (*Arundo donax*) invasion. Biological Invasions 5 (3), 167–177.

Hestir, E.L., Khanna, S., Andrew, M.E., Santos, M.J., Viers, J.H., Greenberg, J.A., Rajapakse, S.S., Ustin, S.L., 2008. Identification of invasive vegetation using hyperspectral remote sensing in the California Delta ecosystem. Remote Sensing of Environment 112 (11), 4034–4047.

Hollander, M., Wolfe, D.A., 1999. Nonparametric Statistical Methods, second ed. John Wiley & Sons Inc., New York.

Lee, C., Choi, E., 2000. Bayes error evaluation of the Gaussian ML classifier. *IEEE* Transactions on Geoscience and Remote Sensing 38 (3), 1471–1475.

Marcus, W.A., Legleiter, C.J., Aspinall, R.J., Boardman, J.W., Crabtree, R.L., 2003. High spatial resolution hyperspectral mapping of in-stream habitats, depths, and woody debris in mountain streams. Geomorphology 55 (1–4), 363–380.

Milton, E.J., Schaepman, M.E., Anderson, K., Kneubuhler, M., Fox, N., 2009. Progress in field spectroscopy. Remote Sensing of Environment 113 (1), S92–S109.

Ambiente, Ministério do, 1999. Decreto-Lei n°565/99 de 21 de Dezembro: Espécies não indígenas da flora e da fauna. Diário da República I – Série A 295, 9100–9114.

Nagler, P.L., Glenn, E.P., Huete, A.R., 2001. Assessment of spectral vegetation indices for riparian vegetation in the Colorado River delta, Mexico. Journal of Arid Environments 49 (1), 91–110.

Noujdina, N.V., Ustin, S.L., 2008. Mapping downy brome (*Bromus tectorum*) using multidate AVIRIS data. Weed Science 56 (1), 173–179.

Ollinger, S.V., 2011. Sources of variability in canopy reflectance and the convergent properties of plants. New Phytologist 189 (2), 375–394.

Papazoglou, E.G., Karantounias, G.A., Vemmos, S.N., Bouranis, D.L., 2005. Photosynthesis and growth responses of giant reed (*Arundo donax* L.) to the heavy metals Cd and Ni. Environment International 31 (2), 243–249.

Pengra, B.W., Johnston, C.A., Loveland, T.R., 2007. Mapping an invasive plant, *Phragmites australis*, in coastal wetlands using the EO-1 Hyperion hyperspectral sensor. Remote Sensing of Environment 108 (1), 74–81.

Quinn, L.D., Holt, J.S., 2008. Ecological correlates of invasion by *Arundo donax* in three southern California riparian habitats. Biological Invasions 10 (5), 591–601.

Quinn, G.P., Keough, M.J., 2002. Experimental Design and Data Analysis for Biologists. University Press, United Kingdom, Cambridge.

Richards, J.A., Jia, X., 2006. Remote Sensing Digital Image Analysis, fourth ed. Springer, New York.

Roberts, D.A., Nelson, B.W., Adams, J.B., Palmer, F., 1998. Spectral changes with leaf aging in Amazon Caatinga. Trees 12 (6), 315–325.

Rossa, B., TuAers, A.V., Naidoo, G., von Willert, D.J., 1998. *Arundo donax* L. (Poaceae) – a C3 species with unusually high photosynthetic capacity. Botanica Acta 111, 216–221.

Schmidt, K.S., Skidmore, A.K., 2003. Spectral discrimination of vegetation types in a costal wetland. Remote Sensing of Environment 85 (1), 92–108.

Schuft, M.J., Moser, T.J., Wigington, P.J., Stevens, D.L., McAllister, L.S., Chapman, S.S., Ernst, T.L., 1999. Development of landscape metrics for characterizing riparian-stream networks. Photogrammetric Engineering and Remote Sensing 65 (10), 1157–1167.

Swain, P.H., Davis, S.M., 1978. Remote Sensing: The Quantitative. Approach, first ed. McGraw Hill International Book Company, New York.

Steinberg, D., Golovnya, M., 2007. Developers of TreeNet, MARS, RandomForests and Other Award-winning data Mining and Predictive Analytics Tools. CART® 6.0 User's Guide. Salford Systems. San Diego. California, USA.

Taylor, S., Kumar, L., Reid, N., Lewis, C.R.G., 2012. Optimal band selection from hyperspectral data for *Lantana camara* discrimination. International Journal of Remote Sensing 33 (17), 5418–5437.

Thenkabail, P.S., Enclona, E.A., Ashton, M.S., Van Der Meer, B., 2004. Accuracy assessments of hyperspectral waveband performance for vegetation analysis applications. Remote Sensing of Environment 91 (3–4), 354–376.

Tso, B., Mather, P.M., 2009. Classification Methods for Remotely Sensed Data, second ed. CRC Press, Taylor and Francis Group, Florida.

Underwood, E.C., Ustin, S.L., DiPietro, D., 2003. Mapping nonnative plants using hyperspectral imagery. Remote Sensing of Environment 86 (2), 150–161.

Underwood, E.C., Ustin, S.L., Ramirez, C.M., 2007. A comparison of spatial and spectral image resolution for mapping invasive plants in coastal California. Environmental Management 39 (1), 63–83.

Ustin, S.L., Santos, M.J., 2010. Spectral identification of native and non-native plant species. In: Proceedings of ASD and IEEE GRS; Art, Science and Applications of Reflectance Spectroscopy Symposium, vol. II, Boulder, Colorado, February 23–25, pp. 17.

Vaiphasa, C., Ongsomwang, S., Vaiphasa, T., Skidmore, A.K., 2005. Tropical mangrove species discrimination using hyperspectral data: a laboratory study. Estuarine, Coastal and Shelf Science 65 (1–2), 371–379.

Vaiphasa, C., Skidmore, A.K., Boer, W.F., Vaiphasa, T., 2007. A hyperspectral band selector for plant species discrimination. ISPRS Journal of Photogrammetry and Remote Sensing 62 (3), 225–235.

Yang, C., Goolsby, J.A., Everitt, J.H., Du, Q., 2012. Applying six classifiers to airborne hyperspectral imagery for detecting giant reed. Geocarto International 27 (5), 413–424.

Capítulo 5

Optimal attributes for the object-based detection of giant reed in riparian habitats. A comparative study between Airborne High Spatial Resolution and WorldView-2 imagery

5.1 Síntese

O capítulo 5 representa a integração dos resultados obtidos nos capítulos 3 e 4 e um exercício de aplicação de uma metodologia de distinção semi-automática de deteção remota da cana em habitats ripários. Tendo como base os resultados e as conclusões dos capítulos anteriores quanto à particularidade das configurações espaciais (capítulo 3) e ao comportamento espectral distinto das formações de cana face à vegetação das zonas envolventes (capítulo 4), é testado um conjunto de atributos geométricos, espectrais e de textura de imagem no sentido de encontrar a combinação ótima de variáveis para a detetabilidade remota desta invasora. Neste trabalho é utilizada uma abordagem orientada por objetos, que permite combinar informação remota de diferentes categorias, no sentido de criar entidades ao nível da imagem – os objetos- com uma correpondência no mundo real, neste caso, manchas de cana. Estes objetos têm intrinsicamente características de forma, espectrais e de textura, que combinadas permitem melhorar a classificação final, sobretudo em imagens de elevada resolução espacial, produzindo cartografia de maior precisão quando comparada com abordagens somente espectrais. A metodologia é testada em dois tipos de imagens de elevada resolução espacial e de fácil aquisição em Portugal: ortofotomapas com 4 canais e 50 cm de resolução espacial, produzidos pelo Instituto Geográfico Português, e uma imagem do satélite comercial WorldView-2, com 8 canais e 2m de resolução espacial. São utilizadas técnicas de calibração radiométrica relativa e uma combinação de classificadores (Bagging CART) para produzir os mapas de distribuição da cana resultantes da classificação orientada por objeto. A validação dos resultados é realizada por comparação dos mapas produzidos, em termos de área total, configuração das manchas e precisão geográfica, com os mapas produzidos manualmente por fotointerpretação e ratificados em campo. Nos resultados é investigada a relação causal entre a variabilidade do comportamento espectral sazonal da cana e a maior ou menor heterogeneidade da matriz de solo envolvente na distinção remota da cana face às diferentes características espectrais, espaciais e temporais dos dois tipos de imagem. Na parte final é apresentada a adequabilidade da metodologia proposta tendo como base diferentes cenários de habitats ribeirinhos, usos de solo envolventes e distintos objetivos de gestão.

5.2 Artigo

Optimal attributes for the object-based detection of giant reed in riparian habitats: a comparative study between airborne High Spatial Resolution and WordView-2 imagery.

Em revisão como: Fernandes MR, Aguiar FC, Silva JMN, Ferreira MT, Pereira JMC. 2013. Optimal attributes for the object-based detection of giant reed in riparian habitats: a comparative study between airborne High Spatial Resolution and WordView-2 imagery.

Optimal attributes for the object based detection of giant reed in riparian habitats: a comparative study between Airborne High Spatial Resolution and WorldView-2 imagery.

Maria Rosário FERNANDES [a, *], mrfernandes@isa.utl.pt

[a] Universidade Técnica de Lisboa, Instituto Superior de Agronomia, Centro de Estudos Florestais, Tapada da Ajuda, 1349-017, Lisboa, Portugal,

*Author for correspondence (email: mrfernandes@isa.utl.pt; phone: +351 213653380; fax: +351 213653338)

Francisca C. AGUIAR [a], fraguiar@isa.utl.pt

João M. N. SILVA [a], joaosilva@isa.utl.pt

Maria Teresa FERREIRA [a], terferreira@isa.utl.pt

José M. C. PEREIRA [a], jmcpereira@isa.utl.pt

Abstract

Giant reed is an aggressive invasive plant of riparian ecosystems in many sub-tropical and warm-temperate regions, including Mediterranean Europe. In this study we tested a set of geometric, spectral and textural attributes in an object based image analysis (OBIA) approach to map giant reed invasions in riparian habitats. Machine learning techniques (bagging Classification and Regression Tree) were used to select the optimal attributes and to build the classification rules sets. Mapping accuracy was performed using landscape metrics and the Kappa coefficient to compare the topographical and geometric similarity between the giant reed patches obtained with the OBIA map and with a validation map derived from on-screen digitizing. The methodology was applied in two high spatial resolution images: an airborne multispectral imagery and the newly WorldView-2 imagery. A temporal coverage of the airborne multispectral images was radiometrically calibrated with the IR-Mad transformation and used to assess the influence of the phenological variability of the invader.

We found that optimal attributes for giant reed OBIA detection are a combination of spectral, geometric and textural information, with different scoring selection depending on the spectral and spatial characteristics of the imagery. WorldView-2 showed higher mapping accuracy (Kappa coefficient of 77%) and spectral attributes were preferentially selected, although a tendency to overestimate the total invaded area, due to the low spatial resolution (2m of pixel size *vs.* 50 cm) was observed. When airborne images were used, geometric attributes were primarily selected and a higher spatial detail of the invasive patches was obtained, due to the higher spatial resolution. However, in highly heterogeneous landscapes, the low spectral resolution of the airborne images (4 bands instead of the 8 of WorldView-2) reduces the capability to detect giant reed patches. Giant reed display peculiar spectral and geometric traits, at leaf, canopy and stand level, which makes the OBIA approach a very suitable technique for management purposes.

Keywords

Alien species; plant invasions, *Arundo donax*; OBIA; geometric metrics; machine learning techniques; Iberian Peninsula

1. Introduction

Giant reed or cane (*Arundo donax* L.) invades many regions of the world, causing biodiversity damaging, water depletion, obstruction to river flows and habitat degradation (Cushman and Gaffney, 2010; DiPietro et al., 2002; Dudley, 2000; Everitt et al., 2004; Herrera and Dudley, 2003). Though very detrimental, giant reed invasions in Portugal are poorly documented, either concerning the species distribution or the related economic damages. Some information can be found in the national-wide inquiry of Aguiar et al. (1996) on the perception of plant invasions by public and private entities responsible for water resources management. This study revealed giant reed as one of the main plant invaders of Portuguese rivers, being responsible for high financial losses mainly by chocking rivers, trapping sediments and causing inundation in adjoining lands and by impeding human and cattle access to the water. Giant reed is also known to cause serious damages in bridges, weirs and dams. The species is widespread in mainland Portugal, though it is more abundant in centre-west and southern rivers (Aguiar et al., 2007; Aguiar and Ferreira, in press). Pinto and Correia (2012) estimate, by interpretation of aerial photographs, that 430 km of main southern rivers of Portugal are invaded by giant reed. Azores archipelago (Portugal) is also invaded by giant reed, which has directly affected at least 11 endemic vascular plant species (Silva et al., 2011).

Mapping the actual species distribution is an important tool for prioritizing control areas and planning regional management. However, giant reed is a fast-growing species capable of a

rapid dispersal along river corridors, making the hand-mapping monitoring methods and interpretation of aerial photographs very inefficient, due to the quickly updating of actual situation (Yang et al., 2012). Therefore, the development of effective, repeated and reliable semi-automatic techniques are desirable to a successful monitoring of giant reed invasions, thus providing on-the-ground management guidelines.

In the last decade, several remote sensing studies have explored the potential of hyperspectral data to map invasive species in wetlands using per-pixel techniques (Andrew and Ustin, 2008; Hamada et al., 2007; Hestir et al., 2008; Pengra et al., 2007; Underwood et al., 2003). Particularly, DiPietro et al. (2002) and Yang et al. (2012) tested several image classifiers, at southwest US, to identify giant reed spectral signatures using airborne hyperspectral imagery. Although hyperspectral data are known to improve species discrimination, the technique is very time consuming and involves intensive image pre-processing due to the high dimensional complexity and spectral noise (Hestir et al., 2008; Underwood et al., 2003). Additionally, most of spectral separability studies of wetland and riparian plant invaders used hyperspectral data collected by field spectroradiometers (e.g. Adam and Mutanga, 2009; Fernandes et al., 2013; Ge et al., 2008; Schmidt and Skidmore, 2003; Vaiphasa et al., 2007) which are especially devoted to baseline assessments and are not suitable for wide-scale management purposes.

Furthermore, several studies found that multispectral images provide similar classification accuracy than the hyperspectral ones, especially when target plant species have clearly distinct spectral properties from the surrounding vegetation (Belluco et al., 2006; Everitt et al., 2004; 2008; Laba et al., 2008; Laba et al., 2010). This was recently confirmed for the giant reed invasions in Portugal by Fernandes et al. (2013), which found that invasive patches are spectrally separable from the surrounding vegetation, in both vegetative and the senescent period, for broad bands located especially in the red edge region and near infrared, but also in

the visible and mid infrared regions In riparian habitats, and especially in Mediterranean regions, very high spatial resolution (< 5m) is needed to map invasive species due to the limited width and high structural complexity of riparian vegetation patches (Congalton et al., 2002; Goetz, 2006; Muller 1997). High spatial resolution is also essential to identify invasive species in early stages of infestation (Underwood et al., 2007). Nevertheless, high spatial resolution refinement did not correspond necessarily to an increase of the classification accuracy using the traditional per pixel techniques, due to increment of the within class spectral variability and consequent reduction of the statistical separability (Carleer et al., 2005; Hsieh et al., 2001; Ke et al., 2010). In high spatial resolution imagery, a giant reed stand is composed by several pixels and spectral reflectance of individual pixels solely may no longer accurately describe the species. Object based image analysis (OBIA) can overcome this problem by initially aggregate adjacent pixels into spectrally homogeneous regions - the objects - (Blaschke, 2010; Peña-Barragán et al., 2011). In this case, the within-object variance is less than the between-object variance (Laliberte et al., 2004). These objects represent meaningful ground entities (Dronova et al., 2011) and have intrinsic spatial, textural and contextual attributes. In the classification process all these attributes can be used to improve image object classification solving the problem of pixel heterogeneity.

As far as we know, few studies using OBIA have addressed these thematic of mapping invasions in riparian habitats (Laba et al., 2010; Pearlstine et al., 2005). Recent OBIA studies with environmental management purposes used the textural information as main auxiliary data, aiming to increase the consistency and accuracy of spectral classification (Franklin et al., 2001; Johansen et al., 2007; Mallinis et al., 2008; Puissant et al., 2005; Yamagata and Yasuoka, 1993). Textural attributes describe the statistical spatial arrangements of pixels (Maillard, 2003; Tso and Mather, 2009) and are particularly useful in high spatial resolution airborne or satellite imagery where repeated patterns of gray tones characterize the object of

analysis (Pearlstine et al., 2005). Topographic, vertical structure and geometric metrics can be also incorporated as ancillary factors. The latter describes the shape, the spatial configuration, the stretching level, the area and the compactness level (Johnsson, 1994). However, until now, geometric attributes have shown little contribution for vegetation discrimination (Ke et al., 2010; Yu et al., 2006). However a recent study of Fernandes et al. (2011), found that riparian areas highly invaded by giant reed were characterized by peculiar geometric configurations characterized by large, simple and elongated patches, whereas the native riparian forests presented vegetation patches with complex forms and interspersed patterns.

Separability between vegetation classes may be enhanced with the recent supervised machine learning techniques (Dronova et al., 2011). In our study, we used bagging Classification and Regression Trees (CART) to select the optimal set of attributes for the OBIA identification of giant reed. Machine learning techniques are ensemble methods that use a finite set of models to improve the consistency of unique classifiers. CART is amongst the most successfully methods for feature selection in mapping invasive species (Andrew and Ustin, 2008; Hestir et al., 2008) and is increasingly being used in combination with OBIA, since it deals well with a large number of similar objects created during the segmentation process (Blaschke, 2010; Breiman et al., 1984; Mallinis et al., 2008; Ke et al., 2010; Pu and Landry, 2012; Yu et al., 2006; Xie et al., 2008). CART as also the advantage of be very easily to interpreted and to create the classification rules sets used in the following OBIA classification process.

Given the previous findings, the objectives of the present study are to:

- identify the optimal set of spectral, geometric and textural attributes to classify giant reed using OBIA;
- assess the accuracy of the giant reed maps obtained with the optimal set of attributes;
- compare the results of two multispectral high spatial resolution images easily accessible in Portugal, namely a commercial available WorldView-2 image, with eight

bands and 2m of pixel size and an airborne multispectral imagery with four bands and 50 cm of pixel size;

- explore the spectral-temporal variability of giant reed stands on multispectral images.

2. Methods

2.1 Study area

This study was conducted in a highly invaded 2.5km-long stretch of riparian area of River Aveiras, located in Centre-west Portugal, between 39º 06'N, 8º 52'25''W and 39º 05' 15''N, 8º 50' 47''W. Small patches of rice, maize, orchards, vineyards, pastures, and patches of pine, cork-oak and eucalyptus forests characterize the land use of the study area. Beside the riparian habitats, giant reed patches can also be found in the landscape mosaic as windbreaks, or as fences to confine properties. The study area is located in a highly populated region severely impacted by channelization, water abstraction, sand extraction and effluent discharges. Climate in the region is characterized by mild winters and hot dry summers and has frequently irregular interannual fluctuations of precipitation. Flood peaks usually occur in early winter, followed by a slowly declining of flow and a consequent drying during late spring and summer. These winter flood events contribute to the dissemination of the invader by dislodge and disperse downstream the giant reed rhizomes.

2.2 Remote sensing data and preprocessing

2.2.1 Airborne High Spatial Resolution images

High spatial resolution multispectral airborne images (0.5 m spatial resolution) were acquired over the study area, for three dates, namely for November 2004, September 2007 and October

2010 (hereafter scenes Nov04, Sep07 and Oct10). The three coverages were obtained with an Ultracam D and a DMC-Intergraph camera with interference filters, and had a nominal overlap of 60% along flight lines with an imaging altitude of 5800m. Only the innermost part of the images was retained for the final scenes to reduce the effects of bidirectional reflectance and exposure falloff. The data had full 8-bit radiometric resolution and were subjected to orthorectification using a 5 m resolution raster Digital Elevation Model (DEM).The airborne image data set was composed by four bands: blue (0.390-0.580 mm), green (0.420-650 mm), red (0.590-0.690 mm) and near-infrared (NIR) (0.675-0.900 mm). Because this sensor does not have a calibration system on board, we used Digital Numbers (DN) and not ground-reflectance, and performed a relative radiometric calibration (see 2.2.1.1) like the one used by Dronova et al. (2011) and Xie et al. (2008). Each airborne multispectral image has 3669 rows and 2716 columns.

2.2.1.1 Normalization with the IR-MAD transformation

An automatic relative radiometric calibration of the Nov04, Sep07 and Oct10 airborne images was performed with the iteratively re-weighted Multivariate Alteration Detection (IR-MAD) transformation (Canty and Nielsen, 2008) to allow the comparison between airborne images from different dates. A relative radiometric calibration can be used when absolute surface radiances are not required. This calibration is based on the hypothesis that the relationship among at-sensor radiances collected at different times, from features of constant reflectance (so-called invariant features, IFs), composed by no-changed pixels, can be approximate by linear equations. In this study we used the IR-MAD transformation, an automated ordination algorithm, to statistically locate the IFs, instead of the manual selection, highly subjective and time consuming. The IR-MAD procedure is an upgrade of the initially developed MAD

transformation (Nielsen et al., 1998) in identifying IFs where the percentage of no-change pixels in image are reduced, which are the case of our study area, due to seasonal variations in vegetation, especially in the vicinity of riparian corridors. Canonical Correlation Analysis (CCA) was used in the IR-MAD transformation to identify linear combinations amongst two groups of variables (i.e. the spectral bands of the target and the reference images) ordered by correlation between pairs. Differences between those ordered pairs are called MAD variates and after standardization to unit variance, approximately follow a chi-square distribution. By settling a threshold level it is possible to differentiate the change and no-change pixels (Canty et al., 2004; Nielsen, 2007). In this study we used a chi-square threshold of 0.95, and selected Sep07 as the reference image due to its high radiometric quality associated with the month of acquisition (low presence of shadows). Pixel values from the IFs were used to perform the regressions for the calibration between the two points across images with different dates. The quality of the normalized images was evaluated in terms of paired *t*-tests, for means and *F*-tests for variances. Since the results between any two selected images were closer to zero for the *t*-tests, and closer to one for the *F*-tests, images were considered consistent (Yu et al., 2006). All image processing was performed within ENVI remote sensing image analysis environment (version 4.5, ITT Visual Information Solutions, Boulder, CO, USA). The IR-MAD transformation and the radiometric normalization were written in the IDL source code (see Canty, 2007).

2.2.2 Satellite imagery

A WorldView-2 scene was acquired over the study area on July 18, 2010 at 11:00 AM, with 0% cloud cover and a 7º off-nadir look angle. The data were full 8-bit radiometric resolution and were georeferenced to the Universal Transverse Mercator (UTM) coordinate system,

Zone 29 North, World Geodetic System 1984 (WGS84). The WorldView-2 image data set was composed of eight spectral bands with 2.0 m of spatial resolution, including coastal (400-450 nm), blue (450-510 nm), green (510-580 nm), yellow (585-625), red (630-690 nm), red edge (705-745 nm), near infrared 1 (NIR1) (770-895 nm)and near infrared 2 (NIR2) (860-1040 nm) bands. The satellite image covers the same study area as the airborne images and had 1113 rows and 883 columns.

2.3 Object based general procedure

The OBIA methodology used in this study to identify giant reed stands consists in the following phases: 1) image segmentation to obtain the initial giant reed objects, 2) training selection and definition of the spectral, geometric and textural attributes, 3) selection of optimal attributes for giant reed classification using bagging CART, 4) application of the optimal rules set and selection of the criteria decision to generate the final giant reed OBIA map, and 5) validation of the OBIA map by comparing with a ground-truth map. Accuracy assessment was based on a confusion matrix and on a set of landscape metrics.

2.3.1 Image segmentation

Object based identification begins with segmentation, by dividing the image into homogenous regions and representing a semantically main group of neighboring pixels (Blaschke, 2010). In our study image, segmentation should ideally produce polygons that correspond to the real-world giant reed patches. For this purpose we used a hierarchical procedure included in ENVI Zoom module, available in the ENVI software (version 4.5, ITT Visual Information Solutions, Boulder, CO, USA). The segmentation process started with an edge-based

algorithm to delineate the initial objects. Then, the Full λ-Schedule algorithm (Robinson et al., 2002) was used to merge adjacent objects that were similar in spatial and spectral characteristics.

Although there are no preferential techniques, edge-based algorithms have been proved to be more effective than region-based algorithms, for the detection of consistent and contrasting objects within images (Carleer et al., 2005). This is the case of giant reed patches in riparian areas where boundaries of the invader are clearly distinct from the surrounding land use. In the first step, the edge-based algorithm delineates objects throughout the discontinuity property, based on the assumption that two neighboring pixels exhibiting a large difference in their spectral values should belong be different objects (Zhang, 1997). As result, reflectance variance within objects is smaller when compared with reflectance variance between objects (Desclee et al., 2006).The algorithm employs both textural and spectral information for the initial delineation of objects. We selected the scale level for the segmentation process, following the criteria of previous studies (Benz et al., 2004; Laliberte et al., 2004; Pu and Landry, 2012) by using a systematic trial and error approach, validated by visual image inspections of the quality of the objects, which means for this case, how well the objects match with real giant reed patches. In our study we selected a scale level of 40 for the airborne images and 30 for the satellite image. The reason for a smaller scale level of segmentation for the satellite image is the coarse spatial resolution (2 m) when compared with the airborne images (0.50 m) (Gergel et al., 2007).

In the second step (Figure 1), some initial objects were merged to improve the delineation of boundaries and to solve some giant reed over-segmentation. The initial objects were merged if the Full λ-Schedule algorithm found a pair of adjacent objects O_i and O_j following the criterion that merging cost t_{ij} was less than a certain threshold λ value, which ranges from 0 to

100. In our study we choose a lambda value of 90.0 for both airborne images and satellite image. Merging cost t_{ij} is given by equation (1):

$$t_{ij} = \frac{\frac{|O_i|\,|O_j|}{|O_i| + |O_j|}\,\|\mu_i - \mu_j\|^2}{\ell\left(\partial(O_i, O_j)\right)}$$

where:

O_i set of pixels of image object i , and O_j set of pixels of image object j

$|O_i|$ is the area of object O_i

$|O_j|$ is the area of object O_j

μ_i is the average of the spectral value of object O_i

μ_j is the average of the spectral value of object O_j

$\|\mu_i - \mu_j\|$ is the Euclidean distance between the spectral values of objects O_i and O_j

$\ell\left(\partial(O_i, O_j)\right)$ is the common boundary length between the objects O_i and O_j.

2.3.2 Training sampling dataset and attributes selection

We decided to classify our data in two classes: the "giant reed" and the "non-giant reed", which includes all other land uses. We did not introduce any further subcategories from each class to deliberately account with all the intrinsic variation of each class. Giant reed training objects were classified by visual interpretation on the images and confirmed by field visits. Giant reed training samples were manually selected in order to ensure the overall class variability, since they were located in a confined area of imagery. In opposition, the training

objects for the non-giant reed class were randomly selected in order to represent 2% of the total objects in each image. Table 1 summarizes the number of training objects for each class and the total objects obtained for each image after the segmentation process.

The full dataset for the following bagging CART analysis was composed by a matrix, for each image, with three groups of object attributes (Table 2). Group one is composed by geometric attributes related with size, spatial configuration, shape complexity, stretching level and objects orientation. Like was observed by Fernandes et al. (2011) riparian giant reed patches have some peculiar geometric characteristics, very different from the surrounding agricultural and near-natural riparian patches, which can contribute for the giant reed identification through an OBIA approach. Spearman Rank Correlations (R) were initially used to avoid redundancy in the data ($|R| > 0.8$; $p < 0.01$). Group two was composed by the object spectral information based on mean, standard deviation and Normalized Difference Vegetation Index (NDVI). Mean and standard deviation were calculated for each band (four bands for each airborne image and eight bands for the satellite imagery) and are related with the spectral reflectance characteristics of each object type. The NVDI assesses the greenness level of the objects and is associated with primary productivity and vegetation growing. High values of NDVI are usually found in dense and vigorous vegetation which represents a combination of high reflectance values in the near infrared region and small reflectance in the red region. We additionally tested (group three) three first-order statistical texture features (mean, variance and entropy) related with global variation of tone for each image type, using a windows analysis of a 3x3 pixels. This window size has been considered to have suitable dimensions to extract the complementary textural information in other OBIA analysis, for wetland vegetation, using high spatial resolution images (Laba et al., 2010).

2.3.3 Machine Learning Bagging Classification and Regression Trees (CART)

Machine Learning Bagging CART was used to identify the most important attributes for giant reed discrimination using an OBIA approach. CART is a hierarchical classifier that uses a top-down binary splitting mechanism based on a sequence of decision rules (Breiman et al., 1984). This technique maximizes the homogeneity inside each child node relative to the dependent variable (class type). Results are a combination of IF-THEN rules, where each rule chooses a single independent variable (geometric, spectral or texture attribute). The contribution of each independent variable to the final classification is computed through an importance score. This score reflects the variable importance both as primary splitter and as surrogate of the primary splitter (Breiman et al., 1984 and Tso and Mather, 2009).

In this study, we used bagging CART, which is an ensemble of classifiers instead of a single classifier, to improve the reliability of attributes' selection. In the bagging approach (acronym for bootstrap aggregating) each classifier is generated using a random sample with replacement from the original training set of independent variables. Subsequently, the different outputs are combined to create the final result (Breiman, 1996; Safavian and Landgrebe, 1991). By using an ensemble approach the variable importance ranking is stabilized, meaning that the performance of the method is increased by using several independent classifiers. Comparing with other ensemble approaches (boosting or random forests) bagging is considered more robust with variable errors and also having faster calculations (Breiman, 1996). We created a set of ten classification trees and the resulting classifiers were aggregated by majority voting of the class allocation decision for each object. The final ensemble classification was obtained by averaging the results of each optimal bootstrap tree. Accuracy assessment was performed on an independent subset of the training data representing 30% of the total data set. We selected the Gini index criterion of impurity

for node splitting, assuming equal class prior probabilities, and defining that all terminal nodes must contain at least 5 cases, both for the airborne images and the satellite image. We attained a set of optimal bootstrap trees, each one obtained when the curve costs/number of terminal nodes flats. This was considered a good compromise between minimization of the error and the reduction of the tree complexity. The final OBIA map results from a combination of these optimal bootstrap trees, by applying a decision criteria to set as giant reed those objects that meet these conditions We tested two scenarios of criteria decision to classify the giant reed objects in the final object based map: i) Majority scenario and ii) Unanimity scenario. In the Majority scenario we considered as giant reed those objects classified as giant reed by at least five of the ensemble trees. In the Unanimity scenario we set as giant red those objects classified as such in all the ensemble trees.

2.3.4 Mapping classification accuracy

The accuracy assessment performed in the previous subchapter (2.3.3), although useful to evaluate the performance of the ensemble classifiers, does not measure the reliability of the giant reed distribution in the study area. Thus, we performed a mapping evaluation by comparing the giant reed maps obtained with the OBIA with the giant reed maps manually achieved by on-screening digitizing and validated with field visits.

Landscape metrics related with the size, total area, configuration, size variability and number of patches were used to compare the giant reed patches obtained in each method (object based and manual). The accuracy assessment of the OBIA giant reed map was also measured by calculating the confusion matrix and the Kappa coefficient. It should be noticed that confusion matrix was made by comparing the geographical location of all pixels of each object, in both maps and not with a randomized set of points over the OBIA map. Other

366 metrics could be used to assess the imagery segmentation quality, like the topographic and
367 geometric similarly between segment and reference objects develop by Möller et al. (2007).
368 However, the latter tend to assess partial overlapped areas and discrepancies between
369 coordinates of the centroids of segmented and reference objects. By using our procedure we
370 reduce bias but the overall classification accuracy tend to be smaller (Radoux et al., 2008),
371 since total overlap is hardly achieve. Given that we are addressing the giant reed patches
372 along rivers, a filter of proximity to the river banks was applied to the OBIA giant reed map
373 aiming to exclude the giant reed patches with a terrestrial location from the confusion matrix.
374
375 **3. Results**
376 3.1 Selection of optimal attributes for giant reed discrimination
377
378 Table 3 summarizes the overall geometric, spectral and textural characteristics of giant reed
379 comparing with the non-giant reed training objects, for each airborne image and for the
380 satellite imagery. Geometric attributes showed that giant reed objects were higher and had
381 more elongated and complex shapes in comparison with the non-giant reed objects, both in all
382 the airborne images and in the satellite image. Also, giant reed objects had a predominant
383 main direction, coincident with the main axis of the river course, whereas non-giant reed
384 objects displayed a randomized distribution. As was expected, non-giant reed objects revealed
385 high variability for the average at all the spectral bands whereas the giant reed objects showed
386 the typical spectral characteristics of a vegetation class, namely small values of the red band
387 and high values for the NIR 1. Giant reed objects had high NDVI values when compared with
388 other class. Textural variance and entropy showed higher homogeneity for the giant reed
389 objects compared to the non-giant reed, exception for the entropy in the airborne images
390 which was equal for both classes.

391 The bagging ensemble of classifiers revealed differences in the selection of the attributes for
392 the giant reed discrimination according to image type (Figure 2). For all the airborne images
393 the geometric variable area was consistently selected as the most important attribute for giant
394 reed discrimination followed by variables related with spectral characteristics, namely the
395 mean of the red band and the NDVI. The form factor was also selected among the primary
396 variables, while the textural attributes were not considered key variables to distinguish giant
397 reed objects in the airborne images.For the satellite image the spectral attribute NDVI was by
398 far the most important variable (median of variable importance score = 100%) followed by
399 the mean values of the red band (median of variable importance score = 68%). The textural
400 attributes entropy and variance showed a median of variable importance score of 66% and 65
401 %, respectively to distinguish the giant reed from the non-giant reed objects in the satellite
402 imagery, in opposition to the airborne images. The information in the additional WorldView-2
403 bands, such as the near infrared 2, the red edge and especially the yellow band was also
404 considered noteworthy for the identification of giant reed objects. Nevertheless, the area, a
405 geometric variable, showed an overall small importance in the satellite image, although it was
406 selected as one of the most important variables for some bootstrap trees.The ensemble of
407 classifiers revealed high classification accuracy (Table 4) for both classes although slightly
408 higher for the giant reed. Nov04 airborne image showed the lowest classification of the
409 overall images (0.84-0.90) with an independent dataset).
410
411 3.2 OBIA maps for giant reed in riparian areas
412
413 The giant reed OBIA map, for each image type, was composed by a combination of
414 individual maps obtained by applying the decision rules generated for every optimal bootstrap
415 tree. Using the airborne images three to four variables were consistently selected for the

ensemble of optimal trees. Those variables were area, average of the NIR band, NDVI and main direction. For the satellite image the ensemble of optimal trees selected only two of the most important variables: the NDVI and alternately the area, the main direction, the average of the textural values and the average of the red band. Figure 3 shows the grey scale object based map resulting from the sum of the ten binary maps for the satellite image. White areas represent objects classified as giant reed in all the ten optimal bootstrap trees and black areas, objects classified as non-giant reed. For the airborne images, both scenarios revealed a good performance in the identification of the giant reed patches with a riverine location. However, the Majority scenario led to the classification of a high number of giant reed objects with a terrestrial location (Figure 4). Given that the purpose of this study is to discriminate giant reed in riparian habitats, we have chosen the restrictive scenario of Unanimity. For the satellite image, the scenario of Unanimity revealed a poor performance in the identification of the giant red objects due to the lower stability of the ensemble classifier. Thus, we used the Majority criteria to set the final giant red object based map.

3.3 Map accuracy

In general, values of landscape metrics (area, number of patches, configuration, size) were similar for the giant reed patches identified with the OBIA approach and manually, for both image types (Figure 5 and Figure 6). However, we observed two exceptions. For the satellite image, the Mean Patch Size of giant reed objects, using the OBIA approach, was higher than the size of patches obtained with the manual method (Figure 6a). For the airborne images, the spatial complexity of the riverine giant reed patches given by the Mean perimeter-Area ratio obtained with the OBIA methods was higher than the value obtained manually (Figure 6d).

Giant reed patches with a terrestrial location classified with OBIA were composed by ground truth giant reed stands but also by other vegetation types that represent classification errors (Figure 7a). The terrestrial giant reed showed high variability and a large number of complex patches (Figure 6b, c and d), although globally smaller when compared with the riverine giant reed objects (Figure 6a). However, since the present study addresses the riverine giant reed, they were eliminated using a filter of proximity to the riparian area, and were not subject to further map accuracy analysis.

The Kappa coefficient (Table 5) revealed a higher mapping accuracy for the satellite image (K=0.77) in comparison with the airborne images (K ranging from 0.55 to 0.73). In the airborne images the producer's accuracy was smaller than the user's accuracy, indicating that misclassification occurred especially due to omission errors. Contrarily, in the satellite image the producer's accuracy was higher than the user's accuracy reveling especially commission errors. The airborne image Nov04 show the worst mapping accuracy amongst all scenes (K=0.55).

4. Discussion

4.1 Optimal attributes for OBIA classification

The major advantage of the object based approach is the possibility of customizing the remote identification of the interesting features by using a combination of attributes that can unequivocally discriminate them. In this study, we used bagging CART to identify the most important variables of a set of geometric, spectral and textural attributes, for the detection of giant reed in riparian systems. We also compared the results of two image types: High Spatial Resolution airborne images and the commercial WorldView-2. When we used airborne images, the geometric attributes, especially the size of the patches were the most important

variables to distinguish the giant reed from the non-giant reed objects. These are innovative results in this kind of studies, since geometric metrics are usually considered to have little contribution in vegetation discrimination (Ke et al., 2010; Yu et al., 2006). However, a recent study (Pu and Landry, 2012), using WorldView-2 imagery, identified a geometric metric (number of edges) as a significant feature to discriminate and map urban trees species. Our results are supported by the previous study of Fernandes et al. (2011) where landscape metrics showed the distinctiveness of the giant reed geometric attributes. Giant reed stands are characterized by simple, large and elongated patches clearly distinct from the near natural riparian stands that presented very complex and meandering forms. The High Spatial Resolution of the airborne images used in our study (50 cm of pixel size) allow to capture in detail, the configuration of the giant reed patches, since form factor and elongation were selected amongst the most important variables. The spectral attributes NDVI and the average values of the red band, were also considered significant variables, in the airborne images, to distinguish the giant reed from the non-giant reed class. These results, more predictable, are supported by previous works (Everitt et al., 2004; Fernandes et al., 2013; Schmidt and Skidmore, 2003) where the red edge and the visible region were considered key zones for the spectral separability of the giant reed from the surrounding land cover, especially from other vegetation types. However, in this study NDVI values for the giant reed objects ranged from 0.37 to 0.39, which are clearly higher than the NDVI value indicated in other object based studies. For instance, Peña-Barragán et al. (2011) and Xie et al. (2008) obtained a threshold of 0.20 to distinguish vegetation from non-vegetation features. Pu and Landry (2012) found a threshold of 0.25 and Aksoy et al. (2010) recorded 0.3 in a study of discriminating woody vegetation in agricultural landscapes. The pronounced giant reed greenness level associated with high NDVI values was also described by Fernandes et al. (2013) and it is likely to be

489 related with its high concentration of chlorophyll contents combined with a great biomass
490 production and photosynthetic rates (Papazoglou et al., 2005; Rossa et al., 1998).
491 For the satellite image, the main variable to distinguish giant reed from the non-giant reed
492 objects was the NDVI. Worldview-2 image has a specific band located in the red edge region
493 and thus values used in the calculation of the NDVI ratio (red and near infrared bands)
494 amplify the greenness behavior of the giant reed stands (NDVI average values of 0.70) when
495 compared with the NDVI values of the non-giant reed class. The additional bands of
496 WorldView- 2, comparing with the airborne images, especially the yellow band, were also
497 considered important to distinguish giant reed stands. Previous studies with WorldView-2
498 imagery (Pu and Landry, 2012) have also showed the importance of the newest yellow and
499 red edge bands in woody vegetation discrimination due to its capability of detecting variations
500 of pigment contents in canopies. For this satellite image, the textural attributes, especially the
501 entropy, were selected amongst the most important variables, contrary to the airborne images.
502 This fact can also be explained by the higher spectral resolution of the WorldView-2 image,
503 when compared with the airborne images, which allows discriminating the spectral
504 heterogeneity between the giant reed and non-giant reed classes. However, entropy values in
505 the WorldView-2 image are always lower, when compared with the airborne images, for both
506 classes, probably due to the lower spatial resolution (2 m) of the satellite image which cannot
507 recognize all the local heterogeneity of the objects.
508 Nevertheless, in this study we used only the first order statistical textural attributes, which
509 measure local pixels randomness. Thus, a detailed analysis using second order statistical
510 features that take into account fully grey value distribution can be useful (Puissant et al.,
511 2005) although in other cases did not improve classification accuracy when compared with
512 first order statistics (Dikshit, 1996; Pearlstine et al 2005). Additionally, textural information
513 collected for linear features, which are the case of riverine giant reed stands are highly

514 influenced by neighboring patches and the true textural information is difficult to represent
515 (Laba et al., 2010). High spectral and spatial resolution and small windows analysis are
516 simultaneously required to improve the textural information though comprehensive ecological
517 interpretation of the statistical and structural properties exhibit by these spatial arrangements
518 are very complex.
519 In the airborne images, where geometric attributes were more relevant, the main direction had
520 a moderate contribution to separate giant red patches from the non-giant reed patches.
521 However, in the case of more extended riparian areas, where river flows in several directions,
522 we think that its importance will decrease and thus giant reed patches loses a predominant
523 trend direction. In this case it would be interesting to test other metrics, for instance to assess
524 a parallel direction to river or with the detection of linear features, such as the Gabor filter
525 (Aksoy et al., 2010), to discriminate giant reed stands in riparian habitats.
526
527 4.2 Geometric and topological characteristics of giant reed objects
528
529 Landscape metrics values of giant reed patches identified manually and with the OBIA
530 approach were similar. The observed differences were related with the size and the
531 configuration of the giant reed patches, and can be explained by the variation of the spatial
532 resolution of images. For instance, the coarser spatial resolution of the satellite image inhibits
533 an accurate detection of the patch boundaries. Gaps inside the giant reed stands smaller than
534 2m (pixel size) were not removed, leading to an overestimation of the total invaded area. This
535 was also founded in previous studies were a reduction of mapping accuracy in riparian areas
536 was related with a decrease in images spatial resolution (Baker et al., 2007; Gergel et al.,
537 2007) .Contrarily, in the airborne images gaps were removed and edges were closely
538 delineated, during the segmentation step, reducing the total area of giant reed (Figure 5). This

539 delimitation enhancement in the airborne images increases the geometric complexity of the
540 giant reed patches in both methods (Figure 6d). However, for the OBIA, the higher spatial
541 resolution detects additional spectral variability within giant reed patches, creating virtual
542 boundaries and increasing even more the complexity of the giant reed objects. In opposition,
543 giant reed patches in the manual method have more simple configurations, closer to our
544 perception of the reality.
545 The coarser spatial resolution of the WorldView-2 did not allow to capture in detail the
546 boundaries of very proximal giant reed patches, creating few large objects instead of many
547 small ones (Figure 6a and 6c). Furthermore, the giant reed objects in the satellite image are
548 even larger than those manually digitalized because OBIA creates, in some cases, unique
549 large objects, including both riversides, and manual method differentiate the two riverbanks,
550 creating for the same giant reed area, two patches.
551
552 4.3 Terrestrial giant reed objects
553
554 The giant reed class with terrestrial location was composed by truly giant reed and by other
555 vegetation types. Giant reed stands are largely widespread in western and southern areas of
556 Portugal, not only in riverbanks, but also as windbreaks, to confine properties and as tutors for
557 creeper-cultivated plants (Aguiar et al., 2007). So, in these areas misclassification errors are
558 small in the object based approach. However, the application of the decision rules of the
559 optimal bootstrap trees, led to an erroneous classification of other objects with similar set of
560 characteristics (geometric, spectral and textural) that were selected for the giant reed
561 identification. For instance, in the airborne images, some large vegetation patches with
562 complex forms, like some perennial woods, or elongated woody patches along roadside were
563 misclassified as giant reed. For the satellite image, vegetation patches with a high primary

productivity and intensive vegetative growth, like emergent vegetation near wetland areas or irrigation crops, were inaccurately classified as giant reed. However, these terrestrial giant reed patches can be easily eliminated using simple topological GIS operations, like clipping the riparian area (Yang, 2007) and thus they do not represent a problem for riverine giant reed mapping.

4.4 Classification accuracy and spectral information in airborne and satellite images

Classification was more accurate (Table 5) and less complex (optimal bootstrap trees with two splits instead of three or four) in the satellite image than in the airborne images. A combination of factors can explain these results. Firstly, the high spectral resolution of the WorldView-2 image allows detecting more accurately the peculiar spectral traits at leaf level (e.g. "red-shift" of the red edge) and at canopy level (high foliage density and strata-complexity) which were responsible for the high discrimination of the giant reed patches. However, satellite and airborne scenes were collected in different seasons, and phenological variability of giant reed and of the overall landscape mosaic may influence the classification process. WorldView-2 was acquired in July, the peak of summer, when giant reed stands showed an overall greenish color clearly distinct from yellowish tone of the surrounding senescent landscape. In a previous study, Fernandes et al. (2013) found that giant reed is spectrally separable from the adjacent herbaceous and woody vegetation in both vegetative and senescent period, although the optimal wavelengths to distinguish the vegetation classes vary depending on seasonal period. Thus, it is likely that for other seasons further bands of the WorldView-2 can be selected to classify giant reed in an OBIA approach. Additionally, airborne images have some atmospheric effects and noise, difficult to exclude due to the lack

588 of sensor calibration which could also contribute to increase the misclassification between
589 classes in these images.
590 The phenological variability of giant reed can also explain the higher mapping classification
591 accuracy of the airborne coverage from September 2007 compared with the late autumn
592 scenes. In the Out10 and in the Nov04 scenes the emergence of the annual grasses mixed with
593 bare soil creates soft spectral transitions between the green-yellowish tone of the riverine
594 giant reed patches and the surrounding herbaceous land cover. Smoothing boundaries are
595 more demanding for edge-based segmentation creating initial objects composed by both
596 vegetation types. Nevertheless, these objects were not classified as giant reed in the final
597 OBIA map since they displayed dissimilar geometric and spectral characteristics compared
598 with the main giant red attributes that led to the underestimation of giant reed invasion,
599 translated into omission errors. The lower classification accuracy of the Nov04 scene can be
600 additionally related with some misclassifications due to differences between the senescent
601 yellowish-brown tone of the giant reed and the brownish canopy of the deciduous riparian
602 vegetation, like alders, ashes and willows. Yang et al. (2012) also found misclassifications
603 between giant reed stands subjected to seasonal water stress with surrounding vegetation due
604 to spectral similarities. Transitional seasons, like late autumn and early spring, display
605 heterogeneous landscape mosaics characterized by sparse spatial distribution pattern of bare
606 soil mixed with green and dry herbaceous and woody plants. In these conditions the high
607 spatial and spectral variability founded increases the complexity of remote sensing
608 classifications. As referred by Andrew and Ustin (2008) the “success of remote sensing
609 analysis declines as site complexity increases (species, structural, and landscape diversity and
610 spectral variability)”.
611
612 4.5 Imagery selection for giant reed management in different riparian habitat conditions

Imagery selection for giant reed management and control in riparian habitats must represent a good compromise between spectral and spatial resolution for the effective detection of the invasive species without been cost-prohibitive. Thus, for this study we tested two images with high spatial resolution easily available in our country. The final imagery selection for mapping giant reed invasions in riparian systems should rely on a combination of land cover, management purposes, size of the management area and cost constraints.WorldView-2 image is desirable if the goal is to obtain a global estimation about the level of giant reed invasion and their geographical location. In this case object based classification is primarily supported by spectral variables followed by textural and finally by geometric attributes. The high spectral resolution of this image type, compared with the airborne multispectral images, makes a straightforward and more accurate object based detection. Furthermore, if the surrounding landscape mosaic of the riparian area exhibits a heterogeneous patchiness, the classification process can be very demanding and thus a high number of bands are essential to distinguish the several land uses, especially vegetation ones.

However, the coarser spatial resolution (2m) of this image, compared with the airborne images (50 cm) tends to overestimate the total invaded area, and is not able to delineate accurately the shape and fragmentation patterns of the giant reed stands. So, airborne multispectral imagery are a good choice when local detailed maps of giant reed invasions are necessary, especially when the surrounding mosaic display homogeneous patches with clearly boundaries (e.g. agricultural crops) supporting high spectral vegetation discrimination with few bands.

In our study, object based classification in airborne images was primarily supported by geometric metrics followed by spectral variables. In this case a detailed map of giant reed configurations can give an indication about the degree and the structure of the invasion. For

instance, dense and connected giant reed stands highly invaded areas which represents major efforts to rehabilitate the riparian system. On other hand the detection of gaps in the middle of the giant reed stands or the presence of near-natural woody spots of vegetation inside the giant reed stands indicates a better ecological condition and a higher probability to rehabilitee this zone. WorldView-2 images have the disadvantage of being much more costly (24€/km^2 in memory file) in comparison with the national airborne multispectral images (2.5€/ km^2). However, satellite images provide information in a more revisit periodic basis and cover large areas, contrarily to the airborne images that in Portugal have three-annual coverage. Also, despite the radiometric calibration, airborne images have a small radiometric quality comparing with satellite image and the effect of different looking angles and time acquisition, are not completely eliminate.

5. Conclusions and future prospects

Our study had demonstrated that object based analysis are a reliable method to accurately map giant reed invasions in riparian areas. We found that optimal attributes for giant reed detection are a combination of spectral, geometric and textural information, but their hierarchical importance in a OBIA approach depends of imagery spectral and spatial characteristics. Giant reed shows, simultaneously, peculiar spectral and geometric traits, at leaf, canopy and stand level, which creates objects clearly distinct from the surrounding non-giant reed objects. Spectral information in the near infrared band, in the red edge region or in the form of NDVI ratio are crucial attributes for giant reed discrimination due to the high photosynthetic rates of this species. Also, additional bands of the WorldView-2, especially the yellow band revealed high potential to discriminate this invader. Complementary information can be added to the spectral data, such as the geometric characteristics of the giant reed stands. Giant reed objects

662 are simultaneously large with elongated configurations noticeably different from surrounding
663 non-giant reed objects.
664 Future prospects in the remote detection of giant reed invasions in riparian areas should rely
665 on the early detection and quickly responses. That means evaluating the capability of
666 identifying giant reed stands with other spectral, geometric and textural scenarios to
667 consequently develop semi-automatic routines for riparian management purposes. Giant reed
668 invasions in the early stages are characterized by small patches, highly fragmented and
669 usually mixed with other vegetation types. For instance, Fernandes et al. (2013) found that
670 giant reed regenerated after mechanical harvesting are more spectrally separable form the
671 surrounding herbaceous and the woody vegetation than giant reed patches that were not
672 subjected to control. This stands are morphologically and phenologically similar to the early
673 stages of giant reed and are characterized by highly greenish and homogeneous communities.
674 In this case other combination of optimal attributes can be selected in an object based
675 approach. It also would be interesting to test other type of complementary information. As an
676 example, giant reed can be confused with the morphospecies common reed, which is a native
677 species in riparian Mediterranean areas. Although they have similar spectral signatures in the
678 vegetative period (Fernandes et al., 2013) common reed is preferentially located in the river
679 channel, whereas the giant reed occupies mainly riverbanks and thus a contextual attribute can
680 potentiate the separability between the two species.
681 In invaded areas, giant reed forms dense and compact stands and can reach 6-7 meters of
682 height, very distinct from the vertical structure of the native vegetation, which is usually
683 composed by different vegetation strata. Other techniques, such as Lidar (Light detection and
684 ranging) can provide information on stand-specific vertical structure which may increase the
685 discrimination of giant reed from the surrounding patches.
686

687 **Acknowledgements**

688 This study received backing from the EU funds (ERDF) from the project RICOVER "River
689 Ricovery in the SW Europe" (Interreg IVB - SOE1/P2/P248) and from the Centro de Estudos
690 Florestais, CEF through FEDER/POCI 2010. Maria R. Fernandes and Francisca C. Aguiar
691 were supported by doctoral and post-doctoral scholarships from the Foundation for Science
692 and Technology, Portugal, SFRH/BD/44707/2008 and SFRH/BPD/29333/2006, respectively.

693

694 **List of References**

695

696 Adam, E., & Mutanga, O. (2009). Spectral discrimination of papyrus vegetation (*Cyperus*
697 *papyrus* L.) in swamp wetlands using field spectrometry. ISPRS *Journal of Photogrammetry*
698 *and Remote Sensing, 64*(6), 612-620.

699

700 Aguiar, F.C., & Ferreira, M.T. (accepted). Plant invasions in the rivers of the Iberian
701 Peninsula, South-Western Europe – a review. *Plant Biosystems*.

702

703 Aguiar, F.C., Ferreira, M.T., Albuquerque, A., & Moreira, I. (2007). Alien and endemic flora
704 on reference and non-reference sites from Mediterranean type-streams of Portugal. *Aquatic*
705 *Conservation: Marine and Freshwater Ecosystems, 17*(4), 335-347.

706

707 Aguiar, F.C., Moreira, I., & Ferreira, M.T. (1996). Perception of aquatic weed problems by
708 water resources managers. A Percepção da Vegetação Aquática Infestante pelas Entidades
709 Gestoras dos Recursos Hídricos. *Revista de Ciências Agrárias, 19*(4), 35-56.

710

711 Andrew, M.E., & Ustin, S.L. (2008). The role of environmental context in mapping plants
712 with hyperspectral image data. *Remote Sensing of Environment, 112*(12), 4301-4317.
713
714 Aksoy, S, Akçay, H.G., & Wassenaar, T. (2010). Automatic mapping of linear woody
715 vegetation fetures in agricultural landscapes using very high resolution imagery. *IEEE*
716 *Transactions on Geoscience and Remote Sensing, 48*(1), 511-522.
717
718 Baker, M.E., Weller, D.E., & Jordan, T. E. (2007). Effects of stream map resolution on
719 measures of riparian buffer distribution and nutrient potential. *Landscape Ecology*, *27*(7),
720 973-992.
721
722 Belluco, E., Camuffo, M., Ferrari, S., Modenese, L., Silvestri, S., Marani, A., & Marani, M.
723 (2006). Mapping salt-marsh vegetation by multispectral and hyperspectral remote sensing.
724 *Remote Sensing of Environment*, *105*(1), 54-67.
725
726 Benz, U.C., Hofmann, P., Willhauck, G., Lingenfelder, I., & Heynen, M. (2004).
727 Multiresolution, object-oriented fuzzy analysis of remote sensing data for GIS-ready
728 information. *ISPRS Journal of Photogrammetry and Remote Sensing*, *58*(3-4), 239-258.
729
730 Blaschke, T. (2010). Object based image analysis for remote sensing. *ISPRS Journal of*
731 *Photogrammetry and Remote Sensing*, *65*(1), 2-16.
732
733 Breiman, L. (1996). Bagging predictors. *Machine Learning*, *26*(2), 123-140.
734

735 Breiman, L.J.H., Friedman, R.A., Olshen, R., & Stone, C.J. (1984). *Classification and*
736 *Regression Trees*. Chapman & Hall/CRC, New York.
737
738 Canty, M.J. (2007). *Image analysis, classification and change detection in remote sensing,*
739 *with algorithms for ENVI/IDL.* Taylor and Francis.
740
741 Canty, M.J., & Nielsen, A.A. (2008). Automatic radiometric normalization of multitemporal
742 satellite imagery with the iteratively re-weighted MAD transformation. *Remote Sensing of*
743 *Environment, 112*(3), 1025-1036.
744
745 Canty, M.J., Nielsen, A.A., & Schmidt, M. (2004). Automatic radiometric normalization of
746 multitemporal satellite imagery. *Remote Sensing of Environment, 91*(3-4), 441-451.
747
748 Carleer, A.P., Debeir, O., & Wolff, E. (2005). Assessment of very high spatial resolution
749 satellite image segmentation. *Photogrammetric Engineering & Remote Sensing, 71*(11), 1285-
750 1294.
751
752 Congalton, R.G., Birch, K., Jones, R., & Schriever, J. (2002). Evaluating remotely sensed
753 techniques for mapping riparian vegetation. *Computers and Electronics in Agriculture, 37*(1-
754 3), 113-126.
755
756 Cushman, J.H., & Gaffney, K.A. (2010). Community-level consequences of invasion: impacts
757 of exotic clonal plants on riparian vegetation. *Biological Invasions, 12*(8), 2765-2776.
758

759 Desclee, B., Bogaert, P., & Defourney, P. (2006). Forest change detection by statistical
760 objectbased method. *Remote Sensing of the Environment, 102*(1-2), 1-11.
761
762 Dikshit, O. (1996). Textural classification for ecological research using ATM Images.
763 *International Journal of Remote Sensing, 17*(5), 887-915.
764
765 DiPietro, D., Ustin, S.L., & Underwood, E. (2002). *Mapping the invasive plant Arundo*
766 *donax at Camp Pendleton Marine Base using AVIRIS.* In: Proceedings of 10th JPL
767 airborne visible infrared imaging spectrometer (AVIRIS) Workshop, Pasadena, CA: Jet
768 Propulsion Lab.
769
770 Dronova, I., Gong, P., & Wang, L. (2011). Object-based analysis and change detection of
771 major wetland cover types and their classification uncertainty during the low water period at
772 Poyang Lake, China. *Remote Sensing of Environment, 115*(12), 3220-3236.
773
774 Dudley, T.L. (2000). *Arundo donax*. In: Bossard, C.C., Randal, J. M., Hoshovsky, M.C.
775 (Eds.), *Invasive Plants of California's Wildlands*, first ed. Univ. of California Press, Berkeley,
776 California, pp.53-58.
777
778 Everitt, J.H., Yang, C., Alaniz, M.A., Davis, M.R., Nibling, F.L., & Deloach, C.J. (2004).
779 Canopy spectra of giant reed and associated vegetation. *Journal of Range Management,*
780 *57*(5), 561-569.
781

Everitt, J.H., Yang, C., Fletcher, R., & Deloach, C.J. (2008). Comparison of QuickBird and SPOT 5 satellite imagery for mapping giant reed. *Journal of Aquatic Plant Management, 46*, 77-82.

Fernandes, M.R., Aguiar, F.C., & Ferreira, M.T. (2011). Assessing riparian vegetation structure and the influence of land use using landscape metrics and geostatistical tools. *Landscape and Urban Planning, 99*(2), 166-177.

Fernandes, M.R., Aguiar, F.C., Silva, J.M.N., Ferreira, M.T., & Pereira, J.M.C. (2013). Spectral discrimination of giant reed (Arundo donax L.): a seasonal study in riparian areas. *ISPRS Journal of Photogrammetry and Remote Sensing, 80*, 80-90.

Franklin, S.E., Wulder, M.A., & Gerylo, G.R. (2001). Texture analysis of IKONOS panchromatic data for Douglas-fir forest age class separability in British Columbia. *International Journal of Remote Sensing, 22*(13), 2627-2632.

Ge, S., Carruthers, R.I., Spencer, D.F., & Yu, Qian. (2008). Canopy assessment of biochemical features by ground-based hyperspectral data for an invasive species, giant reed (*Arundo donax*). *Environmental Monitoring and Assessment, 147*(1-3), 271-278.

Gergel, S.E., Stange, Y., Coops, N.C., Johansen, K., Kirby, & K.R. (2007). What is the value of a good map? An example using high spatial resolution imagery to aid riparian restoration. *Ecosystems, 10*, 688-702.

Goetz, S.J. (2006). Remote Sensing of riparian buffers: past progress and future prospects. *Journal of the American Water Resources Association, 42*(1), 133-143.

Hamada, Y., Stow, D.A., Coulter, L.L., Jafolla, J.C., & Hendricks, L.W. (2007). Detecting Tamarisk species (*Tamarix* spp.) in riparian habitats of Southern California using high spatial resolution hyperspectral imagery. *Remote Sensing of Environment, 109*(2), 237-248.

Herrera, A.M., & Dudley, T.L. (2003). Reduction of riparian arthropod abundance and diversity as a consequence of giant reed (*Arundo donax*) invasion. *Biological Invasions, 5*(3), 167-177.

Hestir, E.L., Khanna, S., Andrew, M.E., Santos, M.J., Viers, J.H., Greenberg, J.A., Rajapakse, S.S., & Ustin, S.L. (2008). Identification of invasive vegetation using hyperspectral remote sensing in the California Delta ecosystem. *Remote Sensing of Environment, 112*(11), 4034-4047.

Hsieh, P.F., Lee, L.C., & Chen, N.Y. (2001). Effect of spatial resolution on classification errors of pure and mixed pixels in remote sensing. *IEEE Transactions on Geoscience and Remote Sensing, 39*(12), 2657–2663.

Johansen, K., Coops, N.C., Gergel, S.E., & Stange, Y. (2007). Application of high spatial resolution satellite imagery for riparian and forest ecosystem classification. *Remote Sensing of Environment, 110*(1), 29-44.

Johnsson, K. (1994). Segment-based land-use classification from SPOT satellite data. *Photogrammetric Engineering and Remote Sensing, 60*(1), 47-53.

Laba, M., Blair, B., Downs, R., Monger, B., Philpot, W., Smith, S., Sullivan, P., & Baveye, P. C. (2010). Use of textural measurements to map invasive wetlands plants in the Hudson River National Estuarine Research with IKONOS satellite imagery. *Remote Sensing of Environment, 114*(4), 876-886.

Laba, M., Downs, R., Smith, S., Welsh, S., Neider, C., & White, S. (2008). Mapping invasive wetland plants in the Hudson River National Estuarine Research Reserve using QuickBird satellite imagery. *Remote Sensing of Environment 112*(1), 286-300.

Ke, Y., Quackenbush, L.J., & Im, J. (2010). Synergistic use of QuickBird multispectral imagery and LIDAR data for object-based forest species classification. *Remote Sensing of Environment, 114*(6), 1141-1154.

Laliberte, A.S., Rango, A., Havstad, K.M., Paris, J.F., Beck, R.F., McNeely, R., & Gonzalez, A.L. (2004). Object-oriented image analysis for mapping shrub encroachment from 1937 to 2003 in southern New Mexico. *Remote Sensing of Environment, 93*(1-2), 198-210.

Maillard, P. (2003). Comparing texture analysis methods through classification. *Photogrammetric Engineering and Remote Sensing, 69*(4), 357-367.

Mallinis, G, Koutsias, N., Tsakiri-Strati, M., & Karteris, M. (2008). Object-based classification using Quickbird imagery for delineating forest vegetation polygons in a Mediterranean test site. *ISPRS Journal of Photogrammetry and Remote Sensing, 63*(2), 237-250.

Möller, M., Lymburner, L., & Volk, M. (2007). The comparison index: A tool for assessing the accuracy of image segmentation. *International Journal of Applied Earth Observation and Geoinformation, 9*(3), 311- 321.

Muller, E. (1997). Mapping riparian vegetation along rivers: old concepts and new methods. *Aquatic Botany, 58*(3), 411-437.

Nielsen, A.A. (2007).The regularized iteratively reweighted MAD method for change detection in multi- and hyperspectral data. *IEEE Transactions on Image Processing, 16*(2), 463-478.

Nielsen, A.A., Conradsen, K., & Simpson, J.J. (1998). Multivariate alteration detection (MAD) and MAF postprocessing in multispectral, bitemporal image data: new approaches to change detection studies. *Remote Sensing of Environment, 64*(1-9), 1-19.

Papazoglou, E.G., Karantounias, G.A., Vemmos, S.N., & Bouranis, D.L. (2005). Photosynthesis and growth responses of giant reed (*Arundo donax* L.) to the heavy metals Cd and Ni. *Environment International, 31*(2), 243-249.

Pearlstine, L., Portier, K.M., & Smith, S.E. (2005). Textural discrimination of an invasive plant, *Schinus terebinthifolius*, from low altitude aerial digital imagery. *Photogrammetric Engineering and Remote Sensing, 71*(3), 289-298.

880 Peña-Barragán, J.M., Ngugi, M.K., Plant, R.E., & Six, J. (2011). Object-based crop
881 identification using multiple vegetation indices, textural features and crop phenology. *Remote*
882 *Sensing of Environment, 115*(6), 1301-1316.
883
884 Pengra, B.W., Johnston, C.A., & Loveland, T.R. (2007). Mapping an invasive plant,
885 *Phragmites australis*, in coastal wetlands using the EO-1 Hyperion hyperspectral sensor.
886 *Remote Sensing of Environment*, *108*(1), 74-81.
887
888 Pinto, J., & Correia, S. (2012). Distribuição de cana (*Arundo donax*) no Algarve e contributos
889 para a sua gestão. In Camprodon, J., Ferreira, M.T., Ordeix, M., 2012. *Restauro e Gestão*
890 *Ecológica Fluvial*. Manual de Boas Práticas de Gestão de Rios e Ribeiras. RICOVER Project.
891
892 Pu, R., & Landry, S. (2012). A comparative analysis of high spatial resolution IKONOS and
893 WorldView-2 imagery for mapping urban tree species. *Remote Sensing of Environment, 124*,
894 516-533.
895
896 Puissant, A., Hirsch, J., & Weber, C. (2005). The utility of texture analysis to improve per-
897 pixel classification for high to very high spatial resolution imagery. *International Journal of*
898 *Remote Sensing*, *26*(4), 733-745.
899
900 Radoux, J., & Defourny, P. (2008). Quality assessment of segmentation results devoted to
901 object-based classification. In T. Blaschke, S. Lang, & G. J. Hay (Eds.), *Object Based Image*
902 *Analysis-Spatial Concepts for Knowledge-Driven Remote Sensing Applications*. Berlin.
903 Springer-Verlag
904

905 Robinson, D.J., Redding, N.J., & Crisp, D.J. (2002). *Implementation of a fast algorithm for*
906 *segmenting SAR imagery*. Scientific and Technical Report, Australia: Defense Science and
907 Technology Organization.
908
909 Rossa, B., TuAers, A.V., Naidoo, G., & von Willert, D.J. (1998). *Arundo donax* L. (Poaceae)
910 - a C3 species with unusually high photosynthetic capacity. *Botanica Acta, 111*, 216-221.
911
912 Safavian, S.R., & Landgrebe, D. (1991). A survey of decision tree classifier methodology.
913 *IEEE Transactions on Systems, Man and Cybernetics, 21*(3), 660-674.
914
915 Schmidt, K.S., & Skidmore, A.K. (2003). Spectral discrimination of vegetation types in a
916 costal wetland. *Remote Sensing of Environment*, *85*(1), 92-108.
917
918 Silva, C.M.N., Silva, L., Oliveira, N., Geraldes, P., & Hervías, S. (2011). Control of giant
919 reed Arundo donax on Vila Franca do Campo Islet, Azores, Portugal. *Conservation Evidence*
920 *8*, 93-99.
921
922 Tso, B., & Mather, P.M. (2009). *Classification Methods for Remotely Sensed Data*, second
923 ed, CRC Press, Taylor and Francis Group, Florida.
924
925 Underwood, E.C., Ustin, S.L., & DiPietro, D. (2003). Mapping nonnative plants using
926 hyperspectral imagery. *Remote Sensing of Environment, 86*(2), 150-161.
927

928 Underwood, E.C., Ustin, S.L., & Ramirez, C.M. (2007). A comparison of spatial and spectral
929 image resolution for mapping invasive plants in coastal California. *Environmental*
930 *Management, 39*(1), 63-83.
931
932 Vaiphasa, C., Skidmore, A.K., Boer, W.F., & Vaiphasa, T. (2007). A hyperspectral band
933 selector for plant species discrimination. . *ISPRS Journal of Photogrammetry and Remote*
934 *Sensing, 62*(3), 225-235.
935
936 Xie, Z., Roberts, C., & Johnson, B. (2008). Object-based target search using remotely sensed
937 data: A case study in detecting invasive exotic Australian Pine in south Florida. *ISPRS*
938 *Journal of Photogrammetry and Remote Sensing, 63*(6), 647-660.
939
940 Yamagata, Y., & Yasuoka, Y. (1993). *Classification of wetland vegetation by texture analysis*
941 *methods using ERS-1 and JERS-1 images*. Geoscience and Remote Sensing Symposium.
942 IGARSS Better Understanding of Earth Environment. 4, pp1614-1616.
943
944 Yang, X. (2007). Integrated of remote sensing and geographic information systems in riparian
945 vegetation delineation and mapping. *International Journal Remote Sensing, 28*(2), 353-370.
946
947 Yang, C., Goolsby, J.A., Everitt, J.H., & Du, Q. (2012). Applying six classifiers to airborne
948 hyperspectral imagery for detecting giant reed. *Geocarto International, 27*(5), 413-424.
949
950 Yu, Q., Gong, P., Clinton, N., Biging, G., Kelly, M., & Schirokauer, D. (2006). Object-based
951 detailed vegetation classification with airborne high spatial resolution remote sensing
952 imagery. *Photogrammetric Engineering and Remote Sensing, 72*(7), 799-811.

Zhang, Y.J. (1997). Evaluation and comparison of different segmentation algorithms. *Pattern Recognition Letters, 18*(10), 963-974.

List of Figures

Figure 1 – Partial output of the airborne multispectral image Set07 in true-color composition (red, green and blue bands), a) initial segmentation output with a scale level of 40.0 b) segmentation output with a merged lamdba value of 90.0 to eliminate the over-segmentation.

Figure 2 –Variable importance score of the ensemble bootstrap trees for the three airborne images and the satellite image. (dot = median, 25 and 75 quartile).

Figure 3 – Grayscale image resulting from the sum of the ten binary maps for the satellite image. Red line delineates the riparian area.

Figure 4 – Final giant reed object based map for the airborne Sep07 applying the a) Majority criteria and b) Unanimity criteria. Red line delineates the riparian area.

Figure 5- Area (mean, ± min, max) for the *Arundo donax* patches with riverine and terrestrial locations, classified manually and with an OBIA approach, using airborne multispectral images and the WorldView-2 image.

976 Figure 6- Landscape metrics values (mean, min, max) for the *Arundo donax* patches with
977 riverine and terrestrial locations, classified manually and with an OBIA approach, using
978 airborne multispectral images and the WorldView-2 image.
979
980 Figure 7 – Partial output of the a) final giant reed map obtained with the OBIA approach and
981 b) final giant reed map from on-screen digitizing, superimposed in a true color composite
982 image (red, green and blue) for the airborne Sep07. The red line delineates the objects
983 classified as giant reed with a riverine location, blue line the objects classified as giant reed
984 with a terrestrial location and yellow line the ground truth riverine giant reed patches
985 manually digitalized.

Table 1 – Total number of objects after the segmentation process for the airborne images and the satellite image. Number of training objects for the giant reed and for the non-giant reed classes.

	Total objects after segmentation	Giant reed training objects	Non-giant reed training objects
Airborne image_Nov04	23270	73	464
Airborne image_Sep07	36863	58	736
Airborne image_Oct10	47365	59	946
Satellite image_WorldView-2	6750	37	136

Table 2 – Characterization of the geometric, spectral and textural attributes of the objects used in this study. Acronyms in parenthesis.

Category	Name	Units and range	Description	Calculation
Geometric	Area (AREA)	Square meters]0, ∞[	Basic geometric statistics	Total area without holes
	Form Factor (FORMFACTOR)	None]0, 1]	Objects configuration complexity Circular object=1 Square object=0.785 Low values for complex configurations	Ratio between area and the square of the total perimeter.
	Elongation (ELONGATION)	None [1, ∞[	Object stretching level Square object =1	Ratio between the major axis and the minor axis
	Main Direction (MAINDIR)	Degrees [0, 180]	North/South = 90 degrees East/West = 180 degrees	The angle made by the major axis and the x-axis
Spectral	Mean (AVGBAND_x)	DN [0, 255]	Basic spectral statistics	Average value of the pixels comprising the object in each band
	Standard Deviation (STDBAND_x)	DN [0, 255]		Standard deviation value of the pixels comprising the object in each band
	Normalized Difference Vegetation Index (NDVI)	Normalized DN [-1,1]	Objects greenness level High values for green vegetation	Normalized band ratio between the red band and the near-infrared band.
Texture	Mean (TX_MEAN)	DN [0, 255]	Basic first-order statistics. Continuous measures of pixel values variability	Average value of the pixels comprising the object using a 3x3 window analysis
	Variance (TX_VARIANC)	DN [0, 255]		Average variance of the pixels comprising the object using a 3x3 window analysis
	Entropy (TX_ENTROPY)	DN [0, 255]		Level of image disorder

Table 3 – Minimum and maximum values of the geometric, spectral and textural attributes, mean (± SD) for the giant reed and the non-giant reed classes for the airborne images and the satellite image. Table 2 gives the acronyms of variables.

Category		Giant reed				Non-giant reed			
		Airborne			Satellite	Airborne			Satellite
	Name	Nov04	Sep07	Oct10	Jul10	Nov04	Sep07	Oct10	Jul10
		N= 73	N=58	N=59	N=37	N= 464	N=736	N= 946	N=136
Geometric	AREA	8.1-1078.1 264.3±(232.4)	8.3-1561.3 387.0±(350.5)	37.0-2774.3 372.6±(497.0)	44.0-7140.0 1239.6±(1383)	0.9-1958.2 80.0±(211.5)	0.5-3467.8 51.0±(189.4)	0.2-18783.3 67.1±(642.8)	4.0-12712.0 533.8±(1903.3)
	FORMFACTOR	0.07-0.55 0.25±(0.10)	0.08-0.57 0.27±(0.11)	0.05-0.55 0.22±(0.11)	0.09-0.76 0.33±(0.15)	0.05-0.84 0.47±(0.19)	0.04-0.85 0.49±(0.17)	0.00-0.84 0.50±(0.17)	0.11-0.82 0.52±(0.16)
	ELONGATION	1.07-5.59 2.19±(0.83)	1.20-5.58 2.56±(1.06)	1.01-5.24 2.32±(0.93)	1.02-5.54 2.33±(1.06)	0.82-9.26 1.76±(0.82)	1.00-11.80 1.82±(0.93)	1.00-19.42 1.88±(1.15)	1.00-8.59 1.86±(0.95)
	MAINDIR	18.5-179.1 129.2±(25.6)	11.5-173.1 123.0±(29.1)	3.3-176.8 128.6±(33.1)	1.5-168.2 116.1±(33.0)	0.0-179.8 93.7±(51.1)	0.0-179.64 85.1±(50.5)	0.0-180.0 86.0±(50.7)	0.0-175.6 88.1±(46.6)
Spectral	AVG_coastal	-	-	-	38.8-42.6 41.2±(0.8)	-	-	-	37.8-103.0 47.8±(10.3)
	AVG_blue	65.0-113.5 94.9±(8.7)	54.8-111.7 89.2±11.3	71.6-102.9 87.3±(6.00)	21.6-26.2 24.3±(0.9)	30.0-217.7 100.6±(30.0)	14.8-197.4 82.0±(31.2)	10.7-191.8 88.0±(30.8)	20.2-89.5 31.7±(11.1)
	AVG_green	37.8-143.3 102.2±(18.6)	59.7-127.5 104.5±(12.1)	85.7-131.3 107.3±(8.9)	25.0-38.2 33.0±(2.7)	-7.2-261.0 114.1±(57.6)	7.5-215.2 92.5±(39.1)	30.6-227.8 105.7±(37.2)	20.6-143.5 44.8±(20.0)
	AVG_yellow	-	-	-	21.0-35.0 29.4±(2.9)	-	-	-	17.3-171 50.6±(27.2)
	AVG_red	12.6-131.4 77.1±(22.5)	42.0-96.4 77.7±(11.6)	60.3-113.0 86.0±(10.6)	8.6-16.0 12.6±(1.5)	-36.2-254.4 99.8±(66.2)	2.44-223.3 89.1±(47.0)	25.9-220.9 102.6±(41.4)	7.1-96 26.1±(15.2)
	AVG_red edge	-	-	-	45.2-81.1 68.3±(7.0)	-	-	-	27.2-179 68.6±(25.6)
	AVG_NIR 1	147.43-190.6 173.7±(9.4)	129.2-190.2 169.1±(8.9)	170.0-206.0 188.2±(8.6)	50.4-86.8 73.0±(7.9)	17.6-206.3 166.1±(17.6)	33.0-220.5 140.0±(29.3)	90.7-218.4 162.8±(25.4)	19.5-118.5 55.8±(16.9)
	AVG_NIR 2	-	-	-	74.9-129.1 111.9±(11.6)	-	-	-	32-181.5 87.8±(26.6)
	STD_coastal	-	-	-	0.7-1.8 1.0±(0.2)	-	-	-	0.0-38.5 2.7±(3.8)
	STD_blue	6.6-12.8 9.8±(1.1)	6.9-13.7 11.0±(1.1)	10.8-16.1 13.6±(1.1)	0.8-2.5 1.4±(0.4)	3.1-23.6 10.7±(3.24)	1.8-30.7 11.4±(3.6)	0.0-34.5 13.7±(4.7)	0.0-40.2 3.5±4.0
	STD_green	10.8-23.0 19.1±(2.1)	8.0-16.0 12.4±(1.5)	12.0-17.5 14.8±(1.2)	2.1-5.2 3.4±(0.8)	10.8-23.0 19.1±(2.1)	1.6-29.7 12.5±(4.0)	0.0-39.7 14.9±(4.9)	0.0-72.5 6.9±(7.1)
	STD_yellow	-	-	-	2.1-8.8 4.0±(1.3)	-	-	-	0.0-95.0 8.6±(9.2)
	STD_red	13.2-25.9 20.9±(2.45)	6.8-19.5 13.0±(2.0)	11.0-16.2 13.6±(1.2)	1.0-6.0 2.7±(1.3)	3.6-42.8 20.6±(5.7)	1.1-32.2 13.1±(5.1)	0.0-41.3 14.1±(4.9)	0.0-48.4 5.7±(5.3)
	STD_red edge	-	-	-	5.4-10.7 7.8±(1.3)	-	-	-	0.0-74.4 9.8±(7.11)
	STD_NIR 1	4.8-10.4 7.9±(1.2)	5.8-12.7 9.3±(1.4)	7.4-16.8 11.9±(1.9)	6.13-12.2 9.14±(1.5)	1.4-14.1 7.2±(2.2)	1.0-26.2 11.1±(3.9)	0.0-31.4 10.8±(3.6)	0.0-50.5 8.3±(5.5)
	STD_NIR 2	-	-	-	6.5-17.4 12.6±(2.2)	-	-	-	0.0-75.4 11.94±(7.8)
	NDVI	0.18-0.84 0.39±(0.11)	0.28-0.51 0.37±(0.06)	0.29-0.49 0.37±(0.04)	0.61-0.76 0.70±(0.02)	-0.15-1.79 0.34±(0.34)	-0.25-0.93 0.27±(0.20)	-0.02-0.63 0.25±(0.15)	-0.03-0.77 0.39±(0.17)
Texture	TX_MEAN	63.7-118.8 87.1±(9.8)	55.6-105.8 82.6±(12.1)	66.1-94.5 78.1±(6.2)	38.3-43.8 41.0±(1.1)	21.6-179.4 95.4±(21.6)	16.2-226.4 92.1±(25.8)	49.3-198.6 85.5±(20.6)	38.4-96.9 46.4±(8.8)
	TX_VARIANC	8.6-154.0 64.7±(26.8)	34.0-163.6 89.5±(31.9)	48.5-237.5 140.1±(42.2)	0.4-4.5 1.3±(1.0)	2.1-1150.0 111.7±(100.7)	2.4-857.0 124.9±(116.6)	1.8-2490.9 235.2±(252.2)	0.2-242.8 22.3±(39.8)
	TX_ENTROPY	0.17-0.19 0.18±(0.00)	0.18-0.19 0.18±(0.00)	0.18-0.19 0.18±(0.00)	0.13-0.16 0.14±(0.00)	0.00-0.19 0.18±(0.01)	0.14-0.19 0.18±(0.00)	0.09-0.19 0.18±(0.00)	0.11-0.19 0.16±(0.01)

Table 4 – Classification accuracy matrix for the optimal ensemble trees for the giant reed and non-giant reed. Test was performed on an independent data set.

	Giant reed		Non-giant reed		Overall	
	Learn	Test	Learn	Test	Learn	Test
Airborne_Nov04	0.97	0.84	0.94	0.90	0.94	0.89
Airborne_Sep07	0.97	0.87	0.97	0.98	0.97	0.97
Airborne_ Oct10	0.99	0.88	0.97	0.95	0.97	0.92
Satellite_Jul10	0.97	0.87	0.96	0.96	0.97	0.95

Table 5 – Confusion matrix comparing the riverine giant reed OBIA map and the giant reed map created from on-screen digitizing. Units are in pixels.

On-screen digitizing	Non-giant reed	Giant reed	Total	User's accuracy (%)	Kappa coefficient
Object based					
Airborne_Nov04					**0.55**
Non-giant red	9811415	77747	9889162	99.21	
Giant reed riverine	16400	59442	75842	**78.38**	
Total pixels	9827815	137189	9965004		
Producer's accuracy (%)	99.83	**43.33**			
Airborne_Sep07					**0.73**
Non-giant red	9811011	37449	9848460	99.62	
Giant reed riverine	27828	88716	116544	**76.12**	
Total pixels	9838839	126165	9965004		
Producer's accuracy (%)	99.72	**70.32**			
Airborne_Oct10					**0.67**
Non-giant red	9799951	42667	9842618	99.57	
Giant reed riverine	38294	84092	122386	**68.71**	
Total pixels	9838245	126759	9965004		
Producer's accuracy (%)	99.61	**66.34**			
Satellite_Jul10					**0.77**
Non-giant red	966135	2523	968658	99.74	
Giant reed riverine	3672	10449	14121	**74.00**	
Total pixels	969807	12972	982779		
Producer's accuracy (%)	99.62	**80.55**			

Figure 1 – Partial output of the airborne multispectral image Set07 in true-color composition (red, green and blue bands), a) initial segmentation output with a scale level of 40.0 b) segmentation output with a merged lamdba value of 90.0 to eliminate the over-segmentation.

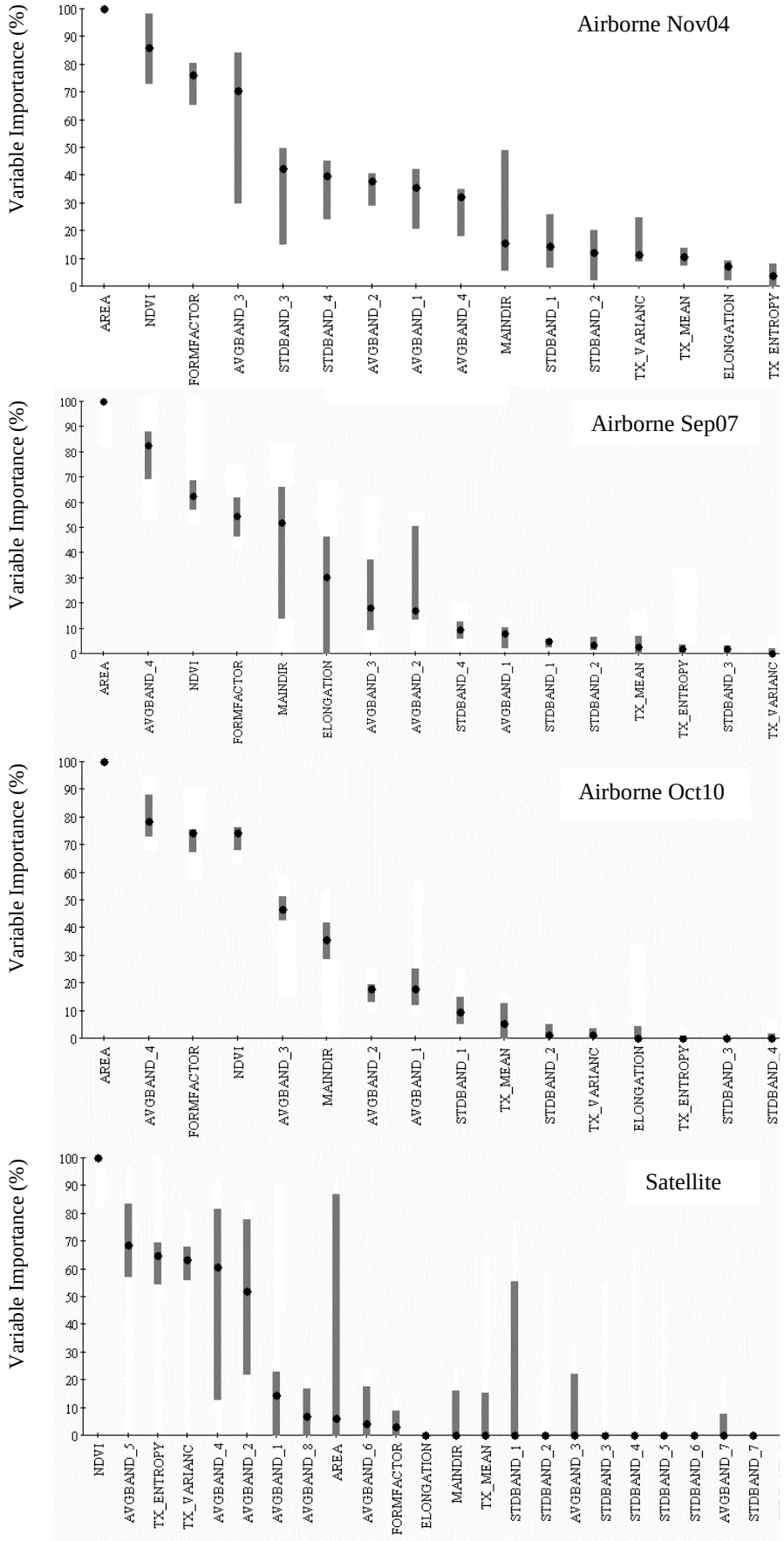

Figure 2 –Variable importance score of the ensemble bootstrap trees for the three airborne images and the satellite image. (dot = median, 25 and 75 quartile).

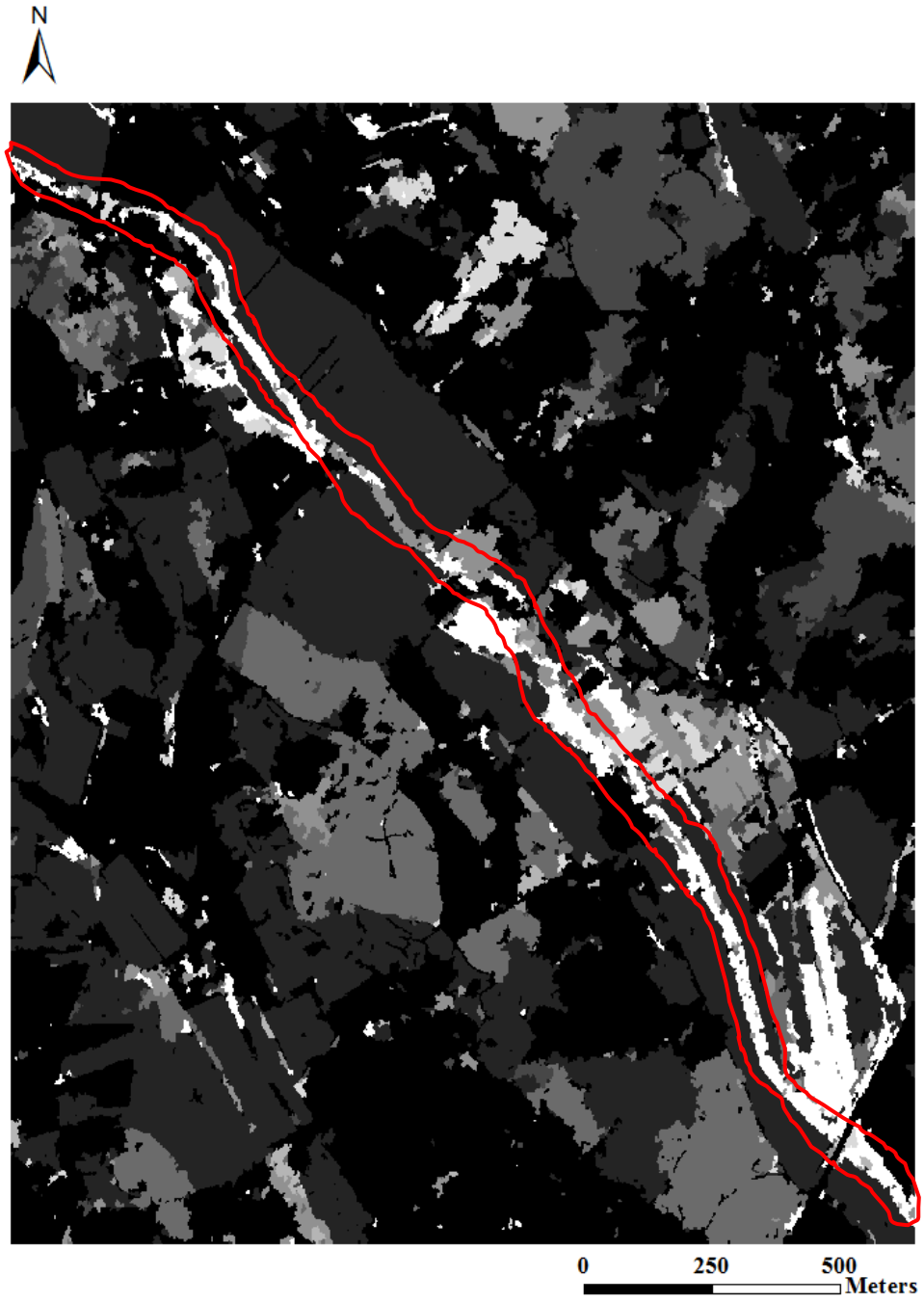

Figure 3 – Grayscale image resulting from the sum of the ten binary maps for the satellite image. Red line delineates the riparian area.

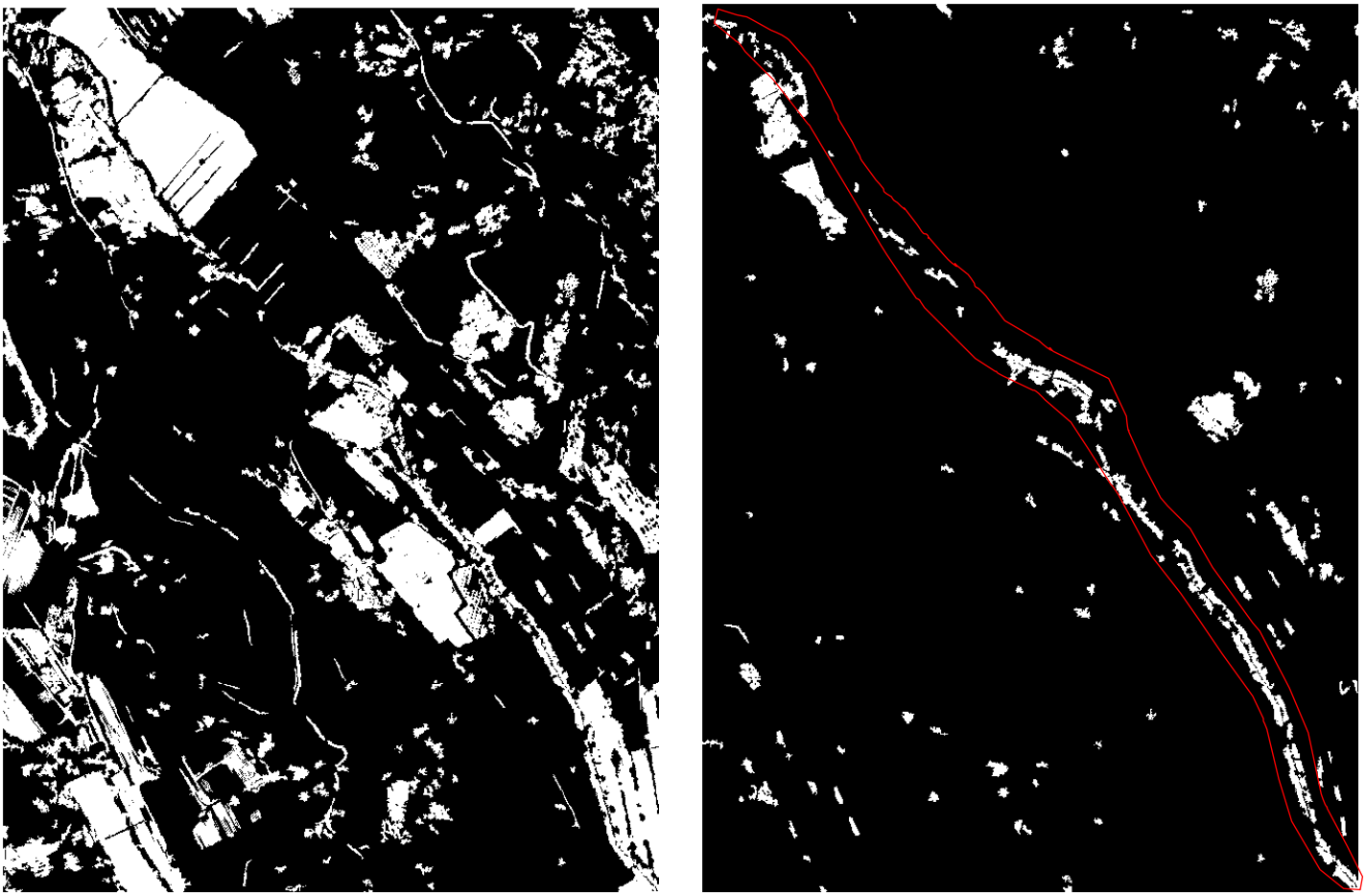

a) b)

Figure 4 – Final giant reed object based map for the airborne Sep07 applying the a) Majority criteria and b) Unanimity criteria. Red line delineates the riparian area.

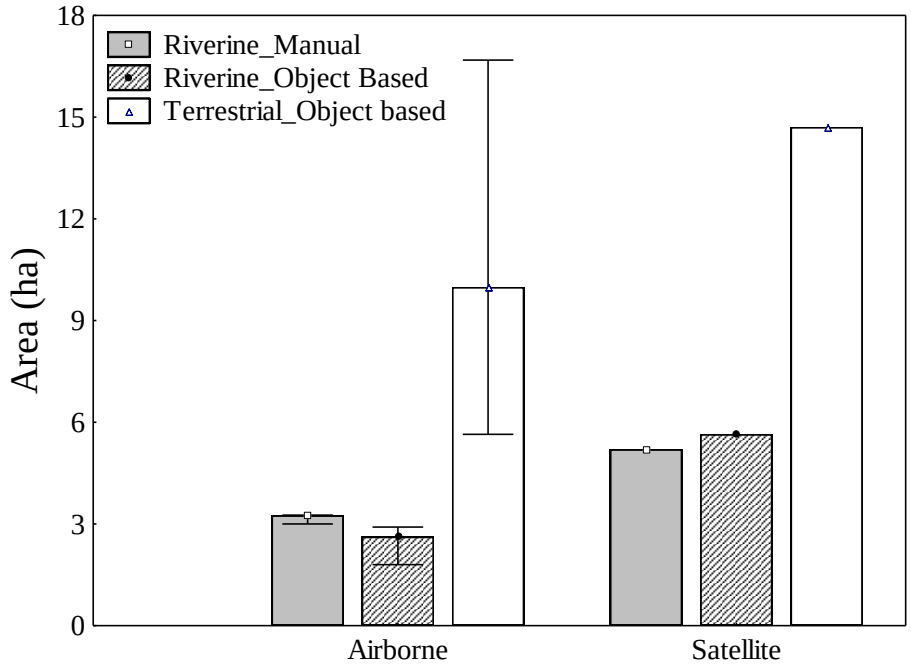

Figure 5- Area (mean, ± min, max) for the *Arundo donax* patches with riverine and terrestrial locations, classified manually and with an OBIA approach, using airborne multispectral images and the WordView-2 image.

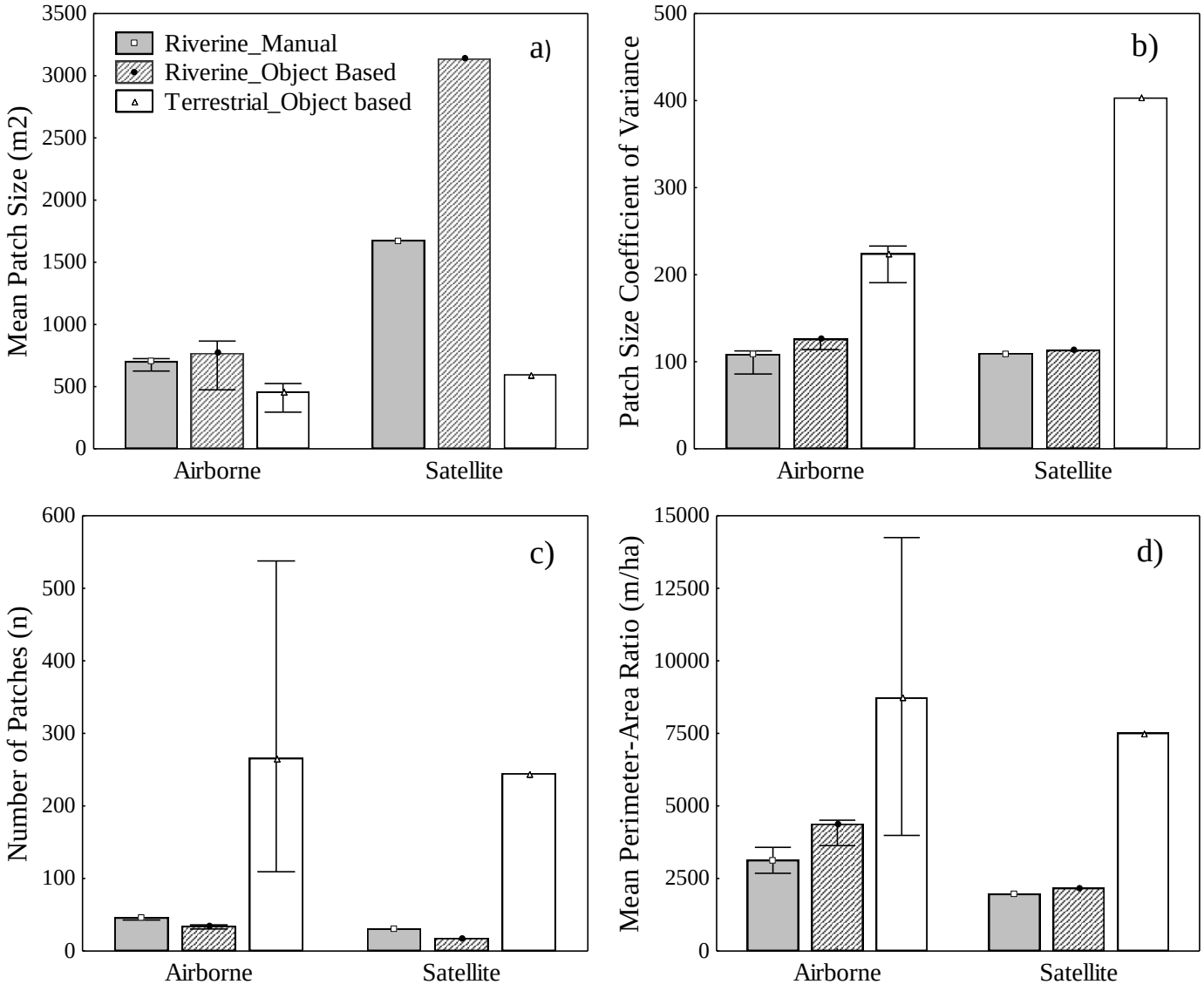

Figure 6- Landscape metrics values (mean, min, max) for the *Arundo donax* patches with riverine and terrestrial locations, classified manually and with an OBIA approach, using airborne multispectral images and the WordView-2 image.

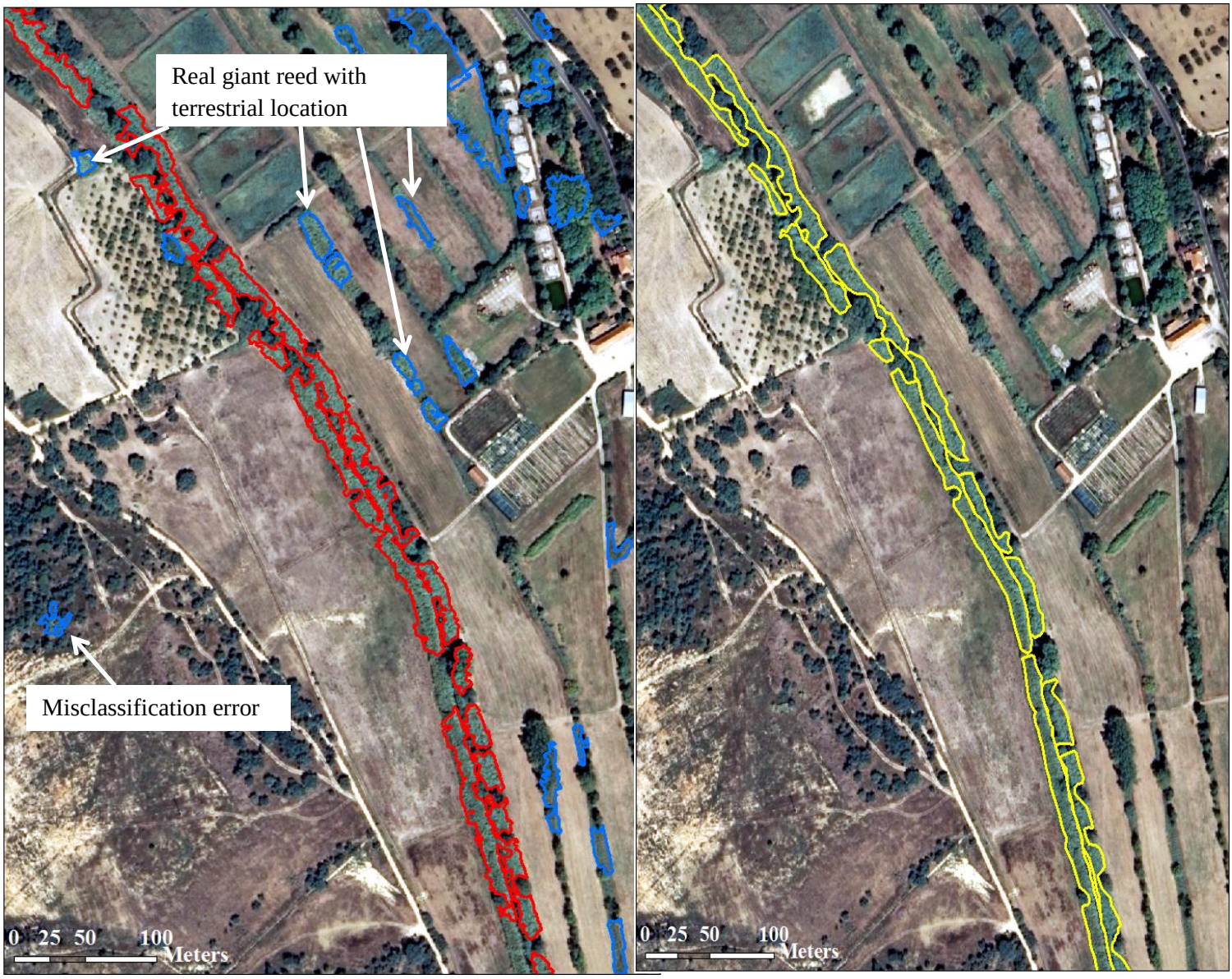

a) b)

Figure 7 – Partial output of the a) final giant reed map obtained with the OBIA approach and b) final giant reed map from on-screen digitizing, superimposed in a true color composite image (red, green and blue) for the airborne Sep07. The red line delineates the objects classified as giant reed with a riverine location, blue line the objects classified as giant reed with a terrestrial location and yellow line the ground truth riverine giant reed patches manually digitalized.

PARTE IV

Discussão

Capítulo 6

Discussão de resultados

6.1 Considerações iniciais

Os trabalhos realizados, no âmbito desta dissertação, permitiram reconhecer a capacidade de identificar e caracterizar os padrões estruturais e composicionais da vegetação ripária, bem como relacioná-los com o estado de integridade ecológica dos corredores fluviais, através da aplicação de técnicas de deteção remota, análises geoestatísticas e Sistemas de Informação Geográfica (SIG). Relativamente aos objetivos particulares desta dissertação, os estudos de separabilidade espectral permitiram reconhecer e caracterizar a dissimilaridade dos traços óticos e das assinaturas espectrais associadas às diferentes tipologias de florestas ripárias nativas existentes em Portugal continental e das respetivas espécies dominantes. A aplicação das métricas de paisagem permitiu a caracterização da estrutura da vegetação ripária, tendo sido possível relacionar os padrões de degradação observados com o gradiente de pressão antropogénico, exercido nas imedições da zona ribeirinha. Os estudos de espectroradiometria possibilitaram o reconhecimento das zonas ótimas do espectro eletromagnético para distinção da cana face à vegetação nativa envolvente, tendo em conta a variabilidade espectral sazonal das diferentes classes de vegetação. Reconheceu-se, ainda, a importância da complementaridade da informação remota descritora de atributos geométricos para a distinção de diferentes tipos de vegetação. Identificaram-se os principais resultados e as respetivas implicações para a gestão e monitorização dos ecossistemas ripários, reconhecendo limitações e identificando prioridades futuras de investigação.

6.2 Caracterização remota dos padrões estruturais e composicionais da vegetação ripária.

6.2.1 Separabilidade espectral de florestas ripárias e padrões espectrais composicionais

A caracterização remota dos padrões composicionais da vegetação ripária foi efetuada através da identificação das assinaturas espectrais, quer das espécies quer das comunidades ripárias nativas e da avaliação do respetivo nível de distinção espectral (capítulo 2). As assinaturas espectrais descrevem a intensidade com que os corpos na natureza refletem ou emitem a radiação eletromagnética nos diversos comprimentos de onda ao longo do espetro eletromagnético. As assinaturas espectrais típicas da vegetação são caracterizadas por valores de reflectância reduzidos na região do visível (400-700nm), com uma ligeira exceção na zona do verde, seguido de uma transição abrupta, designada por “red-edge”, caracterizada pelo aumento da reflectância na região do infravermelho próximo (700-1300nm). A distinção espectral da vegetação ocorre em função das características e dos traços óticos existentes ao

nível da folha, que regulam sobretudo o comportamento espectral na região do visível, e dos traços óticos ao nível da copa, que determinam ainda o comportamento na região do infravermelho (Cochrane 2000; Schmidt e Skidmore 2003).

O comportamento na região do visível está sobretudo dependente da concentração dos pigmentos fotossintéticos e da presença da água no mesófilo da folha, responsáveis pelos padrões de absorção da radiação solar incidente. Apesar de variável em função de espécie e da época do ano, o comportamento da refletância nesta região é mais previsível do que o comportamento na região do infravermelho próximo, uma vez que este é regulado não só pelas características ao nível da folha (padrões de difusão da radiação em função das características do mesófilo e dos espaços intercelulares), mas também pelo efeito conjunto de fatores relacionados com a arquitetura da copa, a complexidade da estrutura vertical, o volume de tronco, a densidade foliar e o grau de coalescência foliar.

As formações ripárias lenhosas existentes em Portugal continental apresentam diferenças ao nível da composição florística, diversidade e grau de cobertura de espécies, em resultado da atuação de um gradiente geomorfológico e climático à escala regional e de variáveis geomorfológicas à escala do segmento (Aguiar et al., 2000). Neste capítulo é postulado que essas diferenças devem-se a um conjunto de traços morfológicos, fisiológicos e ecológicos, que se traduzem numa convergência ótica intraclasse, tornando as florestas ripárias remotamente separáveis entre si. Nas formações lenhosas ripícolas localizadas no extremo do gradiente climático; i.e florestas da zona temperada vs florestas da zona mediterrânica, foi possível reconhecer padrões de separabilidade espectral elevada. As florestas ripárias destas regiões estão sujeitas a distintos constrangimentos ambientais desenvolvendo um conjunto de características, quer ao nível das espécies, quer ao nível da comunidade, com repercussões no comportamento espectral, potenciando a separabilidade ótica destas formações. A singularidade dos padrões espectrais foi sobretudo observada nas florestas ripárias da zona mediterrânica. Estas são formadas maioritariamente por espécies arbustivas perenifólias como o loendro, (*Nerium oleander L*.) ou esclerófilas, como o tamujo (*Flueggea tinctoria* (L.) G.L.) e a tamargueira (*Tamarix africana* Poiret) que apresentam um conjunto de adaptações à secura estival e à elevada intensidade de radiação, quer ao nível das folhas (cor verde escuro, orientação predominantemente vertical, espessamento da epiderme, presença de ceras, reduzida concentração de pigmentos fotossintéticos), quer ao nível da copa (baixa densidade foliar, coalescência foliar elevada, reduzido diâmetro). Estes atributos têm implicações na forma como estas espécies absorvem, difundem e refletem a luz solar (Ollinger, 2011) que se

traduzem num comportamento espectral caracterizado pela reduzida refletância na região do infravermelho próximo e valores de "red-edge" reduzidos, quando comparados com os padrões espectrais típicos da restante vegetação. Em oposição, as formações ripárias da região temperada são formadas maioritariamente por espécies caducifólias, como o amieiro (*Alnus glutinosa* (L.) Gaertner) e o freixo (*Fraxinus angustifolia* Vahl.), apresentando traços, quer ao nível das folhas (elevado conteúdo em água, ângulo de inserção horizontal por forma a potenciar a captação de radiação solar, elevado teor de pigmentos fotossintético), quer ao nível das copas (distribuição homogénea da folhagem, elevada complexidade vertical) que, no geral, dão origem a uma assinatura espectral com valores de reflectância relativamente mais elevados, sobretudo, na região do vísivel e do infravermelho próximo.

Para as florestas ripárias da região de transição não foi possível encontrar valores de separabilidade espectral que as permitam distinguir remotamente das restantes florestas ripárias. A variabilidade espectral da vegetação ripária desta zona é superior à das outras regiões, estando associada a uma maior heterogeneidade florística. As comunidades desta região, embora dominadas por salgueirais, são caracterizadas pela presença de espécies que também ocorrem nas outras duas regiões, como é o caso do amieiro, do freixo, do amieiro-negro (*Frangula alnus* Miller), da tamargueira, embora com frequência de ocorrência e densidades distintas. A reduzida separabilidade espectral desta região face às restantes reconhece-se nos erros de classificação ocorridos entre pixels com comportamentos espectrais semelhantes. Como exemplo, referira-se a similaridade entre as assinaturas espectrais de manchas de vegetação da região de transição compostas por *Fraxinus angustifolia* e *Salix atrocinerea* e as comunidades da região mediterrânica, ambos com valores de reflectância reduzidos.

As florestas ripárias localizadas em rios de média dimensão apresentam valores de separabilidade espectral mais elevada quando comparadas com as florestas localizadas em rios de pequena dimensão. Ao contrário do que seria esperado, a composição florística encontrada nos locais de referência de rios de média dimensão apresenta padrões de reduzida diversidade biológica, quando comparada com a riqueza e composição florística encontrada em rios de menor dimensão, o que conduz a uma menor variabilidade espectral, aumentando a distinção remota entre as florestas ripárais nos rios de média dimensão. Como exemplo, pode referir-se a dominância de amieiros em muitos dos rios de média dimensão na região temperada enquanto em rios de pequena dimensão foi encontrada uma mistura de amieiros, freixos e salgueiros.

Os valores da separabilidade espectral aumentam significativamente, quando em vez das assinaturas espectrais correspondentes à totalidade da variabilidade florística – assinatura espectral da comunidade - se utilizam as assinaturas das espécies ripárias dominantes (espécies de maior frequência e abundância em cada região), designadamente *Alnus glutinosa* para a região temperada, *Salix salviifolia* para a região de transição e *Nerium oleander* para a região mediterânica). A utilização de aspetos peculiares para potenciar a detetabilidade remota de espécies ripárias, em determinadas alturas do ciclo vegetativo, foi anteriormente utlizada com sucesso, na cartografia de (*Populus fremontii* S. Watson) e o (*Salix gooddingii* C.Ball) em zonas áridas (Nagler et al., 2005). No presente trabalho, as análises discriminantes revelaram uma precisão de classificação particularmente elevada para o amieiro, associada a um comportamento espectral claramente distinto das restantes espécies dominantes, caracterizado por valores de refletância elevados na região do visível e do infravermelho próximo. Este comportamento está relacionado com as caraterísticas fenológicas apresentadas por esta espécie no início do período vegetativo (folhas emergentes de cor verde-amarelada) que a tornam distinta da restante vegetação envolvente, quer visualmente quer por técnicas de deteção remota. Por sua vez, o loendro destaca-se por uma floração caracterizada pela presença de flores de uma coloração rosa intensa, embora neste caso, a singularidade do aspetos fenológicos ocorra durante o período de estiagem.

Implicações para a gestão e monitorização de ecossistemas ripários

A caracterização das assinaturas espectrais pode ser utilizada como medida da funcionalidade e integridade dos ecossistemas ripários (capítulo 1). A informação relativa aos padrões espectrais de comunidades localizadas em locais de reduzida perturbação (assinaturas espectrais de referência) permite uma avaliação preliminar da qualidade ecológica através da caracterização da componente composicional. A identificação de comportamentos espectrais, que representam desvios claros em relação às assinaturas espectrais de referência, permite identificar áreas prioritárias para restauro. Por exemplo, a deteção de assinaturas espectrais com valores de refletância elevadas em galerias ribeirinhas localizadas na região mediterrânica poderá indiciar a presença de padrões de degradação associados à presença de espécies invasoras, como é o caso do *Arundo donax* (cana), ou espécies herbáceas higrófilas, uma vez que a assinatura espectral típica das comunidade de referência apresenta valores de refletância naturalmente reduzidos tal como foi referido anteriormente. A deteção das espécies dominantes características de cada tipo ripário é também um indício do bom estado

de conservação da galeria ribeirinha, podendo as assinaturas espectrais destas espécies indicadoras serem usadas na criação de bibliotecas espectrais para posterior utilização na cartografia de zonas ripárias.

6.2.2 Caracterização remota dos padrões estruturais da vegetação ripária e influência do uso do solo.

É postulado que a vegetação ripária pode ser descrita com base em características estruturais (continuidade transversal e longitudinal, largura ripária) e que estas apresentam respostas preditivas à degradação, como o aumento da fragmentação, a diminuição da largura, as alterações dos padrões espaciais de distribuição das manchas de vegetação ao longo da galeria (Schuft et al., 1999) devido à pressão antropogénica exercida nas imediações das zonas ribeirinhas (Inoue e Nakagoshi, 2001; Allan, 2004; Aguiar e Ferreira, 2005). Tradicionalmente, a caracterização da vertente estrutural é realizada com recurso a trabalho de campo exaustivo e moroso ou a avaliações visuais expeditas, mas baseadas em critérios qualitativos, sendo difícil, oneroso e subjetivo replicar estas metodologias em escalas alargadas e/ou em locais de difícil acesso.

No trabalho do capítulo 3 concluiu-se que a estrutura da vegetação ripária pode ser descrita de forma detalhada, utilizando uma metodologia expedita e quantitativa, baseada no cálculo e interpretação de métricas de paisagem estabelecidas com recurso a imagens de elevada resolução espacial (50 cm). As métricas em causa são descritores numéricos de parâmetros relacionados como a densidade (número e tamanho médio), a configuração e complexidade (índice de forma e dimensão fratal), o isolamento e proximidade, o contágio e a interconectividade (índice de interspecção e justaposição) das manchas de vegetação. Nos 80 km de corredores fluviais estudados (afluentes do rio Tejo), as galerias ribeirinhas em bom estado de conservação apresentam manchas de vegetação lenhosa de média a elevada dimensão, com formas complexas e meandrizadas distribuídas de forma equilibrada ao longo da zona ripária. Em oposição, as galerias ripárias em mau estado de conservação são caracterizadas pela presença de um número reduzido de manchas de vegetação lenhosa de pequena dimensão e complexidade, dispostas de forma desequilibrada ao longo da zona ripária. As análises de redundância realizadas revelaram que os padrões de degradação observados estão relacionados com um gradiente de pressão antropogénico exercido na zona envolvente da galeria ribeirinha. No extremo do gradiente de pressão, com reduzidos impactos

físicos e ecológicos sobre o sistema ripário, encontra-se a classe correspondente ao uso agroflorestal, que inclui pastagens naturais, montados, sistemas extensivos e florestas mistas. No extremo oposto do gradiente, encontram-se os usos do solo com ocupações agrícolas em regimes intensivos e uso urbano e industrial. Embora vários trabalhos tenham revelado que o tipo de uso do solo envolvente influencia a estrutura da vegetação ripária (Bunn and Davies, 2000; Bott et al., 2006; von Schiller et al., 2008), este trabalho permitiu concluir que os usos do solo proximais, nomeadamente numa faixa de 30m contígua à zona ripária, apresentam uma maior influência na determinação dos padrões estruturais da vegetação ripária do que os usos do solo mais distais (faixa de 200m). Este resultado vai de encontro às conclusões obtidas num estudo precedente que sugeria que a extensão e a proximidade dos usos envolventes influenciam de forma preponderante os padrões de alteração da vegetação (Aguiar e Ferreira 2005). Contudo, a variabilidade da estrutura ripária não depende apenas dos usos do solo e da repectiva contiguidade, mas também de fatores históricos e/ou sociais, como é o caso de fenómenos naturais, tais como incêndios ou cheias extremas ou fatores humanos, como cortes rasos, extração de inertes e modificações do perfil do canal. Por outro lado, a componente espacial, nomeadamente a existência de autocorrelação espacial, reveste-se de particular importância, na medida em que pode alterar a perceção das relações entre as variáveis estudadas, sendo necessário incorporá-la nos estudos que englobem dados de carácter geográfico. Neste trabalho a utilização de uma subamostragem de dados com independência espacial revelou ser a opção mais adequada para a correta aferição da influência dos usos do solo na estrutura da vegetação ripária.

Interessa referir que, embora este trabalho tenha um delineamento adequado, com uma razoável amplitude de pressões e de degradação da zona ripária, há necessidade de ajustar este referencial a outras tipologias ripárias de outras regiões.

Os padrões de degradação observados caracterizam-se pela presença de galerias fragmentadas com poucas manchas de vegetação lenhosa e de reduzida dimensão. Contudo, padrões estruturais similares podem ser encontrados nas cabeceiras de rios, sem que isso represente um processo de redução de integridade, devido à presença de constrangimentos ambientais que não permitem o desenvolvimento de galerias frondosas e contínuas. Por outro lado, para uma caracterização adequada do estado de integridade, é necessário possuir informação complementar relativa à composição florística, sobretudo ao nível da vegetação arbórea e arbustiva. A presença de galerias ripárias com manchas de vegetação de elevada largura e conetividade longitudinal com configurações simples e lineares podem estar associadas à presença de espécies exóticas (ex, cana), ou de espécies florestais em regime de

produção lenhosa (choupo), estando, nestes casos, a reduzida qualidade ecológica da zona ripária relacionada sobretudo com características composicionais e não estruturais.

Implicações para a gestão e monitorização de ecossistemas ripários

A possibilidade de integração e visualização em ambiente SIG dos resultados da aplicação da métricas de paisagem na avaliação remota da qualidade ecológica das zonas ripárias torna esta metodologia numa ferramenta de elevado interesse para a gestão e monitorização dos sistemas fluviais, permitindo identificar áreas prioritárias para restauro ou sujeitas a medidas de conservação (Aguiar et al., 2011).

Este trabalho permitiu constatar a necessidade de combinar métricas de diferentes categorias para obter uma caracterização detalhada da estrutura da vegetação ripária. No entanto, é possível aligeirar a metodologia, selecionando métricas-chave que permitam classificar as zonas ripárias de acordo com distintos objetivos de gestão. Por exemplo, para restabelecimento da conectividade longitudinal, tendo em conta uma determinada espécie alvo, pode ser utilizada unicamente uma métrica de conectividade, o MPI (índice de proximidade). Esta métrica é calculada em função de uma distância mínima, estabelecida *a priori*, a partir da qual a distância entre manchas de vegetação passa a representar galerias com perda da conectividade, ou seja, galerias onde a função de corredor ecológico deixa de ser garantida, com descontinuidades no habitat e refúgio para aquela espécie, identificadas quando o valor da métrica é zero. Para a cartografia expedita da fragmentação ripária é possível utilizar uma combinação de duas métricas, o MNND (a distância ao vizinho mais próximo) e o MPS (tamanho da mancha). Manchas pequenas e distantes entre si dão uma ideia rápida da localização geográfica dos padrões de degradação associados a processos de fragmentação onde ocorrem perdas na transferência de energia e matéria ao longo da galeria ribeirinha. Por outro lado, a identificação de áreas para a aplicação de medidas de conservação, deverá ser realizada com recurso a métricas que avaliem a configuração espacial e a complexidade das manchas de vegetação, como é o caso do MSI (índice de forma média) e o MPFD (índice de dimensão média fractal) por representarem uma medida de transferência de fluxos ecológicos relacionados com os efeitos de orla e com a dinâmica de espécies associada à conetividade lateral.

Os resultados obtidos relativos à influência preponderante dos usos proximais na estrutura da vegetação poderão servir de suporte para o desenvolvimento de medidas legislativas que

regulem e restrinjam as utilizações humanas nas imediações das áreas ripárias, fomentando os usos do solo ecologicamente sustentáveis, como os sistemas agroflorestais, nas zonas contíguas à zona ripária.

As métricas de paisagem podem ainda ser usadas na identificação de zonas ripárias invadidas por espécies exóticas, como é o caso do *Arundo donax* L (cana). Constatou-se que as galerias ribeirinhas fortemente invadidas por esta espécie tendem a formar manchas de vegetação de grandes dimensões, com formas simples e lineares, sendo possível detetar e cartografar estas particularidades geométricas, utilizando uma combinação de métricas de diferentes categorias, nomeadamente, o MSI (indice de forma) e o MPS (tamanho da mancha).

6.3 Cartografia de *Arundo donax* L. e sua relação com o estado de integridade ripária

Numerosos estudos têm relacionado degradação da qualidade ecológica e funcional das zonas ripárias com a colonização das margens dos rios por espécies exóticas invasoras, nomeadamente pela cana, *Arundo donax* (Everitt et al., 2008; Ge et al., 2008). Esta espécie é responsável pela perda de biodiversidade e pela redução geral da funcionalidade ecológica dos ecossistemas ribeirinhos em diversas regiões do mundo de clima mediterrânico e sub-tropical, como é o caso do sul da Europa e do sudoeste americano (Herrera e Dudley, 2003; Cushman e Gaffney, 2010). Em Portugal, esta espécie encontra-se sobretudo no sul do país e nas bacias hidrográficas do Tejo e das ribeiras dos Oeste, onde terá sido introduzida para controle de erosão, para dividir propriedades agrícolas e como quebra-ventos e tutor de plantas trepadeiras (Aguiar et al., 2007; Aguiar e Ferreira, in press). Silva et al. (2011) refere ainda a presença de invasões de cana no arquipélago dos Açores onde tem sido apontada como responsável pela redução da composição florística endémica. Em ecossistemas ribeirinhos, devido à elevada disponibilidade em água, a cana apresenta um desenvolvimento vegetativo vigoroso e uma elevada capacidade de dispersão e colonização, dando origem a formações vegetais impenetráveis, que todos os anos são responsáveis por elevados prejuízos económicos relacionados com a inundação dos terrenos agrícolas e danos em pontes e açudes provocados pela retenção de sedimentos nos rios.

Apesar dos prejuízos ecológicos e económicos serem amplamente reconhecidos não se sabe ao certo a distribuição geográfica e a abundância desta invasora, nem a eficácia dos meios de luta, geralmente físicos ou químicos ou uma combinação de meios mecânicos e herbicidas. Em Portugal, todos os anos é necessário utilizar medidas de controlo da cana, que são efetuadas por entidades privadas ou públicas com responsabilidades na gestão da água e dos

ecossistemas fluviais. Tradicionalmente, a localização dos canaviais ribeirinhos é conhecida com recurso a campanhas in loco dispendiosas e exaustivas ou por interpretação de ortofotomapas, sendo neste último caso necessária uma validação posterior para reduzir a subjetividade do processo de classificação. Desta forma, o desenvolvimento de metodologias remotas semi-automáticas capazes de cartografar a distribuição de cana e monitorizar em tempo adequado a eficácia das medidas de controlo, são consideradas ferramentas fundamentais para a gestão das zonas ripárias.

6.3.1 Separabilidade espectral e variabilidade sazonal de *Arundo donax* em galerias ribeirinhas

As formações de cana em habitats ribeirinhos são frequentemente monoespecíficas, o que facilitaria o reconhecimento remoto das zonas invadidas, devido à maior homogeneidade espectral do *Arundo donax* face à vegetação envolvente. Contudo, esta espécie apresenta uma acentuada variabilidade espectral sazonal associada a processos de natureza fenológica (floração, senescência), e antropogénica (cortes mecânicos) o que dificulta a sua distinção da vegetação ripária ou da envolvente do corredor fluvial. Da mesma maneira, colocou-se a hipótese que a similaridade morfológica com outras espécies presentes no sistema ripário, como é o caso do caniço *(Phragmites australis* (Cav.) Trin. ex Steud*)*, dificultariam a identificação da cana devido à possível sobreposição das assinaturas espectrais das duas espécies. Neste trabalho, concluiu-se que a cana é espectralmente separável das restantes classes de vegetação envolvente (arbórea, arbustiva e herbácea), tanto no período vegetativo como no período de senescência, embora o número e a localização das bandas que maximizam a distinção variem em função da época e da classe de vegetação considerada. Como esperado, observou-se uma elevada similaridade espectral entre a cana e o caniço. No entanto, as duas espécies têm assinaturas espectrais distintas durante o período de senescência. Neste período, geralmente entre Outubro e Fevereiro na zona Oeste do país, enquanto a cana apresenta formações caracterizadas por uma mistura de folha amarelas (senescentes) com folhas verdes, originando assinaturas espectrais com o comportamento típico da vegetação, o caniço apresenta formações totalmente senescentes com assinaturas espectrais caracterizadas por uma redução acentuada dos valores de refletância na região do infravermelho próximo e na região do verde, devido à acentuada perda dos pigmentos fotossintéticos.

A utilização de espectroradiometria de campo (com 2151 bandas), combinada com um procedimento estatístico hierárquico, usando testes de análise de variância e árvores de

classificação, permitiu identificar as bandas ótimas para discriminação da cana, distribuídas por todo o espectro eletromagnético em análise (350 - 2500 nm), embora com predominância na região do "red-edge" (650nm a 750nm) e do infravermelho próximo (750 nm a 1300nm). Uma combinação de traços morfológicos e fisiológicos, quer ao nível da folha, quer ao nível da copa é responsável pelos padrões de separabilidade da cana face às restantes classes de vegetação. A elevada concentração de clorofila nas folhas desta exótica, combinada com elevadas taxas fotossintéticas e acentuado índice de área foliar (Rossa et al., 1998; Papazoglou et al., 2005) são responsáveis pelo deslocamento do "red-edge" para comprimentos de onda mais elevados (Chen e Chen, 2008; Ollinger, 2011), tal como observado neste estudo, o que potencia a separabilidade desta espécie face às restantes. Ao nível da copa, as diferenças na densidade foliar, complexidade da estrutura vertical e nível de coalescência das folhas, explicam a separabilidade da cana em relação à vegetação em redor. Por exemplo, a cana forma tendencialmente galerias densas com estruturas verticais coesas, enquanto a vegetação arbórea é caracterizada por uma estrutura vertical de elevada complexidade, com muitas lacunas responsáveis pelos fenómenos de retenção da radiação, dando origem a assinaturas espectrais com valores de refletância mais baixos sobretudo na região do infravermelho próximo (Alvarez-Añorve et al., 2008). Contudo, este trabalho conclui ainda que para a distinção da cana em relação à vegetação herbácea são também selecionados comprimentos de onda localizados na região do visível e para a discriminação face à vegetação arbórea são escolhidas bandas na região do infravermelho médio (1300 nm-2500). Enquanto a separabilidade espectral na região do infravermelho médio está sobretudo associada a diferenças no teor em água das diferentes espécies (zonas de absorção da radiação) e aos padrões de difusão da radiação dependentes da complexidade tridimensional da vegetação, a separabilidade na região do visível, sobretudo na região do verde, está maioritariamente relacionada com diferenças na cobertura foliar e respetiva concentração dos pigmentos fotossintéticos. Contudo, os resultados mostram a maior dificuldade do classificador em separar a cana da vegetação herbácea, no período de senescência, devido à grande heterogeneidade florística encontrada dentro da classe herbácea nesta altura do ano, com consequente mistura de "verdes" existente no mosaico da paisagem.

Um dos resultados mais interessantes deste estudo é a elevada separabilidade espectral encontrada entre a cana que regenera após corte (controlo mecânico), designada neste trabalho por cana_RAC (*regenerated after mechanical cutting*), face às diferentes classes de vegetação envolventes, quando comparada com a cana que não foi sujeita a qualquer medida de controlo. A rebentação da cana após o corte ocorre em qualquer altura do ano, estando

sobretudo dependente da disponibilidade hídrica. As formações de cana_RAC são formadas exclusivamente por folhas primárias, i.e, folhas do primeiro ano, mais largas, mais compridas e sem ramificação, quando comparadas com as folhas mais velhas (Decruyenaere e Holt, 2005). Estas características fisiológicas dão origem a formações vegetais homogéneas, de cor verde-escuro, bem distintas das formações de cana sem medidas de controlo, onde há uma mistura de folhas desse ano, com folhas amarelas mais estreitas e outras já senescentes, de anos anteriores. A elevada produção de biomassa e intenso vigor vegetativo da cana_RAC é comprovada neste estudo através do deslocamento da posição do "red-edge" para comprimentos de onda mais elevados, o chamado "*red-shift" of the red edge* quando comparada com a localização para as restantes classes de vegetação, o que potencia a separabilidade desta classe face às restantes classes. Este é um resultado francamente promissor para a gestão de zonas ripárias por deteção remota ao permitir monitorizar os resultados da aplicação das medidas de erradicação da invasora.

Implicações para a gestão e monitorização de ecossistemas ripários

Este trabalho pertence ao grupo dos estudos cujo objetivo é a determinação por deteção remota de parâmetros, que permitam aferir a qualidade ecológica das zonas ripárias, de acordo com a categorização apresentada no capítulo 1 (Quadro 1). A caracterização da variabilidade sazonal das assinaturas espectrais e a identificação das zonas ótimas de separabilidade espectral da cana face à vegetação envolvente, fundamentam escolhas futuras quantas à seleção das imagens mais adequadas para cartografia da cana em habitats ripários. As bandas ótimas de separabilidade identificadas neste estudo só se encontram disponíveis em imagens hiperespectrais, com elevado custo de aquisição e necessidade de programação do voo, no caso de imagens de elevada resolução espacial obtidas utilizando plataformas aéreas. Contudo, os resultados deste trabalho permitiram concluir que a escolha do tipo de imagem varia em função dos objetivos, e nalguns casos poderá não ser necessário um detalhe espectral tão elevado. Por exemplo, a identificação de um número alargado de bandas contíguas na região do visível que potenciam a separabilidade espectral da cana face ao caniço no período de senescência, aponta para possibilidade de seleção de imagens multiespectrais, com cobertura maioritariamente na região do visível. Por sua vez, a distinção da cana face à vegetação arbórea necessita de informação adicional na região do infravermelho médio, e para a cartografia da cana_RAC, as imagens multiespectrais de elevada resolução espacial, como por exemplo as dos satélites comerciais Ikonos ou QuickBird, parecem ser as que se adequam melhor à distinção de manchas de cana em regeneração. Contudo, no caso de uma

matriz paisagística de elevada heterogeneidade florística, só o detalhe das imagens hiperespectrais permite reconhecer diferenças subtis entre as diversas assinaturas espectrais possibilitando a distinção remota da cana.

Nos testes de separabilidade espectral feitos com imagens simuladas, as Landsat apresentam os melhores resultados quando comparadas com as Ikonos e as SPOT. Este resultado deve-se à maior resolução espectral e ao posicionamento de bandas na região do infravermelho médio, identificado como fundamental para discriminação da cana face à vegetação arbórea. No entanto, é importante não esquecer que a resolução espacial das imagens Landsat (30m) só a torna viável para a deteção de cana em habitats ribeirinhos no caso do grau de invasibilidade ser muito acentuado (manchas grandes e com grande larguras), caso contrário os 30m de resolução de cada pixel não são adequados.

6.3.2 Atributos ótimos para a cartografia de *Arundo donax*

Tendo em conta os resultados obtidos anteriormente relativos às particularidades da configuração geométrica (capítulo 3) e ao nível de separabilidade espectral (capítulo 4) das formações de cana face à vegetação envolvente, este trabalho identifica as variáveis mais importantes, num conjunto de atributos geométricos, espectrais e de textura, para cartografia de cana em habitats ripários, utilizando classificação orientada por objeto.

Os resultados demonstram que as características ótimas para cartografia de cana resultam de uma combinação de atributos de diferentes categorias, embora a sua importância varie em função do tipo de imagem utilizada. No caso da classificação ser realizada em imagens aéreas multispectrais, (4 canais e 50 cm de resolução espacial) os atributos geométricos, sobretudo o tamanho das manchas de cana, são primariamente selecionados para distinção da cana face à envolvente, seguidos por atributos espectrais, como o Índice da Vegetação por Diferença Normalizada (NDVI) e a média dos valores na banda do vermelho. A elevada resolução espacial destas imagens (50cm) permite caracterizar com detalhe as configurações geométricas, sendo também considerados importantes os atributos relacionados com a forma e o nível de alongamento das manchas. Estes resultados foram surpreendentes, uma vez que na maior parte dos estudos de classificação orientada por objeto, as variáveis geométricas têm revelado um contributo reduzido na discriminação das diferentes classes de vegetação (Yu et al., 2006). Este trabalho confirma a relevância dos atributos espectrais, sobretudo das bandas do vermelho e infravermelho próximo na discriminação da cana, tal como apontado

anteriormente por outros autores (Schmidt e Skidmore, 2003; Everitt et al., 2004). No entanto, os valores de NDVI encontrados para as manchas de cana, entre 0.37 e 0.39, são claramente superiores aos descritos para outros tipos de vegetação, entre 0.2 e 0.3 (Xie et al., 2008; Aksoy et al., 2010; Peña-Barragán et al., 2011; Pu e Landry 2012). Estes resultados vão de encontro ao referido no capítulo 4, relativamente à elevada produtividade primária e intenso desenvolvimento vegetativo desta invasora face às restantes classes de vegetação, o que potencia a sua distinção por técnicas de deteção remota.

Para a classificação realizada na imagem de satélite WorldView-2, as variáveis espectrais, sobretudo o NDVI, são primariamente selecionadas para discriminação da cana, seguidas dos atributos texturais. Os canais desta imagem (8 canais), face aos quatro canais das imagens aéreas multiespectrais, nomeadamente a banda do amarelo, do red-edge, e do infravermelho médio, permitem detetar com maior precisão os traços óticos, quer ao nível da folha quer ao nível da copa, que parecem ser responsáveis pela maior discriminação da manchas de cana no corredor ripário.

A validação dos resultados revelou uma similaridade elevada entre os mapas produzidos utilizando os atributos ótimos numa classificação orientada por objeto, e os mapas produzidos manualmente por fotointerpretação. A similaridade ocorreu não só em termos de precisão geográfica mas também em termos de área total e de configuração das manchas de cana. A peculiaridade dos traços espectrais e geométricos das manchas de cana torna a classificação orientada por objeto uma técnica adequada para cartografia desta invasora ao permitir a utilização de um conjunto de atributos que a descriminam de forma inequívoca da envolvente.

Implicações para a gestão e monitorização de ecossistemas ripários

Os resultados deste trabalho, de conteúdo fortemente metodológico, fornecem um conjunto de recomendações quanto à escolha da tipologia de imagens (resolução espectral, espacial e temporal) em função de diferentes objetivos de gestão e monitorização ripária, do uso do solo envolvente, da escala de atuação e dos constrangimentos orçamentais. Por exemplo, o maior nível de precisão geográfica (coeficiente kappa=0.77) obtido nos mapas produzidos com recurso à imagem de satélite WorldView-2, em comparação com as imagens aéreas multiespectrais (coeficiente kappa=0.73), recomenda a utilização da imagem de satélite para cartografia geral de cana, sobretudo nos casos em que a matriz de paisagem envolvente à zona ripária apresenta elevada heterogeneidade, sendo fundamental a maior resolução espectral

destas imagens. Porém, as comparações efetuadas entre os mapas obtidos com a classificação orientada por objetos e os mapas obtidos manualmente, utilizando métricas de paisagem, mostram uma tendência para sobreavaliar a área total invadida quando se recorre a imagens WorldView-2. De facto, estudos anteriores (Baker et al., 2007) haviam igualmente relacionado a sobreavaliação da largura e do grau de conetividade em corredores ripários com a menor resolução espacial das imagens. Desta forma, se os objetivos de gestão passam pela produção de uma cartografia de detalhe, as imagens aéreas multiespectrais (50 cm) poderão representar uma alternativa adequada, sobretudo se a matriz espectral envolvente à zona ripária for relativamente homogénea, com a identificação clara das fronteiras entre os diferentes usos do solo. Neste caso, a distinção espectral poderá ser suportada por um número reduzido de bandas. Estão nesta situação as galerias ripárias rodeadas por monoculturas agrícolas em regime intensivo, ou florestas de produção. A caracterização detalhada das configurações espaciais das manchas de cana ao longo do corredor ripário fornece informação quanto ao grau de invasão e consequentemente quanto ao estado de degradação da galeria ripária. Manchas de cana fortemente conectadas, sem a presença de vegetação nativa e zonas de descontinuidades representam galerias ripárias onde o esforço de restauro é elevado. As imagens aéreas multiespectrais utilizadas neste trabalho, produzidas pelo Instituto Geográfico Português, apresentam como vantagem o reduzido custo de aquisição face à imagem de satélite (2.5€/ km^2 vs 24€/ km^2). Contudo a qualidade radiométrica destas imagens é inferior à da imagem de satélite, obrigando à realização de processos adicionais de calibração radiométrica para eliminação dos erros provenientes da aquisição em períodos temporais distintos.

Os resultados obtidos neste trabalho, e nos capítulos anteriores, permitem concluir que não existe época do ano ótima para aquisição das imagens, sendo esta fortemente dependente dos objetivos de estudo, dos traços óticos da vegetação e das características das imagens. Contudo, neste trabalho foram observados mais erros de classificação nas épocas correspondentes a um elevado desenvolvimento vegetativo, situadas no ínicio da primavera e do outono (para as culturas agrícolas de inverno). A similaridade espectral existente nos períodos de transição sazonal foi anteriormente referida por Andrew e Ustin (2008) e Yang et al. (2012), sendo responsável pela redução de precisão nas classificações realizadas com recursos a técnicas de deteção remota.

6.4 Considerações finais

As potencialidades da deteção remota, aplicada ao estudo das comunidades ripárias e como ferramenta de apoio à gestão e monitorização de ecossistemas fluviais, encontram-se largamente evidenciadas, não só ao longo dos trabalhos realizados no âmbito desta dissertação, mas também na vasta bibliografia apresentada A singularidade e complexidade dos ecossistemas ripários obrigam a uma especificidade nas metodologias e materiais utilizados, nomeadamente, no que se refere à utilização de imagens de elevada resolução espacial, que, embora se encontrem largamente disponibilizadas no mercado, apresentam ainda custos de aquisição muito elevados. No entanto, para que as metodologias de avaliação remota se tornem prática comum nas ações de monitorização dos ecossistemas ripários é necessário operacionalizá-las para a escala da bacia hidrográfica, a unidade mínima de gestão dos recursos hídricos. Programas como GMES (Global Monitoring and Environmental Security) desenvolvidos pela Comissão Europeia poderão contribuir para aligeirar esta questão. Os dados proveniente dos novos sensores, disponibilizados de forma tendencialmente gratuita, como é exemplo o sensor ótico Sentinel-2, com uma resolução espectral de 13 bandas estrategicamente localizadas em regiões consideradas fundamentais para a distinção da vegetação representam um manancial de dados para estudos futuros de deteção remota aplicada ao ambiente em geral, e aos ecossistemas ripários e fluviais em particular.

A natureza linear destes sistemas combinada com a elevada variabilidade dos padrões espaciais e a problemática da diferença de escala existente entre as entidades de estudo e a resolução da imagem cria dificuldades adicionais na aplicação das metodologias clássicas de deteção remota, baseadas na componente espectral, aos ecossistemas ripários.

Ao longo desta dissertação foi possível verificar a importância da complementaridade dos atributos geométricos avaliados de forma remota, quer manualmente, quer utilizando metodologias semi-automáticas e a aplicação de filtros espaciais, no aumento da precisão da classificação. Tendo em conta estes resultados, e a tendência observada nas publicações mais recentes, é de prever que os trabalhos futuros apresentem, cada vez mais, uma combinação de diferentes tipos de informação remota (informação espectral, contextual, geométrica, de textura), diferentes tipos de sensores (dados Lidar, fusão de imagens, calibração de imagens em função de dados de campo e/ou outras imagens de maior resolução espacial), mas complementada com procedimentos hierárquicos realizados em ambiente SIG, muitas vezes, desenvolvidos “à medida” de cada aplicação no sentido de minimizar os erros de classificação.

Finalmente, uma das aplicações menos exploradas da deteção remota, mas de elevada pertinência dentro do cenário atual de alterações climáticas, é o desenvolvimento de estudos temporais, que permitam a elaboração de modelos capazes de prever a influência destas alterações nos padrões estruturais e composicionais da vegetação ripária e na integridade dos ecossistemas ripários. Estes trabalhos representam desafios acrescidos por se situarem numa interface multidisciplinar entre a cartografia, a modelação e a ecologia, mas possibilitando o desenvolvimento de propostas fundamentadas para os organismos com responsabilidade de tutela na gestão dos recursos hídricos.

6.5 Referências bibliográficas

Aguiar F.C., Ferreira M.T. 2005. Human-disturbed landscapes: effects on composition and integrity of riparian woody vegetation in the Tagus River basin, Portugal. Environmental Conservation 32 (1), 30-41.

Aguiar, F.C., Ferreira, M.T. (in press). Plant invasions in the rivers of the Iberian Peninsula, South-Western Europe – a review. Plant Biosystems.

Aguiar F.C., Fernandes M.R., Ferreira M.T. 2011. Riparian vegetation metrics as tools for guiding ecological restoration in riverscapes. Knowledge and Management of Aquatic Ecosystems 402, 21.

Aguiar F.C., Ferreira M.T., Albuquerque A., Moreira I. 2007. Alien and endemic flora on reference and non-reference sites from Mediterranean type-streams of Portugal. Aquatic Conservation: Marine and Freshwater Ecosystems 17 (4), 335-347.

Aguiar F.C., Ferreira M.T., Moreira I., Albuquerque A., 2000. Riparian types in Mediterranean basin. Aspects of Applied Biology 58, 221-232.

Allan J.D. 2004. Landscapes and Riverscapes: The influence of land use on stream ecosystems. Annual Review of Ecology, Evolution and Systematics 35, 257-284.

Alvarez-Añorve M., Quesada M., de la Barrer E. 2008. Remote Sensing and Plant Functional Groups. Physiology, Ecology, and Spectroscopy in Tropical Systems. In: Kalacska, M., Sánchez-Azofeifa, A. (Eds.), Hyperspectral Remote Sensing of Tropical and Sub-Tropical Forests, pp. 27-45.

Aksoy S., Akçay H.G., Wassenaar T. 2010. Automatic mapping of linear woody vegetation fetures in agricultural landscapes using very high resolution imagery. IEEE Transactions on Geoscience and Remote Sensing 48 (1), 511-522.

Apan A.A., Raine S.R., Paterson M.S. 2002. Mapping an analysis of changes in the riparian landscape structure of Lockyer Valley catchment Queensland, Australia. Landscape and Urban Planning 59 (1), 43-57.

Andrew M.E., Ustin S.L. 2008. The role of environmental context in mapping plants with hyperspectral image data. Remote Sensing of Environment 112 (12), 4301-4317.

Baker M.E., Weller D.E., Jordan T.E. 2007. Effects of stream map resolution on measures of riparian buffer distribution and nutrient potential. Landscape Ecology 27 (7), 973-992.

Bott T.L., Montgomery D.S., Newbold J.D., Arscott D.B., Dow C.L., Aufdenkampe A. K., Jackson J. K., Kaplan L.A. 2006. Ecosystem metabolism in streams of the Catskill Mountains (Delaware and Hudson River watersheds) and Lower Hudson Valley. Journal of the North American Benthological Society 25, 1018-1044.

Bunn S.E., Davies P.M. 2000. Biological processes in running waters and their implications for the assessment of ecological integrity. Hydrobiologia, 442/443, 61-70.

Chen J., Chen C. 2008. Correlation analysis between indices of tree leaf spectral reflectance and chlorophyll content. In: editors (Eds.), Proceedings of Commission VII. ISPRS Congress Beijing, 3-11 July, Beijing China, pp. 231.

Cochrane M.A., 2000. Using vegetation reflectance variability for species level classification of hyperspectral data. International Journal Remote Sensing 21 (10), 2075-2087.

Cushman J.H., Gaffney K.A. 2010. Community-level consequences of invasion: impacts of exotic clonal plants on riparian vegetation. Biological Invasions 12 (8), 2765-2776.

Decruyenaere J.G., Holt J.S., 2005. Ramet demography of a clonal invader, *Arundo donax* (Poaceae), in Southern California. Plant and Soil 277 (1-2), 41-52.

Everitt J.H., Yang C., Fletcher R., Deloach C.J. 2008. Comparison of QuickBird and SPOT 5 satellite imagery for mapping giant reed. Journal of Aquatic Plant Management 46, 77-82.

Ferreira M.T., Aguiar F.C., Nogueira C. 2005. Changes in riparian woods over space and time: Influence of environment and land use. Forest Ecology and Management 212 (1-3), 145-159.

Ge S., Carruthers R.I., Spencer D.F., Yu Qian. 2008. Canopy assessment of biochemical features by ground-based hyperspectral data for an invasive species, giant reed (*Arundo donax*). Environmental Monitoring and Assessment 147 (1-3), 271-278.

Inoue M., Nakagoshi M. 2001. The effects of human impact on spatial structure of the riparian vegetation along the Ashida river, Japan. Landscape and Urban Planning 53 (1), 111–121

Nagler P.L., Glenn E.P., Hursh K., Curtis C., Huete, A.R. 2005. Vegetation mapping for change detection on an arid-zone river. Environmental Monitoring and Assessment 109 (1-3), 255-274.

Ollinger S.V. 2011. Sources of variability in canopy reflectance and the convergent properties of plants. New Phytologist 189 (2), 375-394.

Papazoglou E.G., Karantounias G.A., Vemmos S.N., Bouranis D.L. 2005. Photosynthesis and growth responses of giant reed (*Arundo donax* L.) to the heavy metals Cd and Ni. Environment International 31 (2), 243-249.

Peña-Barragán J.M., Ngugi M.K., Plant R.E., Six J. 2011. Object-based crop identification using multiple vegetation indices, textural features and crop phenology. Remote Sensing of Environment 115 (6), 1301-1316.

Pu R., Landry S. 2012. A comparative analysis of high spatial resolution IKONOS and WorldView-2 imagery for mapping urban tree species. Remote Sensing of Environment 124, 516-533.

Rossa B., TuAers A.V., Naidoo G., von Willert D.J. 1998. *Arundo donax* L. (Poaceae) - a C3 species with unusually high photosynthetic capacity. Botanica Acta 111, 216-221.

Schmidt K.S., Skidmore A.K. 2003 Spectral discrimination of vegetation types in a costal wetland. Remote Sensing of Environment 85 (1), 92-108.

Schuft M.J., Moser T.J., Wigington P.J., Stevens D.L., McAllister L.S., Chapman S.S., Ernst T.L. 1999. Development of landscape metrics for characterizing riparian-stream networks. Photogrammetric Engineering and Remote Sensing 65(10), 1157-1167.

Silva C.M.N., Silva L., Oliveira N., Geraldes P., Hervías S. 2011. Control of giant reed *Arundo donax* on Vila Franca do Campo Islet, Azores, Portugal. Conservation Evidence 8, 93-99.

von Schiller D., Martí E., Riera J.L., Ribot M., Marks J.C., Sabater F. 2008. Influence of land use on stream ecosystem function in a Mediterranean catchment. Freshwater Biology 53 (12), 2600-2612.

Xie Z., Roberts C., Johnson B. 2008. Object-based target search using remotely sensed data: A case study in detecting invasive exotic Australian Pine in south Florida. ISPRS Journal of Photogrammetry and Remote Sensing 63 (6), 647-660.

Yang C., Goolsby J.A., Everitt J.H., Du Q. 2012. Applying six classifiers to airborne hyperspectral imagery for detecting giant reed. Geocarto International 27 (5), 413-424.

Yu Q., Gong P., Clinton N., Biging G., Kelly M., Schirokauer D. 2006. Object-based detailed vegetation classification with airborne high spatial resolution remote sensing imagery. Photogrammetric Engineering and Remote Sensing 72 (7), 799-811.